RIASSUNTI DI TESI DI DOTTORATO DI RICERCA

MAGMA INTERACTION PROCESSES DURING THE LAST PHASE OF ACTIVITY OF NISYROS ACTIVE VOLCANIC SYSTEM (SOUTH AEGEAN, GREECE)

ELEONORA BRASCHI
Dipartimento di Scienze della Terra, Università di Firenze, Via G. La Pira 4, 50121 Firenze

INTRODUCTION

Understanding the interaction between different magmas is very important for reconstructing the dynamics of the eruptions and the plumbing system configuration of a volcano. One of the best evidence of these processes is represented by mafic enclaves inside evolved host, like lava flow or domes.

Mafic enclaves represent fragment of mafic magma that rapidly crystallize on contact with the cooler more evolved host magma. These two terms are, therefore, considered as the end-members of a system where different liquids interact and generate a variety of characteristics that reflect different condition (P, T, composition). Enclaves are the result of immiscibility processes between two different magmas yielding to mingling.

The work presented here is focused on the understanding of the interaction processes between magmas with different degree of evolution. The aim is to understand how and if these processes can trigger eruptions and if it is possible to find evidence of distinct recharge event of mafic magma inside an evolved shallow reservoir.

The active volcanic system of Nisyros and Yali, in the eastern part of the South Aegean Volcanic Arc, is one of the best place for investigating these processes because its last evolution is characterized by the emplacement of rhyolitic pyroclastic products and extrusion of rhyo-dacitic domes, rich in mafic enclaves.

GEOLOGICAL AND VOLCANOLOGICAL BACKGROUND

Nisyros volcano, near the coast of Turkey, is the easternmost volcanic edifice of the active South Aegean Volcanic Arc. It is the largest of a group of volcanic islands including the islets of Perigusa, Pahia, Strongili and Yali.

Nisyros island is a small entirely volcanic edifice, build up during the last 100 ka. All products have a calc-alkaline affinity varying in composition from basaltic-andesite to ryolite.

The volcanological evolution can be subdivided into two distinct cycle of activity (Di Paola, 1974): the first cycle includes the cone-building activity with effusive and explosive activity. The second eruptive cycle includes the caldera-forming explosive activity, with two distinct phases, each consisting in rhyolitic phreatomagmatic eruption triggering central caldera collapse and extrusion of dacitic-rhyolitic domes and lava flows. The rocks of this cycle are characterized by the presence of mafic enclaves, with distinct petrographic and chemical features, which testify mixing-mingling processes between variously evolved magmas during the last activity of the volcano (Francalanci *et al.*, 1995). In particular, the last phase of the second cycle, is characterized by the emplacement of six domes after the caldera collapse (probably < 24 ka), associated to the Plinian eruption leading to the formation of a thick pyroclastic

deposit (*Upper Pumice*) (Limburg & Varekamp, 1991). The six post-caldera domes were extruded both inside and outside the caldera along a tectonic lineament aligned NE-SW.

The adjoining island of Yali, younger than 24 ky, has a distinctive assessment composed by two different part characterized by different products. The SW part is completely build up by pyroclastic deposits, whereas the NE portion is formed by lava flow and domes, with a small tuff ring on the eastern corner. All products are calc-alkaline, mostly rhyolitic in composition, with few less evolved products, defining a large compositional gap. The latter are present as dense juvenile material (enclaves) inside the youngest pyroclastic unit named *Yali Upper Pumice* sequence.

RESULTS

Based on field observations, Profitis Elias dome is the oldest one, then the Sterna, Trapesina and Nifios domes were emplaced, followed by Karaviotis and then Boriatico dome. Enclaves show round and irregular shapes with sharp contact and convolute surface. Sizes are variable, ranging from about one meter to few centimeters. Abundance and size of these enclaves show quite evident variation among domes depending on the age: from the older to the younger dome, enclaves increase in percentage (from 5-6 to 10-13%) and decrease in size (from 25-30 cm to 5-10 cm as prevalent size).

The sampling has been performed on domes and mafic inclusions, taking several enclaves for each dome to cover all the variability in size, shape, color and texture, trying also to collect the dome-enclave contacts.

The *Upper Pumice* pyroclastic sequence of Nisyros has been sampled from the base (fallout level) to the top (lag-breccia level) in order to investigate possible compositional changing in the feeding magmas. The basal fallout level is characterized by a double juvenile consisting in white pumice and dense, light grey juvenile, whereas only a dense juvenile is found in the lag-breccia level.

The sampling on Yali island has been performed on the *Yali Upper Pumice* sequence (Yup), lava flows and tuff ring products.

Petrographic and geochemical studies were performed on whole rocks of all the samples collected, whereas mineral chemistry and isotope analyses were performed on a selected number of samples.

Finally *in situ* micro-sampling technique, for micro-Sr isotope determinations, has been also applied on three most significant enclave samples.

Petrography

Domes have porphyritic and glomeroporphyritic textures, with criptocrystalline to glassy groundmasses. They show high phenocryst contents (*ca*. 20-30 vol.%) which are constituted by plagioclase, quartz, orthopyroxene, Fe-Ti oxides and rare clinopyroxene, olivine and amphibole. Microlites of plagioclase are present in the glassy groundmass.

Magmatic enclaves have hypocrystalline textures with variable and generally low porphyritic index (< 10 vol.%). They frequently have diktytaxitic voids in the groundmasses and show variable vesicle contents. The dome-enclave contacts are usually characterized by chilled margins in the enclaves, with smaller size of the microlites and/or higher glass content. Chilled margin insure their origin from a magmatic liquid and their inclusion into the cooler dome magmatic bodies. Phenocrysts are constituted by plagioclase, clinopyroxene, and rare amphibole, olivine, Fe-Ti-oxides and orthopyroxene, whereas the groundmasses are formed by a microcrystalline network of acicular plagioclase and amphibole with interstitial clinopyroxene, oxides and small amount of glass. Several enclaves show mega-phenocrysts of

plagioclase with rounded shape and several sieved zones. These crystals are often present near the contact surfaces between the enclaves and the host domes. This characteristic suggests that mega-phenocrysts of plagioclase move from the dome host magma to the enclave body, giving rise to an intense crystal exchange between the two magmas (micro-scale mingling).

Pumices of the *Upper Pumice* sequence have low porphyritic texture (up to 5 vol.%), with glassy, highly vesicular groundmass. Crystals are mostly plagioclase and Fe-Ti oxide with rare pyroxene crystals. The dense juvenile component (both from fallout and lag breccia levels) are similar to the magmatic enclaves, but show a higher vesicular texture. Pyroxene, Fe-Ti oxide and olivine micro-phenocrysts are also present.

Pumices from *Yali Upper Pumice* sequence (Yup) are low porphyritic with glassy, high vesicular groundmass. Plagioclase (micro-phenocrysts) is the main mineral phase together with Fe-Ti oxides. Dense juvenile samples are similar to the Nisyros magmatic enclaves. Lavas and pyroclastic juvenile forming the tuff ring are very low porphyritic (< 1%) with glassy, variously vesiculate, groundmass. Plagioclase represent the main mineralogical phase together with oxides.

Mineral chemistry

Mineral chemistry has been analyzed in 12 representative samples of domes and enclaves.

Mg# ($Mg/Mg+Fe^{2+}$) in clinopyroxene range between 0.58-0.85 and in orthopyroxene between 0.70-0.85, while anorthite contents in plagioclase vary between 20-95%.

Among the enclaves, minerals are characterized by distinct features: plagioclase xenocrysts coming from the host magma show oscillatory zoning and range in composition between An% 25-60, whereas plagioclase of the enclaves magma are mainly micro-phenocrysts and have An% between 70-90. Few intermediate compositions are also present suggesting complex interaction processes.

Amphiboles are classified as tschermakite and are quite homogeneous in composition, with Mg# ranging between 0.70-0.80. The amphiboles of the Profitis Elias enclaves show small, but consistent, variations in Mg#, aluminum content and $Fe^{3+/}Fe^{2+}$ ratio in respect with those of the Boriatico enclaves.

Two *Upper Pumice* samples have been selected for the mineral chemistry analysis. Pumice, have orthopyroxene with homogeneous Mg# of about 0.59, whereas dense juvenile (from the same fallout level) have Mg# of 0.55. On the contrary, plagioclase shows anorthite contents between 25-40% among the pumice and 45-51% among the dense juvenile.

Among the Yali samples, only few analyses were performed on pumice and dense juvenile samples belonging to the pyroclastic sequence of Yup. Clinopyroxene are exclusively present in the dense juvenile sample and show a variation in Mg# between 0.72-0.90. Plagioclase of the pumice shows anorthite contents between 60-75%; those of dense juvenile are wide zoned, ranging from An% 35 in the core to 80 in the rim.

Major and trace element geochemistry

Domes are dacitic and rhyolitic with silica content ranging from 66 wt.% to 72 wt.%. Sterna and Profitis Elias domes have the highest silica contents, whereas Boriatico dome has the lowest silica content. Al_2O_3, TiO_2, CaO and FeO contents are negatively correlated with SiO_2 (Fig. 1), whereas Na_2O and K_2O abundances form positive correlations with silica.

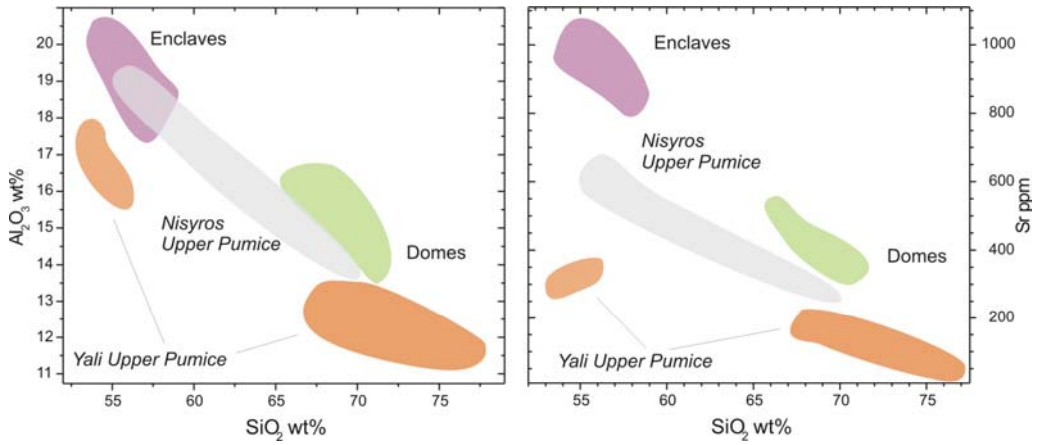

Fig. 1 - Al_2O_3 (wt.%) and Sr (ppm) *vs.* SiO_2 (wt.%) contents for Nisyros and Yali younger products. Light green: domes; violet: enclaves; light grey: Upper Pumice pyroclastics; orange: Yali products.

Enclaves are basaltic-andesites and andesites with silica contents ranging between 54-59 wt.%. A large silica gap between domes and their enclaves is thus present. Among major elements (Fig. 1), Al_2O_3 contents of enclaves show the highest variation and are well negatively correlated with silica, with Karaviotis and Boriatico enclaves having the highest alumina contents. At the same silica content, Boriatico, Karaviotis and some Trapesina enclaves also show lower FeO and TiO_2 abundances than the other enclaves. On the whole, among both the enclaves and domes, the silica content decreases from the oldest to the youngest.

Both major and trace elements of the whole rocks show clear differences between domes and enclaves. For example, K_2O in the enclaves vary from 0.9 to 1.5% and from 2.4 to 3% in the domes. Enclaves show higher contents in compatible elements and lower amounts in incompatible trace elements than domes: Sr contents in the enclaves vary from 850 to 1000 ppm and from 320 to 530 in the domes (Fig. 1), V and Rb contents in the enclaves are 105-155 and 5-25 ppm, respectively, whereas in the domes they are 35-70 and 45-75 ppm, respectively.

The Upper Pumice samples cover a wide compositional range from basaltic-andesite to rhyodacite. They show a small compositional gap between 65% and 69% of silica. This gap discriminates between pumice (69-73% SiO_2) and dense juvenile components (56-65% SiO_2). Among the dense juvenile samples, major and trace element contents are quite homogenous in the lag-breccia samples, whereas they show much more variability in the fallout samples. The latter are intermediate between pumice and lag-breccia dense juvenile.

The Yali products show a wide compositional gap, with rhyolitic lavas and pumices (silica from 67 up to 76%) and basaltic-andesite dense juvenile components.

On the basis of major elements, it is hard to discriminate between pre- and post-caldera products of Nisyros as well as between Nisyros and Yali products. On the contrary, trace elements, especially Sr, highlight systematic differences among the products of the three eruptive events. At same silica content, the Nisyros post-caldera dome-enclave samples are characterized by the highest Sr content, whereas the lowest are found in the Yali products (Fig. 1).

Isotope geochemistry

Sr and Nd isotope data show important variations among the post-caldera samples (domes and enclaves) as well as between products of Nisyros Upper Pumice and Yali samples (Fig. 2).

$^{87}Sr/^{86}Sr$ data show little but significant differences between the enclaves (from 0.70383 to 0.70386). This variation becomes more evident among the domes, where values from 0.70402 to 0.70418 are measured.

$^{143}Nd/^{144}Nd$ values vary from 0.51269 to 0.51273 among the enclaves and from 0.51264 to 0.51266 among the domes. Like silica contents, $^{87}Sr/^{86}Sr$ values decrease, among the enclaves, from the oldest to the youngest ones, whereas among domes, Sr isotope ratios is considerably higher for the oldest domes. The Boriatico system is, therefore, less Sr radiogenic both for enclaves and host-dome, in respect with all the other dome-enclave systems, showing composition closer to those of the enclaves. Nd isotope ratios, are well negatively correlated with Sr isotope ratios (Fig. 2).

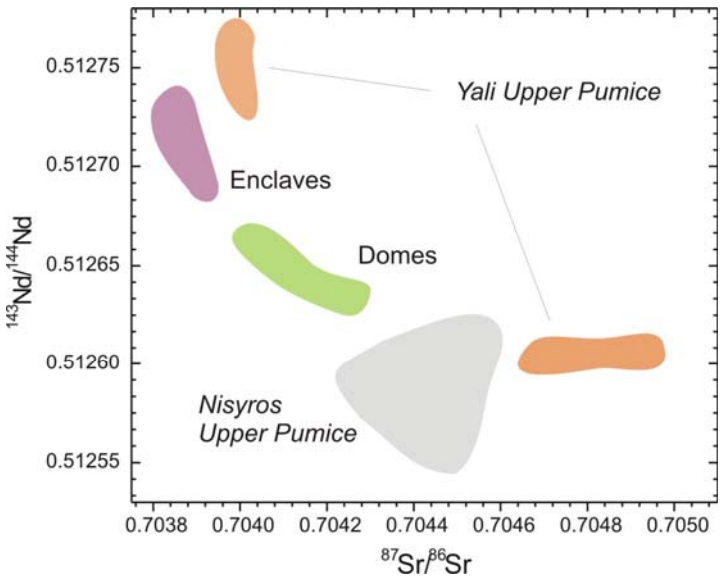

Fig. 2 - $^{87}Sr/^{86}Sr$ *vs.* $^{143}Nd/^{144}Nd$ for Nisyros and Yali younger samples. Field colours as in Fig. 1.

Upper Pumice samples show $^{87}Sr/^{86}Sr$ values ranging from 0.70425 to 0.70456 for lag breccias dense juvenile and pumice respectively, whereas $^{143}Nd/^{144}Nd$ values vary from 0.51255 to 0.51261 in the fallout dense juvenile and pumice, respectively. Among these samples, the Nd and Sr isotope ratios are not well correlates, pointing out the occurrence of complex evolutionary processes inside the pre-caldera plumbing system.

Among the Yali samples, the evolved pumice shows a $^{87}Sr/^{86}Sr$ value of 0.70450 and a $^{143}Nd/^{144}Nd$ of 0.51261, whereas the more mafic dense juveniles have $^{87}Sr/^{86}Sr$ of about 0.70400 and $^{143}Nd/^{144}Nd$ ranging from 0.51273 to 0.51277.

Micro-Sr isotope data

In order to investigate the origin of the plagioclase mega-phenocrysts found in several enclaves, which probably belong to the host-domes, three representative samples from enclaves are selected for *in situ* Sr isotope determinations. They have been chosen from Trapesina, Karaviotis and Boriatico samples.

The results from this forefront technique give important information for the understanding of post-caldera plumbing systems.

Cores of all mega-plagioclase crystals selected for *in situ* determinations (characterized by low anorthite content of 30-35%) show high $^{87}Sr/^{86}Sr$ (ranging from 0.7044 to 0.70452), whereas rims (where anorthite content is up to 70%) show $^{87}Sr/^{86}Sr$ values that range from 0.70415 to 0.70398. The latter

show, therefore, a wider range than cores, and have an isotopic composition similar to that of the domes. Cores have, instead, an isotopic composition that fall inside the Sr isotope range of the *Upper Pumice* products.

Some euhedral plagioclase, with anorthite of 80-90% has been also analyzed. The results give $^{87}Sr/^{86}Sr$ values lower than those of the aforesaid mega-plagioclase rims, down to values lower than the whole isotopic range of the enclaves (0.70380).

DISCUSSIONS AND CONCLUSIONS

Concerning the domes-enclaves interaction, field observations and petrographic examinations tell us that, from the oldest to the youngest domes, the degree of mingling processes increases enhancing the emulsion of mafic magmas (the enclaves) inside the host magma (lava domes). During mingling, several exchange processes also take place at the micro-scale, allowing intense transfer of mineral phases from dome to enclaves (plagioclase and glassy groundmass portions) and vice versa (pyroxenes, olivine and plagioclase microlites due to the crumbling of enclaves).

The latter observation is consistent with the compositional characteristics revealed by mineral chemistry analysis. For example, the evaluation of equilibrium-disequilibrium conditions of the mafic phases (pyroxene and olivine), in respect to the whole host rocks, highlight that several crystals are out of the equilibrium conditions, both in domes and enclaves.

Geobarometric determinations, based on amphibole composition, allow us to suppose a slight decrease in pressure conditions with time, from Profitis Elias to Boriatico dome systems. This means that, probably the level of contact surface between the two magmas rise up during the emplacement of the six post-caldera domes.

Geochemical and isotopic data show variation that can be explained by the concomitance of several processes. Major and trace element compositions indicate a mixing trend between two end-members (rhyolitic and basaltic-andesite magmas), but the real hybrid magmas are lacking.

For the post-caldera domes, rhyo-dacitic rocks show, in effect, evidence of hybridization with the mafic magma of the enclaves (increasing with time). This hybridization is mostly due to the dispersion inside the host magma of micro-enclaves and mineral phases, like a micro-scale mingling.

The generation and differentiation of the enclave magmas, seem mainly due to fractional crystallization, with the concomitance of less contamination processes with the host evolved magma (probably due to small amount of evolved, residual liquid that slip into the enclave body).

Little geochemical variations among the enclaves, belonging to different dome body, have been interpreted as the evidence of different inputs of new magma (at least two different input) inside the shallow magma chamber, before the post-caldera activity. This causes a zoning inside the more primitive magma reservoir underlying the rhyo-dacite magma. Dispersion starts consequently to the instauration of strong convective motions inside the magma chamber (due to the heating and density contrast) and brings up different portions of the mafic magma, generating a complex, variously zoned system. The emplacement of domes allows sampling different portions of the magma chamber, which result in the different characteristics of enclaves.

Finally, micro-Sr results show that most, if not all, the macro-plagioclase are xenocrysts in respect to the enclaves magma and come from the dome evolved magma, but they crystallize from the previous magmatic system that formed the evolved Upper Pumice product.

In this interpretation, the *Upper Pumice* represents the parental system for the post-caldera evolved portion.

Summarizing, all the characteristics of the magmatic enclaves suggest that they represent mafic magmas intruded in the more evolved dome magmas. The presence of a compositional gap between domes and enclaves demonstrates that generation of hybrid magmas, did not really occur, and seems to indicate that the two magmas remained in contact for a short period of time.

The plumbing system of the last magmatic activity of Nisyros can be figure out as a complex system with a zoned magma chamber where several events of renewed intrusion of mafic magma took place, with a clear tendency of the system towards more mafic composition.

Furthermore, it is also evident that Quaternary tectonics play an important role on the volcanic activity of Nisyros volcanic system. Tectonic movements can cause closure or opening of new way out for the deep magma, allowing jumping on the volcanic activity (from explosive to effusive). Indeed, *Upper Pumice* pyroclastics and domes-enclaves systems cover the same silica range (that means same degree of evolution) and undergo similar mingling process, but they are emplaced by different type of activity. This indicates the importance of the tectonic assessment variation from the caldera-forming and post-caldera periods of activity.

Regarding to Yali, the obtained data suggest that it represents an independent volcanic center, fed by a different plumbing system, marginal in respect with the main volcanic area of Nisyros.

REFERENCES

Di Paola, G.M. (1974): Volcanology and petrology of Nisyros island (Dodecanese, Greece). *Bull. Volcanol.*, **38,** 944-987.

Francalanci, L., Varekamp, J.C., Vougioukalakis, G., Defant, M.J., Innocenti, F., Manetti, P. (1995): Crystal retention, fractionation and crustal assimilation in a convecting magma chamber, Nisyros Volcano, Greece. *Bull. Volcanol.*, **56**, 601-620.

Limburg, E.M. & Varekamp, J.C. (1991): Young pumice deposits on Nisyros, Greece. *Bull. Volcanol.*, **54,** 68-77.

ATMOSPHERIC DEPOSITION OF VOLCANOGENIC MAJOR AND TRACE ELEMENTS ON MT. ETNA (ITALY)

SERGIO CALABRESE
Dipartimento di Chimica e Fisica della Terra ed Applicazioni alle Georisorse ed ai Rischi Naturali,
Università di Palermo, Via Archirafi 36, 90123 Palermo

INTRODUCTION

There are a variety of natural and anthropogenic sources of trace elements into the environment, and human activity has drastically changed the biogeochemical cycles and balance of several elements. In the last twenty years many efforts have been spent by the scientific community to better outline the levels of pollutants in the environment on a long-term basis, and to evaluate global large-scale changes. It is generally accepted that volcanic emissions are an important source of gases and particles to the atmosphere, contributing significantly to the natural geochemical cycles of all elements (Nriagu, 1989; Hinkley *et al.,* 1999; Oppenheimer, 2003). Many studies have been carried out on the main volcanic emitters of the world, to estimate and characterise their emissions (Gauthier & Le Cloarec, 1998; Hinkley *et al*., 1999; Cheynet *et al*., 2000; Allard *et al*., 2000; Aiuppa *et al*., 2003; Bagnato *et al*., 2007). By contrast, the atmospheric deposition of trace elements around active volcanoes is poorly constrained. From a literature review, we have recognized the scarcity of investigations on trace element deposition in the surroundings of active volcanoes. Although active volcanoes are widely distributed in the world and their emissions plays a key role on the global geochemical cycles of many elements, only Hawaiian, Japanese, Italian and a few central American volcanoes have been studied from the point of view of major species atmospheric deposition.

This research focuses on the relevant question of the fate of trace metals emitted by an active volcano such as Mount Etna (Italy), and attempts to answer this question by reviewing and interpreting the results of an unprecedented set of trace elements analyses in Etna's precipitation, collected over two years of periodic sampling. The first part of this work is aimed at updating earlier estimates of elemental fluxes released from the volcano, by using classical methodologies. Original data on aerosols chemistry and fluxes, among with the previous estimates, were essential to quantify the *volcanic source*. The second section, focuses on the characterization of atmospheric bulk deposition around the volcano. The obtained large dataset on major, and trace elements concentrations in atmospheric precipitation was used to estimate the deposition rates of the same suite of elements. Finally, in the last part of the thesis, the results for volcanic emissions are compared with atmospheric deposition to highlight the effects of the volcano at local and regional scale.

SAMPLING AND ANALYSIS

Volcanic emissions were collected at Mount Etna from 2004 to 2007. Aerosols in the volcanic plume have been sampled *in situ*, at the rim of the craters (NEC and VOR), by using conventional filtration techniques. Sampling was performed at the rim of the summit craters to avoid excessive dilution of the plume, by pumping the mixture of gases and aerosol for about one hour through an untreated Whatman filter (47 mm cellulose filter disc, with a porosity of 0.45 μm), placed inside a Teflon filter holder (47 mm Teflon® Filter Pack - URG2000); a portable battery-powered pump was equipped with a

flow meter to measure the volume of collected air. The concentrations of metals in the collected aerosols were obtained by ICP-OES and ICP-MS after digestion of the filters. The particles trapped on filters were totally dissolved in a mixture of strong acids (HNO_3, HF, $HClO_4$) by a microwave oven. All determinations were checked by the external standard calibration method, using In as internal standards; analytical errors ranged between 5 and 30% for the analyzed elements. The absolute concentrations were corrected for filters blanks.

Atmospheric precipitation was collected approximately fortnightly on Mount Etna, from April 2006 to December 2007, using a network of five rain gauges, located at various altitudes on the upper flanks around the summit craters of the volcano (Fig. 1). Basing on previous work (Aiuppa *et al*., 2006; Bellomo *et al*., 2007; Martin *et al*., 2009), four rain gauges were installed on the down-wind (eastern) flank, at different distances from summit craters. To define the local atmospheric background, the fifth rain gauge was installed in a site up-wind (INT), in a rural area poorly affected by volcanic emissions. The design and installation of the collectors was conformed to EMEP (European Monitoring and Evaluation Programme) site requirements for precipitation gauges (EMEP, 2001). The rain gauges used for the present research were "Bulk Collectors" because they remained open during the whole sampling period, thus receiving both wet and dry deposition. All water samples were analyzed for 44 elements in the laboratories of the C.F.T.A. department of the University of Palermo, and in the laboratories of the INGV Palermo. Ion chromatography technique was used for the determination of both major anions and cations. The detection limits ($mg \cdot l^{-1}$) were 0.005 for F, 0.01 for Cl and Na, 0.05 for SO_4 and K, 0.05 for NO_3, Mg and Ca, with precision ≤ 3%. Trace and ultra-trace elements were analyzed by inductively coupled plasma-mass spectrometry, with two different ICP-MS instruments (Perkin Elmer ELAN 6100 DRC-e and Agilent 7500ce). The Quality Assurance and Quality control procedures followed in the present research are those adopted by most atmospheric deposition

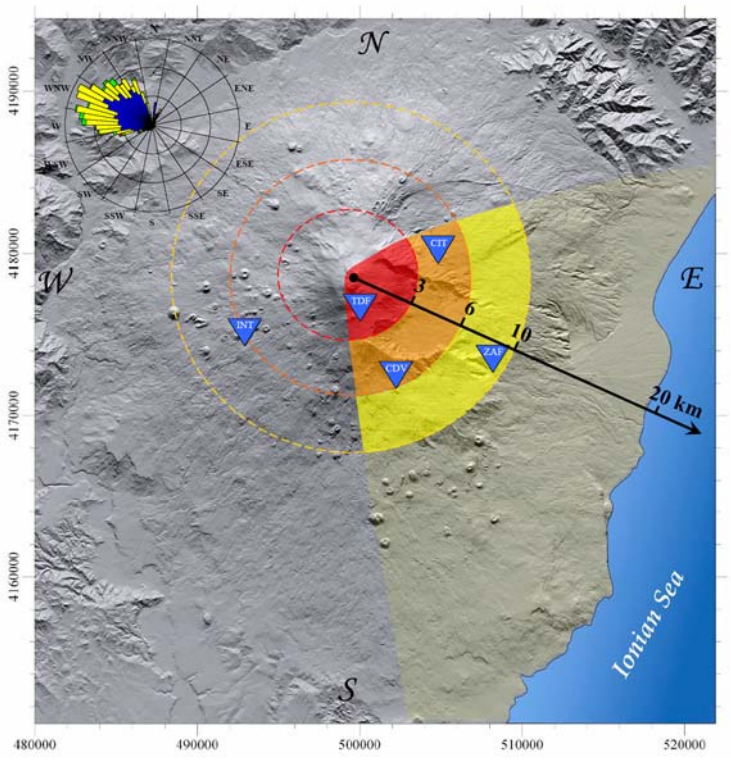

Fig. 1 - Map of Mount Etna and location of the sampling sites of bulk deposition (blue triangles): *Torre del Filosofo* (TDF), *Citelli* (CIT), *Casa del Vescovo* (CDV), and *Zafferana* (ZAF) are the down-wind sites; *Intraleo* (INT) is the up-wind site. The wind rose highlights the prevailing wind directions, referring to the altitude of the summit for the period 2006-2007 (data from Birgi station).

programs and included: field and analytical blanks, cleaning procedures, reference materials, field comparison, and inter-laboratory comparison.

RESULTS AND DISCUSSION

Volcanic emissions

Measured concentrations in solutions from acid digestion of the thirty-one filters were combined with the pumped volume of air (0.5 - 1 m^3) to calculate in-plume element concentration for each sample. Results show that whilst the dominant gaseous species on the filters are Cl, S, and F (from in-tandem filter-pack measurements with base-treated filters), the most abundant metals (in particles) are K, Ca, Mg, Al, Fe, and Ti (1.5 - 50 μg/m^3), which are some of the main constituents of basaltic rocks and magmas. Their abundances on filters reflect the presence of small ash fragments in the plume, which derive from rock fragments eroded from the vent walls, and juvenile fragments of the magma, including glass and silicate minerals. Minor and trace element concentrations in volcanic aerosols range from about 0.01 to 1 μg/m^3, and can be divided into volatile (*e.g.* Se, Cd, Tl, Sb) and non-volatile (*e.g.* U, Th, Cs, La, Rb, Ba) elements (Fig. 2). The non-volatile are lithophile elements with a refractory behaviour because of their strong affinity for the silicate melt, even at low-pressure and high-temperature. In contrast, volatile elements are thought to be extensively partitioned into the gas phase during high-temperature magmatic degassing, likely because of their strong affinity with degassed S and Cl (Aiuppa *et al*., 2003). These elements are assumed to be concentrated into the aerosol phase as magmatic gases cool and oxidize upon interaction with atmospheric air, and gas-to-phase conversion of metal-bearing gaseous precursors takes place. The result of these processes volatile elements are highly enriched in aerosols compared with their original concentrations in the magma.

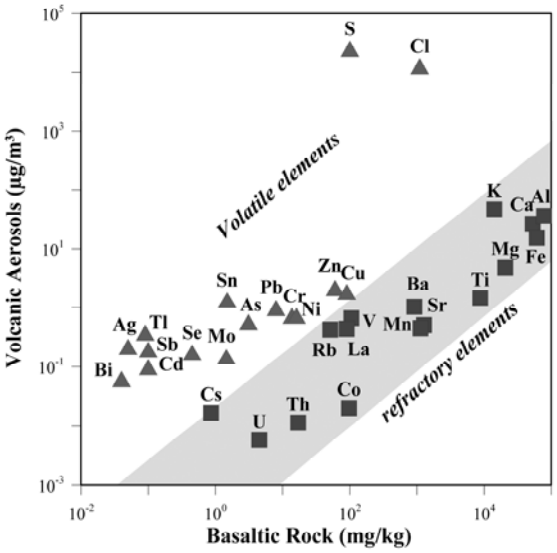

Fig. 2 - Different geochemical behaviour of refractory and volatile elements.

In order to estimate the fluxes, the metal/sulphur ratios (ranging from 10^{-2} to 10^{-8} depending on the elements) obtained from the two craters (NEC and VOR), were calculated, and then related to the total sulphur fluxes daily measured by the INGV of Catania using remote sensing techniques. The average metal fluxes during the study period are showed in Table 1. These measurements are representative of the quiescent degassing activity from the volcano, and do not account for the contribution from eruptive degassing. There is a general agreement between elemental fluxes estimated in this work and previous assessments (Buat-Menard & Arnold, 1978; Andres *et al*., 1993; Gauthier & Le Cloarec, 1998; Aiuppa *et al*., 2003) (Fig. 3). For several elements, the present 2004-2007 fluxes fall at the lower limit of previous estimates; a trend which is consistent with the results of Gauthier & Le Cloarec (1998), which highlighted great differences in emission rates between eruptive and non-eruptive periods. This pattern is consistent

with the lower SO_2 degassing rates in 2004-2007 (mean SO_2 flux, ≤ 2000 t/day; M. Burton, INGV-CT, pers. comm.) than in the 80-90s (mean SO_2 flux, ~ 5000 t/day; Caltabiano *et al*., 2004).

Atmospheric Deposition

Volcanic volatiles and aerosol emitted into the atmosphere ultimately fall on the Earth's surface as wet or dry deposition, and they can influence the environment and the ecosystems at local and regional scales. Therefore, atmospheric deposition plays a key-role in the geochemical cycles, redistributing volcanogenic elements to the ground. The chemical composition of rainwater from the down-wind sites (TDF, CIT, CDV, and ZAF) exhibits a significant enrichment in all elements analyzed, compared to the up-wind site (INT). The enrichment is most evident for elements like S, Cl, F, H, Si, Al, Fe, Cu, As, Se, Cd, and Tl. The rainwater samples with the highest element concentrations were collected at TDF, the closest site to the summit craters. Samples from INT have the lowest element concentrations in the dataset, and the mean values for this site were here considered as representative of the local background.

Table 1 - Volcanic emissions, total deposition on the eastern flank and on the whole etnean area, and percentage of scavenged elements from the volcanic plume (minimum and maximum values are relative to the upper and lower estimation).

	Volcanic emissions	Total deposition on the eastern flank	Total deposition on the whole Etnean area (upper estimation)	Volcanogenic deposition on the whole Etnean area (lower estimation)	Amount of elements scavenged from the Plume		
	(Mg/a)	(Mg/a)	(Mg/a)	(Mg/a)	(%)		
Al	2810	8.0	32	26	0.9	-	1.1
As	31	0.07	0.3	0.1	0.3	-	0.9
Ba	41	0.6	2.3	0.5	1.3	-	5.6
Cd	12.8	0.02	0.1	0.1	0.5	-	0.7
Co	1.9	0.01	0.04	0.02	0.9	-	2.2
Cr	63	0.02	0.1	0.01	0.02	-	0.1
Cs	2.0	0.004	0.02	0.01	0.6	-	0.8
Cu	240	0.6	2.5	1.5	0.6	-	1.0
Fe	505	5.1	21	15.0	3.0	-	4.1
La	8.2	0.01	0.0	0.03	0.4	-	0.6
Li	7	0.03	0.1	0.03	0.5	-	1.7
Mo	84	0.01	0.0	0.01	0.01	-	0.1
Ni	30	0.1	0.3	0.1	0.3	-	1.0
Pb	31	0.07	0.3	0.2	0.6	-	0.9
Rb	38	0.09	0.4	0.2	0.6	-	1.0
Sb	0.7	0.02	0.1	0.0	2.5	-	12
Se	18.9	0.1	0.4	0.1	0.8	-	2.2
Ti	39	0.1	0.4	0.3	0.6	-	0.9
Tl	36	0.03	0.1	0.1	0.3	-	0.4
U	0.1	0.002	0.0	0.0	2.1	-	6.5
V	12	0.3	1.4	0.4	3.0	-	12
Zn	90	2.5	10	2.9	3.2	-	11

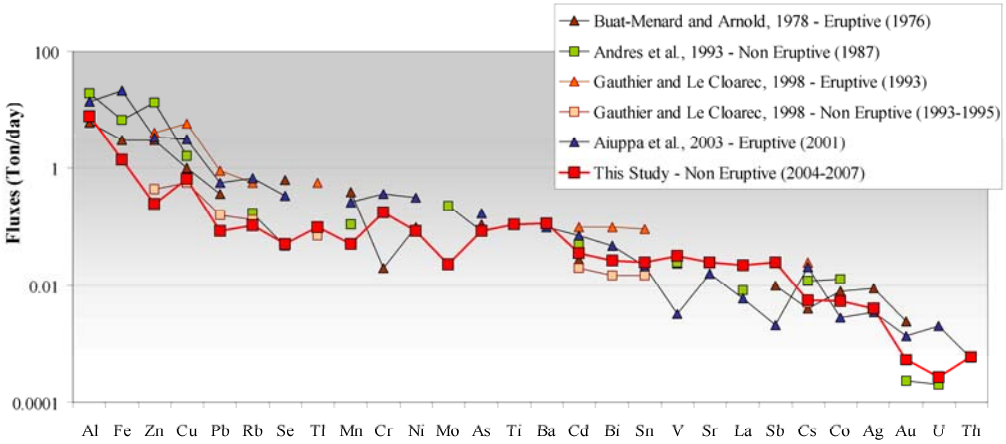

Fig. 3 - Comparison of previous and new estimates of metal fluxes emitted by Mount Etna.

One of the main effects of volcanic emissions on rainwater chemistry is the drastic increase of its acidity, as a direct consequence of the interaction with plume-derived strongly-acidic gases, mainly SO_2, HCl, and HF. The *p*H of rainwater collected at the different sites was highly variable, ranging from 2 to about 8. The concentration of protons show an exponential decrease from TDF site, where it contributes strongly to the total cationic species, to ZAF (the farthest site), where it accounts for only about 1%. The main anionic species are sulphate and chloride in all sites. Fluoride has an almost exclusive volcanogenic origin in the Etnean area (Bellomo *et al.*, 2007), and its concentration in rainwater decreases rapidly moving away from the volcanic source. By contrast, nitrate shows an increase of relative concentrations in the lower sites, while absolute concentrations are nearly constant (median values range from 1.1 to 1.9 mg/l). This reflects a derivation of nitrate from a regional anthropogenic background (NO_x emissions). Calcium is the main cation and its origin can be ascribed to several sources (re-suspended dust either from volcanic or carbonate rocks). Other elements like K and Mg show an almost constant concentration, while the contents of Na, together with Cl, show an increase towards the lowest parts of Mt. Etna, highlighting an increasing sea salt contribution from the Ionian Sea. The concentration of the most investigated elements with respect to the pH is inversely correlated, and high acidity of rainwater is almost always accompanied by high contents of major and trace metals. The relation between volcanogenic anions (SO_4^{2-}, Cl^-, and F^-) and volatiles elements (*e.g.* Cu, As, Se, Cd) displays a positive linear correlation, suggesting that sulphate and halide salt aerosols are adsorbed onto ash particles, and soluble compounds rapidly dissolved in rainwater. The dissolution of the ash's silicate constituents by the corrosive volcanic acid (SO_2, HCl, and HF) explains also the enrichment of several refractory elements, both major (Na, K, Ca, Mg) and trace (*e.g.* Si, Al, Fe, Ti, Sc).

Rainfall provides a major input of elements to the Earth's surface, and the chemical flux of elements can be determined if rain composition is well known. Through the measured concentrations of each element, it is possible to calculate the deposition rates by using the following relation:

$$\Phi x = (Cx \cdot P)\, T^{-1}$$

where Cx is the concentration of each element x in rain; P is the amount of precipitation, and T is the exposition time of the collectors. The average deposition rates of inorganic elements during the study

period were computed for each site (Fig. 4). The average deposition rate at the 5 sites decreases with distance from the volcano (except for nitrogen, as nitrate, and antimony), confirming that volcanic contribution to bulk deposition prevails close to the volcanic source (summit craters). In fact, the deposition rate in the most exposed sites is 1-3 orders of magnitude higher than at the background site INT for many of the major and trace elements analyzed. They include: (i) S, F, H, and Cl, which are due to the dissolution of volcanic acid gases in rainwater; (ii) refractory elements (Al, Fe, Ti, La, and Sc), highlighting the ash contribution to bulk deposition; (iii) the volatile elements (As, Cu, Cd, and Tl), whose excess with respect to the local background values (site INT) is also a clear fingerprint of volcanic contribution, and reflects scavenging of metal-rich aerosols.

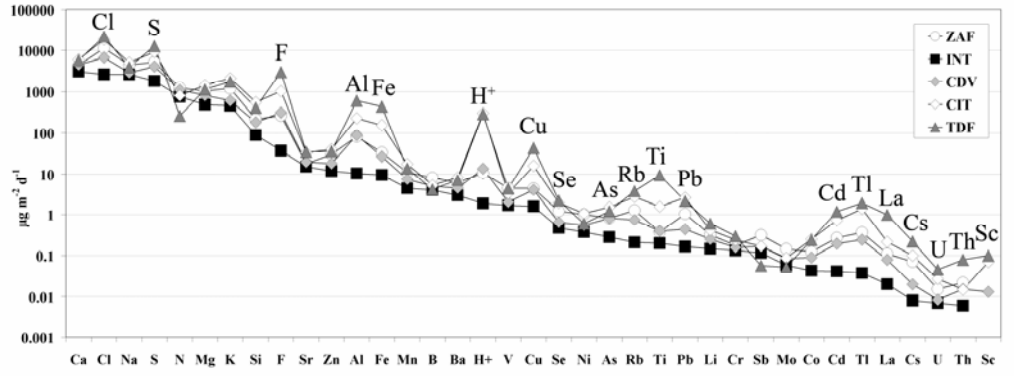

Fig. 4 - Average daily deposition rate for each site; the elements are ordered according to median values of the local background site (INT).

Estimate of the dispersion of volcanogenic elements

On the basis on the deposition rates measured in the present work an attempt was made to estimate the percentage of volcanogenic minor and trace metals scavenged from the volcanic plume. Since the number and position of the rain gauges was inadequate to cover the whole Etnean area (about 1200 km^2), this estimate was performed initially only for the sector downwind of the volcanic source (Fig. 1 and Table 1). Considering that this sector represents about one quarter of the entire volcanic edifice we could hypothesize that the maximum deposition on the whole area would not exceed a value four times that of the downwind sector (upper estimation in Table 1). The deposition values measured at the sampling sites are representative of different sources. In the attempt to discriminate only the contribution of the volcanogenic input, the deposition on the downwind sector has also been calculated by subtracting the values measured at the background site (INT). The obtained "volcanic deposition" values are certainly underestimated because the volcanic input at the local background site, although low, is not completely absent. With the aim to reduce this underestimation the obtained values were multiplied by a factor two. A further multiplication by a factor two was used to extend the estimated "volcanic deposition" to the whole Etnean area considering that volcanic contribution is absent in the upwind sector and in the remaining intermediate sectors "volcanic deposition" contributes only for a half. Hence the obtained values are considered as the minimum values for volcanic deposition on the whole flanks of the volcano (lower estimation in Table 1). Finally, a comparison with the whole plume emission values evidences that

only a very low percentage of the emitted elements is deposited close to the volcano. In particular, the amount of trace elements scavenged from the plume range from 0.1 to 1% for volatile elements such as As, Cd, Cu, Tl, and from 0.5 to 10% for refractory elements such as Al, Fe, Ti. Consequently, more than 90% of volcanogenic trace elements are dispersed at regional and/or global scale.

CONCLUSIONS

Etna's metal output, in 2004-2007 period, confirms that Mt. Etna is an important source of trace metals at the regional and in some cases at the global scale. Etna's emissions are about two or three orders of magnitude higher than the local anthropogenic emissions for several elements (*e.g.* Zn, Cu, Se, Hg, Cd, Ni, Cr), and this highlights that Mt. Etna is the major natural *point-source* of metals in Mediterranean Sea. Meteorological conditions are a determining factor on the direction of volcanic plume dispersion; prevailing wind directions at Mt. Etna area are from W-NW, and the E-SE flank of the volcano is thus receiving the highest deposition. Nevertheless, the active vents are located at more than 3000 m of altitude and its volcanic *output* is thus directly injected above the boundary layer, implying that only a small percentage of the emitted volcanogenic elements return to the Earth's surface close to the volcano (0.1-1% for volatile elements, and 0.5-10% for refractory elements).

ACKNOWLEDGEMENTS

The author thanks F. Parello and A. Aiuppa (CFTA, University of Palermo) and W. D'Alessandro (INGV, Palermo) for their valuable contribution to this work.

REFERENCES

Aiuppa, A., Dongarrà, G., Federico, C., Pecoraino, G., Valenza, M. (2003): Degassing of trace volatile metals during the 2001 eruption of Etna. *In*: "Volcanism and the Earth's atmosphere", A. Robock & C. Oppenheimer, eds. *Geophys. Monogr.*, **134**, 41-54.

Aiuppa, A., Bellomo, S., Brusca, L., D'Alessandro, W. Di Paola, R., Longo, M. (2006): Major-ion bulk deposition around an active volcano (Mt. Etna, Italy). *Bull. Volcanol.*, **68**, 255-265.

Allard, P., Aiuppa, A., Loyer, H., Carrot, F., Gaudry, A., Pinte, G., Michel, A., Dongarrà, G. (2000): Acid gas and metal emission rates during long-lived basalt degassing at Stromboli volcano. *Geophys. Res. Letters*, **27**, 1207-1210.

Andres, R.J., Kyle, P.R., Chuan, R.L. (1993): Sulphur dioxide, particle and elemental emissions from Mount Etna, Italy during July 1987. *Geol. Rundsch.*, **82**, 687-695.

Bagnato, E., Aiuppa, A., Parello, F., Calabrese, S., D'Alessandro, W., Mather, T.A., McGonigle, A.J.S., Pyle, D.M., Wangberg, I. (2007): Degassing of gaseous (elemental and reactive) and particulate mercury from Mount Etna volcano (Southern Italy). *Atmos. Environ.*, **41**, 7377-7388.

Bellomo, S., Aiuppa, A., D'Alessandro, W., Parello, F. (2007): Environmental impact of magmatic fluorine emission in the Mt. Etna area. *J. Volcanol. Geophys. Res.*, **165**, 87-101.

Buat-Ménard, P. & Arnold, M. (1978): The heavy metal chemistry of atmospheric particulate matter emitted by Mount Etna volcano. *Geophys. Res. Letters*, **5**, 245-248.

Caltabiano, T., Burton, M., Giammanco, S., Allard, P., Bruno, N., Mure, F., Romano, R. (2004): Volcanic gas emissions from the summit craters and flanks of Mt. Etna, 1987-2000. *In*: "Mt. Etna: Volcano Laboratory", A. Bonaccorso, S. Calvari, M. Coltelli, C. Del Negro, S. Falsaperla, eds. *Am. Geophys. Union, Geophys. Monogr.*, **143**, 111-128.

Cheynet, B., Dall'Aglio, M., Garavelli, A., Grasso, M.F., Vurro, F. (2000): Trace elements from fumaroles at Vulcano Island (Italy): rates of transport and a thermochemical model. *J. Volcanol. Geotherm. Res.*, **95**, 273-283.

Chuan, R.L., Palais, J.M., Rose, W.I. (1986): Fluxes, sizes, morphology and compositions of particles in the Mt. Erebus Volcanic Plume, December 1983. *J. Atmos. Chem.*, **4**, 467-477.

EMEP (2001): Manual for sampling and chemical analysis. EMEP/CCC Report 1/95 NILU Norwegian Institute for Air Research, Kjeller, Lillestrøm, Norway.

Gauthier, P.-J. & Le Cloarec, M.-F. (1998): Variability of alkali and heavy metal fluxes released by Mt. Etna volcano, Sicily, between 1991 and 1995. *J. Volcanol. Geotherm. Res.*, **81**, 311-326.

Hinkley, T.K., Lamothe, P.J., Wilson, S.A., Finnegan, D.L., Gerlach, T.M. (1999): Metal emissions from Kilauea, and a suggested revision of the estimated worldwide metal output by quiescent degassing of volcanoes. *Earth Planet. Sci. Letters*, **170**, 315-325.

Martin, R.S., Mather, T.A., Pyle, D.M., Watt, S.F.L., Day, J., Collins, S.J., Wright, T.E., Aiuppa, A., Calabrese, S. (2009): Sweet chestnut (Castanea sativa) leaves as a bio-indicator of volcanic gas, aerosol and ash deposition onto the flanks of Mt. Etna in 2005-2007. *J. Volcanol. Geotherm. Res.*, **179**, 107-119.

Nriagu, J.O. (1989): A global assessment of natural sources of atmospheric trace metals. *Nature*, **338**, 47-49.

Oppenheimer, C. (2003): Volcanic degassing. *In*: "The crust", R.L. Rudnick, ed. Elsevier-Pergamon, Oxford, 123-166.

MINERAL-PETROGRAPHIC AND PHYSICAL-MECHANICAL CHARACTERIZATION OF HYBLEAN LIMESTONES

CHIARA CALABRO'
Dipartimento di Scienze della Terra, Università di Catania, Corso Italia 55, 95129 Catania

Since the antiquity, in Eastern Sicily different varieties of Hyblean limestones have been employed in constructive activities (walls, farms, villas, civil and religious architectures), due to the easy availability, workability and extractivity of stones.

After the earthquake of 11th January 1693, which destroyed the major part of Eastern Sicily, an intense reconstruction building activity took place in different urban cities of the Val di Noto (Ragusa, Modica, Scicli, Noto, Siracusa, etc.), allowing to the Sicilian architecture to reach a splendid and autonomous flowering of Baroque forms because of the ability of the local architects and workers and to the easy workability of local stones. The numerous baroque monuments and buildings of Eastern and Western Sicily have been recognised as Cultural Heritage by the UNESCO for their exceptional historical and artistic interest.

Observing the conservation state of these monuments, it is evident that carbonate rocks employed are characterized by different type of degradation and/or alteration.

It is known that degradation depends on the intrinsic characteristics of the materials (mineralogical composition, textural features) and on external factors as the implementation, the conditions of exposure to the atmospheric agents, the rate of environmental pollution and the previous restoration works.

For this reason, we carried out a study on the mineral-petrographic and physical-mechanical features of the carbonate stones used in historical Baroque monuments of the Val di Noto with the purpose of underlining the compositional and textural differences. These characteristics were related to the weathering types both reproduced in laboratory through accelerated ageing tests and directly observed on the monuments. In this study, we used stone parameters that have an influence on durability and depend only upon pore structure: connected porosity, the water absorption coefficient by capillarity, the saturation coefficient. We also used stone parameters with an influence on strength: flexural strength, uniaxial compressive strength, Young's dynamic modulus and ultrasound wave velocity. Analytical methodologies carried out are: thin section microscopic analysis, determination and grain size distribution of the insoluble residue, mineralogical analysis through X-ray diffractometry, mercury intrusion porosimetry, colorimetric analysis, determination of water absorption coefficient by capillarity (UNI EN 1925), determination of water absorption at atmospheric pressure (UNI EN 13755), determination of the open porosity through hydrostatics balance, determination of the drying index (NORMAL 29/88), determination of the resistance to the crystallization of the salts (UNI EN 12370), measure of the speed of sound propagation (NORMAL 22/86), determination of uniaxial compressive strength (UNI EN 1926), determination of flexural strength under concentrated load (UNI EN 12372), determination of the elastic modulus to uniaxial compressive strength (UNI 9724/8-92).

The laboratory analyses were carried out on specimens (n° 467) belonging to five geological formations outcropping in the Eastern and Western Hyblean Plateau for a total of ten sites of sampling. The geological formations examinated are the *Climiti Mountains Formation (Melilli white limestone)*, the *Carrubba Mountain Formation (Lumachelle limestone)*, the *Pleistocene Bench (giuggiulena or ochred*

calcirudite), the *Palazzolo Formation (yellowish and pale cream limestone)* and the *Ragusa Formation (Ragusa, Modica and Scicli limestone)*. The materials have been sampled in historical quarries because they represent the most likely extraction sites of the materials used in historical Baroque monuments of the Val di Noto. The major part of stones object of the study is not currently extracted or used as exception of the Palazzolo Formation limestone. This last one has been in fact quarried both in historical and in recent quarries.

Briefly summarizing, the results of studies conduced so far showed that:

The *Pleistocene ochred calcirudite* from a petrographic viewpoint can be classified as biosparite or grainstone with a grain-supported texture (Fig. 1) formed by fragments of algae, foraminifers and bryozoans shells. The intergranular space is filled with sparry calcite. The porosity determined by optical microscopy is 30-40% and the mean pore diameter is about 1-2 mm whereas the porosity determined by mercury intrusion porosimetry is markedly inferior (11%). This characteristic influences the mobility of

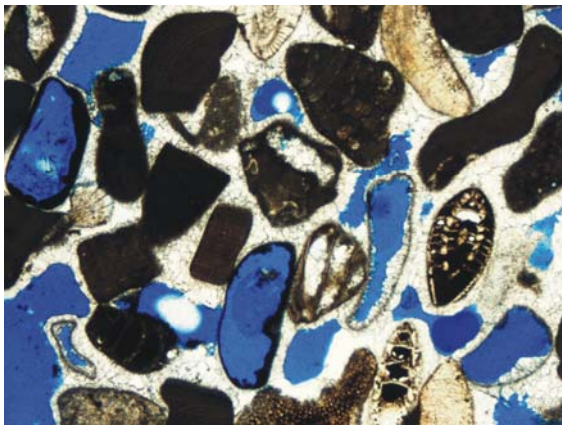

Fig. 1 - Grain supported texture (2.5 x).

the fluids inside the material, in fact, during tests of water absorption by capillarity and by total immersion all the samples produced a "sponge effect" saturating (shortly after 1 minute in the capillarity test) and releasing part of the water for gravity very quickly.

The principal effect of such characteristics is that the material does not degrade during the test of salt crystallization because are not present evident pore of small dimensions ($\phi < 0.1$ mm) and there are not therefore conditions for the development of high pressures of crystallization. From a mechanical standpoint this limestone records low values of uniaxial compressive and flexural strength.

The *Lumachelle limestone*, from a petrographic viewpoint can be classified as biosparite or packstone and shows good petrophysical and mechanical characteristics: high values of uniaxial compressive and flexural strength, high ultrasonic wave velocity, low coefficient of water absorption by capillarity, mean weight loss after salt crystallization test around 17%. Most common types of weathering are selective weathering, granular disgregation and sometimes detachment around shell pile (Fig. 2).

Fig. 2 - Selective weathering and detachment around shells pile.

The *Melilli white limestone*, classified as wackestone or biomicrite, shows high values of water adsorption coefficient by capillarity, high values of porosity, open porosity and coefficient of imbibition. The mean weight loss after salt crystallization test is about 27% and the common

weathering types are flaking, produced by detachments of small, thin, stone flakes parallel to the stone surface, granular disgregation and selective weathering around the accumulation of worms' pipe. From a mechanical viewpoint, they have a middle degree of compactness testified by high ultrasonic wave velocity, high values of uniaxial compressive and flexural strength and elastic modulus.

From a petrographic standpoint the *Palazzolo Formation limestones* can be classified as biomicrite or wackestones.

It is possible to recognize within such formation two different lithofacies: pale cream limestones, represented by the samples quarried near Cassibile (Cassibile historical quarry) and Palazzolo Acreide town (Camelio modern quarry) and yellowish limestones quarried near Ancient Noto (Leone historical quarry) and Noto town (Porcari modern quarry). The first lithofacies is more compact and has a percentage of insoluble residue inferior to 3%; the second results less compact and shows 3% great insoluble residue. In detail, the pale cream limestone displays better mechanical properties than the yellowish one. Indeed it has, higher ultrasound wave velocity, higher values of uniaxial compressive and flexural strength and elastic modulus. (Index of a great compactness and a great specific weight). From a physical point of view the pale cream limestone displays values of the parameters determined (porosity, water absorption coefficient by capillarity, open porosity, coefficient of imbibition, weight loss after salt crystallization test) better then to yellowish one.

Both lithofacies show as principals types of weathering a selective weathering (loss of material takes place around "skolithos") (Fig. 3) and chromatic alteration.

Fig. 3 - Loss of material around "skolithos" during II-VI-XV salt crystallization cycle.

Ragusa Formation limestones can be all classified as biomicrite or packstones. The limestone quarried around Scicli town is the most resistant to the crystallization salt test (mean weight loss is about 34%) that is probably related to the better textural characteristic and to the higher degree of compactness testified by higher ultrasonic wave velocity. The Modica limestone exhibits petrographic features similar to those of the Scicli and Ragusa limestone, although it suffered a higher mean weight loss (64%). During the test of salt crystallization a progressive flaking of the samples occurred parallel to the stratification and it shows a higher percentage of insoluble residue (about 7%). From a physical-mechanical viewpoint the Ragusa limestone is the cheapest within the Ragusa Formation.

The analytical techniques, employed in this study, enabled the characterization of Hyblean limestones used in historical Baroque monuments of Val di Noto and the identification and correlation with their degradation forms.

It is determined therefore that the principal causes of degradation types, with the exception of the ochred calcirudite, are pressures produced by the salt crystallization. This determines nevertheless in the different material forms and different intensity of degradation tied up to the intrinsic characters of the rocks. In fact salt weathering, quantified by the percentage of weight loss after salt crystallization ($Na_2SO_4 \cdot 10H_2O$) is dependent on textural features such as heterogeneities, type and dimension of pores, percentage of insoluble residue, stratification, etc.

Opportune mineral-petrographic and physical-mechanical investigations are therefore necessary in order to perform the correct choice of materials adequate to the architectural site, either for the construction of new buildings or substitutions during the restoration.

Future studies will be focused on the material pore network and changes in physical-mechanical properties of this in response to salt crystallization tests.

STUDY OF GROWTH RATE OF ALKALI FELDSPAR IN PHLEGRAEAN FIELDS TRACHYTES

MARTA CALZOLAIO
Dipartimento di Scienze della Terra, Università di Camerino, Via Gentile III da Varano, 62032 Camerino (MC)

INTRODUCTION

In this thesis my purpose is to study the crystallization kinetics of phlegraean trachytic magmas, reproducing pre-eruptive conditions and through a combined study of textural and mineralogical features of the samples, trying to define magma behavior during the ascent towards the earth surface that is during eruption. The results of this study will allow the increase of specific knowledge of pre- and sin-eruptive processes of the Phlegraean Fields, with the aim of monitoring and forecasting the kind and the evolution of future eruptions, to create evacuation and first-aid plans. Experimental data on nucleation and growth kinetics are lacking now, for shoshonitic and trachytic melts are totally absent and the existing data for different kind of magmas vary of several order of magnitude, due to variations in the chemical composition of the melt, kind of minerals and undercooling degree. In this thesis cooling (at constant P) and decompression (at constant T) experiments on phlegraean natural samples have been performed. The results obtained after this experimental work will be compared with those obtained by Piochi *et al.* (2005) after the study of CSD in natural samples from Monte Nuovo, Phlegraean Fields.

STARTING MATERIAL AND ANALYTICAL METHODS

The starting material used in the present experimental work is a trachytic obsidian, from the basal unit of the Breccia Museo Member, Phlegraean Fields. This obsidian is subaphiric and contains less than 10% in volume of crystals; phenocrystals are mostly alkaline feldspars and secondarily plagioclase, clinopyroxenes, biotite and magnetite, with decreasing abundance, and as accessory phases apatite and titanite (Civetta *et al.*, 1997). This composition has been chosen because the phase relations are well known (Fabbrizio & Carroll, 2008; Calzolaio, 2005) and the composition is very similar to the Monte Nuovo products, both from a chemical and a petrographical point of view. The powder was introduced in Ag_{70}-Pd_{30} capsules with distilled and deionized water. The experiments in H_2O supersaturated condition have been carried out in vertical Cold Seal Pressure Vessels (CSPV, with Nimonic 105 composition) at the Earth Science Department of Camerino University. The oxidation condition of this apparatus is ~ 0.8 log fO_2 units above the NNO buffer (Di Matteo *et al.*, 2004).

Cooling experiments

In this kind of experiments, samples were at first heated above the alkali feldspar liquidus, at a temperature of 850°C (starting temperature, T*i*) and at the experimental pressure, to allow the homogenization of the starting materials contained in the capsules (annealing). After an hour of annealing, water-saturated samples were cooled to the experimental temperature (T*f* = 750, 775, 800, 825 °C) and let crystallize for different time durations (7200, 14400, 21600, 28800, 57600 seconds), to allow the study of the influence on crystal growth of the crystallization time, defined as the time that the sample spends in the alkali feldspar stability field (Fenn, 1977). All the experiments and with a ten-minutes-long quench. In Table 1 the experimental conditions are summarized.

Table 1: Experimental conditions for cooling experiments.

Sample	T (°C)	P (MPa)	ΔT (°C)	theoretical H_2O (wt.%)	time (s)
D1	750	200	15,24	8,00%	14400
D2	750	200	15,24	8,00%	7200
D3	800	100	18,1	6,00%	14400
D4	800	100	18,1	6,00%	7200
D5	800	100	18,1	6,00%	28800
D6	800	100	18,1	6,00%	21600
D7	750	200	15,24	8,00%	57600
D8	750	200	15,24	8,00%	28800
D9	825	50	20	4,00%	57600
D10	825	50	20	4,00%	28800
D11	825	50	20	4,00%	7200
D12	825	50	20	4,00%	14400
D13	775	150	16,19	7,00%	28800
D14	775	150	16,19	7,00%	57600
D15	775	150	16,19	7,00%	7200
D16	775	150	16,19	7,00%	14400
D20	750	200	15,24	8,00%	28800
D23	800	100	18,1	6,00%	21600
D24	800	100	18,1	6,00%	57600
D28	860	50	20	4,00%	14400
D33	840	50	20	4,00%	14400
D34	840	50	20	4,00%	7200

Decompression experiments

Decompression experiments were divided in three series, on the basis of the starting pressure (P*i*). Experiments with P*i* = 100 MPa belong to the Series A, with P*i* = 150 MPa belong to the Series B, with P*i* = 200 MPa belong to the Series C.

Water-saturated samples were lead to 850°C (starting temperature, T*i*), above the alkali feldspar liquidus, and at the same time at the starting pressure. After an annealing time of an hour, temperature was decreased to 750°C (final temperature, T*f*) and pressure was lead to the run value (P*f*), to allow sample crystallization in the different condition of P*f* (150, 100, 50, 30 MPa).

The experiments belonging to the A series (P*i* = 100 MPa) were lead to final pressure of 50 and 30 MPa, while B series experiments (P*i* = 150 MPa) were lead to 100 and 50 MPa and C series experiments (P*i* = 200 MPa) were lead to 150 and 100 MPa. Samples were left at the final conditions for 2, 6 and 14 hrs (7200, 21600 and 50400 seconds, respectively) to study how the growth rate is influenced by the time available for crystallization, that is that time that the sample spends in the alkali feldspar stability field, starting from the moment in which decompression is performed (Fenn, 1977). All the experiments end with a ten-minutes-long quench. In Table 2 the experimental conditions are summarized.

Growth rate calculation

Sample textural analysis is useful to determine crystals dimensions and thus their growth rate. Starting from SEM images of the samples after the runs, crystal dimensions were measured by Adobe Photoshop 7.0. In every sample only the 10 longest feldspar crystals were considered.

From the collected images is evident the presence of many crystalline phases, among which, of course, alkali feldspars, many in crystalline radial aggregates, from which was impossible to gain any

Table 2: Experimental conditions for decompression experiments.

Sample	T (°C)	P*i* (MPa)	P*f* MPa)	time (s)	ΔT (°C)	theoretical H_2O (wt.%)
D39	750	200	150	50400	42,86	8,00%
D55	750	200	150	7200	42,86	8,00%
D37	750	200	150	21600	42,86	8,00%
D51	750	150	100	21600	69,52	6,00%
D53	750	150	100	50400	69,52	8,00%
D38	750	200	100	21600	69,52	8,00%
D40	750	150	100	7200	69,52	7,00%
D42	750	200	100	7200	69,52	8,00%
D27	750	200	100	50400	69,52	8,00%
D49	750	100	50	50400	94,55	5,00%
D46	750	100	50	21600	94,55	5,00%
D45	750	150	50	50400	94,55	6,00%
D43	750	100	50	7200	94,55	6,00%
D50	750	150	50	21600	94,55	6,00%
D30	750	150	50	7200	94,55	7,00%
D47	750	100	30	50400	106,36	5,00%
D48	750	100	30	21600	106,36	5,00%
D44	750	100	30	7200	106,36	6,00%

information on crystallization kinetics, as it was not possible to define the exact dimensions of the minerals. In fact, only K-feldspar single crystals were taken into account to measure their length (L).

In the calculation of the growth rate we referred to Couch (2003). To calculate maximum growth rate on the longest side of the crystal (G_L) was used the relation:

$$G_L = (0.5\ L) / t$$

where L is the length of the crystal and t is the duration of the experiment.

RESULTS

The crystallization process is strongly affected by the undercooling degree (ΔT) and by the pressure decrease in the system, implying variations in texture, on bubble percentage, on abundance and dimension of the present phases.

In the sample analyzed with the SEM, the prevalent phases are:

- Alkali Feldspar, with intermediate composition between albite and orthoclase ($Ab_{60\text{-}90}$ - $Or_{40\text{-}10}$, anorthoclase). This is evident even in the K-feldspars from natural samples from Monte Nuovo.
- Clino-pyroxenes, as shown in the semi-quantitative analysis.
- Glass, with a composition similar to that of the alkali feldspar.

DISCUSSION

The graphs "G_L *vs.* ΔT" correlates undercooling, experiment duration and growth rate (inferred from the longest direction of the crystal, G_L) for cooling (Fig. 1) and decompression experiments (Fig. 2). For low ΔT growth is more helped than for high ΔT where G_L is reduced. With increasing experiment duration there is an apparent growth rate reduction, of about an order of magnitude. Error bars (standard deviation of the growth rate of the 10 alkali-feldspar crystals measured for every sample) are quite large.

This can be explained with the Ostwald ripening theory that predicts that in disequilibrium conditions (short duration experiments) several dimensional classes can form, while approaching equilibrium (increasing experiment duration) there is a homogenization of the dimensions (Cabane *et al*., 2005), with the reduction of error bars, as we can see from graph in Fig. 2.

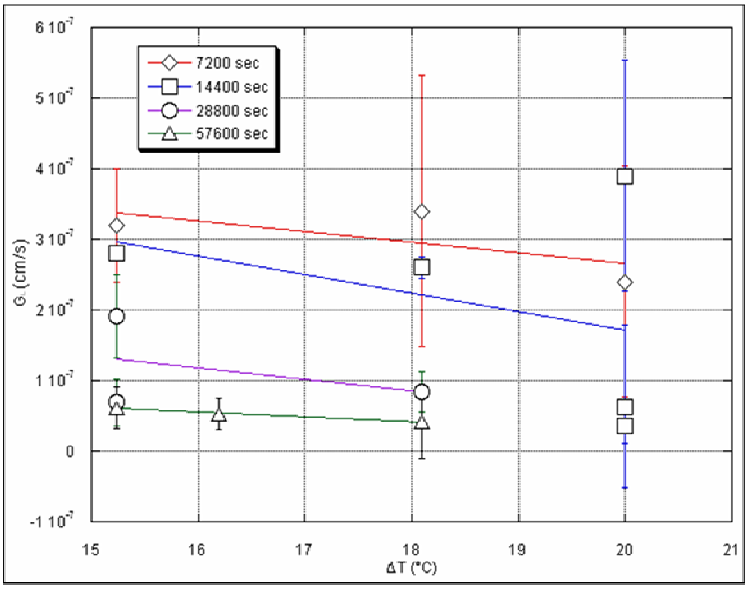

Fig. 1 - Correlation between growth rate and undercooling for cooling experiments.

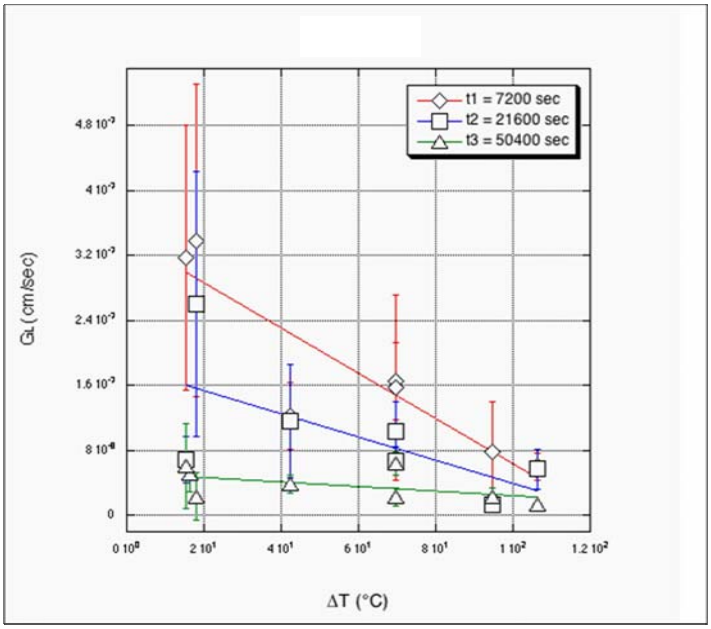

Fig. 2 - Correlation between growth rate and undercooling for decompression experiments.

The graphs "G_L *vs.* t" for cooling (Fig. 3) and decompression (Fig. 4) experiments show that crystal growth is high for short experimental duration, because in this condition the driving force for crystal growth is significant, while, with increasing experimental duration, G_L decreases because the system is approaching equilibrium. Between the shortest and the longest experiment durations there is a difference of about one order of magnitude.

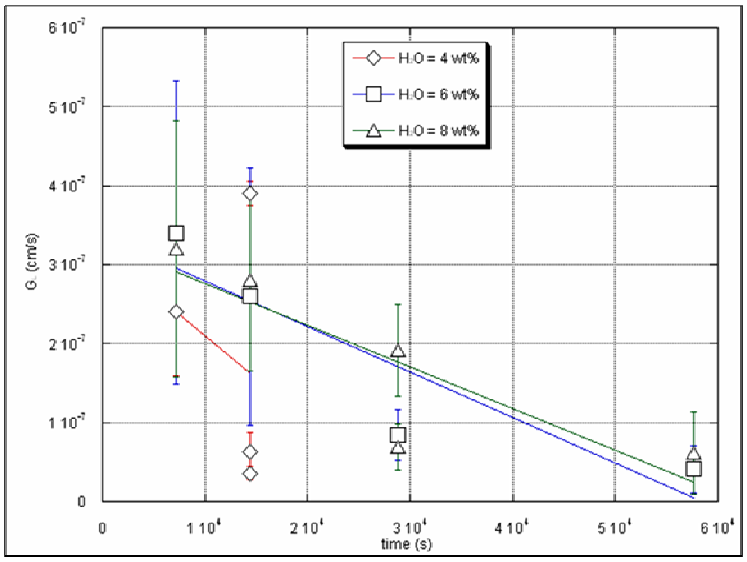

Fig. 3 - Correlation between growth rate and experimental duration for cooling experiments.

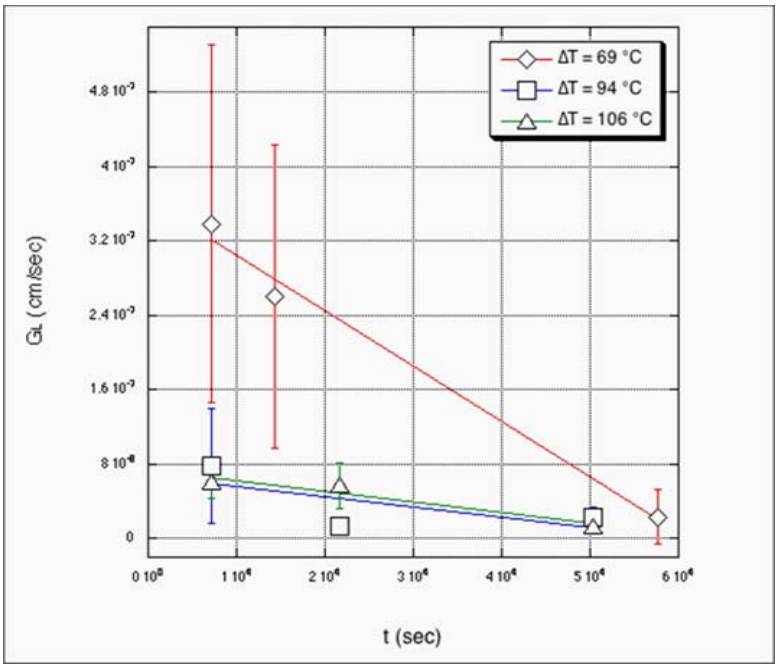

Fig. 4 - Correlation between growth rate and experimental duration for decompression experiments

Comparison between cooling and decompression experiments

Graph "G_L *vs.* t" (Fig. 5) shows a reduction in growth rate (G_L) with increasing experimental duration. It can be highlighted that G_L is a little higher for cooling experiments at constant pressure with respect to the decompressed ones. This behavior is due both to lower ΔT in cooling experiments (that helps growth) and to the exsolution of water during decompression that slows down the diffusivity of the elements inside the melt.

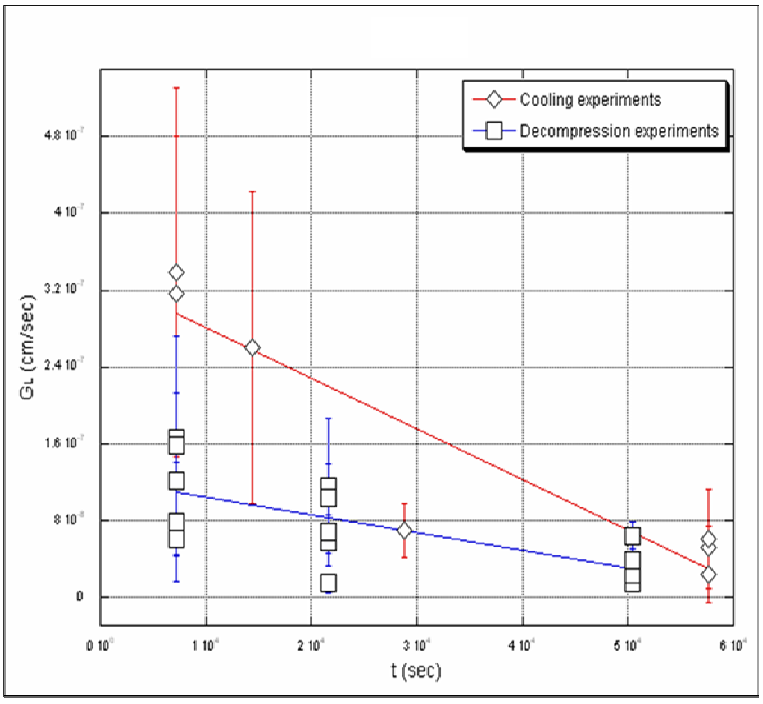

Fig. 5 - Comparison of crystal growth rate obtained in decompression and cooling experiments.

Comparison with previous studies

Studies about K-feldspar growth rate are scarce in the scientific literature: the only ones that calculated G for alkaline feldspars are Swanson (1977) in synthetic granitic melts and Fenn (1977) in an albite ($NaAlSi_3O_8$), orthoclase ($KAlSi_3O_8$) and H_2O mixture.

To allow this comparison between the growth rates obtained in this work and those obtained by Swanson and Fenn through cooling experiments at constant pressure, we considered the values of G obtained at the same experimental temperature (750°C). The order of magnitude of K-feldspar growth rate estimated by Swanson varies between 10^{-8} and 10^{-6} cm/s; in Fenn's results, G has an order of magnitude of 10^{-6} cm/s; in the end in this thesis G varies between 10^{-8} and 10^{-7} cm/s both for decompression and cooling experiments.

Swanson and Fenn studied growth rate in relation to ΔT (that goes from few degrees under the liquidus temperature to about 400°C). Maximum growth rate is obtained with ΔT between 200 and 250°C and trends to decrease with increasing or decreasing undercooling, while the data collected in this work show that growth rate is maximum for low ΔT, while decreases for increasing ΔT.

Besides, Fenn relates G with ΔT and melt dissolved water percentage and shows that for low ΔT (between 20 and 70°C), the increase of water causes an increase in alkali-feldspar growth rates. This

behavior was found in our data as well. The undercooling and the water percentages have similar value to those used in the decompression experiments of the present experimental work, while Fenn's G varies of one or two orders of magnitude with respect to the values of G obtained in this work.

Available application of the collected data

Growth rate is used both in the description of magmas crystallization kinetics and in the study of the Crystal Size Distribution (CSD), to determine residence and ascent times, to forecast future eruptive events and consequently realize an evacuation plan of the phlegraean area.

Crystal Size Distribution is the variation of the number of crystals for each size in natural samples. In a CSD graph [size *vs.* ln(population density)], the slope (s) of the linear regression obtained from the plot of natural samples is (-1/G·t) (after Higgins, 2000, 2002). Known G from experimental studies and s from the observation of natural samples, we can calculate t that is time needed for crystal growth.

Piochi *et al.* (2005) calculated residence and ascent rates during the Monte Nuovo eruption using two values of G:

- 10^{-9} cm/s is the value of G for the crystallization processes inside the magma chamber with low ΔT (Cashman, 1993) and was used to calculate the residence time of the magma;

- $2 \cdot 10^{-8}$ cm/s, on the contrary is the mean value of all the G estimated by Geschwind & Rutherford (1995) and by Couch *et al.* (2003), with no distinction between plagioclases and alkali feldspars. This value was used to calculate ascent time in the conduit towards surface, with consequent decrease of pressure and magma degassing.

The value of G used by Piochi *et al.* (2005) to determine the ascent time is quite similar (10^{-8} cm/s) to the decompression growth rates calculated in this thesis, differing at the most of an order of magnitude. This difference implies significant variations of the rising time. CSD studies on Monte Nuovo products carried out by Piochi *et al.* (2005) to investigate magma dynamics in sin-eruptive conditions, show rising time between 1 and 2 days. On the contrary, using the value of G obtained in this experimental work, we can obtain a new timing for magmatic processes: similar (using 10^{-8} cm/s) or lower (using 10^{-7} cm/s) duration than Piochi *et al.* (2005).

CONCLUSION

We performed two different kinds of crystallization experiments, cooling and decompression ones, to investigate how the kinetics of crystallization are affected by the different changing parameters. We found that for cooling experiments growth rate varies between $3.6 \cdot 10^{-8}$ and $3.9 \cdot 10^{-7}$ cm/s, while for decompression experiments it varies between $1.4 \cdot 10^{-8}$ and $1.7 \cdot 10^{-7}$ cm/s.

Crystal growth rate is higher in experiments with shorter duration, while it decreases with increasing experimental duration. The undercooling degree implies significant variation in the crystallization kinetics: for low ΔT growth is helped, in fact we find values of G higher than experiments with higher ΔT (where the growth slows down). This behavior differs from the theoretical relation between G and ΔT (see for example Peccerillo & Perugini, 2003), probably because the theoretical curve simply encloses all the experimental results, while in the present work different G values experimentally obtained were distinguished for experimental conditions. The percentage of dissolved water in the melt plays a fundamental role in helping growth, as well: collected data show an increase of crystal growth rate with increasing water content in the melt. This behavior is due to the depolymerizing effect of water that reduces magma viscosity and consequently helps atoms mobility inside the magma.

From the comparison between cooling and decompression growth rates we can see that the former are slightly faster than the latter. This is because the amount of dissolved water in the melt depends on the experimental starting pressure. In decompression experiments pressure is lowered and consequently the amount of dissolved water in the melt lowers as well, implying a lower mobility of cations and consequently a lower crystal growth rate.

The estimate of alkali feldspar growth rate together with the study of the CSD is useful to determine residence and rising time of trachytic phlegraean magmas to evaluate eruptive dynamics of volcanic events that can involve the area. The values of G presented here are the same (10^{-8} cm/s) or differ at the most of an order of magnitude (10^{-7} cm/s) from the growth rates used by Piochi *et al.* (2005) for Monte Nuovo, so the rising time that will be calculated will surely be similar or lower than those estimated by Piochi *et al.* (2005).

REFERENCES

Cabane, H., Laporte, D., Provost, A. (2005): An experimental study of Ostwald ripening of olivine and plagioclase in silicate melts: implications for the growth and size of crystals in magmas. *Contrib. Mineral. Petrol.*, **150**, 37-53.

Calzolaio, M. (2005): Effetto dello stato di ossidazione sulla cristallizzazione dei magmi dei Campi Flegrei. MSc thesis.

Cashman, K.V. (1993): Relationship between crystallization and cooling rate insight from textural studies of dikes. *Contrib. Mineral. Petrol.*, **113**, 126-142.

Civetta, L., Orsi, G., Pappalardo, L., Fisher, R.V., Heiken, G.H., Ort, M. (1997): Geochemical zoning, mixing, eruptive dynamics and depositional processes – the Campanian Ignimbrite, Campi Flegrei, Italy. *J. Volcanol. Geotherm. Res.*, **75**, 183-219.

Couch, S. (2003): Experimental investigation of crystallization kinetics in a haplogranite system. *Am. Mineral.*, **88**, 1471-1485.

Couch, S., Sparks, R.S.J., Carroll, M.R. (2003): The kinetics of degassing-induced crystallization at Soufrière Hills Volcano, Montserrat. *J. Petrol.*, **44**, 1477-1502.

Di Matteo, V., Carroll, M.R., Berhens, H., Vetere, F., Brooker, R.A. (2004): Water solubility in trachytic melts. *Chem. Geol.*, **213**, 187-196.

Fabbrizio, A. & Carroll, M.R. (2008): Experimental constraints on the differentiation process and pre-eruptive conditions in the magmatic system of Phlegraean Fields (Naples, Italy). *J. Volcanol. Geotherm. Res.*, **171**, 88-102.

Fenn, P.M. (1977): The nucleation and growth of alkali feldspar from hydrous melts. *Can. Mineral.*, **15**, 135-161.

Geschwind, C.H. & Rutherford, M.J. (1995): Crystallization of microlites during magma ascent: the fluid mechanics of 1980-1986 eruptions at Mount St. Helens. *Bull. Volcanol.*, **57**, 356-370.

Higgins, M.D. (2000): Measurements of crystal size distribution. *Am. Mineral.*, **85**, 1105-1116.

Higgins, M.D. (2002): Closure in crystal size distribution (CSD), verification of CSD calculations, and the significance of CSD fans. *Am. Mineral.*, **87**, 171-175.

Peccerillo, A. & Perugini, D. (2003): Introduzione alla Petrografia ottica. Morlacchi, ed. Perugia, 200 p.

Piochi, M., Mastrolorenzo, G., Pappalardo, L. (2005): Magma ascent and eruptive processes from textural and compositional features of Monte Nuovo pyroclastic products, Campi Flegrei, Italy. *Bull. Volcanol.*, **67**, 663-678.

Swanson, S.E. (1977), Relation of nucleation and crystal-growth rate to the development of granitic textures. *Am. Mineral.*, **62**, 966-978.

SPECTRAL ANALYSES IN THE VNIR OF IGNEOUS ROCKS: SURFACE COMPOSITION CHARACTERIZATION OF TERRESTRIAL PLANETS

CRISTIAN CARLI
Dipartimento di Scienze della Terra, Università di Parma, Via G.P. Usberti 157/A, 43100 Parma

INTRODUCTION

Understanding the geological evolution of the Earth and extraterrestrial planets passes through the knowledge of the lithosphere composition. To this aim, remote spectroscopy has become an important tool for the spectral characterization of the surface composition, particularly during the last decades as a consequence of the improved spatial and spectral resolutions of the sensors. The criteria for the interpretation of the surface composition of extraterrestrial planets can be established through the study of rock samples from terrestrial analogues, using pure minerals, mineral mixtures and rocks (*e.g.*, King & Ridley, 1987; Cloutis & Gaffey, 1991; Burns, 1993; Harloff & Arnold, 2001; Pompilio *et al*., 2007).

The spectra of the most important silicate minerals, like pyroxene, olivine and plagioclase, show several diagnostic absorption feature in the Vis and near-IR range (Burns, 1993). The qualitative evaluation of remote spectra is generally made by comparison with spectra of minerals and rocks measured in the laboratory under controlled conditions. The spectroscopy of rock slabs is still in a developmental stage. The problems include: the discrepancy between rock-slab spectra and mineral mixture spectra with identical compositions; the texture effects on shape and position of the diagnostic absorptions of minerals; and the possibility to resolve the spectral components in a rock spectrum applying mathematical models.

The ongoing MESSENGER (NASA) and the planned Bepicolombo (ESA and JAXA) missions will improve our knowledge about the geologic history of Mercury. Mercury is the extreme rocky planet in our solar system, and so far the less studied. Data from orbit were acquired in the 70's by Mariner10 mission, whereas until the first flyby of MESSENGER in January 2008 the majority of data was collected from ground based observations. According to these data, the known part of Mercury is cratered and ancient, with some similarities with the Moon's surface (see a review in Boynton *et al.*, 2007). The less cratered, younger plains have been interpreted as having a volcanic origin; however the spatial resolution of Mariner10's images was not suitable for a reliable identification of volcanic morphologic features. The knowledge of chemistry and mineralogy of the mercurian surface is based on several ground based observations in the VIS, NIR and MIR intervals. Spectral data revealed no or weak absorption features indicative of low FeO and TiO_2 content, and a systematic red slope, supporting a close similarity to lunar highlands anorthosites.

In this research, sets of rocks belonging to suites from various terrestrial geodynamics contexts were analyzed in the VNIR spectral range, and the relationships between spectral and petrographic parameters were established. These rock suites have been selected as possible analogues for the mercurian surface composition. The influence of texture was also analyzed, using rock powders at different sizes as well as rock-slabs. The spectra collected during this research will also be implemented in a spectral library of possible Mercury's analogues.

TERRESTRIAL ROCK SUITES

Co-genetic rocks from a cumulitic layered intrusion (Stillwater Complex) and two distinct suites of basaltic rocks (Pampas Onduladas Flow and Iceland) from different geological contexts, have been studied. The composition of the principal mineral phases was determined by microprobe analyses made with a CAMEBA SX50 at the microprobe laboratory of C.N.R., Earth Science Department of Padua University.

The Stillwater Complex (SWC) is a portion of a cumulitic layered intrusion, emplaced 2.7 Ga at a depth of 10-15 km. Tectonic deformation and subsequent erosion exposed part of the intrusive complex. The igneous stratigraphy of the SWC consists of genetically related rocks subdivided into three major zones: the Basal Series, the Ultramafic Series (US) and the Banded Series (BS; McCallum, 1996). Two compositionally different magmas built up the SWC: a MgO and SiO_2 rich magma which formed the US and a tholeiitic magma from which the BS was originated.

The samples studied in this thesis were collected in the US and in the BS and show a cumulitic texture. In detail, the US samples have orthopyroxene (Opx), clinopyroxene (Cpx), olivine (Ol) and opaque minerals as cumulus phases, and plagioclase (Pl) as intercumulus phase. The BS samples have Pl as cumulus phase, while Opx, Cpx and Ol could be cumulus or intercumulus phases.

Five ultramafic rocks and five mela-norites have been studied from the US, while the BS samples consist of three anorthosites, two leucogabbros, three gabbronorites, one norite and three Ol-bearing rocks. Ol is more forsteritic (Fo_{85}) in US than in BS (Fo_{78}) samples. Opx and Cpx show narrow ranges of variation in individual samples, but these phases show significant variations when the samples are considered all together, ranging from $En_{59\text{-}88}Wo_{1\text{-}9}$ and $En_{39\text{-}51}Wo_{36\text{-}47}$, respectively. Pl is scarcely zoned but it shows a wide variation (An_{65}-An_{90}) considering the samples all together.

Chromite is present in some US samples.

The Pampas Onduladas Flow (POF) is a very long (181 km) pahoehoe lava flow erupted in the Andean back-ark volcanic province of Payenia, Argentina. The lava flow outpoured during the Late Quaternary from the summit rift of a shield volcano and it is the longest known individual Quaternary lava flow on Earth. It has a hawaiite composition with Ol and minor Pl phenocryst (Pasquarè *et al.*, 2008).

The studied samples were collected from different portions of the lava flow: most of them derive from the proximal portion of the flow; a few samples from the middle and one sample represents the distal portion. They show P.I. index less than 8%, and an intergranular texture of the groundmass. The mineral association consists of Pl, Ol, Cpx and small amounts of opaque minerals. Only one sample shows a hyalopilitic groundmass for the presence of a dark glass.

Ol phenocrysts range from Fo_{72} to Fo_{84}, whereas microcrysts range from Fo_{30} to Fo_{70}. Cpx varies from Ca-rich augite ($En_{42}Wo_{44}$) to diopsidic-augite ($En_{32}Wo_{48}$). Pl varies in composition from An_{61} to An_{68}. Opaques are Chr-spinel.

Iceland is an island developed on the Atlantic middle ridge up to a mantle plume. Active volcanic systems are associated with three different rift-areas which comprise en echelon arrays of volcanic fissure swarms: the Reykjanes Eastern Rift Zones (ERZ), the Reykjanes Western Rift Zones (WRZ), the Reykjanes Northern Rift Zones (NRZ). Volcanic activity is also present in non-rift areas but this volcanic centres lack well-developed fissure swarms.

Different types of volcanic products have been observed in Iceland, but almost 85% consists of basalts with composition varying amount tholeiiti, Ol-rich, and transitional-alkaline, Ol-alkaline or Fe-Ti rich (Basaltic Volcanism Study Project, 1981).

The samples studied in this thesis are from different lava flows of the ERZ and the NRZ. They show a wide range of phenocryst content, with P.I. index from 0 to 85%. Also the groundmass texture is strongly variable: in some samples it is intergranular, in others intersertal or hyalopilitic due to the presence of a dark glass. The mineral association includes Pl, Cpx, opaque minerals and rare Ol.

Ol phenocrysts vary from Fo_{76} to Fo_{87}, whereas microcrysts range from Fo_{61} to Fo_{85}. Cpx is represented by augite, varying in composition from $En_{51}Wo_{44}$ to $En_{35}Wo_{27}$. Pl is scarcely zoned, but it shows a wide variation, ranging from An_{76} to An_{90} among the phenocrysts and from An_{44} to An_{80} among the microlites, considering the samples all together. Ilmenite and magnetite are ubiquitous as opaque minerals.

REFLECTANCE SPECTROSCOPIC DATA

Reflectance spectra were measured in the 0.35 to 2.50 μm interval using two spectrophotometers: a) Perkin-Elmer λ-19 at IFAC Institute of C.N.R., Florence and b) Fieldspec Pro at INAF-IASF Institute, Rome.

In this range of wavelength, several absorption features of silicate minerals are described in the literature (*e.g.*, Burns, 1993), as well as the spectral behaviour of mineral mixtures. In this work the spectra were measured on slabs and powders of rock.

Powdered specimens were however limited to selected representative samples.

The visual inspection of the spectra was useful to recognize the most evident absorption structures, and to assign the absorption bands to electronic and molecular interaction processes by comparison with the literature. Electronic and vibrational absorptions were described and labelled using roman numbers (Band I to V in Fig. 1) and lowercase letters (Band a to d), respectively. Band I (~ 1.00 μm) is due to the presence of Fe^{2+} in M2 of Opx, in M1 or M2 of Cpx and in both M2 and M1 of Ol, Band II (~ 2.00 μm) is due to the presence of Fe^{2+} in M2 of Opx and Cpx, Band V (~ 1.25 μm) is due to the presence of small Fe^{2+} amounts in Pl. Different associations of these bands identify spectral groups that represent "spectral classes" in the sense of Longhi *et al.* (2001); these spectral classes can

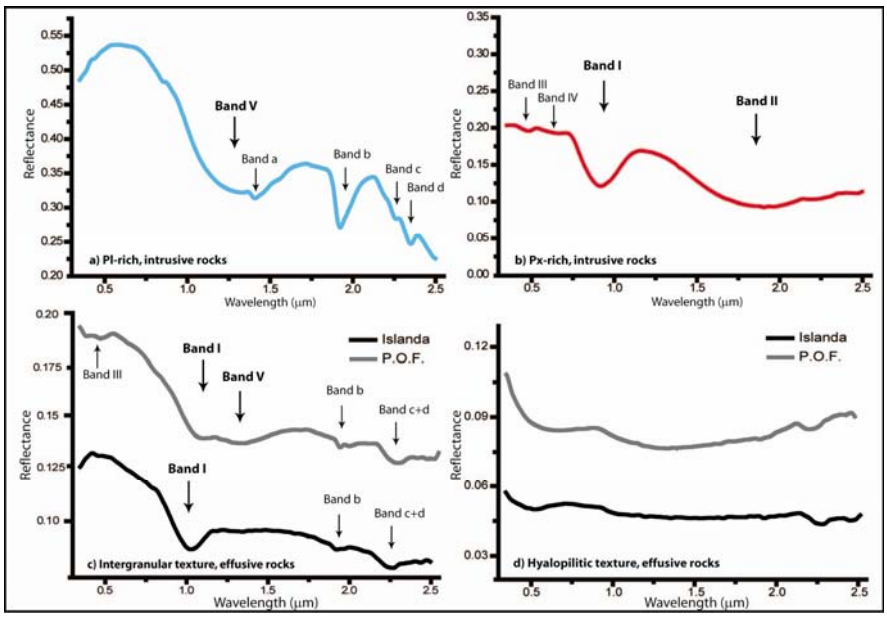

Fig. 1 - a, b) Exempla of slab spectra of first two classes of intrusive rocks (SWC). c, d) Exempla of slab spectra of basalts, samples with intergranular texture show absorption structures of minerals, samples with hyalopilitic texture do not show them.

be compared with petrographic features (rocks composition and texture). The parameters describing individual absorption bands (position on the wavelength axis, intensity and width at half maximum) are related to the mineral composition. For this analysis, statistical methods of spectral analysis (Sunshine *et al.*, 1990; Pompilio *et al.*, 2009) have been used to decompose the spectral curves both measured on slabs and powdered samples.

In general, slab spectra show a blue slope (reflectance decreasing towards IR). Powdered spectra show higher reflectance than the corresponding slab spectra and a horizontal or red slope (reflectance increasing towards IR).

In particular:

1) The slab spectra of SWC rocks are grouped into four classes: One class is characterized by a wide absorption band at about 1.25 μm, that can be due to Fe^{2+} in Pl; these rocks are anorthosites and leucogabbros, with Pl > 80% (Fig. 1a). The second class (Fig. 1b) shows two absorption bands at about 0.93 μm and 2.00 μm, due to Fe^{2+} in M2 site of Opx and in both M1 and M2 sites of Cpx (Burns, 1993). The other two classes, not shown in Fig. 1, comprise spectra characterized by a low reflectance and weak absorption band due to the influence of opaque minerals; and a group of spectra with no clear absorption features, dominated by variously altered Ol.

2) In the slab spectra of basalts the absorption features due to different mineral associations can be recognized in samples with an intergranular or intersertal texture (Fig. 1c). The absorption bands are smoothed in samples with a hyalopilitic texture (Fig. 1d).

Spectral curves measured on powdered samples of the first two groups of SWC rocks allowed us to quantify the spectral parameters and therefore to characterize the absorption features due to the spectrally active "facies". In this case, "facies" indicates an ion in a specific site in a mineral; *e.g.*, the Fe^{2+} content in Pl or in M2 site of Opx and Cpx, or in M1 and M2 sites of Ol.

The spectra of powdered basalts show absorption structures due to two different mineral associations; the absorption bands are well defined for samples with intergranular texture, and are almost absent in those containing dark-glass.

In the following section, the spectral parameters measured on spectra of powdered rocks are compared with the rock compositions.

SPECTROSCOPIC PARAMETERS *VS.* ROCK/MINERAL COMPOSITIONS

As reported above, different associations of absorption bands permit the spectral classification of rocks with different mineral associations and/or textures. The parameterization of these absorption features allows the evaluation of the content of the "facies", so that the relationship between absorption data and mineral chemistry can be established. Several models were proposed in the literature to quantify the absorption bands: empirical methods which measure position, depth and width of the absorption band; models of scattering which involve solving the equation of Radiative Transfer; models of decomposition which use a distribution of Gaussians or modified Gaussians superimposed to a continuum. In this research, a new decomposition model called EGO (Exponential Optimized Gaussian; Pompilio *et al.*, 2009) has been used.

The Band I, clearly expressed in both slab and powder spectra, is particularly diagnostic for Opx, Cpx and Ol. In our samples, it results in a composite band, due to the silicate absorptions of those silicate occurring in a restricted range of wavelength. EGO returns a Gaussian for each absorption process. The

band centre position (b.c.) and the band depth (b.d.) of the Gaussians are compared with the parameters of mineral composition (ferrosilite or forsterite content) and the relative modal abundance of minerals.

The b.c. of Opx and Cpx for intrusive rocks (Fig. 2) and of Cpx and Ol for effusive rocks (Fig. 3) were compared with data from the literature relative to pure minerals (Cloutis & Gaffey, 1991; Burns, 1993).

In both cases, the b.c. positions measured in rocks approximate the correlation curves reported in the literature for pure minerals.

The b.d. or intensity of the absorption band is related to the probability of an electronic transition to occur. For a given allowed transition, the b.d. is related to the abundance of the absorbing phase in a mineral mixture (*e.g.* Opx in Fig. 4). A linear relationship was observed between b.d. and Fe^{2+} content in both Opx and Cpx (*e.g.* Opx in Fig. 5). However, because the band intensity depends on the amount of spectrally active "facies", saturation effects were observed as this amount increases (empty circles in Figs. 4, 5).

On the other hand, the intrusive rocks are classified on the basis of the relative modal abundance of the principal minerals; therefore, it is useful to establish the relationship between the b.d. of the absorption and the modal abundance of the absorbing phase. In fact, a linear relationship was observed between b.d. measured in powder spectra and both Opx mode (Fig. 4) and volumetric Fe^{2+} content, expressed as Fe^{2+} * mod Opx% (Fig. 5).

Similar linear trends are displayed in Figs. 4 and 5 for spectra measured on rock-slab spectra. In this case, however, a so called "bulk effect" is responsible for a strong reduction of b.d. with respect to b.d. measured in spectra of powder samples of the same rocks.

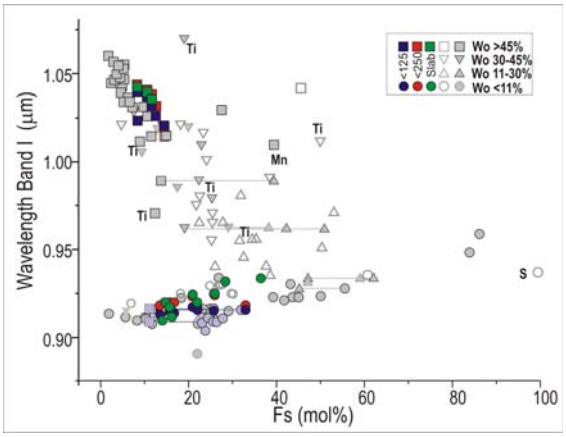

Fig. 2 - Position of Band I *vs.* Fs (mol.%) of pyroxene of SWC. Data of this thesis are colored; literature data are grey (modified after Pompilio *et al.*, 2007).

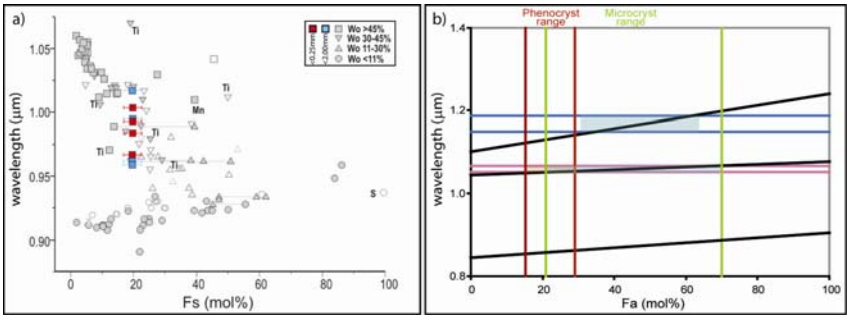

Fig. 3 - a) Position of b.c. *vs.* Fs (mol.%) of Ti-augite of POF. Data of this thesis are colored; literature data are grey (modified after Cloutis *et al.*, 1991); b) position of b.c. (powders < 0.25 µm) *vs.* Fa (mol.%) of Ol, black lines are data from literature (modified after Burns, 1993).

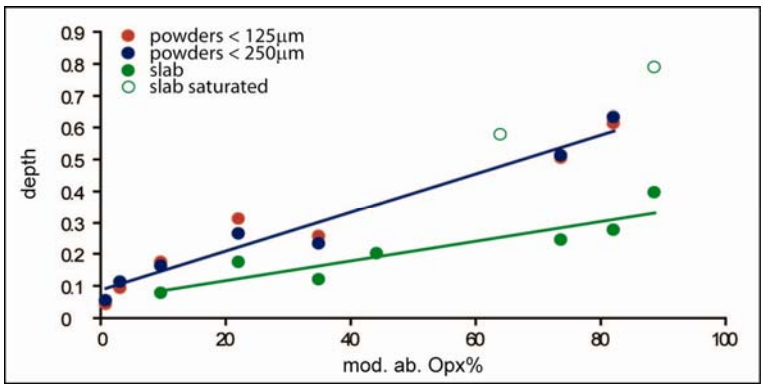

Fig. 4 - Band depth *vs.* mod. ab. of Opx for samples of SWC. Confidence level of 99%.

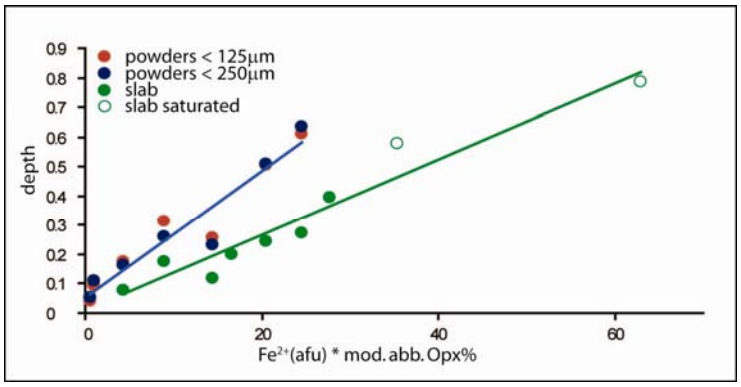

Fig. 5 - Band depth *vs.* modal distribution of Fe^{2+} of Opx for samples of SWC. Confidence level of 99%.

APPLICATION TO SPECTRA OF MERCURY

New data from the first MESSENGER's flyby show that Mercury's surface is morphologically and compositionally more heterogeneous then previously observed (Boynton *et al.*, 2007, and references therein). Areas characterized by different ratios in the VIS and NIR have been associated with distinct surface morphologies (Robinson *et al.*, 2008). Furthermore the spectra show evidence for the presence of pyroxene or olivine richer in Mg than predicted before. Finally, the effect of a darkening agent, possibly Ti-Fe oxides, was proposed.

Spectra of powders measured in this thesis have been recalculated to the slope of the average full-disk spectra of Mercury acquired by MASCS (McClintock *et al.*, 2008). Recalculated spectra show that the absorption band I in norites and gabbronorites is still clearly recognizable. In contrast, the shape of the anorthosite spectra is close to the average full-disk spectra and the basalt spectra do not show clear absorption structures.

Band ratios calculated according to Robinson *et al.* (2008) algorithms show that the basalts follow the trend described for the low reflectance material and the SWC samples partially fall in the range of immature areas, with a wider range of values for the NIR slope due to the presence of the band I (Fig. 6).

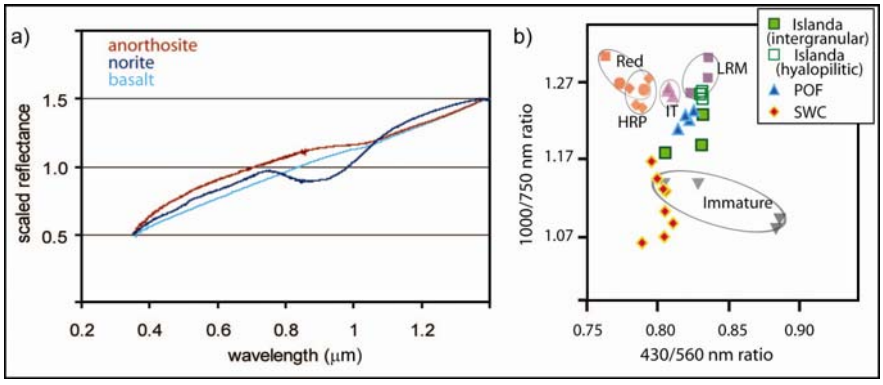

Fig. 6 - a) Recalculated spectra show a clear band I only for pyroxene-rich SWC samples. b) Band ratios calculated according to Robinson *et al.* (2008).

CONCLUSIONS

- Different associations of absorption bands permit the spectral description and the discrimination of the rock compositions of the three studied sites.

- The spectral parameters determined in rock spectra are comparable with those of pure minerals. In particular the b.c. of the modified Gaussians, resulting for the spectra of both slabs and powders match the correlation curves determined for pure minerals (Opx, Cpx and Ol). The b.d. for intrusive rocks always show a linear relationship with modal abundance. However, weaker b.d. were observed for the slabs with respect to the powdered samples of the same rocks.

- Spectra re-calculated according to the algorithms used for MASCS spectra of Mercury show a clear absorption structure of pyroxene for norites and gabbronorites, indeed up to now not detected in Mercury's spectra. However, both the anorthosite and basalts recalculated spectra, although these rocks contain pyroxene, do not show clearly absorption structure clearly indicative of mafic minerals.

REFERENCES

Basaltic Volcanism Study Project (1981): Basaltic volcanism on the terrestrial planets. Pergamon Press, New York, 1286 p.

Boynton, W.V., Sprague, A.L., Solomon, S.C., Starr, R.D., Evans, L.G., Feldman, W.C., Trombka, J.I., Rhodes, E.A. (2007): MESSENGER and the Chemistry of the Mercury's Surface. *Space Sci. Rev.*, **131**, 85-104.

Burns, R.G. (1993): Mineralogical applications of crystal field theory. Cambridge University Press, Cambridge, 551 p.

Cloutis, E.A. & Gaffey, M.J. (1991): Pyroxene spectroscopy revisited: spectral-compositional combinations and relationships to geothermometry. *J. Geophys. Res.*, **96**, 22809-22826.

Harloff, J. & Arnold, G. (2001): Near-infrared reflectance spectroscopy of bulk analog materials for planetary crust. *Planet. Space Sci.*, **49**, 191-211.

King, T.V.V. & Ridley, W.I. (1987): Relation of spectroscopic reflectance of olivine to mineral chemistry and some remote sensing implications. *J. Geophys. Res.*, **92**, 11457-11469.

Longhi, I., Sgavetti, M., Chiari, R., Mazzoli, C. (2001): Spectral analysis and classification of metamorphic rocks from laboratory reflectance spectra in 0.4-2.5 μm interval: a tool for hyperspectral data interpretation. *Int. J. Remote Sensing*, **22**, 3763-3782.

McCallum, I.S. (1996): The Stillwater Complex. *In:* "Layered Intrusions", R.G. Cawthorn, ed. Elsevier, Amsterdam, 441-484.

McClintock, W.E., Izenberg, N.R., Holsclaw, G.M., Blewett, D.T., Domingue, D.L., Head III, J.W., Helbert, J., McCoy, T.J., Murchie, S.L., Robinson, M.S., Solomon, S.C., Sprague, A.L., Vilas, F. (2008): Spectroscopic Observations of Mercury's Surface Reflectance During MESSENGER's First Mercury Flyby. *Science*, **321**, 62-65.

Pasquarè, G., Bistacchi, A., Francalanci, L., Bertotto, G.W., Boari, E., Massironi, M., Rossetti, A. (2008): Very long pahoehoe inflated basaltic lava flows in the Payenia Volcanic Province (Mendoza and La Pampa, Argentina). *Rev. Asoc. Geol. Argentina,* **63**, 131-149.

Pompilio, L., Sgavetti, M., Pedrazzi, G. (2007): Visible and near-infrared reflectance spectroscopy of pyroxene-bearing rocks: New constraints for understanding planetary surface compositions. *J. Geophys. Res.*, **112**, E01004.

Pompilio, L. Pedrazzi, G., Sgavetti, M., Cloutis, E.A., Craig, M.A., Roush, T.L. (2009): Exponential Gaussian approach for spectral modeling: the EGO algorithm, I. Band Saturation. *Icarus,* in press.

Robinson, M.S., Murchie, S.L., Blewett, D.T., Domingue, D.L., Head III, J.W., Head, J.W., Holsclaw, G.M., McClintock, W.E., McCoy, T.J., McNutt, R.L. Jr., Prockter, L.M., Solomon, S.C., Watters, T.R. (2008): Reflectance and color variations on Mercury: Regolith processes and compositional heterogeneity. *Science*, **321**, 66-69.

Sunshine, J.M., Pieters, C.M., Pratt, S.F. (1990): Deconvolution of mineral absorption bands: an improved approach. *J. Geophys. Res.*, **95**, 6955-6966.

SECONDARY MINERALIZATIONS IN BASALTIC ROCKS: EXAMPLES FROM THE LESSINI MOUNTS (ITALY)

MARCO CENNI
Istituto di Scienze della Terra, Università "Carlo Bo", Loc. Crocicchia, 61029 Urbino (PU)

INTRODUCTION AND GEOLOGICAL SETTING

This work focus on the secondary mineralizations affecting the basaltic rocks from the Lessini Mounts (Verona Province) with the main purpose to establish a systematic of the secondary minerals that were formed in the cavities and vesicles determining the morphologies, the chemical compositions, the paragenesis and their areal distribution. Moreover, petrographic, mineralogical and geochemical investigations of volcanic host rocks have been carried out with the aim to explore possible relationships between the host rocks, their secondary minerals and the associated alteration phenomena, trying to carry a contribution to the knowledge of physico-chemical processes which are related to fluids migration through basaltic lava flows.

The Lessini Mounts can be referred to the South-Alpine Domain and a large area of its central-northern sector (now corresponding to the Veneto region) was affected by an intense magmatic activity from the late Paleocene to late Oligocene. The volcanic products related to this activity are now interbedded at various levels in South-Alpine Domain sedimentary rocks and they are described as Veneto Volcanic Province (VVP; Beccaluva *et al*., 2001; Bonadiman *et al.*, 2001). On the basis of tectono-magmatic features the VVP can be divided into three main areas: the western Lessini-Southern Trentino, the Marostica hills and the eastern Lessini.

The study area is located in the eastern Lessini (Verona province) and it is bounded by the Castelvero fault to the West and the Schio-Vicenza tectonic line to the East. In this area the volcanic activity span from the late Paleocene to the late Oligocene with the emplacement of submarine to subaeral lava flows and tuffs, now interbedded in the sedimentary stratigraphic succession. The main tectonic structure of the eastern Lessini area is the Alpone-Agno *Graben*, were the volcanic succession reaches a thickness of about 400 m and represents the most significant sequence of VVP. Within this depression eight volcanic phases have been recognized, from the late Paleocene to late Oligocene (De Vecchi & Sedea, 1995). These volcanics, whose compositions range from basanites, alkali-basalts, transitional basalts to tholeiites, are often deeply weathered and show veins and vesicles frequently filled by secondary minerals.

RESULTS AND DISCUSSION

Petrography, mineral chemistry and geochemistry of the host rocks

From a petrographic point of view all of the studied samples are basaltic rocks with a fairly homogeneous composition. Their paragenesis is Ol ± Cpx ± Pl ± Opq, present in different proportions, their texture ranges from subaphyric to porphyrytic (IP from 2 to 18 wt.%) and the groundmass is oloialine to olocrystalline. Abundant disrupted olivine xenocrysts and mantle xenoliths have been observed. These rocks show variables degrees of vesiculation and alteration. Olivine phenocrysts show an average composition of Fo_{78-84}, with a CaO content varying between 0.22 and 0.44 wt.%, and they did not

reveal the presence of minor elements such as Ni and Cr. The pyroxene shows a wide compositional variability characterized by $Wo_{41-58}En_{35-48}Fs_{2-12}$ and corresponding to the diopside field. The most significant changes are expressed by Ca (from 0.73 to 0.99 apfu) and Mg (from 0.56 to 0.88 apfu), while the TiO_2 content is between 0.33 and 4.78 wt.%; the Al is distributed mainly in the tetrahedron site (^{IV}Al 0.1-0.4 apfu, while ^{VI}Al 0-0.1 apfu). Plagioclase has a composition ranging from andesine to bytownite ($An_{47-89}Ab_{11-51}Or_{0-2}$), with the average of An_{65-75}.

According to the TAS diagram (Le Bas *et al.*, 1986), the studied volcanic host rocks are classified in order of abundances as: basanite, alkali basalts and sub-alkali basalts; K-trachibasalts, hawaiite and mugearite are very subordinate. In particular, the more basics terms show the typical characters of primitive rocks with high Mgv (> 0.5, assuming Mgv = $Mg/Mg+Fe^{2+}$, with $Fe_2O_3/FeO = 0.15$), low FeO_T/MgO (< 1.2), low Al_2O_3 (< 14 wt.%) and high Ni (176-295 ppm) and Cr (225-455 ppm).

As concerns REE, all patterns are sub-parallel with a decrease in LREE and an invariable content of HREE. In particular, the mafic rocks (basanite) have slightly higher contents of LREE compared to the relatively more evolved rocks. $(La/Lu)_N$ ratio range from 11 to 25. $(La/Yb)_N$ ratio varies from 14 for the more basic rocks, to 31 for the more evolved rocks, whereas Eu/Eu* ratio is always > 1 (1.3-2.3). Generally, all samples show a good overlap with the REE patterns of literature samples for this area.

Primordial mantle-normalized (McDonough *et al*., 1992) diagrams for Lessini volcanic host-rocks show sub-parallel patterns characterized by an increase from Rb to Nb (only for basic rocks), a significantly decrease in U and a more regularly decreases from Nb to the couple Tb-Y. A small trough can be seen at Hf. Primitive mantle-normalized (Sun & McDonough, 1989) diagrams for selected Lessini mafic rocks show smooth patterns characterized by a slight concavity downwards with positive peaks at Ba, Nb and La, while Th, U, Pb and K are negative peaks. All the analyzed rocks show patterns resembling that of the literature for this area. The only differences rest on negative Th, U, Pb, and Sm anomalies, which are significantly lower in the studied samples.

On the basis of petrology and chemical characters all the studied rocks are related to alkaline or moderately alkaline magma series, with $Na_2O > K_2O$ and low SiO_2 content (< 46 wt.%), features similar to OIB mantle sources. The data display typical within-plate geochemical signature and the multi-element diagrams show patterns which resemble those of magmas derived from a depleted mantle, similar to MORB or HIMU-type basalts, with the exception of some negative Th, U and Pb anomalies. However, in spite of their similar whole geochemistry, the studied samples evidence significant differences in particular geochemical characters. Elements such as Hf, La and Nb, for example, do not show any correlation with Zr, as it should be in the case of comagmatic rocks. Moreover, some element ratios such as Ba/Nb and Ba/La show no correlation with Zr.

These data seem to indicate that the Lessini volcanics are likely to be generated from substantially similar mantle sources, as suggested by the subparallel incompatible element patterns. However, some geochemical characters suggest that the deepest mantle sources, with an HIMU signature, were probably not homogeneously enriched by metasomatic fluids prior to and/or melting processes, as also well evidenced by recent isotope systematics (Beccaluva *et al*., 2007). The HIMU metasomatizing agents may possibly be related to a convecting mantle plume that is thought to extend from the eastern Atlantic to Europe (Macera *et al*., 2003; Piromallo & Morelli, 2003; Beccaluva *et al*., 2007).

Secondary mineralizations in the Lessini basalts

Vesicles and cavities in the Lessini basalts were partly to completely filled with secondary minerals. The zeolite group constitutes about ~ 90% of the total mineral species and it is represented

mainly by analcime, harmotomo, chabazite, gmelinite, phillipsite and natrolite whereas erionite, offretite, heulandite and stilbite are less common. In some samples very rare zeolites as yugawaralite and willhendersonite were also found, and this the first discovery in VVP. Zeolite minerals are often associated with other silicates as apophyllite, gyrolite, prehnite, pectolite and smectite (*e.g.* saponite, Fe-saponite) and non-silicates as carbonates (calcite, aragonite), sulphates (celestine) and oxides (quartz, tridimite).

Regarding the zeolite group, analcime, gmelinite and natrolite show macroscopic features, optical properties and chemical compositions comparable with the same minerals already described in the literature for other areas of the Lessini Mounts (Vicenza province) as well as other locations (Gottardi & Galli, 1985; Tschernich, 1992; Bish & Ming, 2001). Phillipsite and harmotomo are consistent with the literature data for macroscopic features and optical properties, while in terms of chemical composition, they are predominantly phillipsite-Ca, with subordinate phillipsite-K and very rare phillipsite-Na. These data show a well compositional range between Ba and K contents which significantly extends the miscibility between the two end-members phillipsite and harmotome. The chabazite shows a wide range of morphologies and can also be found with very rare habits. One of them, never seen before in Lessini Mounts, is the result of a geometrically regular growth of lamellae with pseudo-hexagonal shape. Its optical properties are consistent with those of the literature and, with respect to chemical compositions, the studied chabazite is a predominantly chabazite-Ca, whereas chabazite-K is very rare and chabazite-Na is absent. In particular, a significant amount of Sr has been detected in some chabazites and this seems to be systematically related to some unusual morphologies. Among the other zeolites heulandite and stilbite are easily recognizable and their characteristics are consistent with the literature data, whereas erionite and offretite show very similar morphologies and their distinction is only possible through accurate chemical and diffraction analysis. Macroscopic characters, optical properties and chemical compositions are comparable with the literature data; in particular, in the Verona Province, only erionite-Ca and Ca-rich offretite have been found, while erionite-Na and erionite-K are absent or very subordinate. Yugawaralite and willhendersonite are rare in Lessini basalts, but their low spread in other parts of the world makes their presence particularly significant. Moreover, this is the first discovery of these zeolites in the Veneto Volcanic Province.

As regards the other silicates (apophyllite, gyrolite, prehnite, pectolite, pectolite-larimar) and non-silicates (celestine, calcite, aragonite, quartz and tridimite) their distribution is very limited and the analyzed samples show coherent characteristics in terms of macroscopic features, optical and chemical compositions if compared to the literature data.

The study of systematic and paragenesis within cavities and vesicles of the investigated samples suggest that most of the secondary minerals in the Lessini basalts were formed at relatively low temperatures, in the range of 50-150°C. Rarely, the secondary minerals and/or their paragenesis can be related to higher temperatures (> 250°C), probably linked to local situations and/or subsequent crystallization processes.

Considering that: (i) most of the cavities and vesicles is only partially filled by secondary minerals, and they crystallize from the walls toward the centre of the vesicle in which, however, there is still space available, (ii) most of the minerals gives rise to secondary crystals with well-developed morphologies observable even at macroscopic scale, (iii) the mineralization observed in the cavities and vesicles in the studied samples are related to phenomena occurring usually at low temperatures (< 150°C), (iv) this is a wide systematic of minerals mainly referred to the zeolite group, and (v) some of them are characterized

by well-defined chemical compositions, so it can be concluded that these minerals may be related to hydrothermal systems. However, there may be several distinct genetic environments, all related to hydrothermal systems but slightly different with each other and probably overlapped in time and space.

In some cases the presence of low-temperature zeolite paragenesis with high variability at small-scale, connected with a strong alteration of host rocks, is consistent with hydrothermal alteration phenomena produced by high temperature fluids that locally pervade already consolidated basaltic rocks. In other cases, however, the mineralogy of the observed associations and their widespread homogeneity suggest a system characterized by the presence of massive injections of high temperature fluids pervading continuously and homogeneously (and for a long time) large masses of already consolidated volcanic rocks or only partially solidified; this feature is typical of volcanic areas with large volumes of emplaced magma. A further possibility involve the formation of secondary minerals as derived from the simple cooling of lava flows where the heat flux produced by the mass in cooling can interact with water bodies, generating high-temperature fluids which may lead to the formation of secondary minerals. In this case, the presence of gaps and/or important tectonic structures may facilitate the movement of water masses (and thus increase the possibility of interaction with magma bodies) and the increase of temperature (also for the heat generated by friction). Finally, the presence of minerals of high temperature, the absence of zeolites and the complete filling of fractures and veins of irregular shape, may indicate the existence, at least locally, of microsystems in which genetic conditions may be very near to the field of low-grade metamorphism.

The alteration of basaltic rocks can be considered as the result of very complex geological processes which probably develop at different scales and time and space. However, in the area of Lessini Mounts, is recognizable a main phase of alteration which is acting on a regional scale and it is responsible for the observed zoneography in volcanic rocks, and other secondary alteration phases, contemporary or subsequent to the main phase and of local importance, may be responsible for the considerable variability observed in terms of amounts of secondary minerals, mineralogical associations and chemical compositions.

The processes of secondary mineralization not affected systematically all the basaltic rocks of the Lessini Mounts and several variations can be recognized, suggesting the presence of significant relationships between the development of mineralizations and some geological characters such as tectonics, fracturing of rock masses and presence of levels with different degree of permeability. At a small scale, the most common mineralizations are generally located on the roof of volcanic bodies or at the contact with clay levels or compact basaltic bodies. At a large scale, however, the mineralized areas have a distribution that follows the most important tectonic structure in this area (Castelvero fault), which may have acted as surface lifts and mobilization of fluids, causing thermic anomalies. These elements suggest that the formation of secondary mineralization in basaltic rocks in the Lessini Mounts (but probably also in other similar contexts) is strongly linked to the presence of preferential pathways of movement and/or stagnation of fluid masses.

Generally cannot be observed systematic changes or specific relationships between the compositions of host rocks and the associated secondary minerals in terms of paragenesis and chemical compositions, suggesting a greater influence by the composition of circulating fluids rather than that of the host rocks. However, in restricted areas, there are significant changes in the contents of some chemical elements in both host rocks and in related secondary minerals, showing the presence of possible genetic relationship of local character.

Almost all of the secondary minerals in cavities and vesicles in the Lessini basalts are characterized by the peculiar presence of calcium as a single- or dominant-cation, as testified by the presence of phillipsite-Ca, gmelinite-Ca, chabazite-Ca, erionite-Ca, Ca-rich offretite, pure Ca-zeolites like yugawaralite, stilbite and peculiar calcium minerals as pectolite, gyrolite, calcite and aragonite. If it is considered that the volcanic rocks hosting the mineralized cavities not have high ratios Ca/(Na+K), and their primary minerals show an enrichment in calcium if compared to what should be their classical composition (*e.g.* pyroxene), it can be concluded that these rocks cannot be held as responsible for the release of calcium. Thus, the Ca cation was to be extremely abundant in the hydrothermal fluids circulating in the rock masses and its origin could be related to the presence of thick and important carbonate successions surrounding (or interbedded with) the volcanic bodies and/or the entire lava sequences of the Lessini Mounts.

REFERENCES

Beccaluva, L., Bonadiman, C., Coltorti, M., Salvini, L., Siena, F. (2001): Depletion events, nature of metasomatizing agent and timing of enrichment processes in lithospheric mantle xenoliths from the Veneto Volcanic Province. *J. Petrol.*, **42**, 173-187.

Beccaluva, L., Bianchini, G., Bonadiman, C., Coltorti, M., Milani, L., Salvini, L., Siena, F., Tassinari, R. (2007): Intraplate litospheric and sublitospheric components in the Adriatic domain: nephelinite to tholeiite magma generation in the Paleogene Veneto volcanic province, southern Alps. *Geol. Soc. Am., Spec. Paper*, **418**, 131-152.

Bish, D.L. & Ming, D.W. (2001): Natural zeolites: Occurrence, properties, applications. *Rev. Mineral. Geochem*., **45**, 662 p.

Bonadiman, C., Coltorti, M., Milani, L., Salvini, L., Siena, F., Tassinari, R. (2001): Metasomatism in the lithospheric mantle and its relationships to magmatism in the Veneto Volcanic Province, Italy. *Per. Mineral.*, **70**, 333-357.

De Vecchi, G.P. & Sedea, R. (1995): The Paleogene basalt of the Veneto region (NE Italy). *Mem. Ist. Geol. Mineral. Univ. Padova*, **47**, 253-274.

Gottardi, G. & Galli, E. (1985): Natural zeolites. Springer, New York, 391 p.

Le Bas, M.J., Le Maitre, R.W., Streckeisen, A., Zanettin, B. (1986): A chemical classification of volcanic rocks on the Total Alkali-Silica diagram. *J. Petrol*., **27**, 745-750.

Macera, P., Gasperini, D., Piromallo, C., Blichert-Toft, J., Bosch, D., Del Moro, A., Martin, S. (2003): Geodynamic implications of deep mantle upwelling in the source of Tertiary volcanics from the Veneto region (South-Eastern Alps). *J. Geodyn.*, **36**, 563-590.

McDonough, W.F., Sun, S.S., Ringwood, A.E., Jagoutz, E., Hofmann, A.W. (1992): Potassium, rubidium and cesium in the Earth and Moon and the evolution of the mantle of the Earth. *Geochim. Cosmochim. Acta*, **56**, 1001-1012.

Piromallo, C. & Morelli, A. (2003): P-wave tomography of the mantle under the Alpine-Mediterranean area. *J. Geophys. Res.*, **108/B2**, 2065, doi:10.1029/2002JB001757.

Sun, S.S. & McDonough, W.F. (1989): Chemical and isotopic systematics of oceanic basalts: implications for mantle compositions and processes. *In*: "Magmatism in the Ocean Basins", A.D. Saunders & M.J. Norry, eds. *Geol. Soc. Lond., Spec. Publ*., **42**, 313-345.

Tschernich, R. (1992): Zeolites of the world. Geoscience Press, Phoenix, 564 p.

CHEMICAL AND ISOTOPIC CHARACTERIZATION OF ISCHIA HYDROTHERMAL SYSTEM: AN INTERPRETATIVE MODEL OF FLUIDS CIRCULATION

ROSSELLA DI NAPOLI
Dipartimento di Chimica e Fisica della Terra ed Applicazioni alle Georisorse ed ai Rischi Naturali, Università di Palermo, Via Archirafi 26, 90123 Palermo

Ischia Island is an active volcanic area in the Campanian Magmatic Province (CMP). Although currently quiescent, Ischia volcano has been active in historic time, most recently in 1302 A.D.. The present activity is characterised by the widespread occurrence of surface hydrothermal manifestations, such as hot water discharges from wells and springs, steam and gas emissions (fumaroles), and diffuse soil degassing.

High thermal fluxes and the intense hydrothermal circulation at Ischia Island have been a matter of interest since the '50s (Ippolito, 1942; Penta, 1949, 1954; Penta & Conforto, 1951a,b). Thermal manifestations on the island have been interpreted as reflecting the surface discharge of a complex and multi-reservoir hydrothermal system, where fluids of formerly meteoric and/or seawater origin get-heated and chemically modified by the interaction with magmatic volatiles (Panichi *et al.*, 1992; Caliro *et al.*, 1999; Inguaggiato *et al.*, 2000; Chiodini *et al.*, 2004).

Chemical and isotopic features of 120 thermal groundwater samples (collected from wells and springs) concentrated along the coastal areas of the island, and of 5 free gas emissions, located in the major fumarolic areas of the island, are here discussed. Data have been acquired during a series of hydrogeochemical surveys, performed between 2006 to 2007, and are here integrated with previous measurements performed by Istituto Nazionale di Geofisica e Vulcanologia (INGV), Sezione di Palermo, in the attempt to provide a comprehensive model of hydrothermal circulation on Ischia.

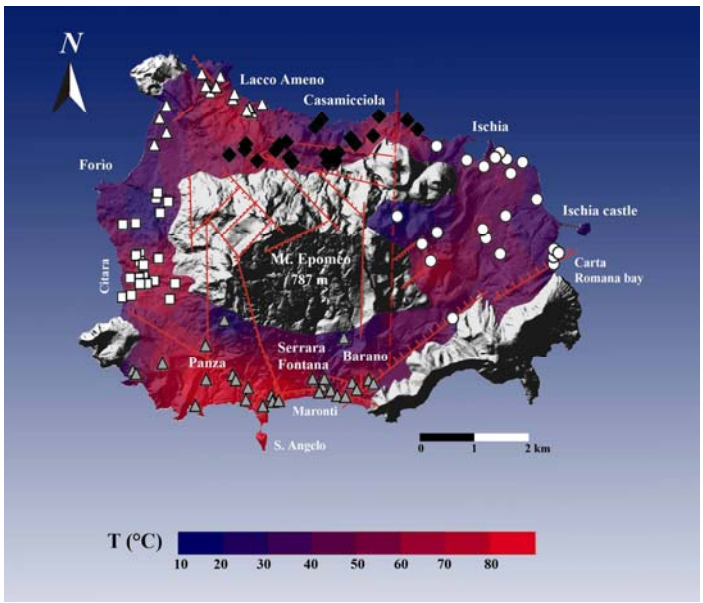

Fig. 1 - Spatial distribution map of discharge temperature of Ischia groundwaters. Samples are distinguished as according to their position: the Eastern-sector (white circles), the Northern-sector (black diamonds), the North-North-Western-sector (white triangles), the Western-sector (white squares) and the Southern-sector waters (grey triangles).

One of the most prominent characteristics of Ischia groundwaters is a remarkable heterogeneity in their chemical composition and physical-chemical parameters. Discharge temperatures measured both in springs and well waters vary in a wide range from 13 to 90°C. Their spatial distribution (Fig. 1) indicates that

the north-western (Casamicciola - Lacco Ameno) and the southern-western sectors (Panza - Serrara Fontana - Barano) are the main thermal areas of Ischia Island, characterised by groundwaters emerging with T > 70°C. In term of temperature, the eastern slope of Mt. Epomeo, a lowland in which volcanism connected with the resurgence phenomenon has been concentrated in the past 10 ka B.P. (Orsi *et al.*, 1991; 2003), is apparently marked by a minor hydrothermal circulation. Indeed, springs and well waters are generally cooler (T ≤ 60°C) than in other areas.

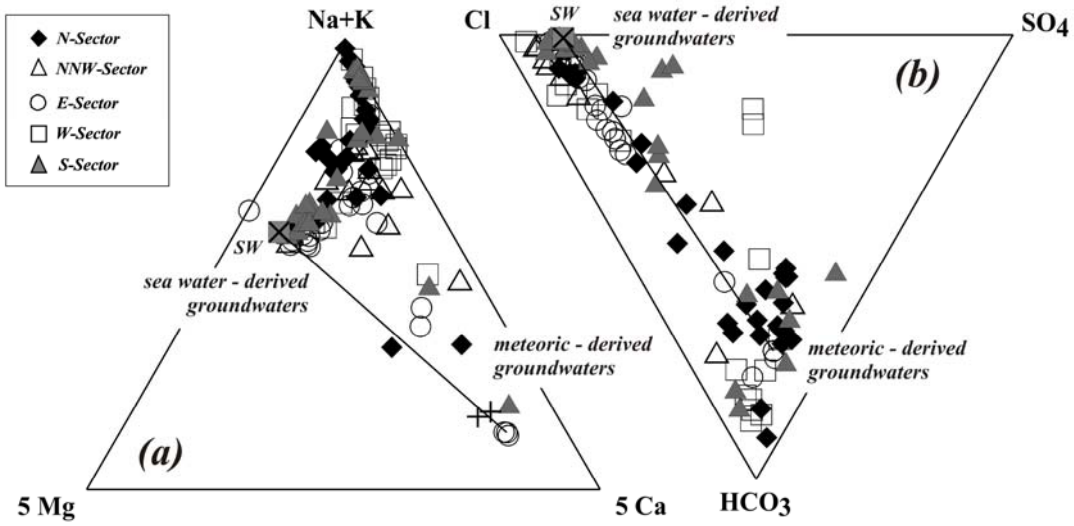

Fig. 2 - In terms of their major dissolved ions, (a) cations and (b) anions, Ischia samples range from calcium-bicarbonate to alkali-chloride groundwaters. Crosses representing rain waters from Vesuvius are from Madonia & Liotta (pers. comm.). The triangular diagrams are drawn from concentrations in mg/l.

The significant heterogeneity of Ischia hydrothermal system is also reflected by total dissolved solids (TDS), which typically increase from inland areas (where more diluted waters with TDS < 1 g/l are recognised) towards coastal areas (where saline waters with TDS > 16 g/l are identified). This trend is an evidence of a multiple recharge of the Ischia hydrothermal system from both sea water and meteoric water, a fact also that fit with major dissolved ion compositions (Fig. 2). For instance, several waters show a clear meteoric signature, having a prevalent bicarbonate composition (Fig. 2b), and being characterised by low TDS, and discharge temperatures (< 25°C) very close to the average annual air temperature. However, only a few data points in Fig. 2 cluster along the meteoric-sea water mixing line. A group of samples plot far below the meteoric-sea water mixing line in Fig. 2b, near the HCO_3 corner: such an enrichment in HCO_3 is also paralleled by higher temperatures (up to 45°C), likely reflecting longer residence time and deeper infiltration in the hydrothermal envelop, where interaction with a CO_2-rich gas phase may occur. On the contrary, saline waters with sea water-like composition have Cl as the prevalent dissolved anion (Fig. 2b), and show enrichments in sodium and potassium and depletion in Mg with respect to sea water composition (Fig. 2a). They likely reflect water-rock interaction processes at high temperatures, which cause leaching of alkali from the reservoir rocks and precipitation of new mineral phases (Mg-bearing) from supersaturated solutions.

The large dataset on the chemical and isotopic composition of groundwater discharges and gas

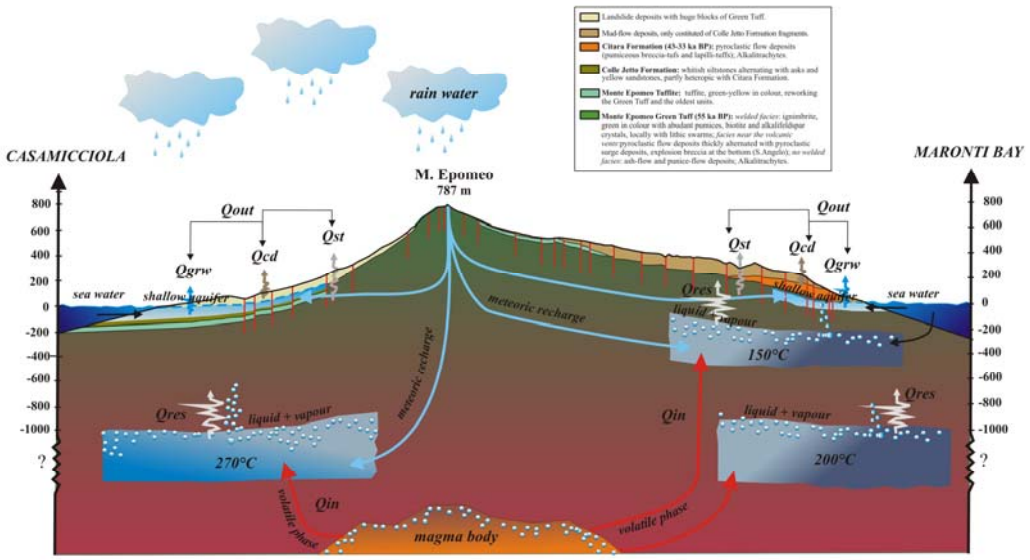

Fig. 3 - Geochemical conceptual model of Ischia geothermal system in a N-S section (from Casamicciola village to Maronti bay).

emissions from Ischia hydrothermal system, presented in this work, has been used to drawn a geochemical model of fluid circulation at depth (Fig. 3), revealing the existence of a complex hydrothermal system composed of at least two superimposed deep reservoirs. As simplified in Fig. 3, the Ischia hydrothermal system is recharged by both meteoric water and sea water. However, groundwater discharges have major and minor ion compositions which can only be partially reproduced by mixing between meteoric and sea water (Fig. 2) requiring that other components (hydrothermal end-members) take part to the mixing processes. Three compositional end-members are identified in this work (Fig. 4), using Mg-depletion in hydrothermal solutions as an index of their maturation, namely an expression of degree of water-rock interaction at high temperature in the deep reservoir. Using this line of reasoning, the chemistry of superficial manifestations suggests, as for the southern Ischia sector, the existence of an hydrothermal end-member (represented by *hydrothermal end-member* "B" in Fig. 4) characterised by low TDS (Cl ~ 1921 mg/l) and isotopically negative ($\delta^{18}O$ ~ -4.98‰) composition. Accepting that this hydrothermal end-member is the surface expression of a deep thermal reservoir, the latter must be thus prevalently recharged by meteoric fluids. On the contrary, *hydrothermal end-member* "C" (Fig. 4), highly saline (Cl ~ 13000 mg/l) and isotopically more positive ($\delta^{18}O$ ~ -0.28‰) than the previous, and thus of likely marine derivation, feeds thermal waters in the western sector of the island (Fig. 3). The chemical dissimilarity between hydrothermal end-members "B" and "C" could seemingly suggests the existence of two distinct reservoirs in the southern and western Ischia sectors. However, this is in conflict with the estimated depths of the thermal reservoirs in the two areas, being remarkably similar. In fact, the deep equilibrium temperatures of *hydrothermal end-members* "B" and "C" (estimated by using classical solute geo-thermometers; Giggenbach, 1983), combined with geothermal gradient data deduced from SAFEN's explorative wells, point to the existence, both at south and west, of a main reservoir located at about ~ 300 m of depth, with equilibrium T ~ 150°C (Fig. 5a,b). In addition, several thermal groundwaters collected in the S-W sector have compositions consistent with the mixing trend between hydrothermal end-members "B" and "C" (see Fig. 4). As such, it is proposed that the same ~ 300 m deep reservoir

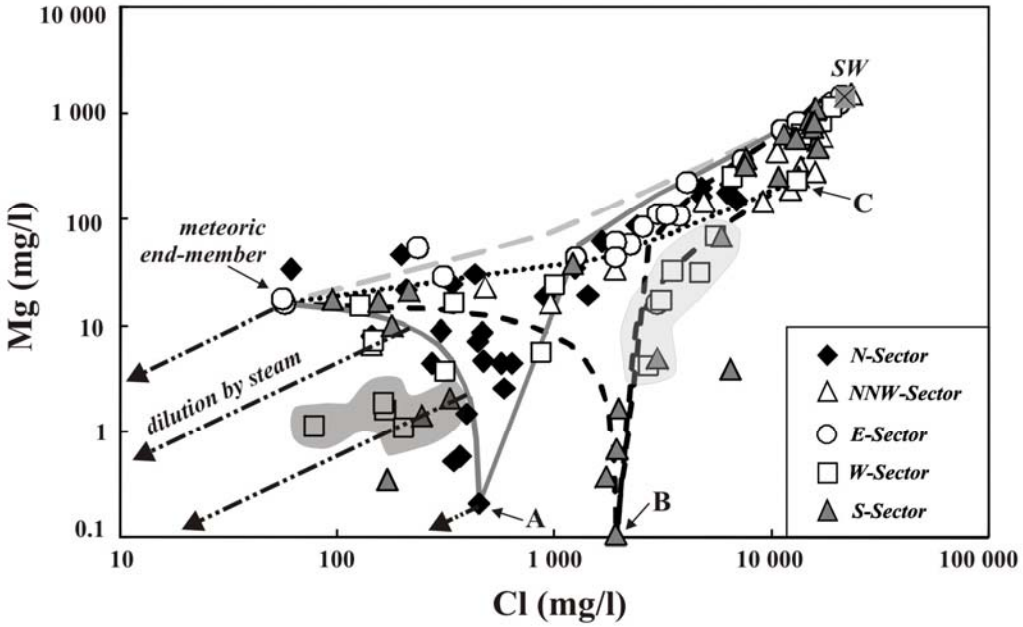

Fig. 4 - Magnesium versus chlorine concentrations. The plot suggests that the compositional range of thermal manifestations on the island reflects the mixing of at least 5 component, namely: i) sea water, infiltrating on coastal areas along the margins of the thermal field; ii) meteoric water; iii) end-member A, iv) B and v) end-member C, Grey dashed line represents the meteoric-sea water mixing, while mixing between meteoric and sea water and the end-members A, B and C are indicated by dark grey solid line, black dashed line, and dotted line, respectively. Some samples collected in the western and southern sectors of the island (plotting within the light grey shaded area) do not follow the trends displayed in this figure, and cluster along a line connecting B and C end-members. The scattering of samples from the above mentioned mixing trends towards Mg and Cl poor compositions (samples into the dark grey shaded area) can be interpreted as resulting from dilution by steam which causes heating of the samples and a general depletion in the dissolved ions.

supplies surface hydrothermal manifestations at S and W (Fig. 3). This relatively shallow reservoir is mainly fed by sea waters in the western Ischia sector, and by meteoric water in the southern portion of the island. In addition, both in the southern and western sectors, the existence of second deeper (> 1000 m) reservoir is supported by thermal waters with equilibrium T > 150°C (Figs. 3 and 5a,b); this hot (~ 200°C) reservoir having been captured by the deepest of the SAFEN drillings in the area. Knowledge about the hydrothermal setting in the northern sector of Ischia is poorer, because of the lack of direct depth-T information from deep drillings. Assuming however that the same geothermal gradient observed in the S and W sectors holds true also at N (see Fig. 5c), the very high equilibrium temperatures (up to ~ 270°C) calculated for thermal waters of the latter area suggest that the reservoir is very deep (>> 1000 m) (Fig. 5c). A shallower depth (350-550 m) for this reservoir (but still deeper than at S and W) can be calculated accepting coexistence of liquid and vapour at depth (as it seems indeed to be suggested by several point overlapping the boiling curves in Fig. 5c). Independently from its location, the composition of the *hydrothermal end-member* "A" in Fig. 4 (Cl ~ 450 mg/l and $\delta^{18}O$ ~ -5.29‰) suggests that meteoric waters feed the thermal reservoir in the northern part of Ischia Island. Again, mixing of "A" with both meteoric and sea water in the shallow thermal groundwater system gives rise to the chemical heterogeneity of surface manifestations at Casamicciola and Lacco Ameno. (Fig. 4)

The significant hydrothermal circulation observed at Ischia requires the existence of a large heat

source in the subsurface, which is likely represented by a cooling and degassing magmatic body at depth. The existence of such a degassing magma is also consistent with the observation of widespread interactions of the hydrothermal system with a deep-originated gas phase, indicated as DGC (deep gas component) and being characterised by CO_2 ~ 97% (on a water-free basis), $\delta^{13}C$ = -3.5‰ and R/Ra = 3.5. It must be noted, however, that the composition of such DGC does not univocally supports its magmatic derivation, since an at least partial crustal or mantle origin cannot be ruled out. It is also clear that the composition of the deep-rising gas phase is strongly modified by interaction with (and fractional dissolution in) hydrothermal aquifers, making interpretation of the chemical and isotopic composition of the DGC more questionable. Contrasting dissolved CO_2 content in groundwaters (expressed as molar fraction) against the corresponding isotopic compositions (see Fig. 6), it can be inferred that the ^{13}C-depleted isotopic compositions of CO_2-poor (low X_{CO2}) samples reflect a prevalent contribution from soil-CO_2 ($\delta^{13}C_{CO2}$ = -25‰ *vs.* PDB) and/or atmospheric-CO_2 ($\delta^{13}C_{CO2}$ = -7.9‰). Instead the more positive isotopic compositions observed on increasing dissolved CO_2 contents converge towards the range of isotopic compositions displayed by free gas samples ($\delta^{13}C_{CO2}$ from

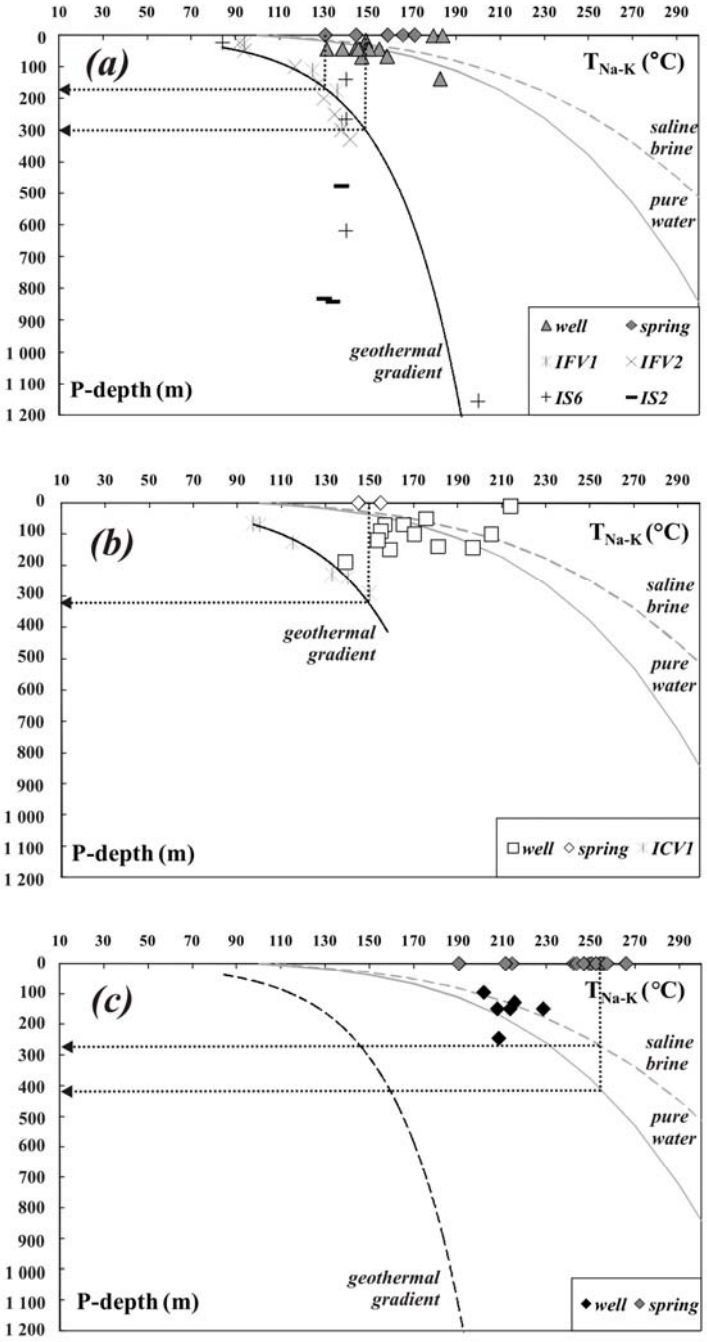

Fig. 5 - Deep equilibrium temperatures for a selection of sampled fluids, calculated from the Na-K geothermometer, are contrasted against the depth of groundwaters below the ground level (0 m for springs). (a) S-sector, (b) W-sector and (c) N-sector. Boiling curves (for pure water and 5% NaCl brine) are drawn to reference. In plots (a) and (b) SAFEN's wells relative to the examined sector are also reported (data from Ippolito, 1942; Penta, 1949, 1954; Penta & Conforto, 1951a,b). See text for explanation.

-6.65 to -2‰). Accepting that the averaged composition of Ischia fumaroles ($\delta^{13}C_{CO2}$ and X_{CO2} of -3.5‰ and 0.97 mol/mol, respectively), computed from samples most enriched in CO_2 (and thus likely near to the features of the deep gas), is representative of the ^{13}C-rich deep-gas component (DGC), the soil-DGC and air-DGC mixing curves have been calculated (dashed grey and solid black lines in Fig. 6). These cover only partially the observed compositional variability in Fig. 6, however, since a significant number of samples have compositions unaccounted for by the above mixing processes. In particular, several samples have $\delta^{13}C_{CO2}$ values far more negative that the model curves could explain. In line with what previously introduced by Caliro *et al*. (1999) and Inguaggiato *et al*. (2000), it can thus be proposed that these ^{13}C-depleted compositions likely reflect the occurrence of isotopic fractionation processes involving the DGC upon its interaction (dissolution) with the aquifer(s). The processes potentially taking place during $CO_{2(g)}$-groundwater interaction have been modelled by using the Rayleigh-type fractionation. Model curves in Fig. 6 were calculated in a range of *p*H (6-8) and temperatures (25 and 100°C) relevant to the system under investigation. In such conditions, model calculations indicate that ^{13}C is preferentially partitioned to the aqueous phase, leading to net ^{13}C-decrease in the residual $CO_{2(g)}$ with a decreasing of residual gas fraction (F) (Capasso *et al*., 1997). The largest fractionations, and the best agreement between modelled and natural compositions, are observed at neutral to basic conditions and at low temperatures (25°C).

In the assumption that magma degassing at depth is currently the driving force for hydrothermal circulation, a simplified thermal budget has been carried to get a first tentative assessment of the volume

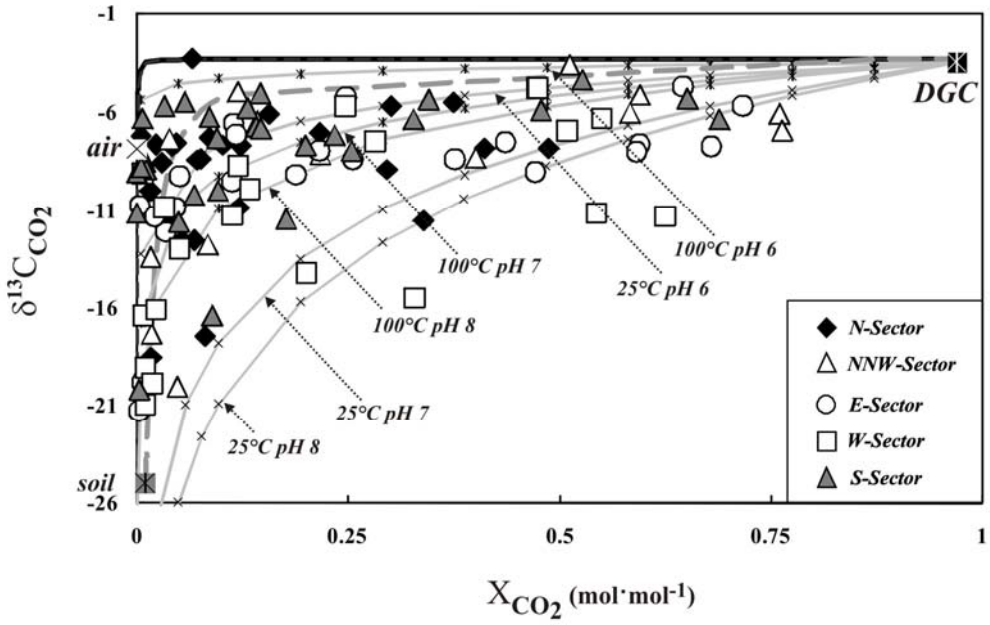

Fig. 6 - Isotopic composition of dissolved CO_2 in equilibrium with groundwaters, plotted versus dissolved CO_2 contents. The isotopic composition of the CO_2-richest waters is consistent with isotopic signature of the hypothesized local magmatic end-member (DGC = deep gas component, with $\delta^{13}C_{CO2}$ of -3.5‰ and X_{CO2} = 0.97 mol/mol). More negative isotopic values reflect mixing between magmatic gases (DGC) and air (black solid line) and/or a soil component (grey dashed line) for soil with CO_2 = 1% in vol.. Departures of samples from the above mixing trends are ascribed to isotopic fractionations involving the rising magmatic CO_2-rich gas phase upon partial dissolution into the shallow aquifer. Solid grey lines, drawn in this plot, model this phenomenon, and represent Rayleigh's fractionation curves calculated at the T and *p*H conditions indicated.

of such a source. At this aim, I have here evaluated the thermal energy dissipated by the shallow hydrothermal system (Q_{out} in Fig. 3) at Ischia at 4.8-6.9·10^{12} kJ/yr. This is calculated summing three different amounts:

- Q_{grw} (in Fig. 3), the heat required to warm the infiltrating waters (meteoric and sea water), feeding the shallow aquifer at an average temperature of ~ 15°C, up to the high temperatures observed in surface discharges;

- Q_{cd} (in Fig. 3), the amount of heat lost from the shallow thermal groundwater system by conduction to the overlying rocks;

- Q_{st} (in Fig. 3), the amount of heat dissipated through steam transport and condensation in the very near-surface (in the soil system) of active fumarolic fields over the island

In a steady-state condition, it is reasonable to hypothesise that the amount of thermal energy dissipated by the shallow thermal groundwater system (which is referred as Q_{out} in Fig. 3) is perfectly balanced by the energy supply from the deep hydrothermal reservoirs (Q_{res} in Fig. 3) through the ascent of a liquid+vapour phase. In turn, heat is supposed to be persistently supplied to deep reservoirs from a degassing and cooling deep magmatic system (Q_{in} in Fig. 3). Thus, the above-calculated surface energy release (Q_{out}) provides a first (though indirect) assessment of the amount of heat Q_{in} (in Fig. 3) convectively transferred from the cooling magmatic body (which is thought to lie at depth in the subsurface of the volcano, but which location and volume are unknown). In addition, the estimated Q_{in} potentially offers a viable pathway for estimating the volume of magma currently feeding heat and volatiles to the hydrothermal system. Making the simplified assumption that this heat is provided to the hydrothermal system in convective form (*e.g.* through the ascent of a water vapour-dominated gas phase released from the degassing magma), it can be estimated that the complete degassing of 2.2-3.2·10^7 m^3 of trachytic magma (with an average value of 2.1 wt.% dissolved H_2O content; Sbrana, 2007) is required every years to account for the release of 1.2-1.7·10^6 tons of magmatic water. Once extrapolated to entire period of quiescence lasting since the last Ischia eruption in 1302 A.D., this volume corresponds to 1.5-2.2·10^{10} m^3 of magma degassed in about 700 years of quiescent activity.

Finally, data presented in this work also contribute to set a baseline for the (minor, non-volcanogenic) temporal changes in the chemistry of Ischia's thermal manifestations; and give indications on the kind of chemical variations which might herald a volcanic unrest in this densely populated area. Accepting that renewal of volcanic activity at Ischia requires replenishment of the volatile-poor alkali-trachytic stored magma with more primitive volatile-rich basaltic magma (Civetta *et al.*, 1991), I suggest that this event might be captured as an increase in the release of magma-derived CO_2 (and possibly He) in the shallow hydrothermal system, here evaluated at ~ 1·10^4 to ~ 7·10^5 tons/yr; a process which should also lead to a shift towards ever more CO_2-rich and ^{13}C-rich compositions in the sampled surface manifestations of the hydrothermal system. An alteration of the mixing relations between the different components (meteoric water, sea water and hydrothermal end-members) could also be anticipated to occur, in response to magma-induced modifications in the structural regime of the island.

REFERENCES

Caliro, S., Panichi, C., Stanzione, D. (1999):Variation in the total dissolved carbon isotope composition of thermal waters of the Island of Ischia (Italy) and its implications for volcanic surveillance. *J. Volcanol. Geotherm. Res.*, **90**, 219-240.

Capasso, G., Favara, R., Inguaggiato, S. (1997): Chemical features and isotopic composition of gaseous manifestations on Vulcano Island (Aeolian Islands, Italy): an interpretative model of fluid circulation.

Geochim. Cosmochim. Acta, **61**, 3425-3440.

Chiodini, G., Avino, R., Brombach, T., Caliro, S., Cardellini, C., De Vita, S., Frondini, F., Granieri, D., Marotta, E., Ventura, G. (2004):. Fumarolic and diffuse soil degassing west of Mount Epomeo, Ischia, Italy. *J. Volcanol. Geotherm. Res.*, **133**, 291-309.

Civetta, L., Gallo, G., Orsi, G. (1991): Sr and Nd isotope and trace element constraints on the chemical evolution of the magmatic system of Ischia Italy. in the last 55 Ka. *J. Volcanol. Geotherm. Res.*, **46**, 213-230.

Giggenbach, W.F., Gonfiantini, R., Jangi, B.L., Truesdell, A.H. (1983): Isotopic and chemical composition of Parbati Valley geothermal discharges, NW-Hymalaya, India. *Geothermics*, **12**, 199-222.

Inguaggiato, S., Pecoraino, G., D'Amore, F. (2000): Chemical and isotopic characterisation of fluid manifestations of Ischia Island. *J. Volcanol. Geotherm. Res.*, **99**, 151-178.

Ippolito, F. (1942): Su alcuni pozzi profondi del napoletano. *Boll. Soc. Nat. Napoli*, **53**, 134-140.

Orsi, G., Gallo, G., Zanchi, A. (1991): Simple-shearing block resurgence in caldera depression. A model from Pantelleria and Ischia. *J. Volcanol. Geotherm. Res.*, **47**, 1-11.

Orsi, G., de Vita, S., Di Vito, M., Isaia, R., Nave, R., Heiken, G. (2003): Facing volcanic and related hazards in the Neapolitan area. *In*: "Earth sciences in cities", G. Heiken, R. Fakundiny & J. Sutter, eds. *Am. Geophys. Union, Spec. Publ.*, Washington, 121-170.

Panichi, C., Bolognesi, L., Ghiara, M.R., Noto, P., Stanzione, D. (1992):. Geothermal assessment of the island of Ischia (southern Italy) from isotopic and chemical composition of the delivered fluids. *J. Volcanol. Geotherm. Res.*, **49**, 329-348.

Penta, F. (1949): Temperature nel sottosuolo della regione Flegrea. *Ann. Geofis.*, **2**, 327-346.

Penta, F. (1954): Ricerche e studi sui fenomeni esalativo-idrotermali e il problema delle "forze endogene". *Ann. Geofis.*, **8**, 317-408.

Penta, F. & Conforto, B. (1951a): Sulle misure di temperatura del sottosuolo nei fori trivellati in presenza di acqua e sui relativi rilievi freatimetrici in regioni idrotermali. *Ann. Geofis.*, **4**, 41-93.

Penta, F. & Conforto, B. (1951b): Risultati di sondaggi e di ricerche geominerarie nell'Isola di Ischia dal 1939 al 1943, nel campo del vapore, delle acque termali e delle "forze endogene" in generale. *Ann. Geofis.*, **4**, 159-191.

Sbrana, A. (2007): Final Report INGV-DPC Project V3_3/11 (Ischia).

ERUPTIVE PROCESSES IN THE AVERNO 2 ERUPTION (CAMPI FLEGREI - ITALY): CONSTRAINTS BY PHYSICAL PROPERTIES OF THE JUVENILE FRAGMENTS

CÉLINE FOURMENTRAUX
Dipartimento di Scienze della Terra, Università di Pisa, Via S. Maria 53, 56126 Pisa

ABSTRACT

The Averno 2 eruption (Av2) occurred 3.7 ka b.p in the northwest sector of the Campi Flegrei caldera (CFc), at the intersection of NE-SW and NW-SE fault systems bordering the resurgent block. The eruption, one of the youngest of the caldera, was followed only by the 1538 AD eruption of Monte Nuovo. 21 representative samples of Av2 deposits were analyzed for grain-size and componentry whereas 16 depositional units (about 100 juvenile clasts each) were sampled to measure bulk density, bulk vesicularity and assess texture characteristics of individual clasts. According to bulk density, vesicularity and textural data, three main pyroclasts types were identified: i) low-density, light coloured, microvesicular, microlite-free; ii) high-density, dark-brown, microlite-rich; iii) banded made up to mm-thick stripes of (i) and (ii) types. The three types record variations of magma properties resulting from various degassing histories and syn-eruptive crystallization of groundmass. Characteristics and relative abundance of juvenile clast types throughout the stratigraphic sequence were used to make inferences and place constrains on temporal variations in magma rise and eruptive mechanisms. Occurrence in the very early fallout bed of dense juvenile clasts suggests the initial disruption of a limited volume of degassed magma. Member A was dominated by type (i) clasts suggesting that plinian episodes were fed by the fast supply of volatile-rich highly evolved magma from below whereas subsequent eruptions were fed by volatile poor-magma less evolved (member C). Members B and C contain (i), (ii), and (iii) types and increasing abundance throughout time of clasts (ii) and (iii) suggests increasing importance of intra-eruption degassing, mostly occurring during time breaks between two successive eruptive pulses. The pulsating activity of Av2 appears to be transitional in style between subplinian and vulcanian and we propose that transitions in eruptive style from plinian to surge activity were controlled by magmatic processes and not by water-magma interaction.

INTRODUCTION

Recent activity in the CFc has been dominated by explosive eruptions of variable magnitude that generated alternating fallout beds and pyroclastic-surge deposits (*e.g.*, Barberi *et al.*, 1988, Wohletz *et al.*, 1995; De Vita *et al.*, 1999; Dellino *et al.*, 2001, 2004). Several authors have emphasized that the explosivity of most events requires in part, the exsolution of magmatic volatiles (formation of pumice) and, in part, the interaction of magma with water (formation of wet, accretionary lapilli-rich, ash deposits). Starting from this concept, several authors have also attempted to discriminate magmatic versus hydromagmatic phases on the basis of different criteria. Some have considered base surge deposits to have been generated by magma-water interaction; others have used clast morphological features (ash grains) to discriminate between different mechanisms of magma fragmentation (Wohletz, 1983; Cioni *et al.*, 1992; Büttner *et al.*, 1999, 2002). However, several studies have suggested that variations in explosive

eruptive style can be explained by changes in magma properties due to groundmass crystallization and corresponding changes in magma rheology. Indeed, recent textural studies of volcanic products from historical Campi Flegrei eruptions (*e.g.*, D'Oriano *et al.*, 2005; Mastrolorenzo *et al.*, 2006) provide evidence that degassing and crystallisation during magma ascent could strongly influence the style and evolution of the eruption. Syn-eruptive degassing/crystallisation has been shown to be a very effective process in controlling Vulcanian style eruptions of calc-alkaline composition. Recent examples include Mount St. Helens (USA) in 1980 (Cashman & Mc Connell, 2005), Galeras (Colombia) in 1992 (Stix *et al.*, 1997; Cruz & Chouet, 1997), Souffrière Hills (Monserrat) between 1995 and 1999 (Druitt & Kokelaar, 2002; Formenti *et al.*, 2003), Guagua Pichincha (Ecuador) in 1999 (Wright *et al.*, 2007).

The Av2, dated at 3700 years BP (Alessio *et al.*, 1971), is one of the youngest and best preserved volcanic structures of the CFc (Fig. 1). Av2 represented a moderate-magnitude event in the volcanic history of CFc and was characterized by complex eruptive activity with alternating plinian to surge

Fig. 1 - View of Averno lake.

activity that generated a sequence of pyroclastic-fall and -ash deposits. According to Di Vito *et al.* (2001) and Braia (2003) deposits are subdivided in three members named A, B, and C (Fig. 2). The lower member A (Fig. 2a and 2b) consists of 6 pumice fallout beds intercalated to thin ash and lapilli beds (surge). The upper members (B and C) are mainly dominated by dry surges beds and minor wet surges (Fig. 2c and 2d). Previous workers have concluded that the explosive activity evolved from prevalent magmatic (member A) to pure hydromagmatic style (members B and C). Thus, the eruption of Av2 provides an ideal case to investigate possible differences between juvenile clasts of varying eruptive dynamics with the aim of better documenting the actual role of magmatic explosivity and its evolution with time. Our research is carried out in order to investigate the responsible mechanisms for the evolution in eruptive style that generated this complex pyroclastic sequence. Here, we present data on the physical properties (bulk density, bulk vesicularity, and macro and micro-texture) of the juvenile clasts. The Av2 eruption represents a possible scenario expected in this sector of the caldera, in case of a future eruption. Therefore, this subject represents a fertile area of research since it improves our knowledge of the CFc eruptions and may be important in terms of volcanic hazard assessment and risk management at CFc.

RESULTS

Macroscopic texture of the juvenile clasts

Pumice clasts from the fallout and surge deposit are heterogeneous and show a large variability in morphology and texture. Clasts are distinct in their colours and differ in density, vesicle content, size,

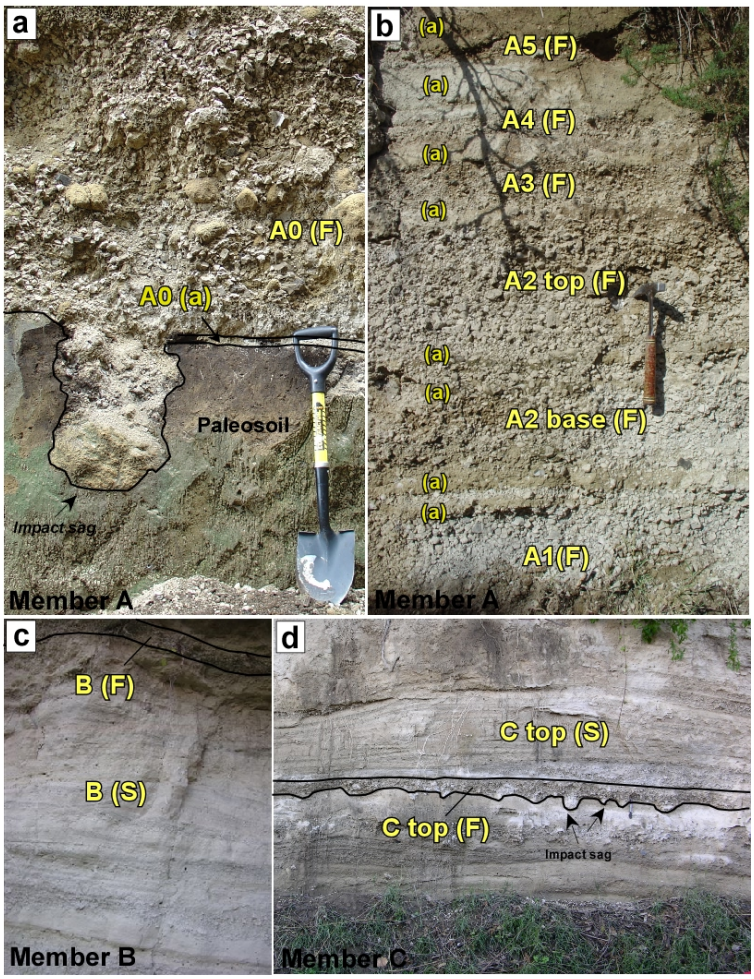

Fig. 2 - (a) Member A fallout bed A0(a) associated with coarse grained A0(F) fallout bed; (b) fallout deposits from A1(F) to A5(F) intercalated to minor ash-surge beds (a); (c-d) Member B and member C respectively, dominated by surge sequence (S) with subordinate fallout beds (F).

shape and spatial distribution. As a result, three morphological clast types are distinguished: light-coloured clasts, banded, and dark-brown coloured clasts (Fig. 3).

i) Light-coloured clasts are microvesicular pumice displaying both isotropic (Fig. 3a) and tubular (Fig. 3b) textures. They are extremely to moderately vesicular, containing vesicles that vary in shape (from tubular to contorted or spherical) and dimension.

ii) Dark brown clasts are, in general, angular and either non-vesicular or very poorly-vesicular, dense with superficial fractures. Some blocks contain angular lithic fragments which can be interpreted as the incorporation of the walls of the conduit during the ascent of the magma in a high shear environment (Fig. 3d).

iii) Banded clasts cover a wide range of morphological features from highly vesicular to poorly vesicular, and are characterized by an alternation of white/yellow and dark or pale grey/brown bands (Fig. 3c). A few banded bomb exhibit breadcrusted forms typical of vulcanian eruptions. Included in this category are clasts with alternating non-vesicular dark-brown coloured and obsidian texture bands (Fig. 3c).

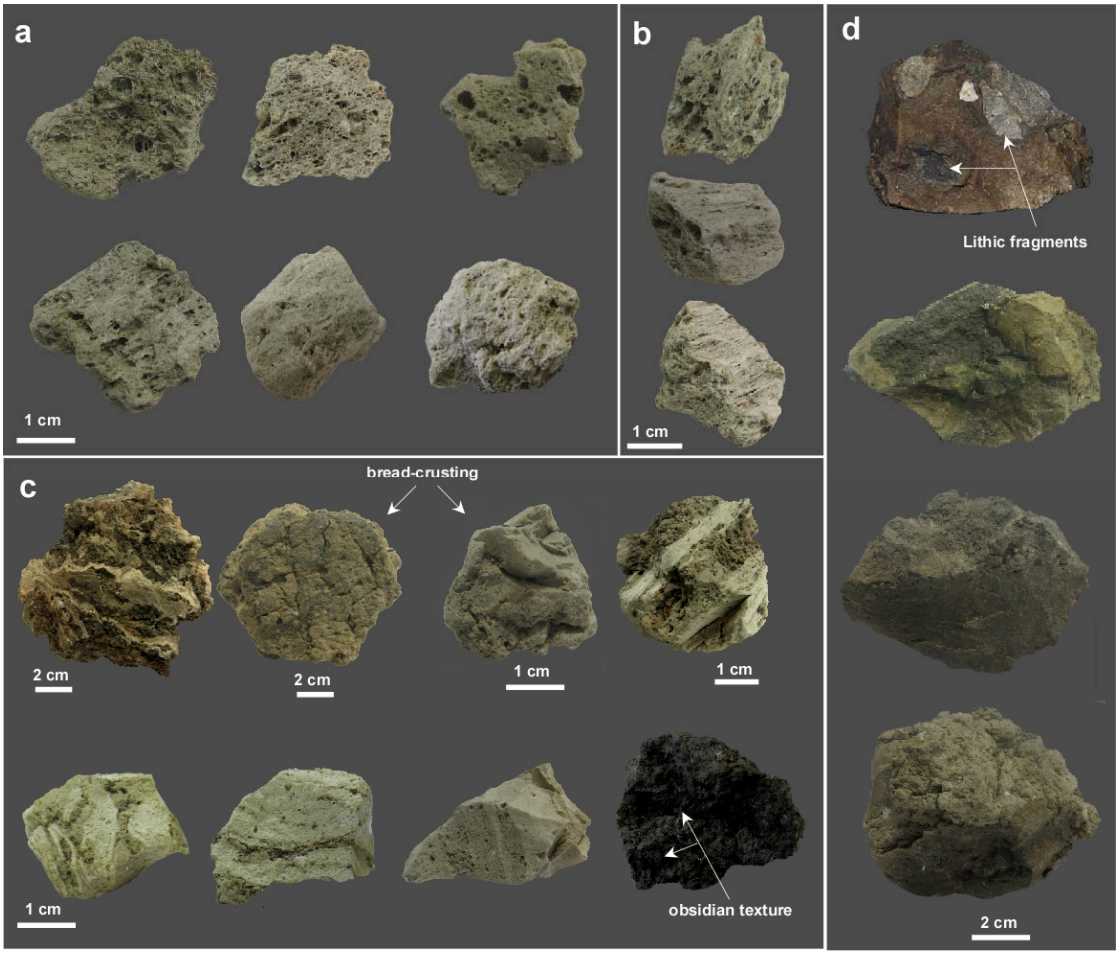

Fig. 3 - Examples of Juvenile products from Averno 2 euption. General view of: (a) light-coloured clasts with isotropic texture; (b) light-coloured clasts with tubular texture; (c) banded pumice with obsidian-like texture and clasts showing bread-crusting; (d) dark-brown coloured types. (c) and (d) show bread-crusting.

Clast density and vesicularity

Density was measured on 1589 clasts taken from 15 layers sampled through the entire stratigraphic sequence (Table 1). In each member, clasts of fallout and surge deposits show a wide variation in density of juvenile clasts ranging from 300 to 2500 kg/m^3 and corresponding to a vesicularity range of 89-8% (Table 1). According to the classification scheme proposed by Houghton & Wilson (1989), clasts range from extremely to poorly-vesicular. To provide a full description of the evolution of parameters during the Averno 2 eruption, we introduced in the density histograms the three morphological clasts type identified (Fig. 4 and 5). It can be immediately observed that, the variation of densities observed in fallout and surge deposits reflects variations in clast types. Microvesicular clasts have the lowest density (530 to 660 kg/m^3), while dark brown clasts have the highest density (1660 1820 kg/m^3). Banded clasts are intermediate with the widest density range from 500 to 1130 kg/m^3. All samples of the member A, except the two lowermost ones A0 and A1, have an uniform density (Table 1 and Fig. 4). In details, the fallout beds of member A are characterized by an unimodal distribution containing uniform pumice assemblage

Table 1 - Average of bulk rock density and vesicularity of Averno 2 juvenile components; n: number of clasts; ρ: density; σ: standard deviation; the second number in the label indicate the number of the outcrop.

Sample	Deposit	Member	n	Average ρ (10^3 kg m^{-3})	σ (10^3 kg m^{-3})	ρ range (10^3 kg m^{-3})	Vesicularity (% vol)	σ (% vol)	Vesicularity range (% vol)
A0- (1)	Fallout	A	100	0.61	0.23	0.3-1.5	77.4	8.7	46.5-89.6
A1- (2)	Fallout	A	100	0.49	0.09	0.4-0.8	81.8	3.2	71.3-88.2
A2 b- (2)	Fallout	A	100	0.57	0.17	0.4-1.5	79.1	6.2	45.7-88.2
A2 t- (2)	Fallout	A	100	0.53	0.12	0.4-0.9	80.6	4.3	67.4-87.6
A3- (2)	Fallout	A	100	0.53	0.12	0.4-1.1	80.5	4.5	58.3-88.5
A4- (2)	Surge	B	102	0.73	0.36	0.4-1.9	73.1	13.3	32.9-88.5
B b- (3)	Fallout	A	100	0.57	0.19	0.4-1.5	79.1	7.1	44.9-87.6
B t- (4)	Fallout	C	99	0.67	0.26	0.4-1.5	75.4	9.4	47.1-88.8
C mb- (5)	Surge	C	119	0.89	0.33	0.4-2.0	67.2	12.2	26.4-85.5
C mb- (7)	Fallout	C	100	0.72	0.26	0.4-1.7	73.4	9.7	39.7-87.7
C t- (5)	Surge	C	109	0.86	0.37	0.4-2.5	68.3	13.5	10.9-85.7
C t- (5)	Surge	C	120	0.56	0.19	0.4-1.9	80.3	5.7	30.8-90.1
C t- (6)	Surge	C	120	0.61	0.20	0.4-1.5	77.6	7.2	46.1-87.5
C mb-s1 (5)	Surge	C	120	0.86	0.37	0.4-2.1	68.3	13.6	23.6-87.6
C mb-s2 (5)	Fallout	C	100	0.75	0.38	0.4-1.9	72.5	13.4	32.3-87.6
C mb-s3 (5)	Fallout	C	109	0.88	0.36	0.4-1.9	67.6	14.0	29.9-85.3

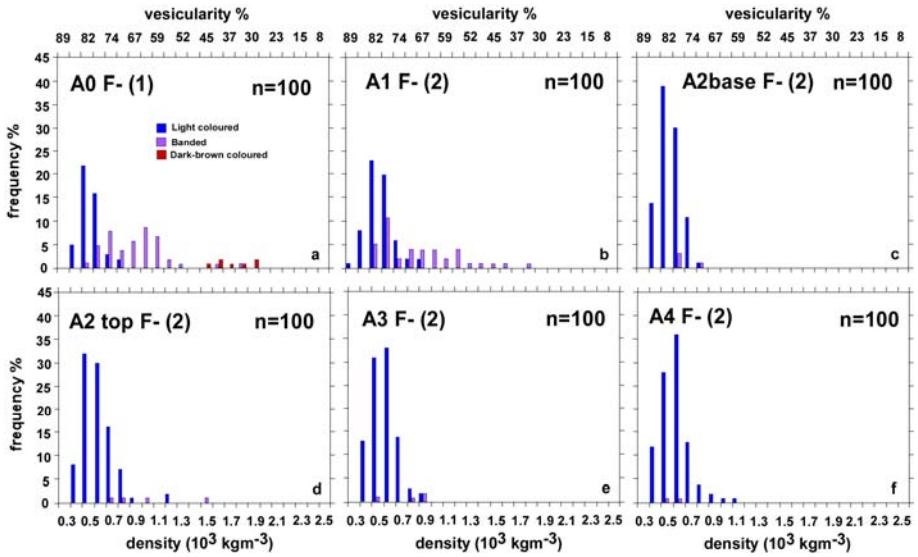

Fig. 4 - (a-f) Density/vesicularity distribution of Averno 2 pyroclasts from each fallout deposit of member A. Excluding A0 F and A1 F, deposits contain uniform pumice assemblages, with a single sharp peak of density and vesicularity of 500 kg m^{-3} and 82% respectively. Letters denote: F, fallout; n, number of analysed clasts. Vesicularity values are derived using a measured DRE value of 2714 kg m^{-3}.

with a single, sharp peak between 500 and 600 kg/m^3 corresponding to a vesicularity range of 82-78%. A0 and A1 fallout are clearly heterogeneous layers exhibiting the widest range in density from 400 to 1900 kg/m^3 and 300 to 1500 kg/m^3 respectively. Density of fallout and surge deposits in member B range

from 400 to 1900 kg/m^{-3} and reflect the large variability of banded clast (Fig. 5a-b). Density distributions of analysed samples of member C from both fallout and surge deposits are bimodal (Fig. 5c-f). Densities

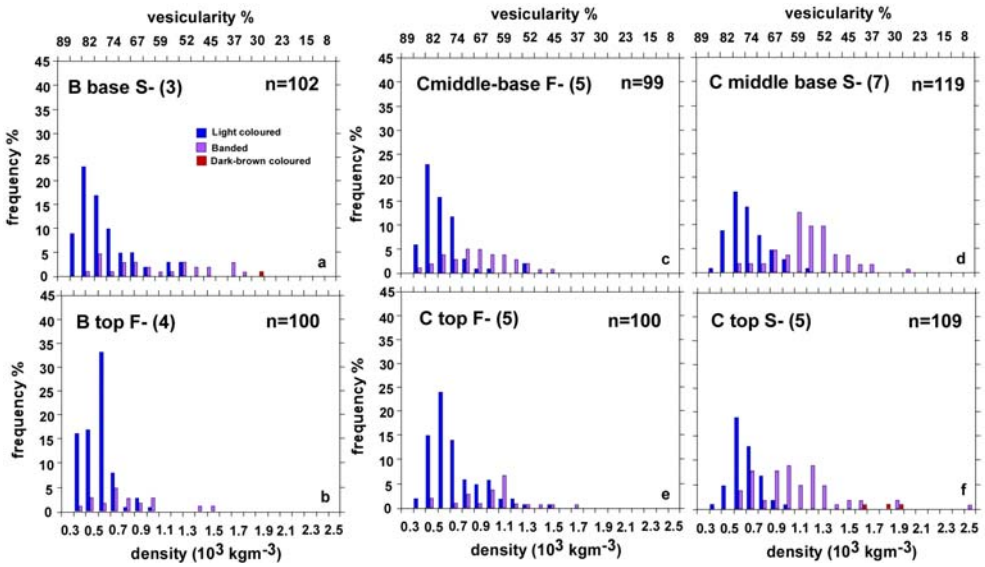

Fig. 5 - (a-b) Density/vesicularity distribution of Averno 2 pyroclasts from fallout and surge deposits of member B. (c-g) Density/vesicularity distribution of Averno 2 pyroclasts from fallout and surge deposits of member C. Letters denote: F, fallout; S, surge; n, number of analysed clasts. Vesicularity values are derived using a measured DRE value of 2714 kg m^{-3}.

cover a wide range from 400 to 2500 kg/m^3. The density shifts from the base (400-1500 kg/m^3) in Cmb-(5) to (400-2500 kg/m^3) in Ct-(5) (Fig. 5). We note that each deposit contains highly vesicular clasts showing peaks at minimum densities 500-600 kg/m^3. The overall deposits of member C are more heterogeneous exhibiting an apparent secondary peak toward to highest densities from 1,000 kg/m^3 to 1,400 kg/m^3 which correspond to a vesicularity range of 63-48%. Clast density/vesicularity data highlights the contrast between member A, B and C. Each heterogeneous sample through the stratigraphic sequence probably represents a mixture of a highly vesiculated magma and partially degassed magma which formed during time breaks at shallow depth.

Microscopic texture of the juvenile clasts

To determine the relationship between density and groundmass crystallinity, we examined thin sections of representative juvenile clasts using both optical microscopy and SEM. Indeed, a positive correlation between microlite crystallization and density and negative correlation with vesicularity is related to variations in rates of magma ascent. This correlation can be directly attributed to the times available for gas loss (Jaupart, 1998) and degassing-induced crystallization (*e.g.*, Hammer *et al.*, 1999). BSE images taken at low magnification offer a general view of each clast types (Fig. 6). On the basis of pyroclasts density and groundmass texture, we have identified the three different pyroclasts types described above. (i) Light coloured, microvesicular clasts which have a low density (ρ) (ρ < 900 kg/m^3) are highly vesicular and found in all deposits. They can exhibit subspherical vesicles whose diameter is

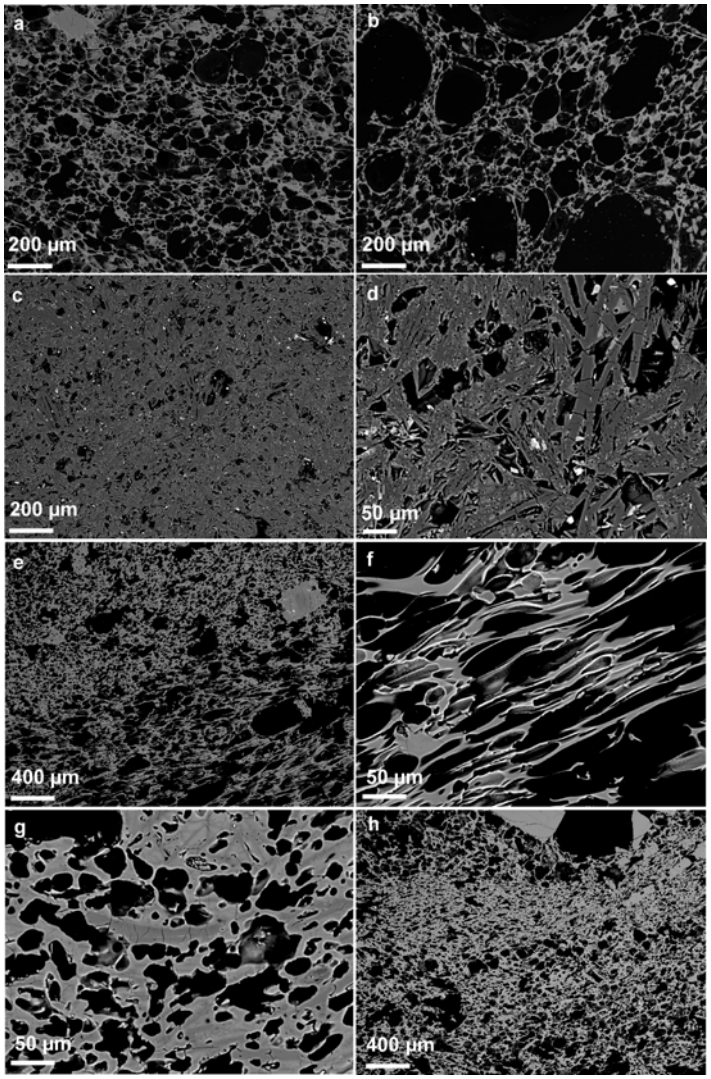

Fig. 6 - Backscattered electron (BSE) images of representative pyroclast types. a-b light-coloured, microvesicular pumice; scale bar = 200 µm; c-d dark brown-coloured clast; scale bars = 200 µm and 50 µm, respectively; e banded pumice clasts of member A; scale bar = 400 µm; f white band in banded pumice clasts of member A; scale bar = 50 µm; g brown dark band in banded pumice clats of member A, scale bar = 50 µm; h banded pumice clast of member C; scale bar = 400 µm. Black irregular shapes are vesicles, grey background is glass, grey crystals are plagioclase and sanidine, white crystals are oxide phases.

generally less than 50 µm in diameter (Fig. 6a) or larger deformed vesicles with a large diameter (up to one millimeter) associated with smaller vesicles which tend to be subspherical in a glassy groundmass (Fig. 6b). Highly elongated and stretched vesicles aligned into a preferred direction are exhibited by tube pumice clasts (Fig. 6f). (ii) Dark brown coloured clasts with the highest density (1500-2100 kg/m^3) have a vesicularity which decreases in terms of both vesicle abundance and dimension (Fig. 6c). These clasts have a holocrystalline texture containing microphenocrysts (up to 250 µm) either as isolated or as clusters (Fig. 6d). (iii) Banded clasts exhibit a wide range of densities (ρ = 400-2000 kg/m^3) reflecting the wide range of morphological features of these clasts. They have a vesicularity and groundmass crystallinity which are organised in bands (Fig. 6e, 6h). The light bands have a heterogeneous vesicularity, with large vesicles from elongated (Fig. 6f) to large or small subspherical whereas in dark bands have large deformed vesicles associated with small spherical vesicles (Fig. 6g). Banded clasts show a range of clasts densities that reflects a variably crystallised groundmass, band with light coloured groundmass exhibit the absence (Fig. 6f) or some microlite while band dark colour are always microlite-rich (Fig. 6g). The banded clasts with obsidian have the highest density (ρ = 2500 kg/m^3). Examination of pyroclastic

obsidian microtexture reveals the alternation of dark brown and glassy bands with spherulitic texture. The obsidian bands have large deformed and elongated vesicles and contain some microlites. The dark-brown bands have a holocrystalline groundmass textures with irregular vesicles (50-100 μm).

DISCUSSION

Using, bulk density, vesicularity and textural data, three main pyroclast types were identified: i) low-density, light coloured, microvesicular, microlite-free clasts; ii) high-density, dark-brown, microlite-rich clasts; iii) banded clasts made up of mm-thick stripes of (i) and (ii) types. The light-coloured microvesicular pumices (heterogeneous vesicles and elongated/deformed vesicles) are typical product of magmatic explosive eruptions. The origin of pumice clasts with different textural and morphological characteristics is attributed in the literature to the development of conduit regions marked by different rheological behaviour (see Cashman *et al.*, 2000; Polacci *et al.*, 2001, 2003). The central part of the conduit is occupied by microvesicular pumice clasts whereas tube-shape pumices are suggested to originate in the region between the center and the conduit walls by both high strain rates in response to shearing at the conduit walls and elongational strain during magma ascent (Sparks *et al.*, 1994; Cashman *et al.*, 2000; Polacci *et al.*, 2001, 2003). Microlite textures are correlated with volatile-loss. Dark-brown coloured clasts are microlite rich and have the lowest vesicularity suggesting that degassing during ascent causes the magma to crystallize. This deduce this with comparison other eruption where occurs the same process (*e.g.*, Cashman *et al.*, 2000, 2005; Hammer *et al.*, 1999). In addition, the occurrence in the deposits of both dark-brown microlite-rich clasts containing foreign lithic fragments inside and obsidian-bearing material suggests that they probably derived from dikes or wall rock fractures filled with "vanguard" magma that, together with wall rocks, were eroded and incorporated into (Rust & Cashman, 2007). We also suggest that banded clast were be formed by pure syn-eruptive mingling of deeper magma with "vanguard" magma that was involved in creating dike fractures and that stalled temporarily at intermediate levels. Also, we propose that the story of Averno 2 eruption can be modelled as follow. During the first phase (member A), the magma that crystallized in response to the degassing was pressurized by new faster-rising magma from depth in the interior part of the conduit, expelled and mingled with the dense and viscous plug producing a heterogeneous fallout bed with a limited amount of dense juvenile clasts (A0 fallout breccia). After this opening stage, 6 fallout beds (from A1(F) to A5 (F)) intercalated by thin ash layers were deposited by pulsatory sub-plinian eruptions with a variable eruptive columns (between 4-10 km high; estimate by Di Vito *et al.*, 2001). This stage was dominated by type (i) clasts (light microvesicular, isotropic and tubular texture) suggesting that, the pulsatory sub-plinian episodes were fed by the fast supply of volatile-rich magma from below. In contrast, the occurrence and increase in abundance of types (ii) and (iii) in the upper unit (member C), suggests the increasing importance of intra eruption degassing, mostly occurring during time breaks between successive eruptive pulses. For each discrete eruptive pulse the progressive decline of the magma supply rate (MSR) and both the reduced pre-eruptive volatile content and the deepening of the fragmentation front (reducing the exit velocity of the gas/pyroclats mixture) favoured the collapse of the eruptive fountain. Intra-pulse degassing was likely responsible for the emplacement of dry to accretionary-lapilli bearing, fine-ash fall out beds separating the surge bedset. The sample from member B represents the transition between the two extremes A and C. Thus, we propose that transitions in eruptive style from plinian to surge activity are the consequence of an eruption controlled by magmatic processes in which each discrete eruptive pulse was fed by the propagation downward of the fragmentation front. Increasing separation between successive

pulses is likely the consequence of a decline of magma supply rate from below. Reduced exit velocities during surge emplacements of B and C members are probably accounted by reduction of magmatic pre-eruptive volatile content and change in magma properties due to degassing and to groundmass crystallization and corresponding changes in magma rheology. Data on juvenile clasts support that fragmentation was dominated by purely magmatic processes, magma-water interaction if present, exerted a subsidiary role in the magma fragmentation and emplacement of surges.

CONCLUSION

The Averno-2 eruption shows a change in eruptive regime through time from dominantly sustained (sub-plinian) to dominantly pulsating (surge). Here, we have shown that data on the physical characteristics (density, vesicularity and macro and micro-texture) of the juvenile clasts are fully accounted by an eruptive mechanism regulated by the interplay of magma supply rate, syn-eruptive degassing and microlite crystallization of magma in the conduit. The implications of this conclusion are many. Firstly, it provides an explanation for producing dense juvenile clasts without calling on interaction with external water. Secondly, it suggests that microlite in these pyroclasts preserve a detailed record of variations in magma ascent and degassing rates throughout the eruptive sequence. Lastly it requires temporary storage of magma at shallow levels before each eruptive pulse. Our interpretation accounts for the occurrence of the juveniles with contrasting densities and texture in the deposits and the increasing abundance through time of dense juvenile (ii) and (iii) types. Although the eruption consisted of a large number of discrete explosive pulses it is likely that the entire eruption occurred within a short period of time (hours to days). In contrast with previous interpretations, our data on the physical nature of the magmatic component also indicates that important involvement of external water is not required to account for the magma fragmentation and eruptive dynamics.

REFERENCES

Alessio, M., Bella, F., Improta, F., Belluomini, G., Cortesi, C., Turi, F. (1971): University of Rome C-14 dates IX. *Radiocarbon*, **13**, 395-411.

Barberi, F., Navarro, M., Rosi, M,. Santacroce, R. (1988): Explosive interaction of magma with ground water: insights from xenoliths and geothermal drillings. *Rend. Soc. It. Mineral. Petrol.*, **43**, 901-926.

Braia, G. (2003): Metodologie quantitative per la ricostruzione dei meccanismi eruttivi di eruzioni esplosive: il caso di Averno 2 nella caldera dei Campi Flegrei. Ph.D. tesi, Università di Bari.

Büttner, R., Dellino, P., Zimanowski, B. (1999): Identifying magma-water interaction from the surface features of ash particles. *Nature*, **401**, 688-690.

Büttner, R., Dellino, P., La Volpe, L., Lorenz, V., Zimanowski, B. (2002): Thermohydraulic explosions in phreatomagmatic eruptions as evidenced by the comparison between pyroclasts and products from Molten Fuel Coolant Interaction experiments. *J. Geophys. Res.*, **107**, 1-13.

Cashman, K.V. & Blundy, J. (2000): Degassing and crystallization of ascending andesite and dacite. *Phil. Trans. R. Soc.*, **358**, 1487-1513.

Cashman, K.V. & Mc Connell, S.M. (2005): Multiple levels of magma storage during the 1980 summer eruptions of Mount St. Helens, WA. *Bull. Volcanol.*, **68**, 57-75.

Cioni, R., Sbrana, A., Vecci, R. (1992): Morphologic features of juvenile pyroclasts from magmatic and phreatomagmatic deposits of Vesuvius. *J. Volcanol. Geotherm. Res.*, **51**, 61-67.

Cruz, F.C. & Chouet, B.A. (1997): Long-period events, the most characteristic seismicity accompanying the emplacement and extrusion of a lava dome in Galeras Volcano, Colombia, in 1991. *J. Volcanol. Geotherm. Res.*, **77**, 121-158.

Dellino, P., Isaia, R., La Volpe, L., Orsi, G. (2001): Statistical analysis of textural data from complex pyroclastic sequences: implications for fragmentation processes of the Agnano-Monte Spina tephra (4.1 ka), Campi Flegrei, southern Italy. *Bull. Volcanol.*, **63**, 443-461.

Dellino, P., Isaia, R., La Volpe, L. (2004): Interaction between particles transported by fallout and surge in the deposits of the Agnano-Monte Spina eruption (Campi Flegrei, Southern Italy). *J. Volcanol. Geotherm. Res.*, **133**, 193-210.

De Vita, S., Orsi, G., Civetta, L., Carandente, A., D'Antonio, M., Di Cesare, T., Di Vito, M., Fisher, R.V., Isaia, R., Marotta, E., Ort, M., Pappalardo, L., Piochi, M., Southon, J. (1999): The Agnano-Monte Spina eruption (4.1 ka) in the resurgent, nested Campi Flegrei caldera (Italy). *J. Volcanol. Geotherm. Res.*, **91**, 269-301.

Di Vito, M.A., Braia, G., Isaia, R., Orsi, G., Piermattei, M. (2001): The Averno2 eruption in the northwestern sector of Campi Flegrei caldera (Italy). GNV - Framework Program 2000/2002 - Project n. 26, 101-106.

D'Oriano, C., Poggianti, E., Bertagnini, A., Cioni, R., Landi, P., Polacci, M., Rosi, M. (2005): Changes in eruptive style during the A.D. 1538 Monte Nuovo eruption (Phlegrean Fields, Italy): the role of syn-eruptive crystallization. *Bull. Volcanol.*, **607**, 601-621.

Druitt, T.H. & Kokelaar, B.P. (2002): The eruption of Soufrière Hills Volcano, Montserrat, from 1995 to 1999. *Geol. Soc. London Mem.*, **21**, 639 p.

Formenti, Y.,·Druitt,·T.H., Kelfoun, K. (2003): Characterisation of the 1997, Vulcanian explosions of Soufrière Hills Volcano, Montserrat, by video analysis. *Bull Volcanol.*, **65**, 587-605.

Hammer, J.E., Cashman, K.V., Hoblitt, R., Newman, S. (1999): Degassing and microlite crystallization during the pre-climatic events of the 1991 eruption of the Mt. Pinatubo, Philippines. *Bull. Volcanol.*, **60**, 355-380.

Jaupart, C. (1998): Gas loss from magmas through conduit walls during eruption. *In*: "The physics of explosive volcanic eruptions", J.S. Gilbert & R.S.J. Sparks, eds. *Geol. Soc. Spec. Publ.*, **145**, 73-90.

Mastrolorenzo, G. & Pappalardo, L. (2006): Magma degassing and crystallization processes during eruptions of high-risk Neapolitan-volcanoes: evidence of common equilibrium rising processes in alkaline magmas. *Earth Planet. Sci. Letters*, **250**, 164-181.

Polacci, M., Papale, P., Rosi, M. (2001): Textural heterogeneities in pumices from the climatic eruption of Mount Pinatubo, 15 June 1991, and implications for magma ascent dynamics. *Bull. Volcanol.*, **63**, 83-97.

Polacci, M., Pioli, L., Rosi, M. (2003): The Plinian phase of the Campanian Ignimbrite eruption (Phlegraean Fields, Italy): evidence from density measurements and textural characterization of pumice. *Bull. Volcanol.*, **65**, 418-432.

Rust, A.C. & Cashman, K.V. (2007): Multiple origins of obsidian pyroclasts and implications for changes in the dynamics of the 1300 B.P. eruption of Newberry Volcano, USA. *Bull Volcanol.*, **69**, 825-845.

Sparks, R.S.J., Barclay, J., Jaupart, C., Mader, H.M., Phillips, J.C. (1994): Physical aspects of magmatic degassing. I. Experimental and theoretical constraints on vesiculations. *In*: "Volatile in magmas", M.R. Carroll & J.R. Holloway, eds. *Rev. Mineral.*, **30**, 413-445.

Stix, J., Torres, R.C., Narvaez, L.M., Cortes, J.G.P., Raigosa, A.J., Gomez, D.M., Castonguay, R. (1997): A model of vulcanian eruptions at Galeras volcano, Colombia. *J. Volcanol. Geotherm. Res.*, **77**, 285-303.

Wohletz, K.H. (1983): Mechanisms of hydrovolcanic pyroclast formation: Grainsize, scanning electron microscopy, and experimental studies. *J. Volcanol. Geotherm. Res.*, **17**, 31-64.

Wohletz, K., Orsi, G., De Vita, S. (1995): Eruptive mechanisms of the Neapolitan Yellow Tuff interpreted from stratigraphic, chemical and granulometric data. *J. Volcanol. Geotherm. Res.*, **67**, 263-290.

Wright, H.M., Cashman, K.V., Rosi, M., Cioni, R. (2007): Breadcrust bombs as indicators of Vulcanian eruption dynamics at Guagua Pichincha volcano, Ecuador. *Bull. Volcanol.*, **69**, 281-300.

MINERALOGICAL, GEOCHEMICAL, AND ISOTOPIC TOOLS FOR THE RECONSTRUCTION OF SUBGLACIAL AND MARINE ERUPTIVE PALEOENVIRONMENTS IN ANTARCTICA

MAURIZIO GEMELLI
Dipartimento di Scienze della Terra, Università di Pisa, Via S. Maria 53, 56126 Pisa

ABSTRACT

The Antarctic continent plays a key role in all the paleoclimatic reconstructions, and affects also the climatic evolution of lower latitudes. Therefore, knowledge of the past evolution of Antarctic ice cover is crucial for all the (paleo)climatic reconstruction.

The study of Cenozoic eruptive sequences in northern Victoria Land is a significant source of information about the presence, extent, thickness and type of this ice cover. In combination with $^{40}Ar/^{39}Ar$ dating, the eruptive environment can be used to draw a picture of ice sheet dynamics in the past. This is particularly true for cold regions where there is little or no surviving evidence for ice cover.

In the field, determination of the eruptive paleonvironment of a volcanic sequence (*e.g.* submarine *vs.* subglacial eruptions) could be a difficult task owing to occurrence of ambiguous sequences of volcanic lithofacies. We propose a new, helpful approach in the determination of eruptive environment, represented by the use of chemical and isotopic composition/evolution of glasses and authigenic minerals in water-cooled lavas to determine the original eruptive paleoenvironment (freshwater *vs.* seawater).

The studied products are from Melbourne and Hallett volcanic provinces in northern Victoria Land and vary from hyaloclastite breccias to lapilli tuffs, characterized by variable degree of alteration. These products have been first characterized by petrographic investigations, mineralogical determinations (XRD) along with chemical analyses (SEM-EDS) on sideromelane, palagonitized glasses and secondary mineral phases such as zeolite, smectite. Then, analyses of specific indicator of eruptive environments have carried out, such as stable isotope systematics (D/H, $\delta^{18}O$) on handpicked glasses and plagioclase crystals separated from the juvenile lapilli along with altered hyaloclastite matrix and B contents on zeolite-rich matrix. (Na+K)/Ca of zeolites and glasses, B content and D/H isotopic ratios on altered matrix and $\delta^{18}O$ on glasses and plagioclase, coupled with $^{40}Ar/^{39}Ar$ data, furnish fundamental information about the evolution of the ice cover during the last 10-12 Ma in northern Victoria Land.

INTRODUCTION

The study of eruptive paleoenvironment of a volcanic sequence can represent a fundamental tool for paleoclimatic reconstructions. At present-day the climate change has a worldwide relevance, and the only way to try to understand the probable climatic evolution is to investigate the past. Current researches on this topic are concentrated on paleoclimatic study of ice cores in Antarctica and Greenland, and marine sediments, integrating stable-isotopes paleotemperature reconstructions from cryosphere-atmosphere records. In the last decades, these investigations are leading to a significant advancement in paleoenvironmental reconstruction even if facing many difficulties such as: complex and expensive logistic (drilling ice or marine sediments in complicated environments), less than 1 million year limit for ice cores, no climate indicators on terrestrial environment.

The Antarctic continent plays an important role in the Earth's climate variations, affecting the climate evolution of lower latitudes and constituting a natural laboratory where temperature variations and evolution are recorded. The volcanic rocks outcropping in Antarctica represent a significant repository of information about the occurrence of ice in the past; in fact, they can register chemical and isotopic variations due to magma-ice or magma-seawater interaction during eruption.

In this work, a multidisciplinary approach has been used to discriminate different eruptive paleoenvironment of volcanic sequences sampled in the Hallett and Melbourne Volcanic Province in northern Victoria Land (Antarctica). This research project takes inspiration from a recent paper written by Johnson & Smellie (2007) on the use of chemistry of zeolites as proxy for eruptive paleoenvironment. This study is not only an application of this pioneering proxy-methodology but it is also the first substantive test of that methodology using a large dataset of new analyses from a different volcanic terrain in other part of Antarctica, and including the first B, δD and $\delta^{18}O$ for volcanic rocks in an eruptive environmental study.

These way, gather different knowledge, some completely new, about magma-ice-water interaction and chemical variations during the eruptions. The field observations coupled with chemical, isotopic and geochronological data provide fundamental information about the evolution of the ice cover during the last 10-12 Ma.

PALEOCLIMATE

The climate change, today, is a topic of worldwide relevance. In the last decade many studies have been carried out, and a lot of hypotheses have been formulated on the temperature evolution of the Earth. These global variations are felt and recorded, particularly, in the polar areas, where the ice masses continuously draw a picture of this fluctuation. In the climate system, the cryosphere (which consists of snow, river and lake ice, sea ice, glaciers and ice caps, ice shelves, ice sheets, and frozen ground) is intricately linked to the surface energy budget, the water cycle, sea level change and the surface gas exchange. The cryosphere integrates climate variations over a wide range of time scales, making it a natural sensor of climate variability and providing a visible expression of climate change. Its relevance for climate variability and change is based on physical properties, such as its high surface reflectivity (albedo) and the latent heat associated with phase changes, which have a strong impact on the surface energy balance. The presence (absence) of snow or ice in polar regions is associated with an increased (decreased) meridional temperature difference, which affects winds and ocean currents. Because of the positive temperature-ice albedo feedback, some cryospheric components act to amplify both changes and variability. However, some, like glaciers and permafrost, act to average out short-term variability and so are sensitive indicators of climate change. Elements of the cryosphere are found at all latitudes, enabling a near-global assessment of cryosphere-related climate changes.

The Arctic area shows the clearest evidence of this variation with the intense reductions in Arctic sea ice extent (Fig. 1). Similar alerts come from the changes of the Antarctic ice cover that affects the climate evolution of lower latitude. Given this, it is not surprising that the poles are also where much of the research concerning global climate change is taking place.

Paleoclimate in Antarctica

Antarctica is a superb natural laboratory for the investigation of climate changes, coupling general climatic elements (*i.e.* orbital variations, greenhouse gas concentration, precipitation change) and

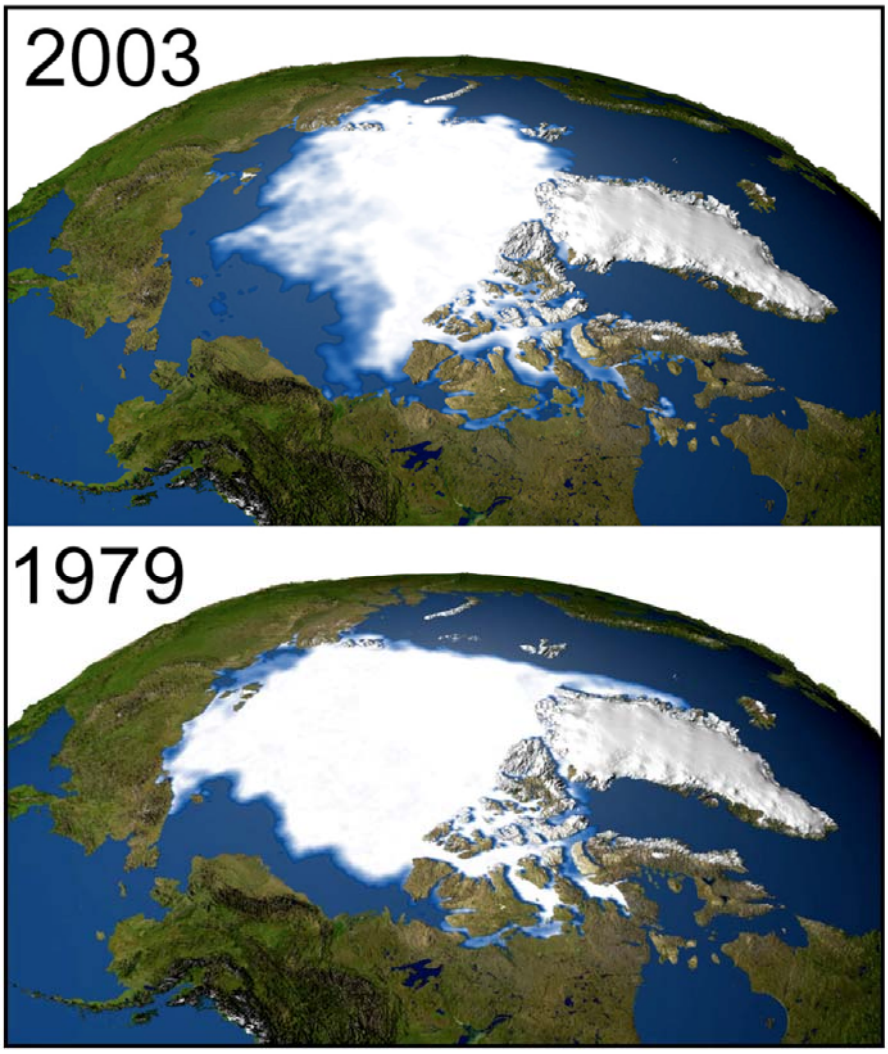

Fig. 1 - Arctic sea ice variations 1979-2003 (www.earthobservatory.nasa.gov).

geodynamic factors, both regional such as the opening of oceanic gateways, and local such as the creation and uplift of mountain ranges (DeConto & Pollard, 2003). The role of polar position of continental Antarctic plate is fundamental, but not fully sufficient to explain the development of the ice sheets, being the position reached in late Cretaceous whereas the ice sheets did not develop until Oligocene time. The set-up of the Antarctic circumpolar current following the opening of the Drake Passage is considered a possible trigger to the main Antarctic glaciation. On the other hand, geodynamic factors like the tectonomagmatic evolution of the West Antarctic Rift System (WARS) (Behrendt *et al.*, 1991; Finn *et al.*, 2005; LeMasurier, 1990; Rocchi *et al.*, 2002), could give rise to the evolution of the Antarctic ice caps. Current research on these topics, in Antarctica, is focused on the forcing role of climate on environment, and aimed to understand how the Antarctic environment – particularly the ice sheets – react to climate variations. These investigations are leading to a significant advance in paleoenvironmental

reconstructions; integrating stable-isotope paleotemperature reconstructions from cryosphere-atmosphere records in the ice cores and hydrosphere record in marine sediments. However, all these methods encounter some difficulties such as: (i) the need for complex and expensive logistics for drilling ice or sediments in extreme environments like Antarctic plateau, ice-shelf (ANDRILL), open-ocean deep water (ODP), (ii) the less than 1 million year age limit for ice cores, (iii) the lack of measurements of climate indicators on terrestrial environment, (iv) the lack of accounting for the possible influence of regional geodynamic factors, such as horizontal and vertical tectonics.

MATERIAL AND METHODS

The studied samples have been collected in northern Victoria Land during the 2005-2006 Antarctic expedition (field season) as a joint operation between Programma Nazionale di Ricerche in Antartide (PNRA) and British Antarctic Survey (BAS). The sampling area (Fig. 2) is distributed along about 400 km, on the Ross Sea margin of East Antarctica, including areas of the Hallett and Melbourne Volcanic Provinces (HVP, MVP). The studied volcanic sequences are in a coastal key position capable to record

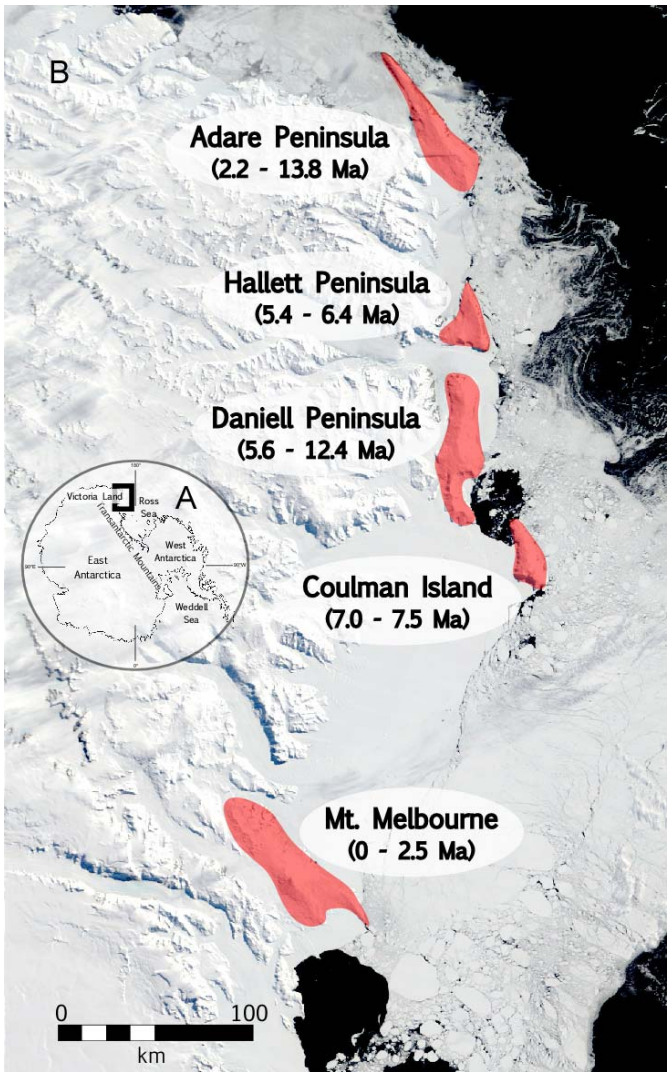

Fig. 2 - A) Antarctica schematic map and location of northern Victoria Land; B) aerial photo of northern Victoria Land. The red sectors represent the principal sampling areas. Age ranges after Armienti & Baroni (1999).

the icesheet or sea level fluctuation in the past; particularly the outcropping volcanic rocks can furnish paleoenvironmental information about the past 10-12 million years.

The sampling strategy was to collect rock samples from volcanic sequences representing magma-water-ice interaction, in order to obtain a potential significant database on the possible fluctuation of ice coverage in northern Victoria Land in the past. Estimates of former ice sheet thickness is one of the principal and most important outputs of lithofacies-based glaciovolcanic studies. However, environmental interpretations based on compositional criteria can also be important (Johnson & Smellie, 2007).

The samples are basanite/basalt - trachyte lavas, fine- or coarse-grained lapilli tuff, hyaloclastites, and pillow. After petrographic characterization, several samples have been selected for mineralogical, geochemical, geochronological and isotopic analyses. The idea was to recognize magma-water interaction considering the chemical and isotopic variation of zeolite-rich matrix, glass and plagioclase of hyaloclastites. From hyaloclastites, zeolite-rich matrix was separated by means of a micro-driller taking care to not include lava clasts/fragments in the powder. The powder obtained was used for XRD analyses, B contents and δD isotopic data. The clasts were crushed and glass and plagioclase were separated for $\delta^{18}O$ isotopic analyses. Glass fragments were concentrated by handpicking under a binocular microscope (excluding any fragment with evidence of micro-crystals and that were not optically clear). They were ultrasonically cleaned in deionized water and dried.

Concerning geochronology (^{40}Ar-^{39}Ar systematics), alkaline lavas were crushed and a representative fraction was sieved to extract groundmass. Lava groundmasses were concentrated from the 150-250 μm and 250-350 μm fractions by handpicking under a binocular microscope, taking care to collect only fresh groundmass chips. In this way 150-200 mg of groundmass was gathered for 21 samples. After petrographic investigation two sanidine-rich lavas were selected to take out sanidine crystals for ^{40}Ar-^{39}Ar analyses. The sanidine crystals were concentrated by means of a Franz Isodynamic separator, were sieved and separated from the 150-250 μm, 250-350 μm and 350-500 μm fractions by handpicking under a binocular microscope. Sample preparation and ^{40}Ar-^{39}Ar data collection were carried out at IGG-CNR, Pisa.

RESULTS AND DISCUSSION

Collection of geochemical data started with SEM analyses on selected thin sections. The selection of the samples was made on the basis of the abundance of secondary minerals and extent of palagonitization. The chemistry of zeolites and glass, points out a lot of interesting linkages between the palagonitization process, taking place during or soon after the eruption, and the zeolitization. Examining the palagonitization development, it is frequently easy to distinguish the two different stages of palagonitization (gel-palagonite and fibrous palagonite). Gel-palagonite, as well as the different stage materials deriving from, it has a spectrum of chemical compositions showing relevant differences from those of the parent fresh glass. Gel-palagonite analyses show a general trend toward lower SiO_2, Al_2O_3, Na_2O, K_2O, CaO but higher TiO_2 and FeO concentrations of the parent glasses.

The zeolites occur as fibrous, elongated and blocky crystals (Fig. 3) and are almost all phillipsites with minor chabazites and analcite. The zeolites have been classified on the basis of alkali ratio using the triangular diagram Ca-Na-K (Ijima & Harada, 1969) (Fig. 4). The studied samples have been grouped into Hallett Volcanic Province (HVP), Melbourne Volcanic Province (MVP) and James Ross Island (JRI) samples.

The alkali ratios of zeolites, is a helpful key feature if used like a tool to discriminate the two

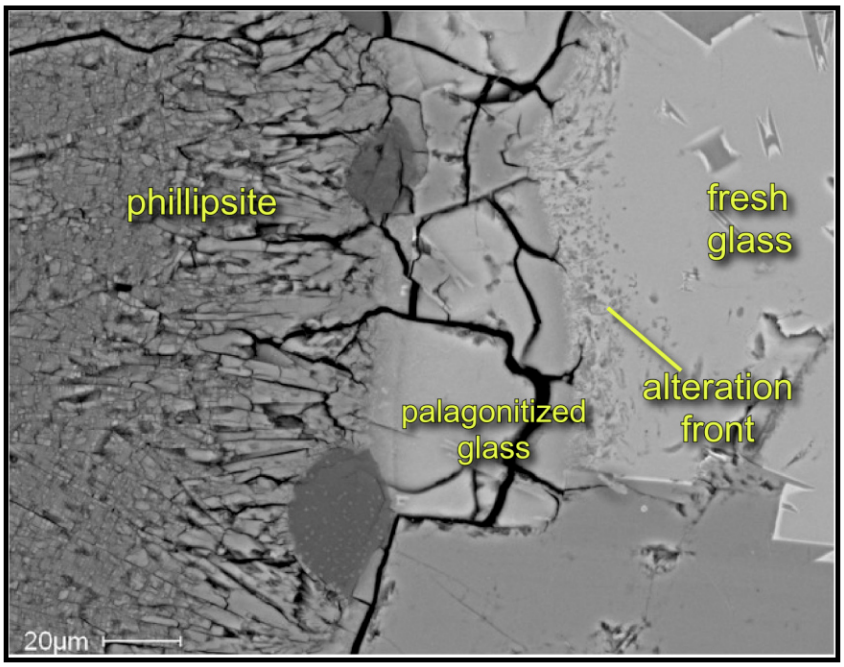

Fig. 3 - SEM picture showing the transition from fresh glass to palagonitized glass and zeolites.

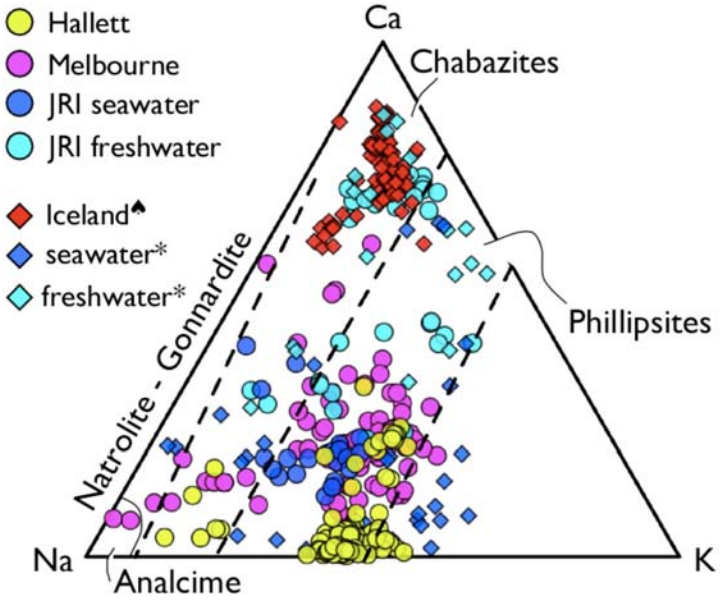

Fig. 4 - Ca-Na-K zeolite triangular classification diagram after Ijima & Harada (1969), Smellie (2008), Johnson & Smellie (2007). Circles represent zeolite analyses made in this work. Diamonds represent literature data.

different eruptive settings (freshwater *vs.* seawater). The zeolite chemical data for the HVP and MVP have been plotted in diagrams considering alkali ratios, Si/Al and freshwater *vs.* seawater (Fig. 5). For comparison, in the diagrams are also plotted the JRI samples and literature data (Abollino *et al.*, 2001; Borghini & Bargagli, 2004; Johnson & Smellie, 2007; Smellie, 2008). The data distributions, plotted using the diagram (Na+K)/Ca *vs.* Si/Al (Fig. 5), indicate that HVP zeolites have a more marine signature in comparison with those of MVP.

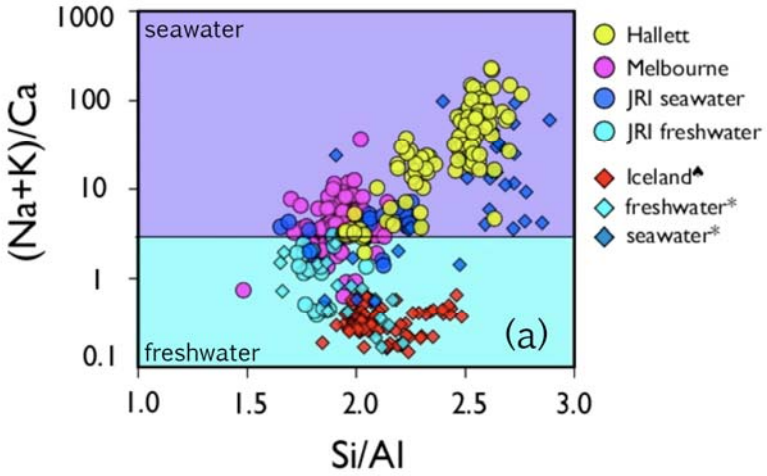

Fig. 5 - (Na+K)/Ca *vs.* Si/Al diagram for a) phillipsites, and b) chabazites. The (Na+K)/Ca ratio 3 is an empirical discrimination value to classify freshwater and seawater zeolites (Smellie, 2008; Johnson & Smellie, 2007). Circles represent zeolite analyses made in this work. Diamonds represent literature data.

The B analyses have been carried out on zeolite-rich groundmass of hyaloclastites from HVP, MVP and JRI. Boron is an element that can be used as a marker for the water-magma interaction in order to determine the paleoeruptive environment, because the boron is abundant in seawater (4.5 ppm; Stumm & Morgan, 1981) in comparison with freshwater boron content. The average of the boron contents for the HVP (-70.8 ppm) and MVP (-93.7) reveal clear differences between the two volcanic provinces. Apart from some samples more close to coastline, we can acknowledge that MVP samples have lower B content with respect to the HVP samples.

The isotopic analyses on zeolite-rich matrix, glass and plagioclase of lapilli, were performed to obtain information about different processes regarding magma-water interaction. A total of 40 zeolite-rich groundmass were analyzed to obtain the δD isotopic ratio, and 13 glass fragments and 13 plagioclase to obtain the $\delta^{18}O$ isotopic ratio. The analyzed samples come from HVP, MVP and JRI. The δD ratio varies from -43 to -119‰ but the variation range for HVP and MVP is different. The HVP samples show values from -56 to -92‰ with a median value of -69‰, whereas the MVP have more negative values, ranging from -71 to -120‰ with a median value of -93‰. The JRI samples have less negative values than MVP with δD ratio varies from -42 to -78‰ with a median value of -57‰.

The $\delta^{18}O$ isotopic ratios were measured for glass particles and plagioclase of hyaloclastite glassy clasts. The $\delta^{18}O$ ratio of glasses varies from 4.95 to 6.73‰ taking into account all samples. The $\delta^{18}O$ ratio of plagioclase, coming from the MVP, ranges from 6.5 to 8.5‰, whereas the sample coming from the HVP and JRI show higher values 6.4-12.3‰ and 16.5-21.3‰ respectively.

A total of 23 samples were dated. Ten lava groundmass and 1 sanidine for HVP samples and 11 lava groundmass and 1 sanidine for MVP. Step-heating technique was used to analyze lava groundmass splits and single-grain total fusion technique to analyze sanidine crystals. The MVP samples show ages ranging from 0.063 to 2.9 Ma and HVP ages ranging from 7.05 Ma to 9.95 Ma.

CONCLUSION

The ^{40}Ar-^{39}Ar dating of HVP and MVP samples carried out from this work, give a great contribution to reconstruction of volcanic history in northern Victoria Land. The age distribution combined with reconstruction of eruptive paleoenvironment, contributes something important for

paleoclimatic evolution. The magma-ice-water interaction recorded by the HVP and MVP volcanic rocks gives information about ice sheet dynamics during the late Miocene and middle Pliocene- Pleistocene.

The interpretation of volcanic sequences in the HVP indicates an interaction with thin ice cover during eruption. The chemistry of zeolites records the interaction that occurred and suggest, as shown by high alkali ratios, B contents and isotopic values, an interaction with seawater or alkali-rich water. In this scenario, melting of snowbanks could generate alkali-rich water. In the Melbourne area, the analyses of volcanic sequences indicates that, during middle Pliocene, eruptions have occurred under a thick-ice cover. The chemical and isotopic data of zeolites for MVP samples show marine signature as indicated by zeolite chemistry and a subglacial or subaerial eruptive environment confirmed by the low B contents and high negative δD ratio. The marine signature of zeolites indicates a marine aerosol influence also on the MVP samples. The lower alkali concentration in zeolites in respect of HVP samples could be ascribed to the younger exposure age or sea level variations due to tectonic dynamics.

REFERENCES

Abollino, O., Aceto, M., Gioia, C.L., Sarzanini, C., Mentasti, E. (2001): Spatial and seasonal variations of major, minor and trace elements in Antarctica seawater. Chemometric investigation of variable and site correlations. *Adv. Environ. Res.*, **6**, 29-43.

Behrendt, J.C., LeMasurier, W.E., Cooper, A.K., Saltus, R., Bosum, W., Cooper, A.K. (1991): Geophysical studies of the West Antarctic Rift System. *Tectonics*, **10**, 1257-1273.

Borghini, F. & Bargagli, R. (2004): Changes of major ion concentrations in melting snow and terrestrial waters from northern Victoria Land, Antarctica. *Antarctic Sci.*, **16**, 107-115.

DeConto, R.M. & Pollard, D. (2003): A coupled climate-ice sheet modeling approach to the Early Cenozoic history of the Antarctic ice sheet. *Palaeogeogr. Palaeoclimat. Palaeoecol.*, **198**, 39-52.

Finn, C., Müller, R.D., Panter, K.S. (2005): A Cenozoic diffuse alkaline magmatic province (DAMP) in the southwest Pacific without rift or plume origin. *Geochem. Geophys. Geosyst.*, **6**, Q02005, doi:02010.01029/02004GC000723.

Ijima, A. & Harada, K. (1969): Authigenic zeolites in zeolitic palagonite tuffs on Oahu, Hawaii. *Am. Mineral.*, **54**, 182-197.

Johnson, J.S. & Smellie, J.L. (2007): Zeolite compositions as proxies for eruptive paleoenvironment. *Geochem. Geophys. Geosyst.*, **8**, Q03009, doi:03010.01029/02006GC001450.

LeMasurier, W.E. (1990): Late Cenozoic volcanism on the Antarctic Plate: an overview. *In*: "Volcanoes of the Antarctic plate and southern Oceans", W.E. LeMasurier & J.W. Thomson, eds. *Am. Geophys. Union, Antarctic Res. Ser.*, **48**, 1-17.

Rocchi, S., Armienti, P., D'Orazio, M., Tonarini, S., Wijbrans, J., Di Vincenzo, G. (2002): Cenozoic magmatism in the western Ross Embayment: role of mantle plume *vs.* plate dynamics in the development of the West Antarctic Rift System. *J. Geophys. Res.*, **107**, 2195.

Smellie, J.L. (2008): Basaltic subglacial sheet-like sequences: Evidence for two types with different implications for the inferred thickness of associated ice. *Earth Sci. Rev.*, in press.

Stumm, W. & Morgan, J.J. (1981): Aquatic chemistry. Wiley, New York, 780 p.

UPLIFT AND EROSION RATES AND PALEOCLIMATE ANALYSIS FROM PLIO-QUATERNARY AULETTA BASIN (SOUTHERN APENNINES, ITALY)

DARIO GIOIA
Dipartimento di Scienze Geologiche, Università della Basilicata, Viale dell'Ateneo Lucano 10, 85100 Potenza

Recent study on tectonically active mountain chains have suggested strong coupling and feedbacks between climate, tectonics and topography. Understanding the roles of tectonics and climate in mountain building and erosion processes requires necessarily the acquisition of multidisciplinary data (Burbank & Anderson, 2001; Schiattarella *et al.*, 2008). The study of the interplay, links, and feedbacks between climate and erosion and among these factors and tectonics, and morphogenesis had already strongly addressed the international scientific community and the Italian geoscientists as well (*e.g.*, Burbank & Anderson, 2001; Pazzaglia & Brandon, 2001; Schiattarella *et al.*, 2003; 2006; Bishop, 2007) to get estimates of parameters, *i.e.* uplift and/or erosional rates in different climate scenarios. The comprehension of morphotectonic evolution of southern Italy is indeed strictly dependent on the estimation of such parameters.

The aim of this work is to reconstruct the Plio-Quaternary morphotectonic and sedimentary evolution of the Auletta basin (Ascione *et al.*, 1992; Barchi *et al.*, 2007), a wide tectonic depression of the axial zone of southern Italian Apennines. In addition, uplift and erosion rates have been calculated using geomorphological, stratigraphic and structural data. In order to better constrain the estimation of uplift and erosion rates, relative and absolute dating methods have been used for a better definition of the ages of the morphotectonic marker. To understand the role of different paleoclimate scenarios in controlling the landscape evolution, geomorphic and stratigraphic data have been integrated with a detailed mineralogical and geochemical study of soils, paleosols and weathering profiles. Information on the paleoclimatic evolution during Quaternary times has been obtained by the analysis of distribution of clay minerals in continental pelitic sediments, paleosols, and weathered horizons developed in depositional and erosional surfaces of different age from key-areas of the basin. In addition, the mineralogical data have been integrated with a detailed study of the geochemical properties of a selected number of samples.

The Auletta basin coincides with the lower valley of the Tanagro River, an hydrographic catchment of the axial zone of the southern Apennines. Upper Pliocene to lower-middle Pleistocene sediments, both of marine and continental origin filled the basin and are shaped by erosion land surfaces and fluvial dissection. The depression has a tectonic origin, being bordered by two main N 120-130° trending fault line scarps and/or recessed fault slopes, related to listric faults with polyphased kinematics. The master fault of the Auletta basin is a NE dipping high-angle listric fault, located at its SW margin. This fault controlled the stratigraphic, structural and morphological setting of the area. Structures with a similar orientation and also NE-SW striking faults are diffused in the Mesozoic carbonate mountains surrounding the basin and in the Quaternary basin itself. In addition, morphometric analysis of the drainage net demonstrated a general tilting of the Tanagro River toward the SW, related to the activity of the master (*i.e.* southern) fault of the basin. As a consequence of the Tanagro River migration, an asymmetric valley developed.

Besides faulting, both the carbonate bedrock and the Pliocene and Quaternary clastic sediments are affected by several order of regional planation and local erosion sub-horizontal surfaces. The

morphostructural evolution of the Auletta basin is characterized by stages of uplift alternated with periods in which the erosional surfaces developed. In the catchment basin and surroundings, five generations of erosional land surfaces have been investigated on the basis of both field survey and map analysis. The age of these surfaces has been defined from their morpho-stratigraphic relationships with Pliocene and Quaternary deposits. The uplift rates have been calculated on the basis of the difference in height between the absolute (sea level) or local (present-day talweg) erosion base levels and the several generations of land surfaces. Regional uplift rates are settled on a value of about 0.6 mm/yr, whereas the local rates are nearly coincident with the magnitude of the fault slip rates. The similar values of the local and regional uplift rates suggests that the major part of energy of relief of the Auletta basin can be ascribed to the tectonic activity of the basin-bounding faults.

In order to relate the different erosion processes to tectonic mobility of the axial zone of the chain, a geomorphic quantitative analysis has been carried out and the eroded volumes of rocks forming both the Mesozoic-Cenozoic bedrock and the Pliocene to Quaternary clastic deposits have been calculated, using cartographic methods and also converting the fluvial turbid transport data as evaluated by geomorphic parameters (Schiattarella *et al.*, 2008). The annual average erosion rate is about 0.2 mm/yr. In order to understand the roles of paleoclimate in controlling the landscape evolution, morphotectonic data have been integrated with those derived from mineralogy and geochemistry. Such a multidisciplinary approach allow to define the weathering conditions of geological and morphological features in different times during their history. Being these conditions suitable proxies, it is therefore possible to get indirect information on paleoclimate scenarios which characterized the landscape through time. To this end, 56 samples of the late Pliocene to Holocene continental succession of the Auletta basin were collected. In particular, the sampled succession was composed by lacustrine and swamp deposits, weathered horizons and paleosols. XRD analysis of the mineralogy of bulk samples and of the clay fraction (< 2 μm grain-size fraction) allow to recognize three different arrangement of the mineralogical phases distribution of the samples (mineralogical assemblage A, B and C in Fig. 1).

The lacustrine deposits, late Pliocene in age, are composed by 40-60 wt.% of illite-smectite mixed layers, 20-35 wt.% of calcite and by a lower content of quartz. In all the sample, a small amount of plagioclase and k-feldspar was found. The clay mineralogy of these samples is mainly composed by smectite-rich illite-smectite mixed layers and by caolinite, illite and chlorite. The mineralogical assemblage of the late Pliocene deposits is similar with respect the lower Pleistocene swamp deposits, although the latter are characterized by a higher amount of illite e chlorite. However, weathering horizons developed within the lower Pleistocene fluvial deposits show a different mineralogical assemblage than both the lacustrine and swamp deposits, being characterized by a higher content of poorly crystallized kaolinite and kaolinite-smectite mixed layers and by the absence of the chlorite. In the weathering horizons, low content of goethite has been detected.

The mineralogy of the middle to late Pliocene paleosols is characterized by phyllosilicates (60-80%), quartz, K-feldspar, plagioclase and goethite. The phyllosilicates are represented by high amount of kaolinite-smectite mixed layers, illite and kaolinite with a low degree of crystallinity. Also, a lower halloysite content has been detected in some samples.

Holocene swamp deposits are mainly composed of phyllosilicates, calcite and quartz with a lower content of plagioclase and k-feldspar. The clay mineralogy of this samples is mainly illite-smectite mixed layers, illite, kaolinite, vermiculite and Al-vermiculite.

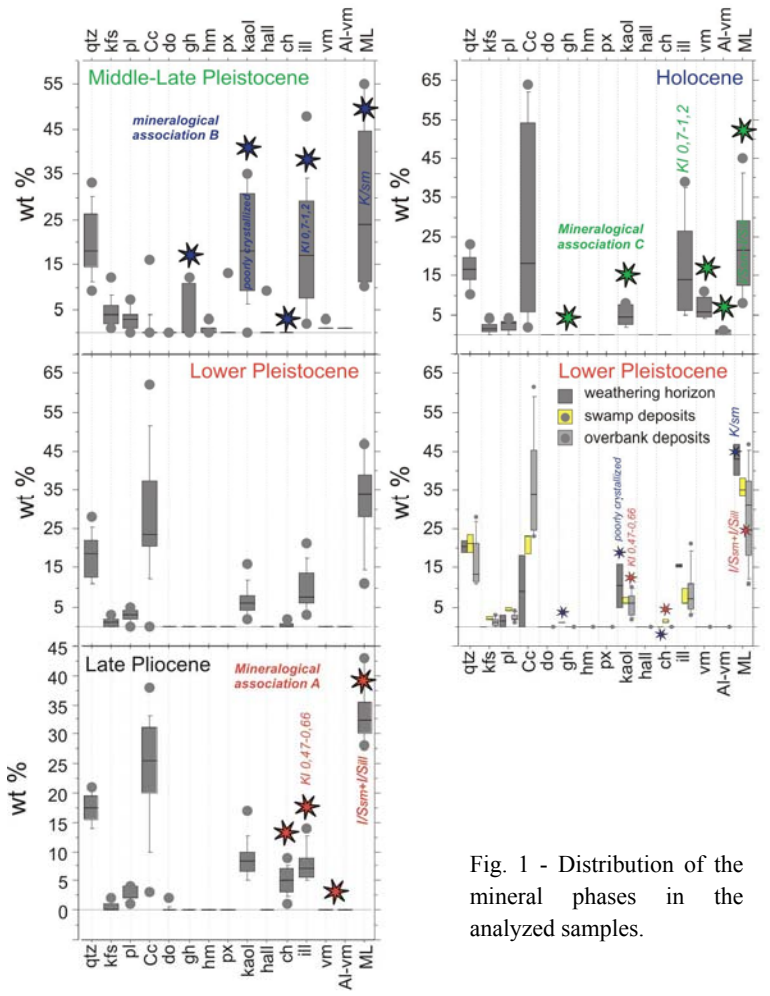

Fig. 1 - Distribution of the mineral phases in the analyzed samples.

In order to evaluate the degree of weathering of the studied samples, the CIA (Chemical Index of Alteration, Nesbitt & Young, 1989) and the A-CN-K diagram (Nesbitt & Young, 1989) have been analyzed. The highest values of the CIA have been observed in the middle to late Pleistocene paleosols, suggesting a strong degree of weathering that it is consistent with warm and humid climates with alternating rainy and dry seasons (Quaternary interglacials). These conditions are also in agreement with the mineralogical assemblage of this samples. Indeed, the results of the mineralogical analysis indicate that the main components of the samples are kaolinite-smectite mixed layers, kaolinite and goethite. Kaolinite minerals have shown low crystallinity, typical of very intense weathering conditions. These conditions promote intense weathering of primary minerals and leaching of cations released from crystal lattices (in turn enhancing the formation of these mineral species), growing in intensity according to an increase of the time span of pedogenesis (Scarciglia *et al.*, 2006, and references therein; Di Leo *et al.*, 2008). It is worthy of note that at the Monte Pozzillo quarry (*i.e.* eastern part of the basin) the paleosols are covered by a 20 cm thick tephra layer made of brown silt with small-size sanidine clasts. Radiometric dating using the $^{39}Ar/^{40}Ar$ method indicate an age of the tephra of 106±1.6 Ka, suggesting that the stage of intense weathering responsible for the mineralogical arrangement of the paleosols was related to the Late Quaternary interglacials. A similar paleoclimate scenario characterized by temperatures and precipitation higher than today seems to be relate to the formation of the weathering horizons during Lower Pleistocene times. On the other hand, the distribution of mineral phases in the late Pliocene to lower Pleistocene lacustrine and swamp deposits suggests a weathering developed in more temperate conditions. Moreover, the abundance of chlorite and kaolinite with a high degree of crystallinity indicates a detrital origin of this mineral, probably related to the denudation of the sicilide units.

Geomorphological and stratigraphical data as well as chronological constraints based on radiocarbon dating indicate that the Holocene deposits ranging from the Boreal to the Subboreal periods. The assemblage of clay minerals within the Holocene swamp deposits, such as illite, illite-smectite mixed layers and vermiculite suggest a moderate weathering environment (Barnhisel & Bertsch, 1989) typical of the Early Holocene paleoclimate setting. However, the mineralogical and geochemical features of the younger samples - which on the basis of the radiocarbon dating can be dated at the Atlantic-Subboreal transition - suggest a more intense stage of weathering, related to the warmest phase of the entire Holocene where also the climatic optimum was reached (Ravazzi, 2003).

This results have been confirmed through a multivariate statistical analysis using PCA method. Using the distribution of the mineral phases in the samples and the sum of several mineral phases typical of temperate (vermiculite, Al-vermiculite, illite-smectite mixed layers and illite, 1st stage of weathering, see Fig. 2) and warm/humid (kaolinite-smectite mixed layer, goethite and kaolinite, 2nd stage of weathering, see Fig. 2) climate as variables in the input matrix of the PCA method, it can be observed that

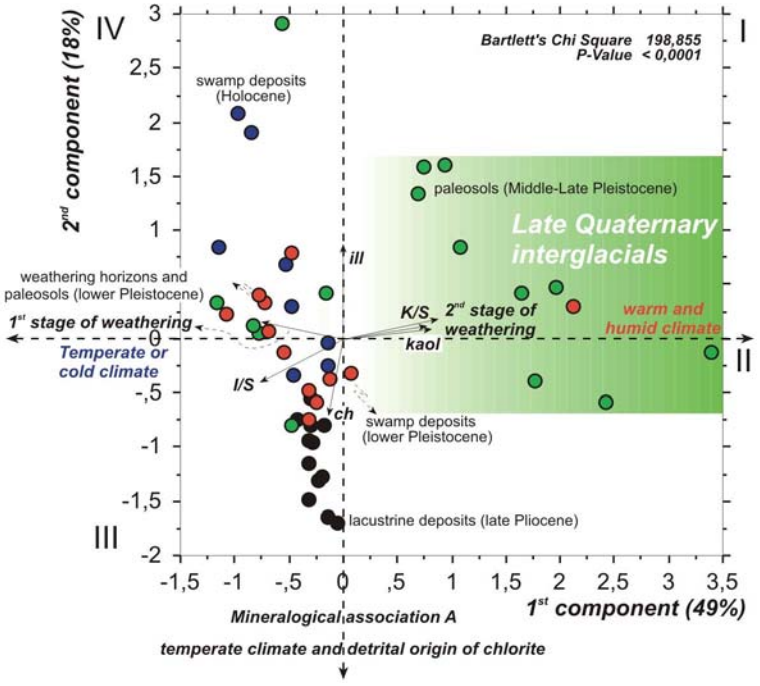

Fig. 2 - PCA analysis based on an input matrix composed by the wt.% of the mineralogical phases. Orthogonal plot of the multivariate statistical analysis carried out using Principal Component Analysis (PCA) as extraction method. As variables in the input matrix of the PCA method, the distribution of the mineral phases in the samples and the sum of several mineral phases typical of temperate (vermiculite, Al-vermiculite, illite-smectite mixed layers and illite, 1st stage of weathering) and warm/humid (kaolinite-smectite mixed layer, goethite and kaolinite, 2nd stage of weathering) climate have been used.

the first component (49% variance) groups together kaolinite-smectite mixed layers, kaolinite and 2nd stage of weathering with high positive component loadings, and 1st stage of weathering and illite-smectite mixed layers with a negative component loading. The second component (18% variance) shows illite with high positive component loadings, and chlorite with a negative component loading.

In the 1st component *vs.* 2nd component plot, most of the samples from middle to late Pleistocene paleosols group together in the direction of maximum variation of kaolinite-smectite, kaolinite and 2nd stage of weathering, representing the mineral phases typical of warm and humid climate setting. late Pliocene to lower Pleistocene lacustrine and swamp deposits group in the direction of the maximum variation of chlorite, testifying a strong influence of the sedimentary input related to the denudation of the sicilide units on the mineralogical features of this samples.

Similar information about paleoclimate scenario can be inferred from the results of geochemical analyses. In particular, the samples related to an intense stages of weathering (*i.e.* lower Pleistocene weathering horizons and middle to late Pleistocene paleosols) shown a light rare earth element (LREE)-enriched pattern of rare earth element (REE). In warm and humid climates, the high rare earth element (HREE) are indeed removed from the soil profile to result in a greater depletion in the medium rare earth element (MREE) and HREE than the LREE (Aubert *et al.*, 2001; Zhou *et al.*, 2008). Although this work is only preliminary and further investigations are needed in the future, the REE pattern appear to be a powerful proxy for past climate.

In this work, the multiproxy approach based on geomorphological, stratigraphical, mineralogical and geochemical data allow to reconstruct the paleoclimate conditions active in different stage of landscape evolution. Moreover, the comparison between uplift and erosion rates suggests that the fluvial erosion did not match the tectonic uplift of the study area, which therefore could result a non-steady system. In this key, landslides affecting also Holocene formations may be the effect of a system in an unrest state.

REFERENCES

Ascione, A., Cinque, A., Tozzi, M. (1992): La valle del Tanagro (Campania): una depressione strutturale ad evoluzione complessa. *Studi Geol. Camerti*, *Spec. Vol.*, **1992**, 209-219.

Aubert, D., Stille, P., Probst, A., Gauthier-Lafaye, F., Pourcelot, L., Del Nero, M. (2002): Characterization and migration of atmospheric REE in soils and surface waters. *Geochim. Cosmochim. Acta*, **66**, 3339-3350.

Barchi, M., Amato, A., Cippitelli, G., Merlini, S., Montone, P. (2007): Extensional tectonics and seismicity in the axial zone of the Southern Apennines. *Boll. Soc. Geol. It., Spec. Vol.*, **7**, 47-56.

Barnhisel, R.I. & Bertsch, P.M. (1989): Chlorites and hydroxy-interlayered vermiculite and smectite. *In*: "Minerals in soil environments", J.B. Dixon & S.B. Weed, eds. Soil Science Society of America, Madison, 729-788.

Bishop, P. (2007): Long-term landscape evolution: linking tectonics and surface processes. *Earth Surf. Proc. Landforms*, **32**, 329-365.

Burbank, D.W. & Anderson, R.S. (2001): Tectonic geomorphology. Blackwell, Oxford, 274 p.

Di Leo, P., Giano, S.I, Gioia, D., Mattei, M., Pappalardo, A., Perri, E., Pescatore, E., Schiattarella, M. (2008): Evoluzione geomorfologica, paleoclimatica e tettonica del bacino di Sanza in Appennino campano-lucano durante il Quaternario. *In*: "Studi di base sull'interazione tra clima, tettonica e morfoevoluzione in Italia meridionale durante il Quaternario", F. Boenzi, D. Capolongo, S.I. Giano & M. Schiattarella, eds. Dibuono Edizioni, Villa d'Agri (PZ), 62-83.

Nesbit, H.W. & Young, G.M. (1989): Formation and diagenesis of weathering profiles. *J. Geol.*, **97**, 129-147.

Pazzaglia, F.J. & Brandon, M.T. (2001): A fluvial record of long-term steady state uplift and erosion across the Cascadia forearc high, Western Washington State. *Am. J. Sci.*, **301**, 385-431.

Ravazzi, C. (2003): An overview of the Quaternary continental stratigraphic units based on biological and climatic events in Italy. *Il Quaternario*, **16**, 11-18.

Scarciglia, F., Pulice, I., Robustelli, G., Vecchio, G. (2006): Soil chronosequences on Quaternary marine terraces along the northwestern coast of Calabria (Southern Italy). *Quatern. Int.*, **156-157**, 133-155.

Schiattarella, M., Di Leo, P., Beneduce, P., Giano, S.I. (2003): Quaternary uplift *vs.* tectonic loading: a case-study from the Lucanian Apennine, southern Italy. *Quatern. Int.*, **101-102**, 239-251.

Schiattarella, M., Di Leo, P., Beneduce, P., Giano, S.I., Martino, C. (2006): Tectonically driven exhumation of a young orogen: an example from southern Apennines, Italy. *In*: "Tectonics, climate, and landscape evolution", S.D. Willett, N. Hovius, M.T. Brandon & D. Fisher, eds. *Geol. Soc. Am., Spec. Paper*, **398**, 371-385.

Schiattarella, M., Beneduce, P., Capolongo, D., Di Leo, P., Giano, S.I., Gioia, D., Lazzari, M., Martino, C. (2008): Uplift and erosion rates from the southern Apennines, Italy. *Boll. Geofis. Teor. Appl.*, **49**, 470-475.

Zhou, H., Wang, Q., Zhao, J., Zheng, L., Guan, H., Feng, Y., Greig, A. (2008): Rare earth elements and yttrium in a stalagmite from Central China and potential paleoclimatic implications. *Palaeogeogr., Palaeoclimat., Palaeoecol.*, **270**, 128-138.

USE OF SAWING AND POLISHING ROCK INDUSTRIAL WASTES FOR LIGHTWEIGHT EXPANDED AGGREGATES PRODUCTION

SOSSIO FABIO GRAZIANO
Dipartimento di Scienze della Terra, Università "Federico II", Via Mezzocannone 8, 80134 Napoli

INTRODUCTION

Wastes produced from geomaterials working processes represent a cost to dump and can have a remarkable environmental impact.

In this light it is clear the importance of scientific researches finalized to the reuse of this wastes as raw material for other industrial purposes.

During this research, sawing and polishing wastes from granitic rocks and ceramics were considered.

Dimension stones working processes generate muds amounts of 25% in weight of the raw material while the grès tiles ones about 50.000 metric tons/year only for Italy (ANPA, 2002).

This muds reveal a low abrasive (SiC) and steel filings amount (1-2%), so CER 010410/13 and 10129 are the corresponding European codes for this kind of wastes.

Nowadays only a small part of this muds are reused even if there is a lot of scientific literature about this matter.

This research prove that ceramic muds chemical composition both with the presence of some SiC percentages cause the expansion of the material after thermical treatments and make it suitable for lightweight aggregates production (de Gennaro *et al.*, 2007a, 2007b).

This muds can be also used like expandent additives in wastes from zeolitized rocks to obtain lightweight aggregates (de Gennaro *et al.*, 2007a, 2007b).

Aim of this research is verify the reusing of working processes granite muds for the production of lightweight expanded aggregates (hereafter LEA) and their behaviour in concrete manufacturing.

RESULTS

The first portion of the research focused on understanding the mechanisms determining the expansion of geomaterials when thermally treated. A wide variety of rock types commonly used in the building industry from a Brazilian and some different Italian industrial districts, having different chemical (carried out by XRF) and mineralogical compositions (carried out by XRD), was selected for study (Table 1). Rocks with high or low silica contents were selected, characterized by different amounts of alkaline and earth alkaline metal oxides and of Fe and Mn. It was thus possible with these samples to evaluate the influence of the SiO_2-Al_2O_3 ratio on fluxing.

Thanks to this characterization it was possible to identify the potentially expandable ones in relation to their chemical composition.

By plotting the chemical composition in the Riley diagram (1951) it was clear that only muds which were in the highlighted area were potentially expandable (Fig. 1).

On pellets produced with this muds, first fire treatments were conducted to verify their expandability.

Table 1 - Muds description.

ITALIAN muds	
AM1	Cutting mud from several marbles
AM2	Cutting mud from several granites
AM3	Cutting mud from several marbles and granites (main pool)
CAB70	Cutting mud from Campanian Ignimbrite
MM1	Cutting mud from several marbles
MM2	Cutting mud from several granites
REV	Cutting mud from Reventino green stone
SER	Cutting mud from Serizzo stone
SIL	Polishing machine mud from Calabrian granite
BRAZILIAN muds	
BRZ1	Polishing machine mud from several granites
BRZ2	Cutting mud from Verde San Francesco & Purangau stones
BRZ3	Cutting mud from Bianco Greco & Purangau stones
BRZ4	Cutting mud from River Giallo & Four Season stones
BRZ5	Cutting mud from Purangau stone
BRZ6	Cutting mud from Verde Ubatuba & Emerald Quartz & Gold fields stones

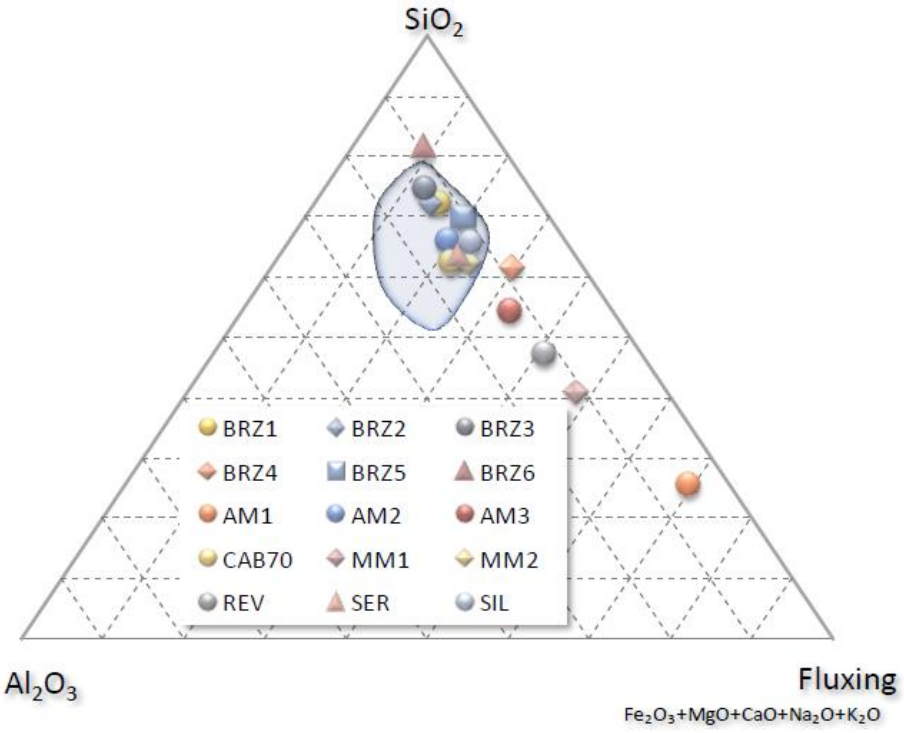

Fig.1 - Riley diagram (1951).

The working conditions for this tests were: temperature 1300°C and firing time 300 sec. The physical parameters of the aggregates are shown in Table 2.

Those aggregates present bulk density values almost always more than unit (>1 g/cm^3) , only BRZ1 and SIL specimens, respectively produced from a Brazilian and an Italian granite polishing machine mud and got from two different plants both using SiC like abrasive, were expandable.

If expansion did not occur spontaneously or if the resulting aggregates did not possess the required features, an expanding agent was chosen for addition. Among the available expanding agents, SiC was used, either on the basis of previous results or because SiC can be present in those materials as a result of polishing processes.

Table 2 - Produced aggregates bulk density.

Brazilian muds	g/cm^3
BRZ1	0,73
BRZ2	1,03
BRZ3	1,14
BRZ4	melted
BRZ5	1,67
BRZ6	1,52

Italian muds	g/cm^3
AM1	1,46
AM2	1,59
AM3	1,65
CAB70	1,41
MM1	3,31
MM2	1,37
REV	1,82
SER	1,11
SIL	0,74

New tests were repeated, mixing dimension stones muds with grès polishing muds (hereafter GPM) like expanding additive.

The main physical features of all lightweight aggregates produced with these mixtures are shown in Table 3.

Table 3 - Produced aggregates physical features.

%	BRZ1	BRZ2	CAB70	SER	SIL	GPM	Bulk Density (g/cm^3)	Compressive Strength Single Grain (kN)
Mix1	35	35				30	0,87	0,55
Mix2	25	25				50	0,83	1,35
Mix3	25	25	25			25	0,95	0,51
Mix4				70		30	1,16	0,91
Mix5				50		50	0,68	0,32
Mix6			25	25	25	25	0,73	0,18
Mix7				25	25	50	0,62	0,12
Mix8				35	35	30	0,7	0,04
ALFA				50		50	Bulk Density (g/cm^3)	Weight stack (kg/m^3)
							0,8-0,9	500
							H_2O absorption (%)	Strength in pile (1lt) (MPa)
							2,1	2,0

On the basis of physical property results and of data analysis, a multivariate statistical analysis was carried out to obtain an empirical model for the dependence of bloating on chemical and mineralogical composition of the raw materials, grain size and packing of the crude powders, the amount and quality of the glassy phase, and the microstructure of the fired product.

Granulometric distribution, weight stack, strength in pile (European-suggested standards UNI EN 13055-1, 2002), and water absorption (European-suggested standards UNI EN 1097-6, 2002) of the mixture with the best bulk density and single grain compressive strength results were determined.

Five litres of aggregates were prepared using a rotative kiln model. Nannetti TO-R150-15 with working conditions: temperature 1300°C and rotational speed 3.5 laps/min.

The compositions giving the best LEA physical properties were then used to produce larger amounts necessary for complete characterization and, finally, for evaluating their use in the production of structural lightweight concretes.

The physical parameters of the selected mixture are almost similar even if the mixture Mix5, made by Serizzo (50%) and grès tiles muds (50%), show suitable values for concrete producing (de Gennaro *et al.*, 2007).

With this mixture, hereafter ALFA ("first letter in Greek alphabet" for first kind of those aggregates) 36 litres of aggregates were produced using new sintering conditions to obtain grains bulk density values between 0.8 and 0.9 g/cm^3 (Table 3).

According to European-suggested standards UNI EN 11013, two concrete mixtures C1 and C2, were prepared and some ingredients amounts were corrected for experimental requirements.

The compositions of the two mixtures are shown in Table 4.

Sand Normal (European-suggested standards UNI EN 196-1); Cement CEMENTIR CEM II/A-LL 42.5R; ALFA aggregate; Additive ADDIMENT 39/T40 (only in C1 mixture) were used.

The use of the additive lowered water requirement in C1 mixture. For this reason the water/cement ratios are 0.53 for C2 and 0.49 for C1.

The Slump test (European-suggested standards UNI EN 12350-2 and UNI EN 206-1) permitted to evaluate the fresh mixtures consistence by measuring the fresh dough falling from the Abrams cone.

A set of five cubic specimens (15 cm sided) were prepared for both the mixtures.

Concrete drying had two phases, the first one (3 days) in air atmosphere with costant temperature (20°C), the second one (till 28 days) in water pools always with constant temperature (20°C).

Table 4 - Mixtures components and concretes physical features.

Mixtures	C1	Corr.	C2	Corr.	Unit
Cement	7		7		kg
Normal sand	10		10		kg
Water	3,5	-0,56	3,5	+0,21	l
ALFA	9		9		kg
Additive	0,07		0		cc
w/c Ratio	0,49*		0,53		
Concretes					
Slump test (mm)	250		160		
Consistency class	S5		S4		
Wet mass (kg/m^3)	1630		1610		
Dry mass 7d – 28d (kg/m^3)	1620 -1600		1610 - 1600		
Compressive strength 7d (MPa)	27,5		22,9		
Compressive strength 28d (MPa)	29,73		30,2		

* w/c Ratio + additive according to UNI EN 11013

Dry mass (European-suggested standards UNI EN 12350-6) and compressive strength (7 days and 28 days after hydration beginning) on dried specimens were evaluated (Table 4).

The physical features of C1 and C2 concretes can be included in lightweight structural concrete field (Compressive strength 28 days > 20 MPa and Dry mass 1400-2000 kg/m^3) and they are similar to other commercial concretes (Fig. 2).

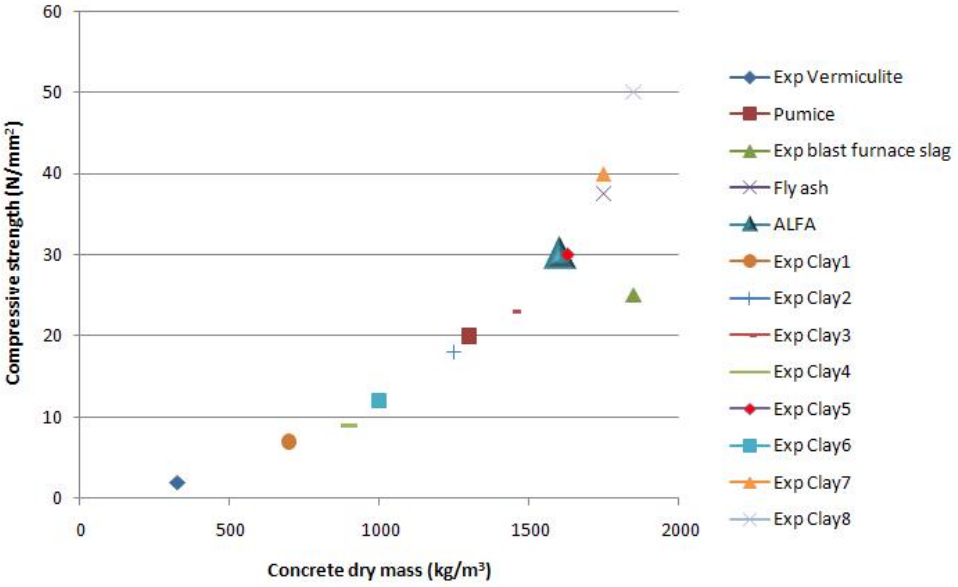

Fig. 2 - Comparison between some lightweight concretes and ALFA concrete (1Mpa = 1 N/mm^2).

DISCUSSION AND CONCLUSIONS

Wastes from dimension stone and grès tiles working processes represent a great environmental problem due to the founding of idoneous dumping sites.

This is also a cost that greatly affect the finished product.

It should be helpful propose alternative solutions for the reuse and the transformation of this wastes.

This research demonstrates that there is a concrete possibility of reuse in the production of lightweight aggregate suitable for the preparation of structural lightweight concrete.

Specifically sludge used with a chemical composition that allows for expansion into kitchen and a small percentage of abrasive used in any process which produces gas at a temperature of softening.

The main difference between the clusters obtained in the manner proposed in this research and those made from expanded clay is the low water absorption of the first due to the vitrified surface, compact and homogeneous.

This feature, together with good strength values in the heap, makes the lightweight aggregate used in the preparation of structural lightweight concrete as demonstrated by the tests in compression and the bulk density, falling perfectly within the limits suggested by the European-suggested standards UNI EN 196-1 (> 20 MPa; 1400-2000 kg/m^3).

Since the use of additive is now routine in achieving concrete results in an acceleration of the drying of these, it is believed that the good results already obtained could be further improved by appropriately adjusting of additive and water amounts in C1 mixture.

The benefits that this proposal would have to be recognized as a possible use in a continuous development of safe waste sawing and polishing that are currently available on the landfill by allocating the product thus obtained processing to packaging to obtain a structural CLS product of excellent quality with an economy likely cost of manufacture.

The replacement of the traditional clay with industrial wastes entails the added benefit of reducing the environmental impact caused by mining for the supply of raw materials.

REFERENCES

ANPA (2002): Rapporti - 18/02 - Rifiuti industriali, metodologie di calcolo dei coefficienti di produzione.

de Gennaro, R., Cappelletti, P., Cerri, G., de' Gennaro, M., Dondi, M., Graziano, S.F., Langella, A. (2007): Campanian Ignimbrite as raw material for lightweight aggregates. *Appl. Clay Sci.*, **37**, 115-126.

Riley, C.M. (1951): Relation of chemical properties to the bloating of clays. *J. Am. Ceram. Soc.*, **34**, 121-128.

UNI EN 12350-6 (2001): Massa volumica del calcestruzzo fresco.

UNI EN 12350-2 (2001): Prova di abbassamento al cono (Slump test).

UNI EN 1097-6 (2002): Prove per determinare le proprietà meccaniche e fisiche degli aggregati. Determinazione della massa volumica dei granuli e dell'assorbimento d'acqua.

UNI EN 11013 (2005): Aggregati leggeri. Argillo e Scisto espanso. Valutazione delle proprietà mediante prove su calcestruzzo convenzionale.

UNI EN 196-1 (2005): Metodi di prova dei cementi - Parte 1: Determinazione delle resistenze meccaniche.

UNI EN 206-1 (2006): Calcestruzzo - Specificazione, prestazione, produzione e conformità.

CHEMICAL AND STRUCTURAL STUDY OF ANIONIC AND CATIONIC SITES IN TRIOCTAHEDRAL MICAS AT RT AND HT TEMPERATURES

MARIA LACALAMITA
Dipartimento Geomineralogico, Università di Bari, Via Orabona 4, 70126 Bari

INTRODUCTION

Micas are a group of minerals with a complex crystal chemistry, characterized by substitutional disorder that may involve tetrahedral (Si, Al, Fe, Ti), octahedral (Mg, Mn, Fe^{2+}, Fe^{3+}, Ti^{3+}, Ti^{4+}, Al, Cr, Li, □), interlayer (K, Ba, Ca, Na, NH_4, □, H_2O) sites, as well as the anion (OH^-, O^{2-}, Cl^-, F^-) site. Many of the mutually substituting atoms may enter more than one site of the mica structure and involve more than one substitution mechanism (Waters & Charnley, 2002; Righter *et al.*, 2002). In addition, some elements may be characterised by variable valence state (Fe, Ti, etc.).

The geological importance of these minerals depends on their occurrence in many geological environments and on their potentiality as petrogenetic indicators. More specifically micas from volcanic rocks could allow to infer pre-eruptive magmatic conditions and discriminate between processes that occurred during the igneous phase of mica crystallization and those due to post-crystallization events, provided that complete chemical analyses and detailed knowledge of the substitution mechanisms, are available (Laurora *et al.*, 2007; Scordari *et al.*, 2008). In addition, the knowledge of the biotite behaviour at high temperature has implications for the characterizations of petrologic and geological systems.

In this work, the crystal chemistry of Mt. Vulture trioctahedral micas has been extensively investigated at room and high temperature using a combination of several independent analytical techniques. In particular, Electron Probe Micro Analysis (EPMA), Secondary Ion Mass Spectrometry (SIMS), Single Crystal X-Ray Diffraction, (SCXRD), Mössbauer Spectroscopy (MS) and Fourier Transform Infrared (FTIR) spectroscopy analyses have been used, in order to:

1) investigate the crystal chemistry of trioctahedral micas with particular attention to substitution mechanisms and anionic site chemical composition that form the basis from which reliable activity-composition models may be developed;

2) examine in detail how the structure of trioctahedral micas of complex composition responds to heating;

3) use the crystal chemical data of micas to get an insight into the geological processes the host rock underwent.

The mica crystals considered here have been separated from deposits belonging mainly to the oldest (~ 740 ka) and to the intermediate (~ 720÷570 ka) volcanic episodes of Mt. Vulture activity. Detailed stratigraphic classification of these deposits is reported in Giannandrea *et al.* (2006). In the present work, mica samples (labelled Vut215, IgnA, IgnB, LCR, and Pg5) used for the room temperature analyses were collected from the oldest volcanic deposits belonging to the Foggianello Synthem. Specifically, Vut215 micas, selected from lava fragment of the Molara Ignimbrite, belong to the Campanile Subsynthem, whereas IgnA, IgnB, LCR, Pg5 samples belong to the Fara d'Olivo Subsynthem. For high temperature investigations, one sample labelled SA, from intermediate deposits (Barile Synthem, Rionero Subsynthems) has been considered.

CHEMICAL CHARACTERIZATION

The chemical results, obtained from EPMA, and, for some sample, from SIMS investigations, have shown that:

1) Pg5 and LCR biotites are characterized by significant intercrystalline chemical variations particularly regarding the Mg/Fe, Ti and F contents. Indeed, Pg5 samples are characterized by remarkable chemical inhomogeneity, as revealed by the generally large ranges in oxide wt.%: 32.8÷36.6 for SiO_2, 15.9÷22.0 for MgO, 6.1÷13.4 for FeO_{tot}, 0.38÷2.4 for TiO_2, 0.8÷3.3 for BaO, 0.7÷1.4 for F. LCR micas have shown inter-grain variability pronounced for TiO_2 (2.8÷5.0 wt.%), F (0.83÷2.73 wt.%, SIMS data), BaO (0.07÷1.8 wt.%) and H_2O (1.24÷3.37 wt.%, SIMS data). This trend is also documented by previous investigations on other Mt. Vulture micas selected both from different and from the same stratigraphic layer (Schingaro *et al.*, 2001, 2005; Mesto *et al.*, 2006);

2) IgnA, IgnB, Vut215 and SA samples turned out to be relatively homogeneous. However, for Vut215 micas were found higher TiO_2 (<4.6> wt.%), BaO (<2.2> wt.%) and Na_2O (<0.7> wt.%) contents than the other samples.

Finally, the $Mg/(Mg+Fe_{tot})$ ratio or "Mg number" ranges from ~ 0.60÷0.90, and generally it decreases with increasing Ti atoms p.f.u.

MÖSSBAUER AND FTIR INVESTIGATIONS

Mössbauer investigation evidenced that in all samples Fe was in octahedral coordination. Indeed, all spectra showed three absorption bands at approximately -0.2, 1.0 and 2.3 mm/s which corresponded respectively to i) the sum of low energy lines of $^{VI}Fe^{2+}$ and $^{VI}Fe^{3+}$ doublets, ii) the high energy line of the $^{VI}Fe^{3+}$ doublet, and iii) high energy component of the $^{VI}Fe^{2+}$ doublet. There was no clear evidence for tetrahedral Fe^{3+} (whose high energy component occurs at ~ 0.5 mm/s) in the samples. The fitting according to the QSD method yielded the following results:

1) Fe^{2+} (%) = 42.3(34), Fe^{3+} (%) = 57.7(34) for IgnA;
2) Fe^{2+} (%) = 65.7(21), Fe^{3+} (%) = 34.3(21) for IgnB;
3) Fe^{2+} (%) = 61.5(69), Fe^{3+} (%) = 38.5(69) for Pg5.

For samples Vut215 and SA the results of previous Mössbauer investigations were used, which provided Fe^{2+} (%) = 11.21(35), Fe^{3+} (%) = 88.79(35) for Vut215 (Matarrese, 2007) and Fe^{2+} (%) = 11.21(35), Fe^{3+} (%) = 88.79(35) for SA (Scordari *et al.*, 2006).

The FTIR investigations were carried out in order to characterize the local environment of the anionic site O4. Measurements were performed on single crystals in the range 4000-600 cm^{-1}. The OH-stretching region for most of the analysed samples extended in the range ~ 3740-3600 cm^{-1} and consisted of normal and impurity bands associated only to fundamental vibrations of the OH groups. On the contrary, for three out of the five investigated LCR samples (LC6_R7, L6_R29 and LC7_R2), the OH stretching region was affected by overlapping of bands that extends up to ~ 2500 cm^{-1}. The results of fitting have shown:

1) a prominent band at ~ 3540 cm^{-1} assigned to OH with two Fe^{3+} and a vacancy, whereas a shoulder at ~ 3621 cm^{-1} is attributed to OH bonded to two Al and a vacancy (Libowitzky & Beran, 2004, and reference therein);

2) a series of overlapping band arising from about 3400 to 2800 cm^{-1} due to the ammonium ion (NH_4^+) and water (H_2O) normal modes of vibration.

Therefore, for LCR samples the total hydrogen content determined by SIMS encompasses different species, *i.e.* OH groups but also NH_4^+ groups and H_2O molecules, both of which substitute for K^+ at the interlayer site (Sadofosky & Bebout, 2000; Cesare *et al.*, 2003). It can be concluded that in this work FTIR analyses have significantly contributed to investigate the hydrogen speciation, the occurrence of octahedral vacancies, Fe-oxy substitution mechanism and, in general, to assess the correct structural formula of the analysed samples.

STRUCTURAL AND CRYSTAL CHEMICAL CHARACTERIZATION

Micas studied here belong to the 1*M* polytype. About 30 single crystal structure refinements have been performed in space group *C*2/*m*.

The samples Vut215, IgnA, IgnB, Pg5 and SA showed structural details (short *c* cell parameter, bond distances and distortion parameters such as t_{int}, t_{oct}, and $t_{K\text{-}O4}$; high value of $shift_{M2}$) which were consistent with the following occurrence of oxy-type substitutions (Cesare *et al.*, 2003; Matarrese *et al.*, 2008; Scordari *et al.*, 2006; Ventruti *et al.*, 2008):

- R^{3+}-oxy, $^{VI}Fe^{2+} + (OH)^- \leftrightarrow {}^{VI}R^{3+} + O^{2-} + ½\ H_2$;
- Ti-oxy, $^{VI}Fe^{2+} + 2(OH)^- \leftrightarrow {}^{VI}Ti^{4+} + 2O^{2-} + H_2$.

On the basis of the cell parameters (especially the *c*-cell parameters) the LCR samples could be divided into two groups: the first one, characterized by $c \sim 10.23$ Å, encompasses three samples (LC6_R7, LC6_R29 and LC7_R2); the other two samples (LC7_R4, LC7_R5) constitute the second group, which has $c \sim 10.14$ Å. These differences pointed to different extents of substitutions at the O4 hydroxyl site (Cesare *et al.*, 2003, and references therein; Matarrese *et al.,* 2008). Micas of the Group 1 were affected by the following substitution mechanisms:

- Ti-Tschermak, $^{VI}Fe^{2+} + {}^{IV}2Si^{4+} \leftrightarrow {}^{VI}Ti^{4+} + {}^{IV}2Al^{3+}$;
- Al, Fe^{3+}-vacancy, $3\,^{VI}Fe^{2+} \leftrightarrow 2\,^{VI}M^{3+} + {}^{VI}\square$;
- Ti-vacancy, $2\,^{VI}Fe^{2+} \leftrightarrow {}^{VI}Ti^{4+} + {}^{VI}\square$;
- Ti-oxy, $^{VI}Fe^{2+} + 2(OH)^- \leftrightarrow {}^{VI}Ti^{4+} + 2O^{2-} + H_2$
- $Fe^{2+} + K^+ \rightarrow Fe^{3+} + H_2O + K^0\downarrow$
- $3\ Fe^{2+} \rightarrow 2\ Fe^{3+} + \square + Fe^0\downarrow$
- $NH_4^+ \rightarrow K^+$

In Group 2 micas $^{VI}Ti^{4+}$ and $^{VI}Fe^{3+}$ enter the structure through oxy-type substitution mechanisms involving deprotonation at O4 as see above.

KINETICS OF FE-OXYDATION/DEPROTONATION PROCESS

Recent investigation have ascertained that oxy substitution mechanisms involving deprotonation at O(4) site play a major role in phlogopites (Virgo & Popp, 2000; Righter *et al.*, 2002; Scordari *et al.*, 2006). Feeley & Sharp (1996) pointed out that the H_2 released by these reactions can combine with the O_2 in the melt, thus increasing the volatile components and the explosive nature of volcanism.

In the second part of this work, the kinetics of the Fe-oxidation/deprotonation process at T = 600 and 700°C in SA samples (labelled SA_14 and SA_9) with composition analogous to those submitted to thermal investigation by Ventruti *et al.* (2008) has been studied. These authors observed the Fe-

oxidation/deprotonation reaction in an *in situ* high temperature X-ray single-crystal diffraction experiment in the temperature range -173-750°C. Ventruti *et al.* (2008) found that the process take place starting from T > 550°C and causes a shortening of the unit cell parameters and, consequently, of the cell volume. In that paper, it was demonstrated that the process is irreversible. It remained questionable, however, whether it was a one-step or a multi-step reaction.

Under isothermal condition the unit-cell parameters decrease following an exponential law and the most pronounced variations occur along the *c* axis. Equilibrium was reached in a time scale of ~ 10^4 and ~ 10^3 min at 600 and 700°C, respectively. The reversal experiment in the temperature range 950-25°C has shown:

1) the irreversibility of the Fe-oxidation/deprotonation process;

2) the superimposition of the linear expansion curves obtained for the two crystals, suggesting a same degree of deprotonation achieved at the two temperatures.

Therefore, the process occurs in an unique step. Structural modifications were also observed by comparing FTIR spectra in the OH stretching region collected before and after heating at 700°C. The most pronounced variations occur to normal and impurity OH stretching bands associated to $^{VI}Fe^{2+}$ and $^{VI}Fe^{3+}$ local environments. Relationships among the amount of Fe^{2+} that is oxidized, the amount of deprotonation, and the *b* and *c* parameters shortening have also been quantitatively estimated. They were found to be consistent with variation of crystal chemical formula before and after heating.

CONCLUSION

1) On the basis of their mineral chemistry, the analysed samples were "biotites" in the sense of the IMA classification of micas (Rieder *et al.*, 1998). Among the analysed micas, two samples (Pg5 and LCR) displayed significant intercrystalline chemical variations, whereas the others (IgnA, IgnB, Vut215 and SA) turned out to be relatively homogeneous.

2) Typical structural features of dehydrogenated micas were generally present in the analyzed biotites. The *c* parameter was reduced with respect to those measured in close-to-end-member annite (10.3235(4) Å, Redhammer & Roth, 2002) and phlogopite (10.310(5), synthetic sample Phl#2 in Redhammer & Roth, 2002).

3) Most of analysed samples are characterized by prevalence of oxy-type substitutional mechanisms that involve deprotonation at O4. On the contrary, some LCR micas show prevalence of vacancy-bearing substitutions and the occurrence of H_2O and NH_4^+ at the interlayer. These samples features were likely the result of the hydrothermal alteration of brown micas (the most common in Vulture deposits), which started their crystallization at high temperature (about 900°C) and low pressure (about 2 Kbar) conditions.

4) For IgnA, IgnB, Pg5 and SA samples were found Fe^{2+}/Fe^{3+} ratios similar to other Vulture samples and likely very close to magmatic values (Matarrese, 2007). On the contrary, for Vut215 micas were obtained $Fe^{3+}/Fe^{2+} >> 1$. Therefore, Vut215 biotites, selected from lavas, very likely underwent post-magmatic thermal oxidation processes.

5) The study of trioctahedral mica SA in the temperature range 25-950°C showed the occurrence of an irreversible deprotonation process with a consequent $Fe^{2+} \rightarrow Fe^{3+}$ oxidation starting from about 600°C and a phase transition implying no symmetry change. Kinetics of Fe-oxidation/deprotonation followed an exponential law, as shown by the trend of the lattice parameters and the volume measured at 600 and 700°C as a function of time. The results obtained in the present study confirmed the occurrence

of the Fe-oxidation/deprotonation process in a unique step, as previously found in other high temperature studies on micas (Tutti *et al.*, 2000; Chon *et al.*, 2006). The effects of the Fe-oxydation/deprotonation process were also observed on some OH stretching bands in the FTIR spectrum of an SA sample before and after heating.

REFERENCES

Cesare, B., Cruciani, G., Russo, U. (2003): Hydrogen deficiency in Ti-rich biotite from anatectic metapelites (El Joyazo, SE Spain): Crystal-chemical aspects and implications for high-temperature petrogenesis. *Am. Mineral.*, **88**, 583-595.

Chon, C.M., Lee, C.K., Song, Y., Kim, S.A. (2006): Structural changes and oxidation of ferroan phlogopite with increasing temperature: *in situ* neutron powder diffraction and Fourier transform infrared spectroscopy. *Phys. Chem. Minerals*, **33**, 289-299.

Feeley, T.C. & Sharp, D. (1996): Chemical and hydrogen isotope evidence for *in situ* dehydrogenation of biotite in silicic magma chambers. *Geology*, **24**, 1021-1024.

Giannandrea, P., La Volpe, L., Principe, C., Schiattarella, M. (2006): Unità stratigrafiche a limiti in conformi e storia evolutiva del vulcano medio-pleistocenico del Monte Vulture (Appennino Meridionale, Italia). *Boll. Soc. Geol. It.,***125**, 67-92.

Laurora, A., Brigatti, M.F., Mottana, A., Malferrari, D., Caprilli, E. (2007): Crystal chemistry of trioctahedral micas in alcaline and subalkaline volcanic rocks: A case study from Mt. Sassetto (Tolfa district, Latium, central Italy). *Am. Mineral.*, **92**, 468-480.

Libowitzky, E. & Beran, A. (2004): IR spectroscopic characterisation of hydrous species in minerals. *In* "Spectroscopic methods in mineralogy", A. Beran & E. Libowitzky, eds. Eötvös University Press, Budapest, 227-279.

Matarrese, S. (2007): Cristallochimica comparativa di flogopiti del Monte Vulture. PhD Thesis, University of Bari, Italy, 160 p.

Matarrese, S., Schingaro, E., Scordari, F., Stoppa, F., Rosatelli, G., Pedrazzi, G., Ottolini, L. (2008): Crystal chemistry of phlogopite from Vulture-S.Michele Subsynthem volcanic rocks (Mt. Vulture, Italy) and volcanological implications. *Am. Mineral.*, **93**, 426-437.

Mesto, E., Schingaro, E., Scordari, F., Ottolini, L. (2006): Electron microprobe analysis, secondary ion mass spectrometry and single crystal X-ray diffraction study of phlogopites from Mt. Vulture, Potenza, Italy: Consideration of cation partitioning. *Am. Mineral.*, **91**, 182-190.

Redhammer, G.J. & Roth, G. (2002): Single-crystal structure refinements and crystal chemistry of synthetic trioctahedral micas $KM_3(Al^{3+},Si^{4+})_4O_{10}(OH)_2$, where M = Ni^{2+}, Mg^{2+}, Co^{2+}, Fe^{2+}, or Al^{3+}. *Am. Mineral.*, **87**, 1464-1476.

Rieder, M., Cavazzini, G., D'Yakonov, Y.S., Frank-Kamenetskii, V.A., Gottardi, G., Guggenheim, S., Koval, P.V., Müller, G., Neiva, A.M.R., Radoslovich, E.W., Robert, J.-L., Sassi, F.P., Takeda, H., Weiss, Z., Wones, D.R. (1998): Nomenclature of micas. *Can. Mineral.*, **36**, 905-912.

Righter, K., Dyar, M.D., Delaney, J.S., Vennemann, T.W., Hervig, R.L., King, P.L. (2002): Correlation of octahedral cations with OH^-, O^{2-}, and F^- in biotite from volcanic rocks and xenoliths. *Am. Mineral.*, **87**, 142-153.

Sadofsky, S.J. & Bebout, G.E. (2000): Ammonium partitioning and nitrogen-isotope fractionation among coexisting micas during high-temperature fluid-rock interactions; examples from the New England Appalachians. *Geochim. Cosmochim. Acta*, **64**, 2835-2849.

Schingaro, E., Scordari, F., Ventruti, G. (2001): Trioctahedral micas-1*M* from Mt. Vulture (Italy): Structural disorder and crystal chemistry. *Eur. J. Mineral.*, **13**, 1057-1069.

Schingaro, E., Mesto, E., Scordari, F., Brigatti, M.F., Pedrazzi, G. (2005): Cation site partitioning in Ti-rich micas from Black Hill (Australia): a multi-technical approach. *Clays Clay Miner.*, **53**, 179-189.

Scordari, F., Ventruti, G., Sabato, A., Bellatreccia, F., Della Ventura, G., Pedrazzi, G. (2006): Ti-rich phlogopite from Monte Vulture (Potenza, Italy) investigated by a multianalytical approach: substitutional mechanisms and orientation of the OH dipoles. *Eur. J. Mineral.*, **18**, 379-391.

Scordari, F., Schingaro, E., Ventruti, G., Lacalamita, M., Ottolini, L. (2008): Red micas from basal ignimbrites of Mt. Vulture (Italy): interlayer content appraisal by a multi-methodic approach. *Phys. Chem. Minerals*, **35**, 163-174.

Tutti, F., Dubrovinsky, L.S., Nygren, M. (2000): High temperature study and thermal expansion of phlogopite. *Phys. Chem. Minerals*, **27**, 599-603.

Ventruti, G., Zema, M., Scordari, F., Pedrazzi, G. (2008): Thermal behavior of a Ti-rich phlogopite from Mt. Vulture (Potenza, Italy): An *in situ* X-ray single-crystal diffraction study. *Am. Mineral.*, **93**, 632-643.

Virgo, D. & Popp, R.K. (2000): Hydrogen deficiency in mantle-derived phlogopites. *Am. Mineral.*, **85**, 753-759.

Waters, D.J. & Charnley, N.R. (2002): Local equilibrium in polymetamorphic gneiss and the titanium substitution in biotite. *Am. Mineral.*, **87**, 383-396.

THE LIGURIDE ACCRETIONARY WEDGE IN THE CALABRIA-LUCANIA BORDER AREA (SOUTHERN APENNINES): A THERMOCHRONOLOGICAL AND STRUCTURAL STUDY

SALVATORE LAURITA
Dipartimento di Scienze Geologiche, Università della Basilicata, Viale dell'Ateneo Lucano 10, 85100 Potenza

Accretionary wedges represent a long-lasting tectonic environment where rock bodies can be underplated at great depths and subsequently exhumed in a relatively short time interval (Platt, 1986; Ernst, 1988). Exhumation mechanisms are still not well understood and much effort has been focused in understanding how the HP rocks return to the surface.

The accretionary wedge is considered as an open system (Platt, 1986), in which the material is removed by tectonic processes or by erosion (Ring & Brandon, 1994). In many cases, extensional shear zones have been recognised (Platt, 1986).

The Liguride Complex (Ogniben, 1969) represents the uppermost structural unit of the Southern Apennines (Patacca & Scandone, 2007, and reference therein). This mountain belt, resulting from convergence of different paleogeographic domains of the European and the Adria plates, developed during Neogene time with ENE vergence (Patacca & Scandone, 2007, and references therein). The Liguride Units represent the remains of a Jurassic ocean, which laid between the Calabrian and Apulian terrains. Late Cretaceous - Tertiary subduction of this oceanic domain gave rise to the Liguride accretionary wedge that finally collided with the Adriatic margin during the Late-Oligocene early-Miocene times (Knott, 1987, 1994).

During this evolution the accreted material was divided into two main tectonic units: the metamorphic Frido Unit (Amodio Morelli *et al.*, 1976; Bonardi *et al.*, 1988) and the non-metamorphic Nord Calabrese Unit (Bonardi *et al.*, 1988). The Frido Unit mainly consists of polydeformed metasediments, showing a low-grade metamorphic overprint, with associated blocks of oceanic and continental crust (Monaco & Tortorici, 1995; Knott, 1987, 1994; Spadea, 1982, 1994).

The meta-sedimentary rocks of the Frido Unit (Monaco *et al.*, 1995; Monaco & Tortorici, 1995) can be subdivided in a lower phyllite subunit, consisting of phyllites, meta-arenites, quartzites and isolated bodies of meta-limestones, and in an upper calcschist subunit mainly consisting of meta-limestones. Bodies of continental crust rocks, generally overlying slices of serpentinites (Spadea, 1982), are mainly composed of altered garnet gneisses, garnet biotitic gneisses and leucocratic gneisses. Often gneisses contain lenticular bodies of amphibolite, generally crosscut by mafic dikes (Spadea, 1982).

Petrographic and structural studies on the rocks of the Frido Unit shows that this entire domain was subjected to high pressure-low temperature conditions during the Alpine evolution (Spadea, 1982). In more detail, Spadea (1982) identified high pressure and low temperature mineral assemblages in the continental crust rocks. According to Knott (1987, 1994) the mineral assemblage of the HP/LT overprint formed during subduction by underplating processes. The HP/LT metamorphism evolved in the greenschist facies during exhumation of the lower portions of the accretionary wedge. According to Monaco *et al.* (1991) and Spadea (1982), the HP-LT metamorphic event was connected to crystallization of glaucophane-lawsonite in mafic rocks and aragonite in metasedimentary rocks.

Even though the main structural and petrographic features of the Liguride Units have been already described in the literature, the evolution of the Liguride accretionary wedge is still matter of debate. Two main hypotheses have been proposed in the literature to explain the geodynamic evolution of the Liguride units. The first hypothesis considers the Liguride terrains as elements of an Apulia-verging accretionary wedge (*e.g.* Ogniben, 1969; Knott, 1987; Monaco & Tortorici, 1995; Cello & Mazzoli, 1999), related to the Late Cretaceous to Oligocene subduction of the neotethyan oceanic crust. The second hypothesis considered these terrains as remnants of an Europe-verging Alpine wedge of Cretaceous-Eocene age, later incorporated in the construction of the Apulia-verging Apennine chain during the Oligocene-Miocene times (*e.g*. Amodio Morelli *et al.*, 1976; Bonardi *et al.*, 1988).

The thesis work aims to define more clearly the evolution of the Liguride accretionary complex by means of structural, microstructural, petrographical, mineralogical and geochronological data. In particular, age determinations on the exhumation of underplated have been used to reconstruct the internal dynamics of the accretionary wedge and the age of the subduction process. Mineralogical data for the metasediments provided more precise determinations of the metamorphic conditions that have been compared with petrological evidence obtained from ophiolitic and continental crust rocks. Structural and microstructural data gave new indications on the deformation history and on the shear sense of the major mylonitic levels. These new data provide new constraints in the geodynamic modelling of the western Mediterranean area and on the thermotectonic evolution (*sensu* Brandon, 1992; Hasebe *et al.*, 1993; Tagami & Dumitru, 1996) of the Liguride wedge.

Field, mineralogical and petrographical data allowed to subdivide the Liguride accretionary complex into three main tectonic units: i) the uppermost Frido Unit, characterized by low-grade metamorphic conditions; ii) the intermediate M. Tumbarino Unit, characterized by metamorphic conditions intermediate between anchizone and diagenesis; iii) the lowermost North Calabria Unit, showing only diagenetic conditions.

The study has been concentrated on the Frido Unit that documents deformation and metamorphic features typical of the deep portions of the Liguride accretionary wedge. Geological mapping has been carried out in five significant areas (from the East to the West: Seluci-Perruttieri-M. Nandiniello, Gallizzi, Cropani-Episcopia, Timpa delle Murge and M. Tumbarino), where the main lithologies and structures of the Frido and M. Tumbarino units crop out (Fig. 1).

In the Frido Unit the ophiolitic rocks are characterized by differences in deformation features and metamorphic grade. The more widely exposed metabasites show well-developed foliation and lineation. They consist of meta-pillow lavas, meta-pillow breccias and meta-hyaloclastites. Frequently, these rocks are in contact with metalimestones and phyllites. In turn, blocks of metabasites (metadolerites) associated with serpentinites are devoid of planar and linear fabrics.

The detailed structural analysis carried out in the study area allowed to recognize structures related to a polyphase deformation history, well developed in metasedimentary rocks of the Frido Unit. Structures and fabric elements related to two early deformation phases (D1 and D2) are overprinted by a later phase developing decametre D3 E-W oriented folds.

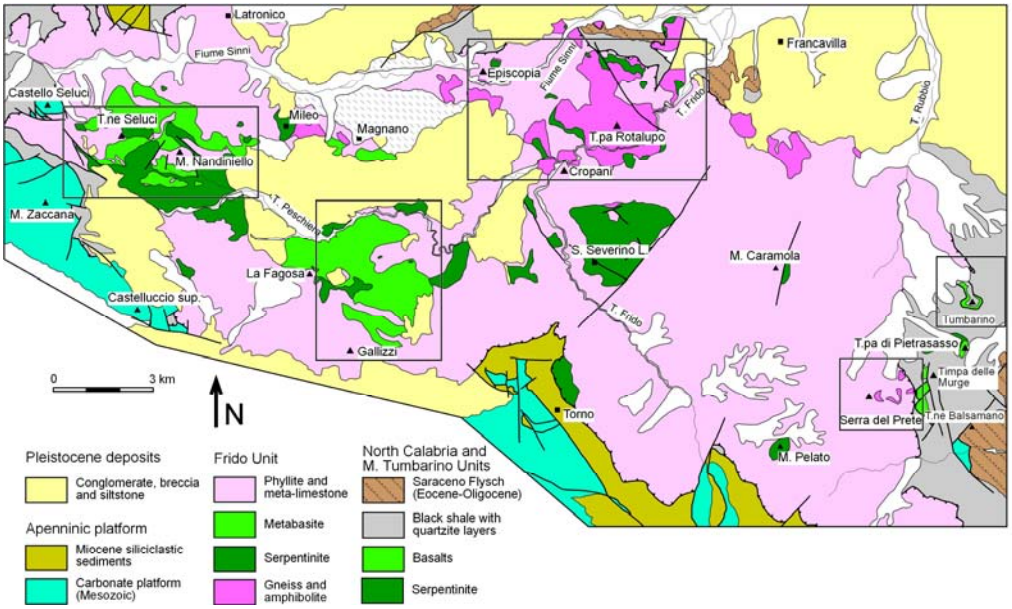

Fig. 1 - Geological sketch map of the Liguride Units in the Calabria-Lucania border area. Boxes outline the areas where detailed fieldwork has been carried out.

D1 foliation is associated with metamorphism under blueschist facies conditions. In places, metabasites affected by D1 mylonitic foliation are overprinted by static crystallisation of euhedral lawsonite porphyroblasts, indicating that high-pressure conditions outlasted the D1 deformation. Later D2 folds and crenulations overprint the previous fabrics, producing a well-developed crenulation cleavage. Local occurrence of riebeckite along the crenulation cleavage suggests that HP-LT conditions operated also during the D2 deformation.

Shear sense indicators obtained from mylonitic bands are mainly coherent with top-to-the-W and top-to-the-NW shear sense. However, indicators showing S- to SE-directed shear have been also found.

A mineralogical and petrological analysis of metabasites, which represent the major component of the ophiolitic sequences of the Frido Unit, has been performed by means of optical microscopy and electron microprobe. Mineral and whole-rock analyses have been used to document the composition of minerals belonging to the HP-LT assemblage and to reconstruct the P-T path.

In the present work the P-T conditions of selected samples of metabasites in the blueschist zone have been estimated using thermobarometric methods. Estimates have been done for glaucophane-omphacite- and jadeite-bearing rocks using the Theriak/Domino software (de Capitani, 1994). This software allows the construction of P-T phase diagrams that have been applied in order to reconstruct the P-T path in metabasites.

The common blueschist facies mineral assemblage in the massive metadolerites consists of sodic amphibole + sodic pyroxene + chlorite. Sodic pyroxene forms prismatic crystals, commonly replaced at the rims by glaucophane. P-T conditions of the blueschist facies metamorphism are estimated to 8-12 kbar and 300-400°C. In particular, absence of lawsonite in metadolerites indicates that pressure did not

exceed about 13 kbar. The blueschist facies metamorphism was followed by a decrease in pressure and temperature up to the pumpellyite stability field.

Metamorphic conditions deduced in mafic rocks have been compared with mineralogical data obtained by X-ray diffraction in low-grade metasediments. This analysis has been performed by using methods taken from studies on diagenesis or anchimetamorphism, such as illite crystallinity (Frey & Robinson, 1999), the percentage of $2M_1$ polytipe (Maxwell & Hower, 1967) and the b_0 parameter of illite-muscovite (Sassi & Scolari, 1974). By these means, an average temperature of 250°C and a pressure ranging between 7 and 9 kbar can be estimated for the Frido Unit. Estimated pressures are coherent with the widespread presence of aragonite in the metalimestones. Even higher pressures (and, possibly, temperatures) are probably recorded in the southern sector (Seluci-Perruttieri-M. Nandiniello and Gallizzi areas) where quartz veins in phyllites contain carpholite. Metapelites of the M. Tumbarino Unit show a metamorphic overprint occurring at a distinctly lower temperatures (about 200°C) and pressures (about 6 kbar).

In this study the exhumation age of the underplated material has been investigated by the fission track (FT) method. This allows to obtain information on the thermotectonic evolution of the Liguride accretionary wedge, now incorporated within the Southern Apennine chain. Fission track analyses are a useful tool to unravel the cooling history experienced by rocks at low temperatures, generally acquired by upper crustal levels. In particular, closure temperatures of fission tracks in zircon are close to maximum temperatures reached by the Liguride Units during the HP-LT metamorphism.

The fission track method (FT) has greater sensitivity to metamorphic overprinting at temperatures between 200-320°C (Tagami *et al.*, 1996) or 240±50°C (Hurford, 1986) or 260°C (Liu *et al.*, 2001) compared with other techniques and thus is well suited for low-temperature thermochronology. The temperature of 260°C (Liu *et al.*, 2001) corresponds to the limit between the prehnite-pumpellyite facies and the greenschist facies metamorphism (Naeser, 1979; Gleadow *et al.*, 1983; Green *et al.*, 1989). Coupling petrological data with FT analyses is possible to fix the paleogeothermal gradients during exhumation of the HP-LT rocks.

Thermotectonic evolution of continental crust slices from the Liguride accretionary wedge is presently unknown. Here we report the first results of FT analyses of zircons from continental crust fragments (garnet gneiss, garnet-biotite gneiss and metagranite) and a metapelite sample from the Frido Unit. The minor thermal input provided by HP/LT metamorphism, eventually coupled with the later greenschist facies overprint, was likely capable to reset the zircon fission track geochronometer.

Results indicate that FT in zircons from the main continental crust slice of Timpa Rotalupo (Cropani-Episcopia area) record exhumation ages of about 65-56 Ma, corresponding to the Paleocene. A younger Oligocene event is supported by “mixed” ages obtained in some metagranitoids and in a basement slice from the Episcopia area. A sample of low-grade metasediments yields poorly constrained Cretaceous ages, indicating that locally FT in zircons were not reset during the HP-LT event.

Geochronologic data of continental crust rocks indicate that possibly the Liguride Complex underwent a multistage subduction and exhumation history. However, the overall evolution took place under a low geothermal gradient, typical of HP-LT metamorphism. This is well documented by the presence of HP-LT parageneses statically overgrowing the D1 mylonitic foliation and growing syntectonically along the D2 crenulation cleavage. Paleocene ages can be related to the early evolution of the “Alpine” accretionary wedge, as documented by the W- to NW-directed shearing found in some

mylonitic bands. On the other hand, Oligocene ages possibly record the incorporation of the Liguride Units in the Apennine chain.

Finally, we propose that the exhumation processes recorded in HP-LT rocks from the Frido Unit shows some similarities with respect to the evolution recognised in the Franciscan Complex. In particular, both subduction complexes are characterized by exhumation taking place in an overall "cold" environment. In the Frido Unit this is clearly shown by the widespread occurrence of well-preserved HP/LT minerals (glaucophane, Na-pyroxene, lawsonite, riebekite and aragonite) and by the lack of a significant overprint in the greenschist facies.

REFERENCES

Amodio Morelli, L., Bonardi, G., Colonna, V., Dietrich, D., Giunta, G., Ippolito, F., Liguori, V., Lorenzoni, S., Paglionico, A., Perrone, V., Piccarreta, G., Russo, M., Scandone, P., Zanettin Lorenzoni, E., Zuppetta, A. (1976): L'Arco Calabro-Peloritano nell'Orogene Appenninico-Maghrebide. *Mem. Soc. Geol. It.*, **17**, 1-60.

Bonardi, G., Amore, F.O., Ciampo, G., De Capoa, P., Micconet, P., Perrone, V. (1988): Il complesso Liguride. Auct.: stato delle conoscenze e problemi aperti sulla sua evoluzione pre-appenninica ed i suoi rapporti con l'Arco Calabro. *Mem. Soc. Geol. It.*, **41**, 17-35.

Brandon, M.T. (1992): Decomposition of fission-track grain-age distributions. *Am. J. Sci.*, **292**, 535-564.

Cello, G. & Mazzoli, S. (1999): Apennine tectonics in Southern Italy: a review. *J. Geodyn.*, **27**, 191-211.

de Capitani, C. (1994): Gleichgewichts-Phasendiagramme: Theorie und Software. *Ber. Deutsch. Mineral. Gesell.*, **6**, 48.

Ernst, W.G. (1988): Tectonic history of subduction zones inferred from retrograde blueschist P-T paths. *Geology*, **16**, 1081-1084.

Frey, M. & Robinson, D. (1999): Low grade metamorphism. Blackwell, Oxford, 313 p.

Gleadow, A.J.W., Duddy, I.R., Lovering, J.F. (1983): Fission-track analysis: a new tool for the evaluation of thermal histories and hydrocarbon potential. *Austr. Petrol.Explor. Ass. J.*, **23**, 93-102.

Green, P.F., Duddy, I.R., Laslett, G.M., Hegarty, K.A., Gleadow, A.J.W., Lovering, J.F. (1989): Thermal annealing of fission-tracks in apatite. 4: Quantitative modelling techniques and extension to geological time scale. *Chem. Geol., Isotope Geosci. Sect.*, **79**, 155-182.

Hasebe, N., Tagami, T., Nishimura, S. (1993): Evolution of the Shimanto accretionary complex. A fission-track thermochronologic study. *In*: "Thermal evolution of the Tertiary Shimanto belt, Southwest Japan: an example of ridge-trench interaction", M.B. Underwood, ed. *Geol. Soc. Am. Spec. Pap.*, **273**, 121-136.

Hurford, A.J. (1986): Cooling and uplift patterns in the Lepontine Alps, south central Switzerland and an age of vertical movement on the Insubric fault line. *Contib. Mineral. Petrol.*, **92**, 413-427.

Knott, S.D. (1987): The Liguride Complex of southern Italy-a Cretaceus to Paleogene accretionary wedge. *Tectonophys.*, **142**, 217-243.

Knott, S.D. (1994): Structure, kinematics and metamorphism in the Liguride Complex, southern Apennines, Italy. *J. Struct. Geol.*, **16**, 1107-1120.

Liu, Y.S., Gao, S., Jin, S.Y., Hu, S.H., Sun, M., Zhao, Z.B., Feng, J.L. (2001): Geochemistry of lower crustal xenoliths from Neogene Hannuba basalt, North, China craton: implications for petrogenesis and lower crustal composition. *Geochim. Cosmochim. Acta*, **65**, 2589-2604.

Maxwell, D.T. & Hower, J. (1967): High grade diagenesis and low-grade metamorphism of illite in the Precambrian Belt series. *Am. Mineral.*, **52**, 843-857.

Monaco, C., Tansi, C., Tortorici, L., De Francesco, A.M., Morten, L. (1991): Analisi geologio-strutturale dell'Unità del Frido al Confine Calabro-Lucano (Appennino Meridionale). *Mem. Soc. Geol. It.*, **47**, 341-353.

Monaco, C. & Tortorici, L. (1995): Tectonic role of ophiolite-bearing terranes in the development of the southern Apennines Orogenic Belt. *Terra Nova*, **7**, 153-160.

Monaco, C., Tortorici, L., Morten, L., Critelli, S., Tansi, C. (1995): Geologia del versante nord-orientale del massiccio del Pollino (confine calabro-lucano): nota illustrativa sintetica della carta geologica alla scala 1:50000. *Boll. Soc. Geol. It.*, **114**, 277-291.

Naeser, C.W. (1979): Fission-track dating and geologic annealing of fission track. *In*: "Lectures in isotope geology", E. Jager & J.C. Hunziker, eds. Spriger, New York, 154-169.

Ogniben, L. (1969): Schema introduttivo alla geologia del confine Calabro-Lucano. *Mem. Soc. Geol. It.*, **8**, 453-763.

Patacca, E. & Scandone, P. (2007): Geology of the Southern Apennines. *Boll. Soc. Geol. It., Spec. Vol.*, **7**, 75-119.

Platt, J.P. (1986): Dynamics of orogenic wedge and the uplift of high-pressure metamorphics rocks. *Bull. Geol. Soc. Am.*, **97**, 1037-1053.

Ring, U. & Brandon, M.T. (1994): Kinematic data for the Coast Range fault and implications for exhumation of the Franscican subduction complex. *Geology*, **22**, 735-738.

Sassi, F.P. & Scolari, A. (1974): The b_0 value of the potassic white mica as a barometric indicator in low-grade metamorphism of pelitics schists. *Contrib. Mineral. Petrol.*, **45**, 143-152.

Spadea, P. (1982): Continental crust rocks associated with ophiolites in Lucanian Apennine (southern Italy). *Ofioliti*, **2/3**, 501-522.

Spadea, P. (1994): Calabria-Lucania ophiolites. *Boll. Geofis. Teor. Appl.*, **34**, 271-281.

Tagami, T. & Dumitru, T.A. (1996): Provenance and thermal history of the Franciscan accretionary complex: constraints from zircon fission track thermochronology. *J. Geophys. Res.*, **101**, 8245-8255.

Tagami, T., Carter, A., Hurford, A.J. (1996): Natural long-term annealing of the zircon fission-track system in Vienna Basin deep borehole samples: constraints upon the partial annealing zone and closure temperature. *Chem. Geol., Isotope Geosci. Sect.*, **122**, 249-258.

STRUCTURAL STUDY OF Pb-Bi SULFOSALTS FROM VULCANO (AEOLIAN ISLAND, ITALY) BY TRANSMISSION ELECTRON MICROSCOPY

DONATELLA MITOLO
Dipartimento Geomineralogico, Università di Bari, Via Orabona 4, 70126 Bari

INTRODUCTION

The first Transmission Electron Microscopy (TEM) investigations are performed on some Pb-Bi sulfosalts from the high-temperature fumaroles (T ~ 400°C) of Vulcano, Aeolian Islands, Italy.

Among the sulfosalts belonging to the PbS-Bi_2S_3 system, the TEM investigation has been performed on two natural sulfosalts of the Lillianite Homologues Series (LHS) (Makovicky, 1981), lillianite and heyrovskýite, which are very abundant at Vulcano and unique examples Ag- and Cu-free sulfosalts known in nature, and on one analogues synthetic Phase II (85.7 mol.% PbS). In addition, TEM investigation was also extended to natural crystal of galenobismutite, which was never structurally investigated by transmission electron microscopy.

The structure of lillianite, ideally $Pb_3Bi_2S_6$, and heyrovskýite, ideally $Pb_6Bi_2S_9$, is based on ordered intergrowths of "galena-like" slabs cut parallel to $(131)_{PbS}$ and stacked along $[010]_{lill}$ (*Bbmm* setting). Any two slabs are twin related and diverse members of this series differ by the thickness of the "galena-like" slabs and, consequently, by the frequency of the *chemical twinning* (Makovicky, 1977).

The most of studies on natural heyrovskýite and lillianite concern minerals containing monovalent cations, such as Ag, Cu. It is also known that these monovalent cations play a role in stabilizing structure (Price & Yeomans, 1984; Skowron & Tilley, 1990).

Due to the particular sensitivity of sulfosalts, to the heating effect of the ion beam during preparation and electron beam during observation (Loginov & Brown, 1992; Skowron & Tilley, 1986; Tilley & Wright, 1982), a particular attention has been given to the preparation techniques of the samples and some precautions were also taken during TEM observations (*i.e.*, low intensity of the electron beam and low exposition of the crystal to the electron beam).

Three different methods, ion-milling, crushing and ultramicrotomy, have been used to prepare several sufficiently thinned samples for TEM investigation. Among these, the ion-milling technique is resulted to be one of the most powerful techniques to prepare sulfosalts, allowing to obtain uniformly and widely thin transparent regions of sulfosalts samples, following the procedure suggested by Barna (1992).

Two different electron microscope have been used to specimens investigation: JEOL JEM 2010 and JEOL JEM 4000, operating at 200 kV and 400 kV, respectively.

The investigated lillianite and heyrovskýite from Vulcano appear as discrete phases, showing a perfectly ordered sequence of slabs 4,4 and 7,7, respectively, with very few stacking faults and/or dislocations. In addition, all the lillianite crystals and few heyrovskýite crystals result non modulated structure. Also the natural galenobismutite crystals appear as a well-ordered structure. On the contrary the most of heyrovskýite crystals showed interesting modulations. This is the first report of the presence of modulations in the natural heyrovskýite structure, never observed in natural Ag-bearing sample (Makovicky *et al.*, 1991) and in synthetic analogue (Pring *et al.*, 1999; Pring & Etschmann, 2002; Prodan *et al.*, 1982).

ORDERED NON MODULATED STRUCTURES

The lillianite crystals from Vulcano show a well-ordered structure with a constant average periodicity of approximately 20.6 Å along *b* direction (Fig. 1a). All the analyzed crystal fragments do not show streaks and/or additional reflections, but only sharp reflections corresponding to the lillianite-like structure (Fig. 1b). Really, subordinate and little areas with low crystallinity could be seen only in the ion-milled lillianite, explained as either a reaction effect under the electron beam or a sublimation phenomenon under the vacuum conditions during the preparation of the sample (Skowron & Tilley, 1986). But, during TEM observations, no dynamic processes, like formation of other phases or chemical reaction, were observed in the lillianite crystals from Vulcano. As a consequence, we exclude that the observed low crystallinity is related to the electron beam and we consider highly probable that it can be ascribed to sublimation phenomena of the sample under the vacuum conditions of the Precision Ion-Polishing System (PIPS) instrument.

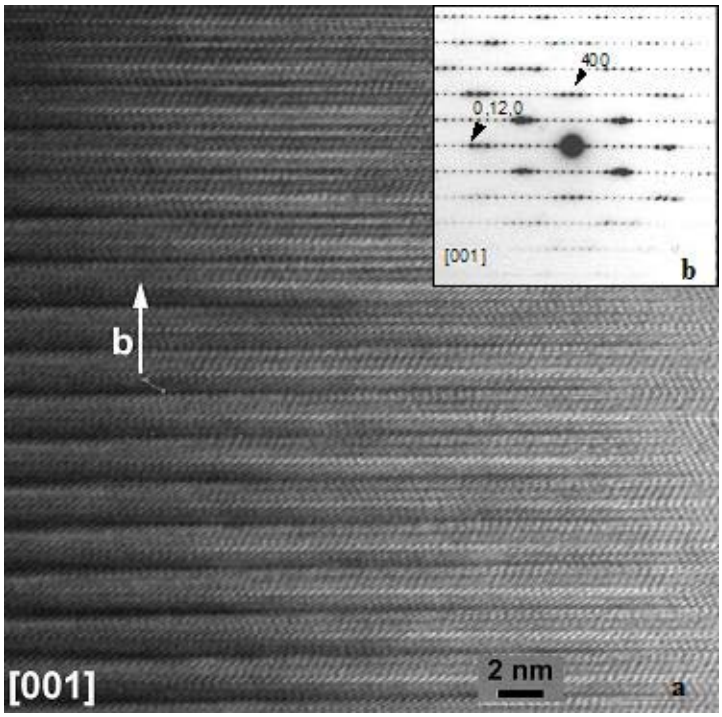

Fig. 1 – HRTEM image (a) and SAED pattern down the [001] zone (b) of well-ordered lillianite (crushed sample).

Analogous ordered structures without any modulation have been observed in some ultramicrotomed heyrovskýite crystals (Fig. 2a), both natural and synthetic (85.7 mol.% PbS), as testified by the absence of streaks and satellite reflections in electron diffraction patterns (Fig. 2b). No substantial differences between natural and synthetic crystals could be observed, except rare stacking faults in the synthetic Phase II observed at low magnification. A perfect constant periodicity of the slabs of approximately 31.2 Å was determined for both the natural phase and its synthetic analogue. This lead us to confirm the structural similarity between the Ag-free heyrovskýite from Vulcano and the synthetic analogue here analyzed. The results obtained in this work on synthetic heyrovskýite are highly comparable with those obtained by Prodan *et al.* (1982) for the same material but prepared and analyzed under different conditions (crushed sample, investigated at 125 kV). This analogy of the results indicates that ultramicrotomy and crushing are preparation tecniques substantially equivalent each other, which can

be usefully used in TEM investigations on sensitive materials. In addition, the absence of structural defects in the samples from Vulcano, support the evidence that disorder stacking sequences are connected with the induced heating during TEM investigations (Skowron & Tilley, 1986, 1990; Colaïtis *et al.*, 1981), rather than with the sample preparation procedure.

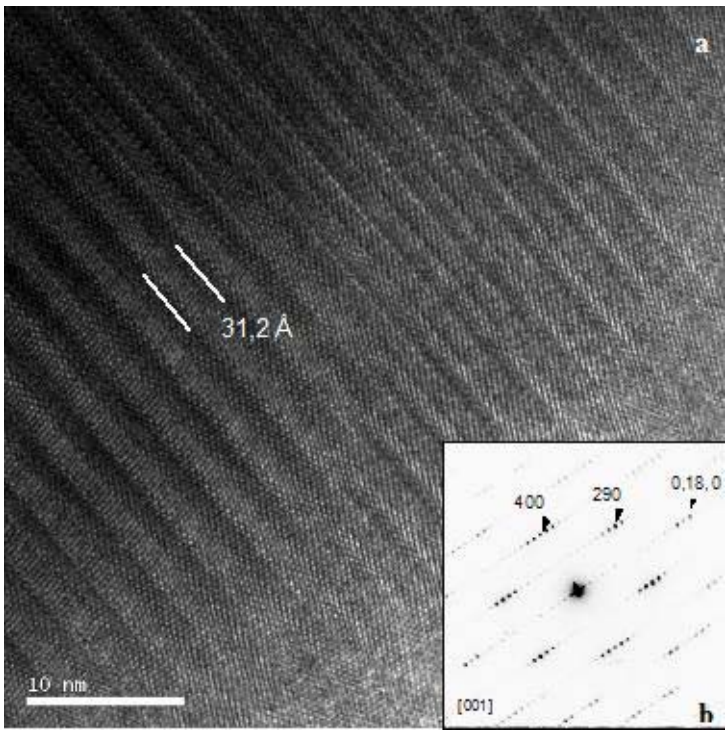

Fig. 2 – HRTEM image (a) and electron diffraction pattern down the [001] zone (b) of heyrovskýite (ultramicrotomed sample).

Also ordered structures without any modulation have been observed in the ultramicrotomed galenobismutite crystal from Vulcano. A perfect constant periodicity of the slabs of approximately 11.8 Å was determined. No HRTEM images, which refers to for comparison, are available in literature neither on natural or synthetic galenobismutite. Only some SAED patterns on synthetic Phase IV are reported (Colaïtis *et al.*, 1981; Tilley & Wright, 1986). Our preliminary results are highly comparable with those reported by Colaïtis *et al.* (1981) for the synthetic Phase IV, suggesting that natural galenobismutite is characterized by an ordered structure without modulations. More experimental work on this matter is obviously desirable for the future.

INTERGROWTHS

A lamella of heyrovskýite (about 145 nm wide) intergrown in a lillianite crystal has been observed in one sample prepared by ion milling. This is a structural features quite uncommon in lillianite and heyrovskýite from Vulcano, but frequently occurring in analogues natural Ag-bearing samples from other localities (Pring & Etschmann, 2002; Pring *et al.*, 1999; Makovicky *et al.*, 1991). In this case too, lillianite presents a well-ordered structure but heyrovskýite appears again as an ordered incommensurate modulated structure. In addition, some planar defects, like edge dislocations, are clearly visible near the observed boundary between lillianite and heyrovskýite. These defects, whose occurrence is well documented in literature, play an important role in the detwinning process. As a matter of fact,

detwinning would be facilitated by the movement of the dislocation from sheet to sheet of the twinned structure, because the dislocation movement decreases substantially the number of chemical bonds that have to be broken to allow the structural change and makes it an energetically feasible process (Skowron & Tilley, 1986). Similar processes were observed as artefacts in transformations of lillianite and heyrovskýite into a galena matrix (Skowron & Tilley, 1986), and they were interpreted as due to the combined effect of the heating induced by the electron beam and of the surrounding vacuum with loss of Bi atom or Bi_2S_3, rather than as due to chemical reaction (Tilley & Wright, 1982; Skowron & Tilley, 1986). In the investigated sample the interruption of the slabs of heyrovskýite are clearly evident, and the presence of the edge dislocations near the boundary of heyrovskýite and lillianite phases suggests that elastic strain energy may also be significant.

Stacking disorder is also observed in the crushed, natural heyrovskýite crystal investigated at 400 kV. This evidence is suggested by the presence of pronounced streaks along the **b*** direction in the electron diffraction pattern. Taking into account that the damage rate induced by electron beam decreases with the increase of operating voltage (Klimentidis & Mackinnon, 1986) and the secondary microstructural defects increase linearly with increasing electron beam flux (Loginov & Brown, 1992), we exclude that the observed disorder could be associated to the different working conditions used for TEM observations (400 kV accelerating voltage instead than 200 kV).

ORDERED INCOMMENSURATE MODULATED STRUCTURES

Ordered incommensurate modulated structures have been observed in a number of natural heyrovskýite crystals investigated in this work. Such modulated structures are characterized by long-range fluctuations visible as dark bands which break the original arrangement of the atomic structure. These fluctuations appear continuous and well developed in two directions, with an average wavelength of about 80 Å (Fig. 3a). The incommensurability has been deduced from the electron diffraction pattern showing satellite spots surrounding the Bragg reflections, making an angle of 15° with **b*** (Fig. 3b). The attempt to investigate structure modulations observed from HRTEM images by means of a single-crystal synchrotron X-ray diffraction experiment did not give the expected results. Although data collection at the synchrotron facility was performed by increasing the crystal-to-detector distance (90 mm), no satellite reflections with period of 80 Å could be observed. The absence of satellite reflections in the synchrotron X-ray single-crystal pattern can be explained by the presence of a modulation diffused in very narrow domains of the crystal structure.

The observed structure modulations in the heyrovskýite from Vulcano can be related either to a cation ordering in the metal sites or to the presence of vacancies. According to Balić-Žunić *et al.* (2007) in the Ag-free heyrovskýite from Vulcano, the M1 site, situated on the mirror plane that connects the adjacent, mirror-related galena-type layers, is a pure Pb site (Fig. 4). The octahedral sites Me2 and Me3, located in the central zone of PbS-like slabs, are pure Pb sites, whereas those closer to the boundary $(311)_{PbS}$ planes (M4 and M5 sites) are mixed (Pb, Bi) sites, with almost equal occupancy. The compositional nature of the modulation in Ag-free heyrovskýite from Vulcano can be related to a sort of ordering between Pb and Bi through the mixed sites Me4 and Me5. It can be expected that if Me4 has Bi then the nearby Me5 will have Pb, and so on. However, the occurrence of vacancies could also lead to the modulations. The presence of vacancies connected to the substitution $3Pb^{2+} \rightarrow 2Bi^{3+} + \square$ were first proposed by Takeuchi & Takagi (1974) in the pure synthetic heyrovskýite $Pb_{6-x}Bi_{2+2x/3}S_9$ and, recently, the structure refinement of an Ag-free heyrovskýite crystal from Vulcano suggested ~ 0.04 *pfu* of vacancy

in the sole Me3 site (Balić-Žunić *et al.*, 2007). It is noteworthy that the M3 lies at about 15° with respect to the b axis, thus forming an angle comparable with the angle that the satellite reflections form with respect to **b*** axis (Fig. 3).

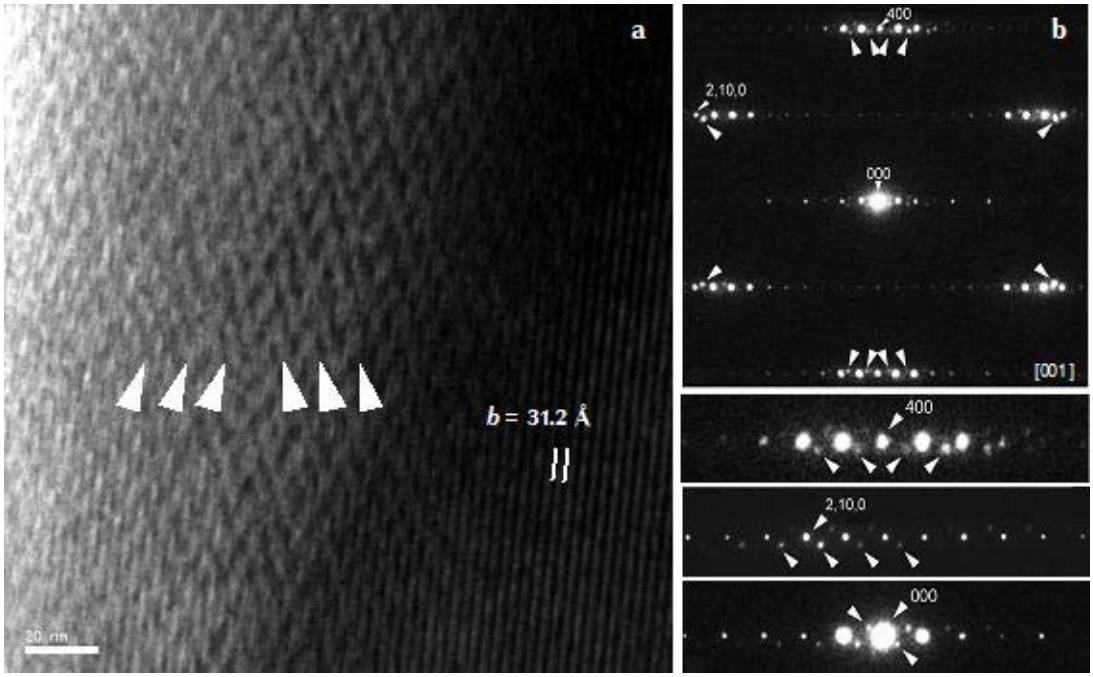

Fig. 3 – Modulated structure (arrows) of heyrovskýite from Vulcano (ion-milled sample): (a) low magnification image; (b) SAED patterns down the [001] zone.

Whereas, the presence of modulations only in Ag-free heyrovskýite and not in Ag-free lillianite can be found by looking at the structure peculiarities of the two mineral phases. As a matter of fact, lillianite and heyrovskýite are two homologues of the lillianite series (Makovicky, 1977; Makovicky & Karup-Møller, 1977a, 1977b) which differ only in the width of the PbS-like slabs mirror related on $(311)_{PbS}$ planes, represented by the number N of octahedra running diagonally across an individual slab, N = 4, for lillianite, and N = 7, for heyrovskýite. Recent studies have shown that, in the structure of Ag-free lillianite from Vulcano, Pb and Bi are statistically distributed among the only two cation sites of the PbS-like slabs (*i.e.* M1 and M2), with almost the same occupancy in both sites (Pinto *et al.*, 2006). Thus, the greater stability of Ag-free lillianite with respect to Ag-free heyrovskýite from Vulcano can be due to either the different thickness of the galena-like slabs or the different distribution of Pb and Bi among the cation sites inside the slabs of these two structures. According to Aizawa and co-workers (Aizawa *et al.*, 1983), the stability of members of the lillianite homologous series is related to their elastic strain energy (E), described as a force performed in twin planes from their unstrained state (E_s) less any energy dissipated by inelastic deformation (E_r). They demonstrated that the total strain energy depends on the distribution of cations, *i.e.* Pb and Bi, over the cation sites of the structure and that, although lillianite and heyrovskýite are the most stable sulfosalts of PbS-Bi_2S_3 system, a rather small change in cation distribution, affects greatly the elastic strain energy of these two phases, thus influencing their stability. Moreover, they noted that, depending on the cation distribution, the elastic strain energy could decrease

or increase when the width of the slabs increases. Thus, this local/widespread "instability" of Ag-free heyrovskýite, can be associated to the higher elastic energy and that the variation in the Pb/Bi ordering would allow to achieve a minimum strain energy that stabilize the structure.

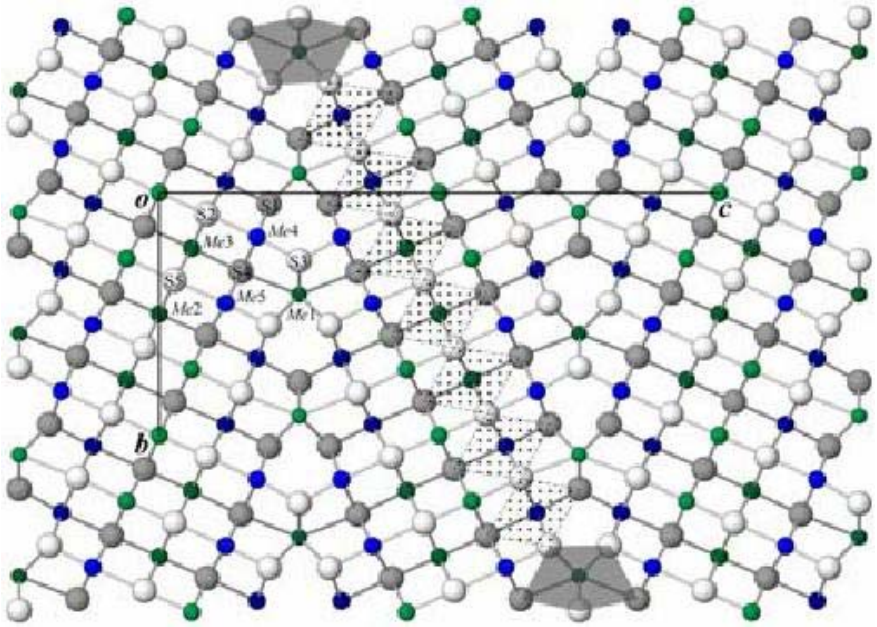

Fig. 4 - The crystal structure of Ag-free heyrovskýite from Vulcano. Projection on (001). Green: Pb; blue: mixed Pb-Bi sites; grey: S. Lightly and darkly shaded circles indicate atoms at z = ½ and z = 0, respectively, along the ~ 4 Å axis. Stippled: chain of octahedra running diagonally across the PbS-like layer, grey shaded: bicapped trigonal prisms of Me1 (by Balić-Žunić *et al.*, 2007).

Taking into account that the presence of small amounts of monovalent cations as Ag (or Cu) allow to stabilize these crystal structures (Makovicky, 1977; Makovicky & Karup-Møller, 1977a, 1977b), it is possible to explain why no structure modulations were observed to date from previous HTREM studies of heyrovskýite, which were only performed on Ag-bearing samples (Makovicky *et al.*, 1991; Takéuchi & Takagi, 1974).

This evidence allows to conclude that the modulations in the heyrovskýite from Vulcano are originally present in the crystals and they are not artefact induced by ion beam and/or surrounding vacuum. It is highly probable that their nature is connected to the very particular depositional environment of these phases, which at Vulcano is characterized by:

1. rapid cooling of the fumarolic fluid from which they form;
2. extreme variability of the Pb/Bi ratio in the fluid phase;
3. continuous variation in the abundance of compounds acting as carriers for the metals (HCl, H_2S etc.);
4. dynamism of the environment of formation which gave reason of the mineral deposition under non-equilibrium conditions.

Finally, the TEM analyses lead us to affirm with a good approximation that no sub-phases in the natural Ag-free phases of lillianite homologous series are present, although in the recent investigations on

heyrovskýite from Vulcano Borodaev and coworkers (Borodaev *et al.*, 2003) suggested the existence of a number of "heyrovskýites", with N_{chem} values substantially different from the ideal value N = 7 (N ~ 5 or N ~ 6).

REFERENCES

Aizawa, K., Iguchi, E., Tilley, R.J.D. (1983): The elastic strain energy stability of some idealized lead-bismuth sulphides. *Solid State Chem.*, **48**, 284-294.

Balić-Žunić, T., Garavelli, A., Pinto, D., Vurro, F. (2007): Structural investigation on the Ag-free heyrovskýite from Vulcano (Aeolian Island, Southern Italy). Geoitalia 2007, Rimini, 12-14 settembre 2007, abstr., 436.

Barna, Á. (1992): Topographic kinetics and practice of low angle ion beam thinning. *Mater. Res. Soc.*, **254**, 3-22.

Borodaev, Y.S., Garavelli, A., Garbarino, C., Grillo, S.M., Mozgova, N.N., Paar, W.H., Topa, D., Vurro, F. (2003): Rare sulfosalts from Vulcano, Aeolian Islands, Italy. V. Selenian Heyrovskýite. *Can. Mineral.*, **41**, 429-440.

Colaïtis, D., Van Dyck, D., Amelinckx, S. (1981): Electron microscopic study of the system mPbS-$n$$Bi_2S_3$. *Phys. Stat. Sol. (a)*, **68**, 419-438.

Klimentidis, R.E. & Mackinnon, I.D.R. (1986): High-resolution imaging of ordered mixed layer clays. *Clays Clay Miner.*, **34**, 155-164.

Loginov, Y.Y. & Brown, P.D. (1992): 100 keV electron beam induced decomposition of II-VI compounds. *Phys. Stat. Sol. (a)*, **132**, 323-337.

Makovicky, E. (1977): Chemistry and crystallography of the lillianite homologous series. III. Crystal chemistry of lillianite homologues. Related phases. *N. Jb. Mineral. Abh.*, **131**, 187-207.

Makovicky, E. & Karup-Møller, S. (1977a): Chemistry and crystallography of the lillianite homologous series. I. General properties and definition. *N. Jb. Mineral. Abh.*, **130**, 264-287.

Makovicky, E. & Karup-Møller, S. (1977b): Chemistry and crystallography of the lillianite homologous series. II. Definition of new minerals: eskimoite, vikingite, ourayite, and treasurite. Redefinition of schirmerite and new data on the lillianite-gustavite solidsolution series. *N. Jb. Mineral. Abh.*, **131**, 56-82.

Makovicky, E. (1981): The building principles and classification of bismuth-lead sulphosalts and related compounds. *Fortschritte der Mineralogie*, **59**, 137-190

Makovicky, E., Mumme, W.G., Hoskins, B.F. (1991): The crystal structure of Ag-Bi-bearing heyrovskýite. *Can. Mineral.*, **29**, 553-559.

Pinto, D., Balić-Žunić, T., Garavelli, A., Makovicky, E., Vurro, F. (2006): Comparative crystal-structure study of Ag-free lillianite and galenobismutite from Vulcano, Aeolian Islands, Italy. *Can. Mineral.*, **44**, 159-175.

Price, G.D. & Yeomans, J. (1984): The application of the ANNNI model to polytypic behaviour. *Acta Crystallogr.*, **B40**, 448-454.

Pring, A. & Etschmann, B. (2002): HRTEM observations of structural and chemical modulations in cosalite and its relationship to the lillianite homologues. *Mineral. Mag.*, **66**, 451-458.

Pring, A., Jercher, M., Makovicky, E. (1999): Disorder and compositional variation in the lillianite homologous series. *Mineral. Mag.*, **63**, 917-926.

Prodan, A., Bakker, M., Versteegh, M., Hyde, B.G. (1982): A microscopic study of synthetic PbS-rich homologues nPbS-mBi_2S_3. *Phys. Chem. Miner.*, **8**, 188-192.

Skowron, A. & Tilley, R.J.D. (1986): The transformation of chemically twinned phases in the PbS-Bi_2S_3 system to the galena structure. *Chemica Scripta*, **26**, 353-358.

Skowron, A. & Tilley, R.J.D. (1990): Chemically twinned phases in the Ag_2S-PbS-Bi_2S_3 system. Part I: Electron microscope study. *J. Solid State Chem.*, **85**, 235-250.

Takéuchi, Y. & Takagi, J. (1974): The structure of heyrovskýite ($6PbS \cdot Bi_2S_3$). *Proc. Japan. Acad.*, **50**, 76-79.

Tilley, R.J.D. & Wright, A.C. (1982): Chemical twinning in the PbS region of the PbS-Bi_2S_3 system. *Chemica Scripta*, **19**, 18-22.

Tilley, R.J.D. & Wright, A.C. (1986): Non-stoichiometric forms of Sb_2S_3 occurring in the $PbSb_2S_4$-Sb_2S_3 region of the Pb-Sb-S phase diagram. *J. Solid State Chem.*, **64**, 1-21.

LITHOSTRATIGRAPHIC SEQUENCES IN THE CENOZOIC VOLCANIC ROCKS OF CENTRAL-SOUTHERN SARDINIA: COMPOSITIONAL VARIATIONS AND DISTRIBUTION OF ZEOLITES AND OTHERS SECONDARY MINERALS IN THE ALLAI AND ASUNI UNITS

ANGELA MORMONE
Dipartimento di Scienze della Terra, Università "Federico II", L.go S. Marcellino 10, 80138 Napoli

INTRODUCTION

The Oligo-Miocene volcano-sedimentary succession of central Sardinia is composed by five ignimbritic units, mostly emplaced in subaerial environments. These units are locally interbedded with the so-called Asuni Unit (ASU; Assorgia *et al.*, 1995), a volcano-sedimentary complex mainly emplaced in sub-aqueous environments. A similar unit is the Allai Unit (ALU; Assorgia *et al.*, 1995), which consists of several overlapping ash and pumice flows, emplaced over a short period of time in a subaerial depositional environment. Mineralogical composition of ALU is akin to that of ASU, but the welding degree is different. Both units are characterized by a zeolitization process, which leads to crystallization of mordenite + clinoptilolite (± analcime) association as main secondary phases. Recent studies have pointed out a quite widespread late zeolite crystallization affecting volcanic deposits of central Sardinia, and mostly related to a transformation process of glassy components (Cappelletti *et al.*, 2001; Brotzu *et al.*, 2006; Palomba *et al.*, 2006).

This work deals with a detailed study of the distribution of main secondary phases occurring in ASU and ALU, aimed to infer the role of different depositional environments in the minerogenetic processes. Then, 27 representative stratigraphic sequences of these units have been sampled in a NW-SE area located between the villages of Asuni and Allai.

METHODS

Detailed sampling work, carried out in different localities of the study area, has been mainly focused to zeolitized horizons within volcanic sequences. Besides, in each section, ignimbritic layers were sampled and investigated to verify the possible relationships between volcanological layering and zeolitization. Over 100 representative samples were collected for the considered sections, taking into account the best exposed areas. A preliminary petrographic study on thin sections was carried out for all samples. Then, rock mineralogy was investigated by powder X-ray powder diffraction (XRPD), using a Panalytical X'pert PRO PW 3040/60 equipped with a curved graphite diffracted-beam monocromator (Cu*K*α radiation, 40 kV, 30 mA scanning interval, step size = 0.020°, counting time 30 sec/step). Micro-morphological observations by scanning electron microscopy (SEM) and EDS microanalysis were carried out by a JEOL JSM 5310 operating at 15 kV (CISAG, University "Federico II", Napoli). Quantitative chemical data were processed by LINK AN10000 and INCA software. Natural and synthetic minerals were use as standards. Quantitative mineralogical analyses were performed using the Reference Intensity Ratio (RIR) technique, which is an evolution of the internal standard technique proposed by Chung (1974), the matrix- flushing method for quantitative multicomponent analysis, later developed and

improved by Chipera & Bish (1988). In order to test the accuracy of these quantitative analyses, some samples where also analyzed by the Rietveld method, using GSAS package.

RESULTS AND DISCUSSION

The whole data set obtained by multi-analytical approach indicate as follows: 1) the strongly welded ignimbrites are unzeolitized; 2) analcime grains mostly occur within vugs and cavities; in association with well-formed quartz and k-feldspar crystals (Fig. 1a); 3) this zeolite mineral is sometimes corroded and lacking in the southern sector; (Fig. 1b) 4) clinoptilolite laths grow on cuspate shards (Fig. 1c), on cineritic matrix and often as vug filling (Fig. 1d); 5) acicular fibres of mordenite grow on both matrix (Fig. 1e) and tabular clinoptilolite crystals (Fig. 1f) and it frequently forms radiating aggregates as vug lining.

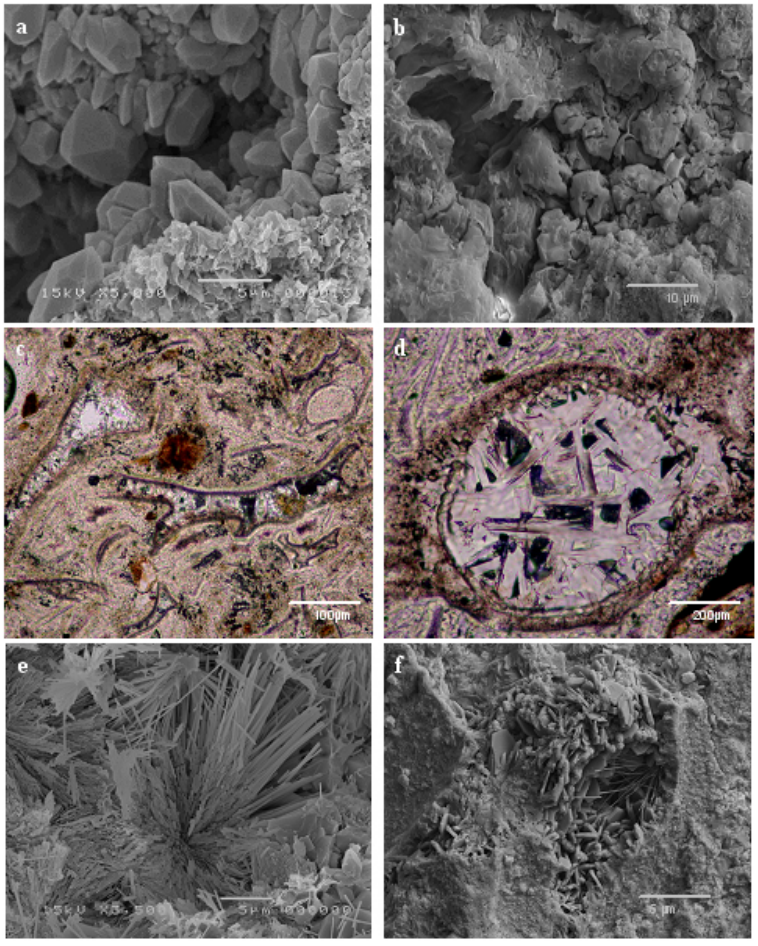

Fig 1 - (a) Analcime crystals associated with K-feldspar and bipiramidal quartz; (b) corroded analcime in vugs; (c) tabular clinoptilolite growing in a glass shard, and (d) in a subsferical cavity; (e) fibres mordenite growing on matrix, and (f) on clinoptilolite crystals.

As regards ALU, the extraframework cation variations of clinoptilolitic zeolite are plotted in Fig. 2a. Clinoptilolite is a Ca-rich variety with average contents of Na, Ca+Mg, and K equal to 23, 56, and 21 afu , respectively. Mordenite fibres, plotted in Fig. 2b, show a distinct sodic feature with mean amounts of Na, Ca+Mg, and K of 46, 42, and 2 afu, respectively. It is worth to note that, with the exception of few samples, narrow compositional variation is observed between the clinoptilolite and mordenite growing on cuspate shards and those occurring in vugs. On the basis of RIR and Rietveld quantitative analysis, a wide variation in the content of newly-formed phases can be emphasized. Anyway a clear mineral zoning does not appear in the sections sampled for this work. In several levels, clinoptilolite content often is higher than 30 wt.%, and the maximum mordenite amount is 31 wt.%. Smectite content is on average lower than 5 wt.%, analcime amount is lower than 21 wt.%.

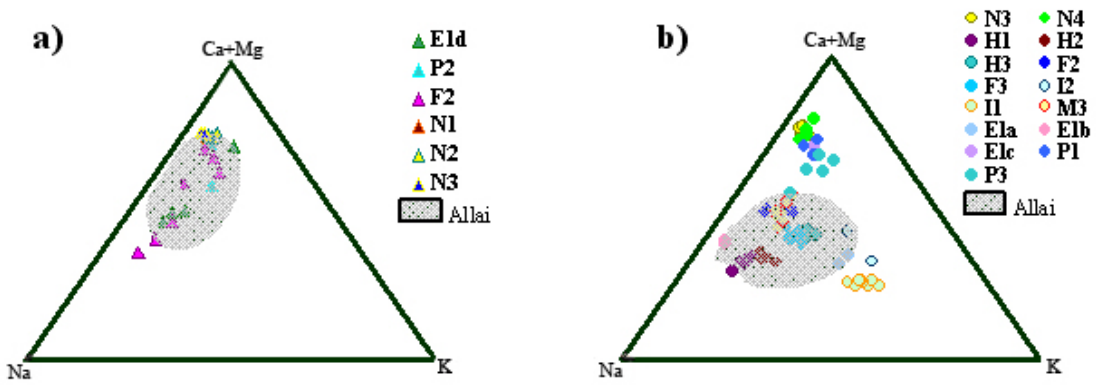

Fig. 2 - (a) Extraframework cations of clinoptilolite, and (b) mordenite plotted in (Ca+Mg)-Na-K ternary diagram for Asuni Unit. The grey area represents the clinoptilolite and mordenite compositional variation for Allai Unit.

ASU is formed by several and diversified lithologies ranging from variably welded ash and pumice pyroclastic flows to epiclastic and laminated levels mainly formed by volcanic materials with carbonized and silicified vegetal remnants. The main authigenic phases are represented by mordenite, clinoptilolite and smectite. As regards vertical distribution of secondary phases in twelve sequences studied here, any sharp vertical mineral zonation can be recognized. Comparative analyses between different lithologies demonstrate that the overall textural feature is similar to that observed in ALU. On average, chemical composition of tabular clinoptilolite shows Na, Ca+Mg, and K amounts of 28, 58, and 4 afu, respectively (Fig. 2a). Mordenite is a Ca-Na-K- rich variety, with Na equal to 32 afu, Ca+Mg equal to 45 afu, and K equal to 23 afu (Fig. 2b)

Only in few samples, quantitative analyses display high mordenite and clinoptilolite contents (over 28 wt.% in zeolite content).

CONCLUSIONS

The vertical distribution of the authigenic minerals recognized in two volcanic and volcano-sedimentary units from central Sardinia cannot be interpreted according to a single genetic model. Taking into account a likely similar starting materials (*i.e.* rhyolitic glass), peculiar physical and chemical conditions are required to promote the observed newly-formed phases and to cause large differences in

alteration degree of volcanic products immediately after their emplacement. In particular, regarding local temperature differences, ALU is characterized by mineral parageneses testifying higher temperature than ASU; this is perfectly in line with the geological evidence that ALU is more close to the emission sector. The wide chemical compositional variation of ASU zeolites is probably related to the presence of a transitional fluid. These data, together with differences in fluids/glass quantitative ratios, may explain the observed scenario.

REFERENCES

Assorgia, A., Balogh, K., Lecca, L., Ibba, A., Purcu, A., Secchi, F., Tilocca, G. (1995): Volcanological characters and structural context of Oligo-Miocene volcanic successions from Central Sardinia (Italy). Acc. Naz. Sci., Atti Conv. Rapporti Alpi-Appennino.

Cappelletti, P., Cerri, G., de' Gennaro, M., Langella, A., Naitza, S., Padalino, G., Rizzo, R., Palomba, M. (2001): Natural zeolites mineralization on the Oligocene-Miocene volcano-sedimentary succession of Central Sardinia (Italy). *Stud. Surf. Sci. Catal.*, **135**, 10-18.

Bish, D.L. & Chipera, S.J. (1988): Problems and solutions in quantitative analysis of complex mixture by X-ray powder diffraction. *Adv. X-Ray Anal.*, **31**, 295-307.

Brotzu, P., Ghiara, M.R., Cincotti, F., Lonis, R., Fercia, M.L., Sau, A. (2006): Distribuzione dei minerali autigeni nei flussi piroclastici dell'Unità di Allai (Sardegna Centro-Meridionale). 85° Congresso SIMP, Fluminimaggiore, 27-30 Settembre 2006, abstr.

Chung, F.H. (1974): Quantitative interpretation of X-ray diffraction patterns of mixtures. I. Matrix-flushing method for quantitative multicomponent analysis. *J. Appl. Crystallogr.*, **7**, 519-525.

Morbidelli, P., Ghiara, M.R., Lonis, R., Petti, C. (2001): Quantitative distribution and chemical composition of authigenic minerals in clinoptilolite-bearing ignimbrites from northern Sardinia (Italy): inferences for minerogenetic models. *Per. Mineral.*, **70**, 71-97.

Palomba, M., Padalino, G., Marchi, M. (2006): Industrial mineral occurrences associated with Cenozoic volcanic rocks of Sardinia (Italy): Geological, mineralogical, geochemical features and genetic implications. *Ore Geol.*, **29**, 118-145.

ARCHAEOMETRICAL INVESTIGATIONS ON MORTARS AND PAINTINGS AT POMPEII AND EXPERIMENTS FOR THE DETERMINATION OF THE PAINTING TECHNIQUE

REBECCA PIOVESAN
Dipartimento di Geoscienze, Università di Padova, Via Giotto 1, 35137 Padova

INTRODUCTION

The characterisation of building materials, such as mortars and plasters, can give useful and unique indications when several technological, artistic and historical questions require answers (such as the definition of various construction periods, knowledge of technology and identification and provenance of raw materials). This may also be applied to the study of wall paintings, which aims to identify the nature of pigments, recipes, and techniques adopted.

A series of samples of mortar-based building materials (127 fragments) and paintings (73 fragments) from varying functional and chronological contexts were collected from the southern and northern areas of the Temple of Venus (Pompeii). Venus is the main polyad divinity of Pompeii, and her temple is one of the most important buildings in the town, located in the south-west area. This site has a long and complex history of construction and reconstruction (Curti, 2008). The present building itself underwent numerous restorations until the eruption of Vesuvius in 79 AD. Most of the samples were archaeologically dated from the end of the 4th Century BC to the 1st Century AD.

The aim of this study was to characterise these building materials and to determine their production techniques, to relate them with the function of the various buildings or rooms, and to follow their evolution over time. Experiments were also performed in order to determine objective criteria for the identification of the wall-painting technique adopted. Optical Microscopy (OM), Scanning Electron Microscopy (SEM, ESEM), X-ray diffraction (XRD), infrared spectroscopy (micro-ATR, FT-IR), Mössbauer spectroscopy, microprobe (EMPA) and colorimetric analyses were carried out to characterise materials, and then integrated with image analysis to define ratios among textural elements of the mortars (*i.e.*, aggregate, binder, porosity) with greater accuracy.

MORTARS

The mortars were preliminarily grouped into three macro-groups according to the architectural features of their provenance: walls, floors, and hydraulic structures (conduits, wells, cisterns), and then analysed petrographically and microstratigraphically. Identified aggregate particles were also compared with samples of sand collected from seven localities along the Neapolitan coastline, from Torre Annunziata to Castellammare di Stabia, and with four alluvial sand samples from borehole cores drilled in the area in front of the Temple of Venus, in attempt to identify the quarrying areas of the raw materials.

The three classes of mortar-based building materials analysed here had differing petrographic and microstructural features, and are briefly described below. Results showed that the aggregate in mortars is mainly composed of a volcanic sand composed of leucite-bearing volcanic rock fragments and volcanic scoria, leucititic or trachytic in composition, associated with abundant crystals of green and colourless clinopyroxene, black and yellow fragments of altered volcanic glass, rare crystals of feldspar and flakes

of mica, and very rare crystals of melanitic garnet. These components are typical of the Somma-Vesuvio volcanoclastic deposits (Santacroce, 1987) and indicate an aggregate made with raw materials of local provenance. This was also confirmed by petrographic comparisons with the sand samples collected from the Neapolitan coastline and from borehole cores.

The differing amounts of components in wall samples distinguished two main groups; one characterised by the prevalence of fragments of volcanic rocks (Fig. 1a), and one by the abundance of clinopyroxene crystals (Fig. 1b). The mortars were often covered by a set of fine-grained layers of plaster, differentiated into several subtypes on the basis of the petrographic nature of the aggregate: i) silicates and silicate rocks (*intonachino*); ii) crushed pottery (*cocciopesto*); iii) limestone or crystals of calcite (*marmorino*).

Both floors and hydraulic structures were composed of two types of mortar, *cocciopesto* (Fig. 1c), or an aggregate of volcanic fragments (Fig. 1d). Pottery inclusions were helpful in further subdividing the *cocciopesto* fragments into two subgroups: *cocciopesto* made either of vulcanite or of quartz and feldspar crystals. The former was related to local production, and the latter indicated re-use of imported materials.

Observations by optical microscopy and measurement of the hydraulicity index (HI = Al_2O_3+Fe_2O_3+SiO_2 / CaO+MgO) of binder and lime lumps, identified two main types of binder - both composed of pure lime, but displaying different HI values, which turned out to be correlated to the extent of hydraulic reaction between binder and aggregate. Pozzolanic aggregates (*i.e.*, in mortars including

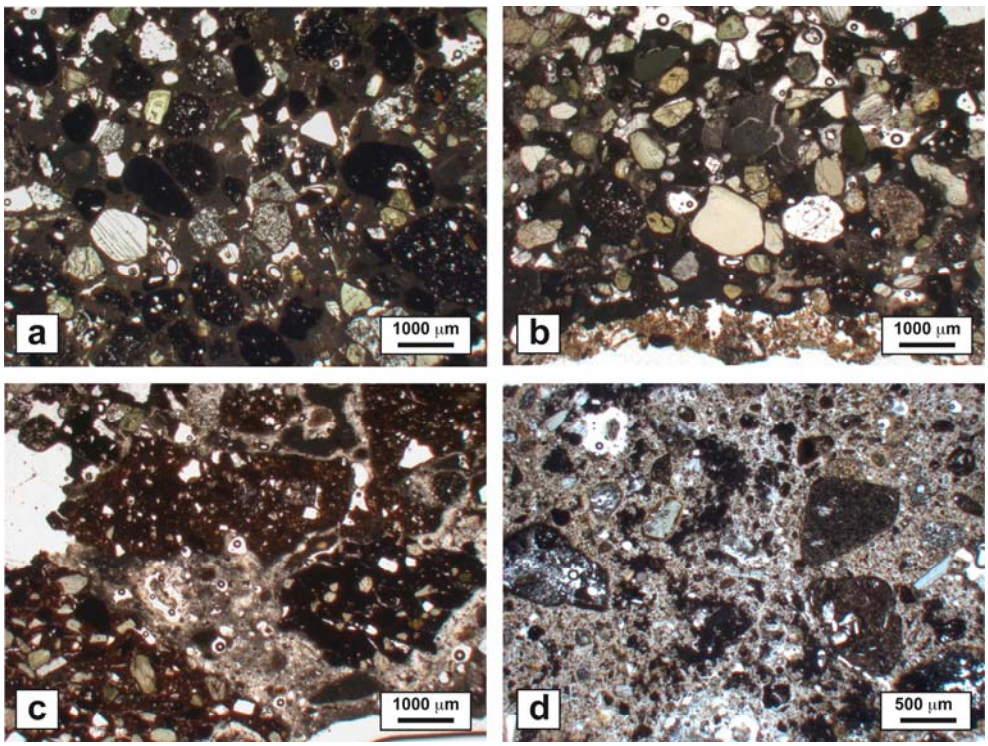

Fig. 1 - Polarising light micrographs of mortar samples. Walls: a) volcanic scoria-rich; b) clinopyroxene-rich. Floors: c) ceramic-rich; d) volcanic scoria-rich. All images taken in PPL.

cocciopesto and volcanic sand) reacted with the lime, producing a hydraulic binder with useful hydraulic properties. Only lime lumps in hydraulic structures had higher HI, with values between 0.08 and 0.27, indicating that true hydraulic lime was probably used to create these architectural features. The data showed that craftsmen could accurately select the materials on the basis of these characteristics, in order to ensure specific physical and/or aesthetic performance.

The occurrence of lime lumps in a large number of samples also indicates that some of the lime did not react completely with water during slaking or with atmospheric CO_2 (Hughes *et al.*, 2001) after application. This provides strong evidence that lime, water and aggregate were mixed without due attention, perhaps because of workers' lack of technological skills or acceptance by buyers of such wares.

As regards time evolution, recipes and raw materials were homogeneous from the 4th Century BC to the 1st Century AD, indicating that technological knowledge was already well established in the 4th Century BC and suggesting the persistence of technological tradition. The various types of mortars were correlated with architectonic structures and therefore with their specific function, such as the case of hydraulic structures, where pozzolanic aggregate was always used.

As regards image analysis, the approach adopted here allowed computation of the textural parameters of silicate aggregate. This approach turned out to be a powerful tool in determining the specific characteristics of the mortars - *i.e.*, aggregate:binder ratio and porosity - although the total porosity was underestimated. Nevertheless, further study is required to improve and test this approach before making it routine in studying mortars.

IDENTIFICATION OF PAINTING TECHNIQUE

Identification of the painting technique adopted by an artist is often a matter of debate in studies on the characterisation, restoration and conservation of mural paintings. During this research, an experimental study was undertaken in order to define objective criteria and analytical procedures to identify the *fresco* (*buon fresco*, *i.e.*, true *fresco*) and *mezzofresco* (lime-painting) techniques. In the case of the *fresco* technique, a very fine-grained pigment is diluted in water and laid on a damp, fine-grained plaster. Plasters only conserve their optimal characteristics for use as a background in *fresco* painting for a very short time (about eight hours), called the "golden period", during which they have a high degree of humidity. In the case of *mezzofresco*, pigments are mixed with slaked lime and spread on dry plaster (Botticelli, 1992).

In this study, two groups of 15 coloured strips were painted using various traditional pigments, including lime white, following both *fresco* and *mezzofresco* techniques. Samples were prepared as polished sections and analysed by optical and scanning electron microscopy for determination of microstratigraphy and microtextural features. Comparison of microstratigraphic sequences and distribution of chemical elements in each of the two sets of samples displayed systematic differences between *fresco* and *mezzofresco* techniques, independently of the pigment used, suggesting distinctive objective criteria and standardised operating procedures.

In the case of *fresco*, the pigment-bearing layer was relatively thin (generally below 50 μm) and its surface was rough and irregular. Coarser grains of pigment did not penetrate the plaster, but remained on the surface, bound by a thin film of calcite. In the case of *mezzofresco*, the pigment-bearing layer was systematically thicker (up to 650 μm), with a smooth surface. Grains were always regularly and completely distributed within a uniform layer of calcite. The distinction between the two painting techniques was even more evident with SEM. The elemental distribution maps of *mezzofresco* show a

high-density, Ca-rich layer, a few dozen microns thick, typically found on the more superficial portion of the plaster, as shown in Fig. 2a. This evidence was more pronounced when SEM-BSE images of *fresco* and *mezzofresco* paints were compared (Fig. 2). Pores also progressively decreased towards the surface of the plaster and increased dramatically within the painted layer, highlighting the thin dense layer between the two. Similar dense, Ca-rich layer was also found on the surface of the paint in both *fresco* and *mezzofresco* techniques.

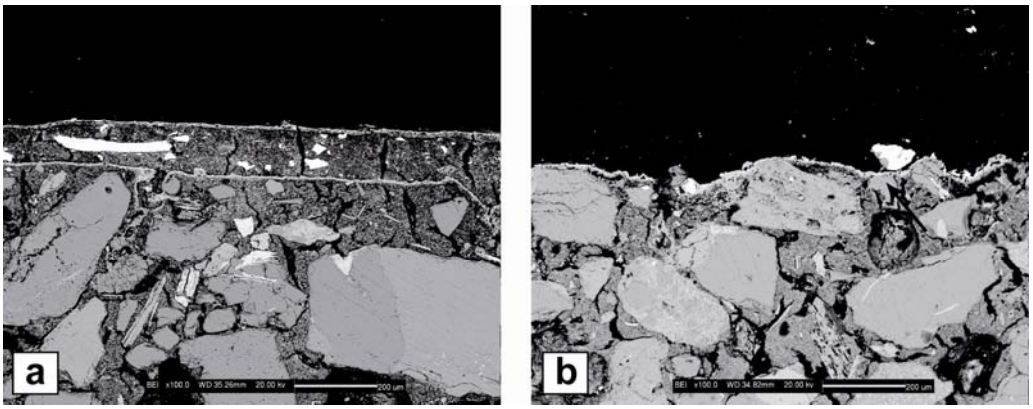

Fig. 2 - SEM-BSE images of azurite paint spread according to a) mezzofresco, and b) fresco techniques, respectively.

Five samples from the Chiaravalle Abbey (Milan) for which the use of *fresco* and *mezzofresco* is well documented, were also analysed, and results were compared with experimental data to validate the proposed diagnostic criteria. Comparisons showed that the features of painted layers, their microstratigraphy, and the location of Ca-rich levels identified in these historical *fresco* and *mezzofresco* samples were very similar to those identified the experimental samples.

Microstratigraphic evidence in *fresco* and *mezzofresco* wall painting is closely related to the carbonation process, which takes place as the plaster and painted layers gradually dry. Good adherence depends on the reaction of the $Ca(OH)_2$, which is the binder, with atmospheric CO_2, producing $CaCO_3$ and releasing water. This process is more efficient on the surface, where the CO_2 concentration is higher and water evaporation more effective. It causes superficial hardening and porosity reduction, which both inhibit and retard carbonation in the inner portion of the underlying plaster. In the *mezzofresco* technique, drying and carbonation may take place before the pigment is applied, since the painted layer is applied to the plaster many hours later. This produces a dense carbonated crust on the plaster surface exposed to the air. When $Ca(OH)_2$ mixed with pigment is then applied to this layer, a new process of drying and carbonation starts on the surface of the paint, so that a second dense, carbonated level is created. In the case of *fresco* painting, a mix of water and pigment is applied on damp plaster, which has not yet undergone drying or carbonation. In this situation, the water guarantees good initial adhesion of the pigment to the plaster surface. Subsequently, evaporation and carbonation cause calcite to precipitate in the painted layer and the more superficial portion of the plaster, so that the painted layer is one with the upper portion of the plaster underneath. For this reason, with the *fresco* technique, the superficial carbonated layer includes all

the grains of pigment, which are completely encased in a thin film of calcite. Moreover, no second, deeper carbonation level can form, since layers are continuously applied without interruption. On the basis of these pieces of evidence, microstratigraphic analysis of a wall painting can provide useful information defining whether the *fresco* or *mezzofresco* technique was used.

PAINTINGS

In the last section of this study, 73 fragments of wall paintings from the Temple of Venus were characterised and the painting technique was identified applying the criteria described above.

Results showed that the palette of colours used to decorate the Temple of Venus was varied, although not so extensive as that found in other buildings in Pompeii. The pigments are similar to those used elsewhere in Pompeii and in the Roman Empire, and also with the palette described both by Pliny and Vitruvius, with the exception of a volcanic natural yellow glass. The palette is composed of several natural earths, such as red, yellow and brown ochres and green earth (mostly celadonite), and other artificial pigments, such as whitewash, carbon black and Egyptian blue. The precious pigment cinnabar was also detected (Table 1). All pigments are of good quality. In particular, red ochre turned out to be haematite with a high degree of crystallinity, and cinnabar and the two types of Egyptian blue were made of very pure, well-selected cinnabar crystals and cuprorivaite, respectively, with negligible contents of

Table 1 - Preparation recipes. Number of samples and constituent pigments.

Recipes	**N° of samples**	**Pigments**	
		Major components	Minor components
Black 1	4	Coal black	-
Black 2	1	Burnt ochre	-
Black 3	1	Red ochre, coal black	-
Red 1	13	Red ochre	Yellow ochre
Red 2	4	Red ochre, yellow ochre	Clays, green earth, yellow glass
Red 3	4	Cinnabar	Red ochre
Yellow 1	3	Yellow ochre	Red ochre
Yellow 2	9	Yellow ochre and red ochre	Yellow glass, clays
Yellow 3	1	Red ochre, yellow glass	-
Yellow 4	1	Yellow and brown glass	Yellow ochre
Light blue	2	Egyptian blue	Yellow ochre, yellow glass
Green 1	4	Celadonite	Red and yellow ochre, Egyptian blue
Green 2	1	Red and yellow ochre, Egyptian blue, celadonite	Brown glass
Green 3	1	Celadonite, Egyptian blue	Red and yellow ochre
Grey	3	Yellow, red and brown ochre, Egyptian blue	Brown glass, cinnabar, glauconite
White 1	16	Lime, calcite	-
White 2	5	Lime	-

other mineral impurities. As regard Egyptian blue, the identification of malayaite ($CaSnSiO_5$) in one group of samples, and an unspecified K-Ca-Fe-bearing phase as tiny inclusions in pigment grains in another, clearly indicates that two different processes were used to prepare this specific pigment. In particular, the occurrence of malayaite indicates that the copper was derived from bronze, whereas the absence of malayaite suggests a different origin for copper, *e.g.*, a deposit of copper ore. Mössbauer spectroscopy on both red and yellow ochres confirmed that these pigments are basically composed of a single phase (*i.e.*, haematite and goethite, respectively) and that other Fe-bearing mineral phases are absent. In two cases, nano-sized oxide/oxyhydroxide particles were also identified. It is also worth noting that the Mössbauer spectra were acquired by a newly designed Mössbauer portable spectrometer, tested on wall paintings for the first time. The statistics of the spectra were sufficiently good, and the acquisition time was reasonably short, confirming the applicability of this new application of Mössbauer spectroscopy.

Paints were either composed of pure pigments or prepared as mixtures of pigments following a series of 17 recipes (Table 1), to obtain different hues and shades. Most of the recipes are quite simple and involve one or two main pigments, sometimes with the addition of minor impurities. In order to make colours darker or lighter, especially yellow and red, carbon (lampblack) and calcite (whitewash), respectively, were mixed with the appropriate pigment. In other cases, the paints contain the same pigments, but were mixed in different relative proportions according to different recipes (*i.e.*, recipes *yellow 1* and *red 1*), yielding a variety of hues. *Grey* and *green 2* were the most complex recipes, involving four different pigments and several minor components. In particular, grey colour was made by deliberately mixing yellow, red and brown ochre, Egyptian blue, brown glass, cinnabar and glauconite in precise proportions to obtain the desired hue. There are no analogies in the literature of such a complex admixture of pigments, which may reflect the painter's skill.

An additional important observation is that some of the colours, such as black, red, green and yellow, were prepared using various pigments. The adoption of differing recipes for the same colour suggests the presence of several groups of painters working in the Temple of Venus who had preferences for different methods to produce their colours. Chronological data show that the most common and inexpensive recipes are also widespread over time, such as pure haematite in *red 1*, haematite and goethite in *yellow 2* and *marmorino* in *white 1*. *Black 1* seems to be the most frequently used recipe for black paint, at least from the 1st Century BC to the 1st Century AD (Julio-Claudian Age). Egyptian blue in light blue paints seems to have been exclusively used in the Imperial Age, although this pigment had certainly been used since the end of the 4th Century BC, as demonstrated by its identification as a component in green admixtures. It is also important to note that the various methods adopted to produce Egyptian blue in the Imperial Age suggest that it was purchased from several different producers.

In addition, a new yellow-brown pigment, never before identified, was found and characterised. It is composed of fragments of a yellow or brown natural volcanic glass, chemically compatible with vulcanites from Somma-Vesuvius. This suggests that this pigment, which is undocumented even by Pliny and Vitruvius, was produced locally. It is relatively common in many paints, either as one of the main components (*yellow 3*, *yellow 4*) or as a minor one (*red 2*, *yellow 2*, *light blue*, *green 2*).

All the data, particularly the absence of a carbonation layer between paint and *intonaco* and of any trace of organic binders, confirmed that the most frequently used painting technique was *fresco*. All samples have very thin painted layers, with well-dispersed fine-grained pigment particles and sometimes medium to coarse grains coated by calcite (Fig. 3a,c). In the coloured samples, with strips or figures

painted on a coloured background, the thickness of the painted layers and the presence of a carbonation layer between the two coloured layers (Fig. 3b,d) suggests that the more superficial paint was applied with the *mezzofresco* technique.

In conclusion, the importance and prestige of the Temple of Venus is also reflected in the quality and value of the pigments, and in the careful preparation of the mortars.

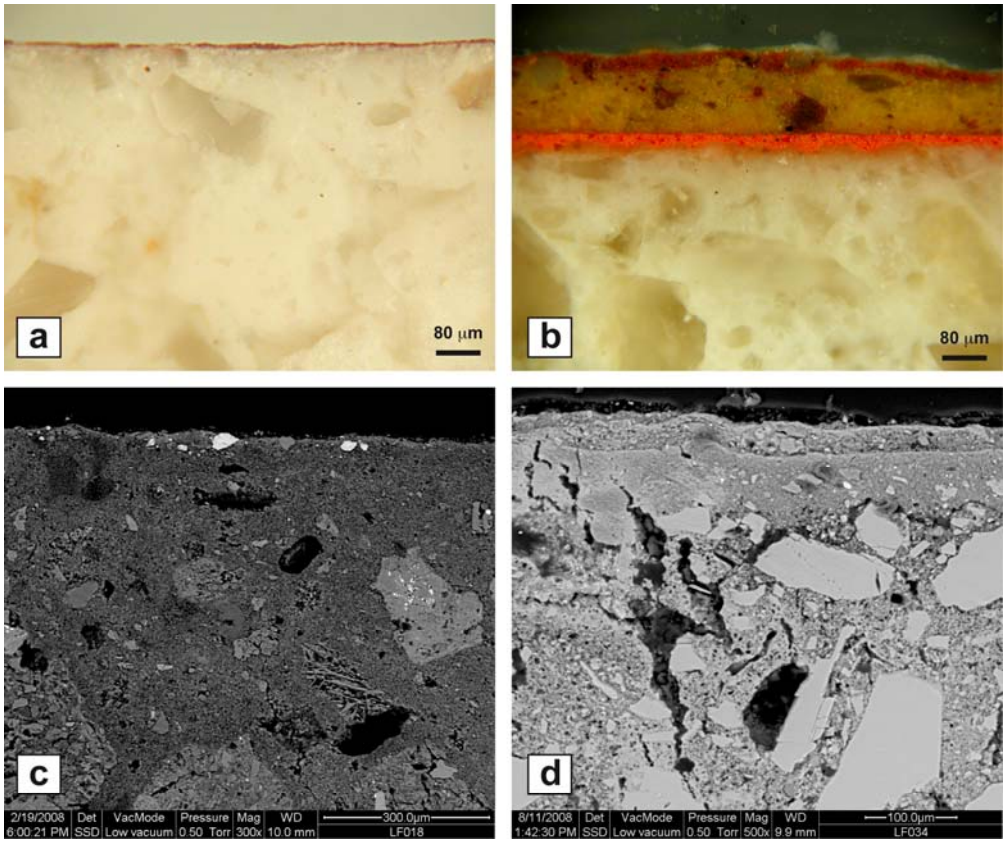

Fig. 3 - Reflected light micrographs of samples of wall paintings: a) single-layer painting; b) multi-layer painting. BSE images of wall paintings: c) *fresco* technique; d) *mezzofresco* technique.

REFERENCES

Botticelli, G. (1992): Metodologie di restauro delle pitture murali. Centro Di, Firenze, 176 p.

Curti, E. (2008): Il tempio di Venere Fisica e il porto di Pompei? *In*: "Nuove ricerche archeologiche nell'area vesuviana (scavi 2003-2006)", P.G. Guzzo & M.P. Guidobaldi, eds. Roma, 47-60.

Hughes, J.J., Leslie, A., Callebaut, K. (2001): The petrography of lime inclusions in historic lime based mortars. *In*: Proceedings of the 8th Euroseminar on "Microscopy Applied to Building Materials", Athens, Greece, September 2001, 359-364.

Santacroce, R., ed. (1987): Somma-Vesuvius. Quaderni de "La Ricerca Scientifica", CNR, Roma, 251 p.

ORIGIN AND EVOLUTION OF THE BACK ARC MAGMATISM OF ECUADOR (NORTHERN VOLCANIC ZONE, ANDES): EL REVENTADOR AND SUMACO ACTIVE VOLCANOES

MATTEO PUERINI
Dipartimento di Scienze Geologiche, Tecnologie Chimiche e Ambientali, Università "Carlo Bo",
Loc. Crocicchia, 61029 Urbino (PU)

INTRODUCTION

The subduction of the Nazca and Antarctic plates under the continental west margin of South America is responsible for the Plio-Quaternary magmatic activity along the Andean Cordillera. This volcanism is divided into four separate provinces (Northern Volcanic Zone or NVZ, Central Volcanic Zone or CVZ, Southern Volcanic Zone or SVZ and Austral Volcanic Zone or AVZ), each one separated from the others by the presence of a volcanic gap, due to segments of flat slabs: the Peruvian, Pampean, and Southern Chile subduction, being this latter linked with the subduction of an active oceanic ridge.

Offshore of the Ecuador an aseismic Ridge is present, the Carnegie Ridge, which is interpreted to be the track of the Galàpagos hot spot on the Nazca plate. Unlike Perù or Chile, in Ecuador the volcanic gap is not present: the Ecuadorian volcanism is characterized by intense activity which is localized both trenchward and in the back arc direction (Bourdon *et al.*, 2003).

The Plio-Quaternary Ecuadorian volcanic arc (NVZ) is constituted by the Western Cordillera (fore-arc) and the Cordillera Real (main-arc). Other volcanoes, including El Reventador and Sumaco, are also present in the rear-arc zone (far from the trench). In this zone it is difficult to explain the occurrence of both calc-alkaline and alkaline products distinctively erupted by these two Quaternary volcanoes, located only 50 km far each other and over the same basement rocks: Jurassic granitoid intrusions covered by volcanoclastic formations (Misahuallì) and Cretaceous metamorphosed sedimentary sequences (Hollin, Napo and Tena formations; Fig. 1).

This study is going to deal with the processes responsible of such geochemical differences. In fact, simple subduction-related geodynamic models do not match with the presence, in the back-arc area and at the same distance from the trench, of both medium to high-K calc-alkaline (El Reventador) and alkaline (Sumaco) volcanic products. More than 300 rock samples were analysed in thin section (200 for El Reventador and 100 for Sumaco). On the basis of petrographic observations, selected samples were chosen for mineral chemistry and whole-rock chemistry (major-trace elements and Pb-Sr-Nd isotopic ratios).

VOLCANOLOGICAL BACKGROUND AND ERUPTIVE HISTORY

El Reventador is a stratovolcano of the Ecuadorian sub-Andean zone and it consists of a calderic amphitheatre (4 × 3 km), opened to the East, which accommodates the young active cone rising up approximately for 1300 m (Hall, 1977). The most recent eruption of El Reventador started on November 2002 (Hall *et al.*, 2004; Ridolfi *et al.*, 2008), with an explosive event (VEI = 4), followed by a sequence of lava flows which are discontinuously coming until now (May 2009).

The morphological, structural and chronologic evolution of El Reventador was characterised by a large stratocone (Old Volcanic Edifice, OVE) followed by a second stratovolcano which grew up

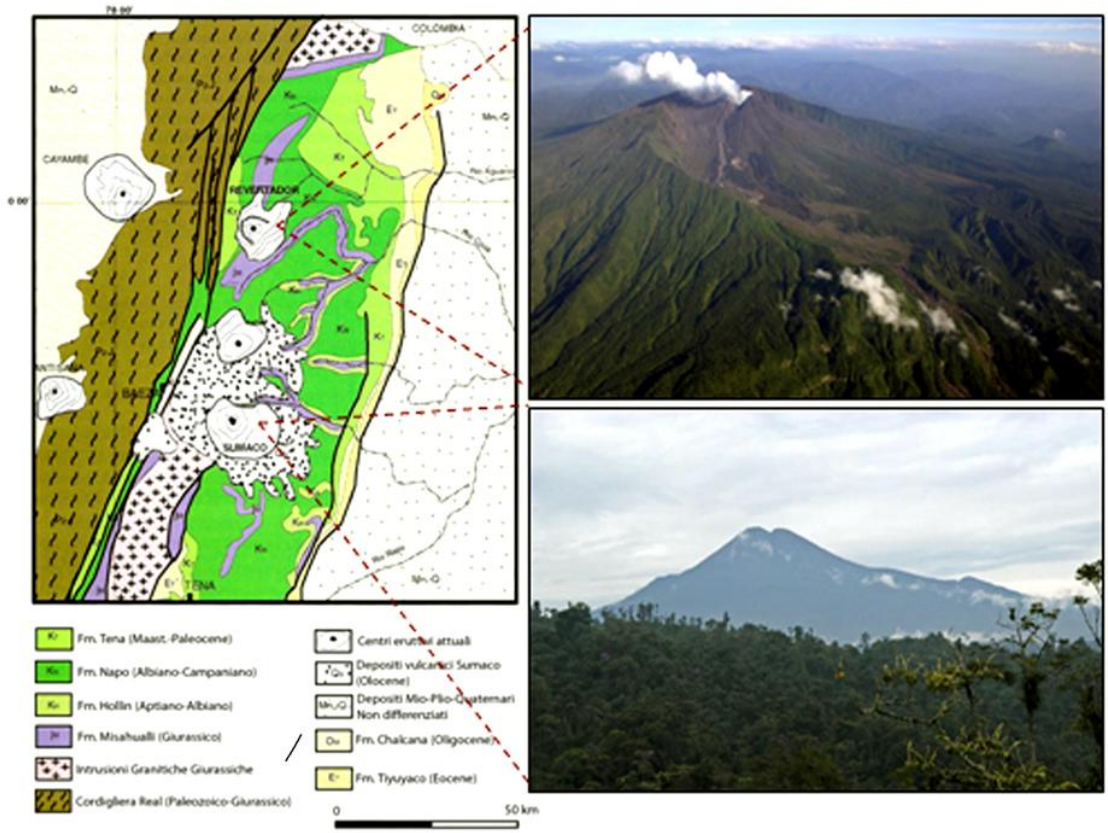

Fig. 1 - Geological sketch of the Ecuadorian sub-andean zone (from Barragàn & Baby, 2004); El Reventador (top) and Sumaco (bottom) volcanoes are also shown on the right.

asymmetrically with prevalent eastern development (Paleoreventador, PR). Paleoreventador underwent two major sector collapses with relative debris avalanche deposits. Currently, that is during the third stage of evolution, the activity is restricted to the young cone (Present Cone, PC) with an activity made of prevalent lavas and subordinate pyroclastic flows and ash fallouts.

Sumaco morphology is dominated by the presence of a conic structure with a basal radius of about 12 km, at the centre of which a symmetric stratocone, rising up for 2800 m, developed. This volcano is poorly known, with respect to the other Ecuadorian volcanoes, because of the difficulty to the access for the presence of the rain forest. The youngest eruptive activity may be ascribed at 1933 (Hantke & Parodi, 1966), although some local people eyewitnessed explosive activity in 1958 as well. The Sumaco structural evolution can be divided into two main stages: Paleosumaco (PS), the old edifice affected by an enormous sector collapse of the northeastern flank, and Neosumaco (NS), the youngest cone made of recent effusive and explosive products.

PETROGRAPHY AND MINERAL CHEMISTRY

The products of El Reventador are mainly represented by porphyritic lava, ranging from basalts to rhyolites (Aguilera *et al.*, 1988; Ridolfi *et al.*, 2008) and characterized by a phenocrysts assemblage made

of plagioclase, clinopyroxene, opaque minerals, ± orthopyroxene, ± olivine, ± amphibole (± sanidine). Micro- to crypto-crystalline groundmass mainly consists of pyroxenes, plagioclases and Fe-Ti oxides.

Some gabbroic nodules, with cumulate texture, were found as cognate inclusions in the lavas. They are made of plagioclase, clinopyroxene, orthopyroxene, Ti-magnetite, amphibole and rare olivine.

One distinctive feature of El Reventador products is the presence of different kinds of amphibole breakdown coronas, which were well investigated and explained. The Al-in-amphibole geothermobarometry for the products erupted during November-December 2002 (Ridolfi *et al.*, 2008) was also discussed.

The products of Sumaco consist of porphyritic lavas with a common pilotaxitic groundmass and they vary from basanite to phonolite being characterized by the presence of modal feldspathoid (mostly haüyne and subordinate nepheline). The most common phenocrysts are represented by clinopyroxene and plagioclase. Olivine (in basanitic samples) apatite, amphibole, magnetite and K-feldspar may be also present among the investigated rocks. Titanite and pyrite are additional accessory phases (Colony & Sinclair, 1928; Barragàn *et al.*, 1998).

GEOCHEMISTRY

The oldest El Reventador products (OVE) are represented by the widest compositional range, from basalts to rhyolites with silica contents from 48.7 to 71.2%, and total alkali contents from 4.3 to 8.7%. Among all the products a small compositional gap is present between 63.0 and 66.0% of SiO_2. Al_2O_3 (21.9-15.8%), CaO (1.9-9.5%), MgO (0.4-6.7%), Fe_2O_3 (1.7-10.6%) and TiO_2 (0.2-1.2%) values show good negative linear correlations with SiO_2. P_2O_5 fix the apatite saturation at about 57.0% of silica. From PR to PC the most recent activity (PC), the most abundant products have intermediate composition: basaltic andesite and andesite. El Reventador volcano belong to a medium to high-K calc-alkaline series (Fig. 2).

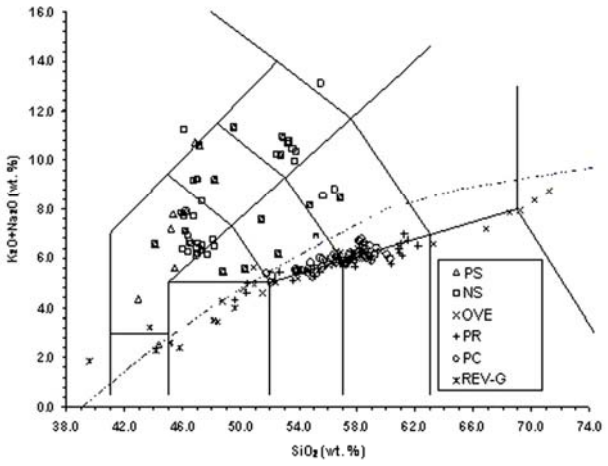

Fig. 2 - Total-alkali *vs.* Silica diagram; PS = Paleosumaco, NS = Neosumaco, OVE = El Reventador Old Volcanic Edifice, PR = Paleoreventador, PC = El Reventador Present Cone, REV-G = El Reventador cumulate gabbro nodules. Dashed line is from Irvine & Baragar (1971).

By contrast, all the Sumaco products (from basanites to phonolites; Fig. 2) are characterized by an alkaline to high-K alkaline affinity (Fig. 3).

Basanites are the most common lavas of Sumaco (both for PS and NS) and their total alkali content ranges from 4.4 to 6.7%, whilst SiO_2 varies from 43.0 to 48.2%.

Some major elements concentrations, such as K_2O (2.1-5.0%), P_2O_5 (0.2-1.1%) and Na_2O (3.5-8.1%) are very high for lowest silica values (*i.e.* 45.2-56.5%) with respect to all volcanic products of the NVZ (Barragàn *et al.*, 1998; Bourdon *et al.*, 2003; Bryant *et al.*, 2006).

Although both volcanoes show the typical Nb-Ta-Ti negative anomaly as the result of a subduction-related environment, trace elements concentrations are markedly different between El Reventador and Sumaco. Small enrichment in incompatible trace elements with silica increase are typical of El Reventador lavas, especially for LREE (*i.e.* La = 20.5-38.6 ppm; Ce = 42.2-72.9 ppm; Pr = 5.4-8.8 ppm). By contrast, the Sumaco lavas are strongly enriched in all incompatible elements and show very low values of LILE/HFSE and LILE/REE ratios (*i.e.* Ba/Nb 35-105 and Ba/La 13-28). These ratios are close to those observed in some ocean island basalts (OIB, Barragàn *et al.*, 1998) even if some calcalkaline basalts (CAB) may also show similar ratios.

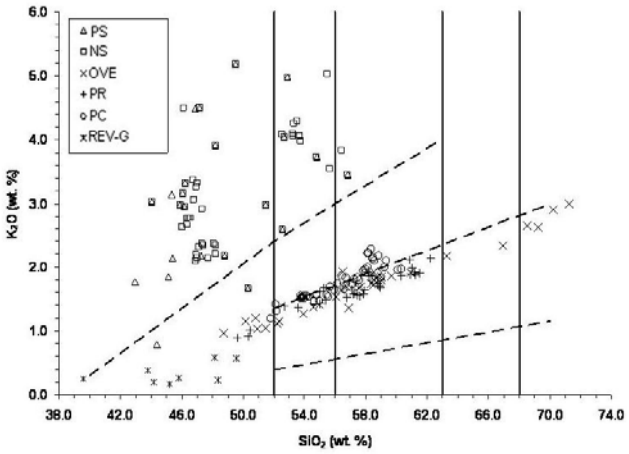

Fig. 3 - K_2O *vs.* Silica diagram; Symbols and abbreviations as in Fig. 2.

La/Yb ratios are higher for Sumaco samples than those for El Reventador, but both are similar to values observed by Hichey *et al.* (1986) in the SVZ of the Andes and interpreted as the result of low degree of partial melting of the mantle wedge. For both volcanoes La/Nb ratios are quite similar, although LREEs of Sumaco lavas are much higher with respect to those of El Reventador because the former is characterized by a very high abundance of Nb.

La/Sm_N ratios (up to 6.8 for Sumaco; 1.7-4.0 for El Reventador) point out the highest values for the Sumaco among all the lavas (with the same silica content) of the NVZ of the Andes. Sumaco geochemical affinity seems to be similar to some Nb-rich basalts which are associated to the adakitic magmatism of some volcanic arcs (Sajona *et al.*, 1996).

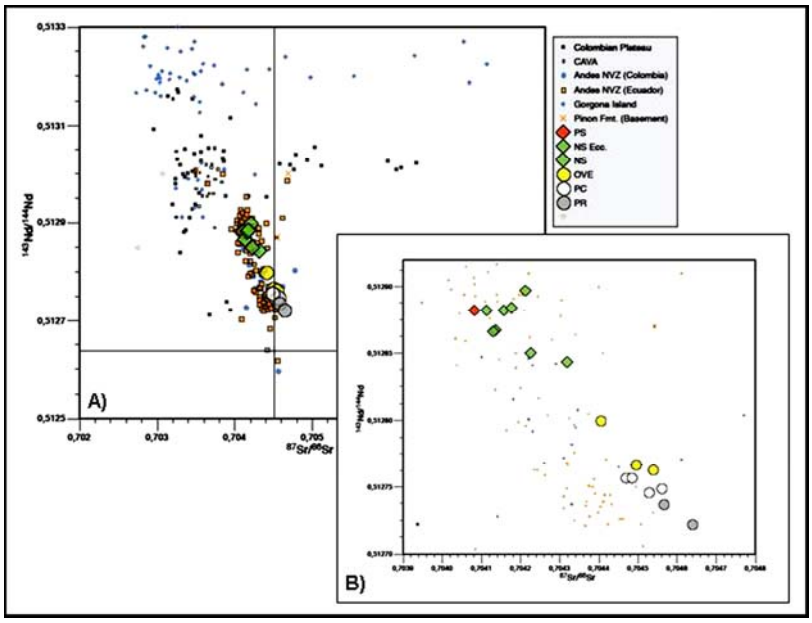

Fig. 4 - $^{87}Sr/^{86}Sr$ *vs.* $^{143}Nd/^{144}Nd$ isotopic ratios variation diagram (a), and relative inset (b) for El Reventador and Sumaco volcanic products; data from the literature are also shown (see legend). Symbols and abbreviations as in Fig. 2. The intersection of the horizontal and vertical lines in (a) represents the BSE (Bulk Solid Earth) composition, CAVA = Center America Volcanic Arc. NSecc = Neosumaco eccentric vents.

Radiogenic isotope data of El Reventador samples exhibit higher $^{87}Sr/^{86}Sr$ (0.70440-0.70464) and lower $^{143}Nd/^{144}Nd$ (0.51272-0.51280) with respect to Sumaco ($^{87}Sr/^{86}Sr$ from 0.70408 to 0.70432 and $^{143}Nd/^{144}Nd$ from 0.51284 to 0.51297; Fig. 4a). It is worth noting that the two distinct fields of El Reventador and Sumaco back-arc volcanoes are well within the Ecuadorian NVZ variation range ($0.7035 < {}^{87}Sr/^{86}Sr < 0.7047$; $0.5126 < {}^{143}Nd/^{144}Nd < 0.5130$). Nevertheless, El Reventador Sr isotopic ratios are among the highest values among the Ecuadorian volcanic rocks from the literature (Fig. 4b).

Lead isotope ratios show more complex variations. Whereas $^{207}Pb/^{204}Pb$ ratios are similar and almost constant, it is worth to note that El Reventador lavas have got lower values for $^{208}Pb/^{204}Pb$ and $^{206}Pb/^{204}Pb$, which are clearly separated from all the other Ecuadorian volcanoes data from the literature (Fig. 5).

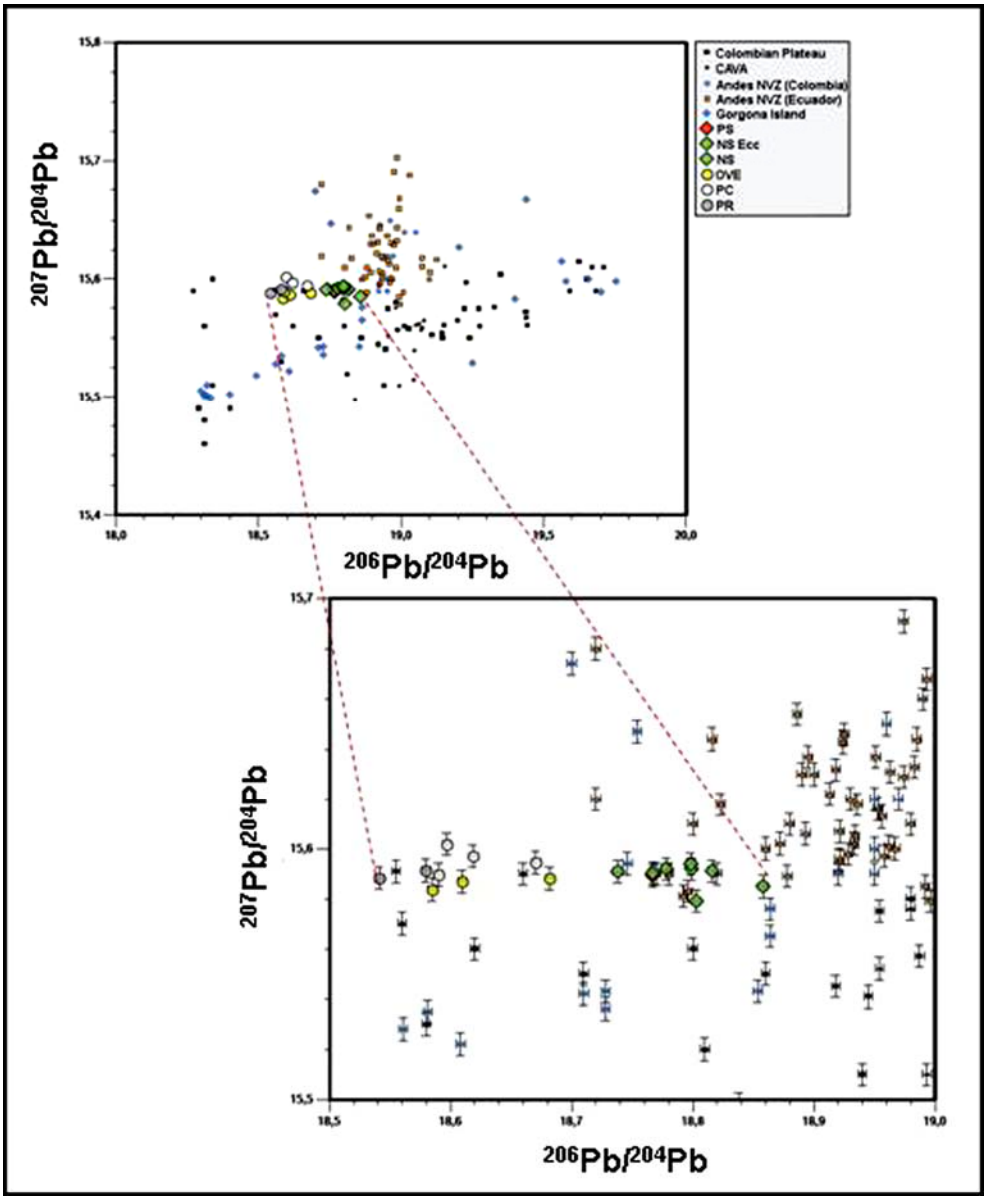

Fig. 5 - $^{207}Pb/^{204}Pb$ *vs.* $^{206}Pb/^{204}Pb$ isotopic ratios variation diagram for El Reventador and Sumaco lavas (and relative inset). Symbols and abbreviations as in Fig. 4.

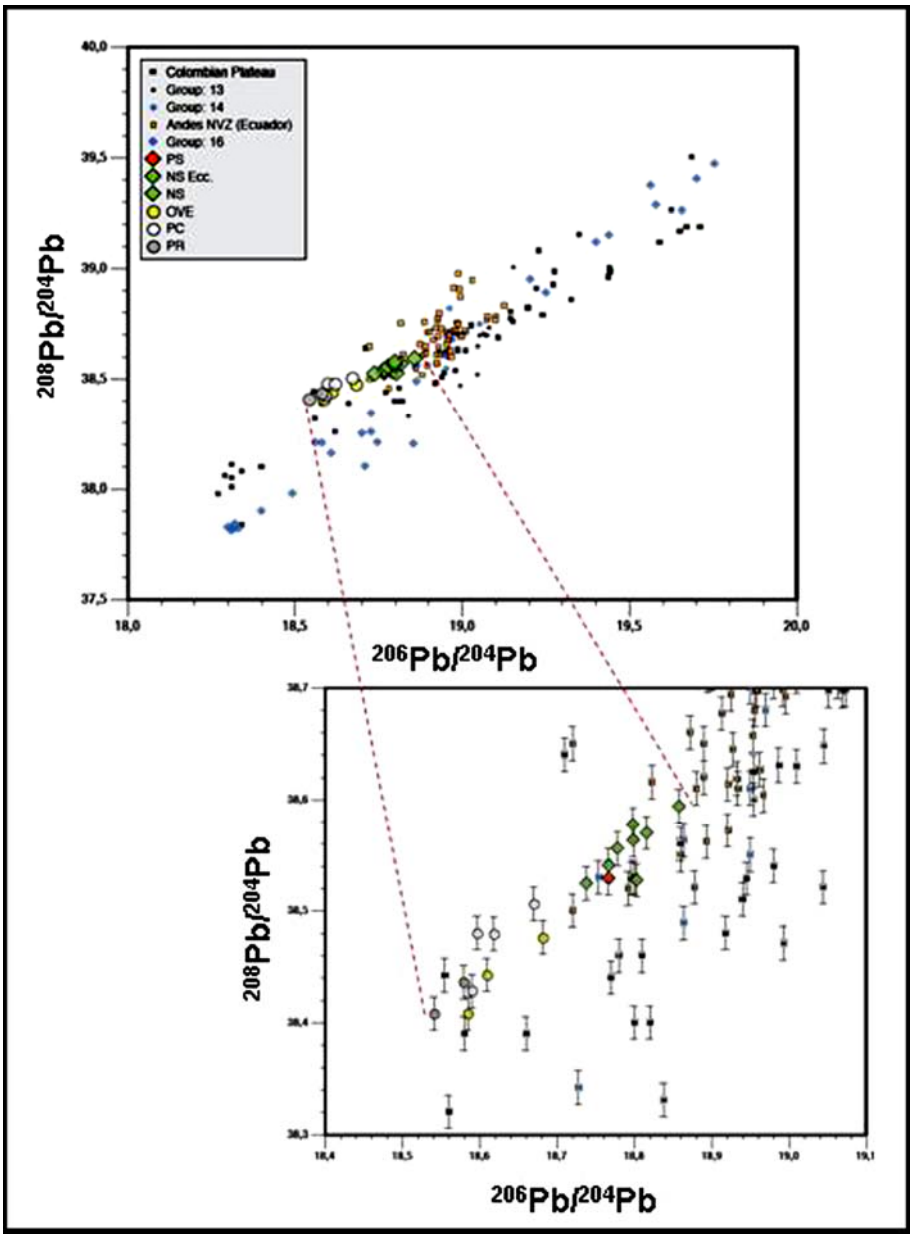

Fig. 6 - $^{208}Pb/^{204}Pb$ *vs.* $^{206}Pb/^{204}Pb$ isotopic ratios variation diagram for El Reventador and Sumaco lavas (and relative inset). Symbols and abbreviations as in Fig. 4.

In more detail, the studied rocks show a positive correlation between $^{208}Pb/^{204}Pb$ and $^{206}Pb/^{204}Pb$ for both volcanoes (Fig. 6). Lead isotope data for Sumaco ($18.738 < ^{206}Pb/^{204}Pb < 18.858$; $15.579 < ^{207}Pb/^{204}Pb < 15.594$; $38.525 < ^{208}Pb/^{204}Pb < 38.594$) are comparable with the global Ecuadorian variation field ($18.700 < ^{206}Pb/^{204}Pb < 19.150$; $15.575 < ^{207}Pb/^{204}Pb < 15.700$; $38.450 < ^{208}Pb/^{204}Pb < 38.950$) whereas those of El Reventador confirm different values from all the other Ecuadorian volcanoes and the lowest $^{208}Pb/^{204}Pb$ and $^{206}Pb/^{204}Pb$ ratios ($18.541 < ^{206}Pb/^{204}Pb < 18.682$; $15.584 < ^{207}Pb/^{204}Pb < 15.602$; $38.408 < ^{208}Pb/^{204}Pb < 38.506$; Figg. 5 and 6).

PETROGENETIC PROCESSES

Identification of magma sources in continental magmatic arcs, such as the Andean Cordillera, is a very complex geochemical task. This is more difficult when the subduction geometry (Benioff plane) is complex and not well defined by geophysical data because of the lacking or scarce seismicity of the subducted plate (Garrison & Davidson, 2003; Gutscher *et al.*, 1999). Physical structure of the Ecuadorian subduction zone suggests that different components may play a significant role in magma genesis: the mantle wedge, the subducted oceanic lithosphere, the physical-chemical characters of the slab, especially referring to the amount and type of the subducted sediments, and the nature and composition of the continental crust that the magmas pass through.

El Reventador and Sumaco volcanic products show completely different mineralogical and geochemical composition, even if they are located nearly at the same distance from the trench (360 km for Sumaco and 350 km for El Reventador), they grew upon the same basement rocks and they are located over mantle wedges with the same characters. The only geodynamic differences may be constituted by different subduction angles and, possibly, the occurrence of a subduction slab tearing close to Sumaco (Gutscher *et al.*, 1999).

Erupted products from both volcanoes show Nb and Ta negative anomalies, which are slightly less marked in the Sumaco lavas. Fluid mobile elements are enriched with respect to the immobile ones: this is a peculiarity generally related to the release of the subduction fluids (Tatsumi & Eggins, 1995). El Reventador lavas, with their Sr/Y ratios between 40 and 75 and Y contents of 12-21 ppm, seems to have an adakitic-like signature (Barragàn & Baby, 2004) similar to the volcanoes of the Cordillera Real (*e.g.* Antisana and Cayambe; Monzier *et al.*, 1997) and the Western Cordillera (*e.g.* Pichincha; Bourdon *et al.*, 2002).

Differences in the geometry and/or age of the subducted slab may be responsible for heterogeneous kind of fluids ± melts which can “induce” different extent of metasomatism in the mantle wedge where the basic magmas of the active continental margin originate. In particular, metasomatism of the mantle wedge is usually stronger in correspondence of the main-arc.

The subduction of the slab may also generate some mantle wedge movement like “corner flows” (Tatsumi & Eggins, 1995) in which mantle metasomatized rocks are carried far from the trench.

New geochemical data collected during this work show different enrichments of the back-arc magmas of Ecuador, due to the subduction component. The subduction component may re-fertilize the mantle and normally triggers partial melting: trace elements and isotope data point out that the Sumaco Volcano is characterized by the smallest amount of this component and consequently by the lowest degree of partial melting of the mantle wedge among the Ecuadorian volcanoes. By contrast El Reventador lavas show geochemical peculiarities similar to other arc-lavas but with marked isotopic differences that are clearly visible considering lead isotopes, suggesting a carbonatic sediment signature (*e.g.* DSDP495 carbonatic sample; Plank & Langmuir, 1998; Pedersen & Furnes, 2001) as subduction-related melts which could have metasomatized the mantle wedge source.

We can summarize the origin and the evolution of the Sumaco magmas through the following steps:

(i) Small amounts of fluids, coming from both the subducted sediments and the alterated oceanic crust are added to the Sumaco mantle source;

(ii) Alkaline basic magmas are generated by low degrees of partial melting of the metasomatized mantle wedge. These primary melts are strongly enriched in incompatible elements, and have low

LILE/HREE and LILE/HFSE ratios, probably because of an OIB component coming up from the asthenosphere (maybe linked to the presence of a slab tearing; Gutscher *et al.*, 1999);

(iii) Partial melting of the subducted slab is not involved in the origin of the Sumaco primary magmas. Mantle-derived basic magmas rise through the continental crust without significant contamination processes and the evolution from basanite to phonolite is mainly driven by fractional crystallization.

On the other hand, El Reventador lavas may derive from the following petrogenetic processes:

(i) A role is played by the subducted slab-derived fluids (sediments, metamorphosed oceanic basalts and serpentinites) for the mantle wedge metasomatism;

(ii) Another component responsible for mantle wedge modification should be carbonatic sediment melts of the subducted slab. This latter component is the main responsible of the peculiar Pb isotopic composition (low $^{206}Pb/^{204}Pb$ and low $^{208}Pb/^{204}Pb$);

(iii) Basic magmas are generated by partial melting of the mantle wedge metasomatized as above. These magmas evolve by fractional crystallisation in crustal magma chambers, as testified by the abundant cognate gabbro cumulates, with negligible crustal contamination. Melts directly derived by partial melting of the oceanic lithosphere slab (adakite magmas *stricto sensu*) seem to be therefore absent.

REFERENCES

Aguilera, E., Almeida, E., Balseca, W., Barberi, F., Innocenti, F., Coltelli, M., Pasquarè, G. (1988): El Reventador: an active volcano in the sub-andean zone of Ecuador. *Rend. Soc. It. Mineral. Petrol.*, **43**, 853-875.

Barragàn, R., Geist, D., Hall, M.L., Larson, P., Kurz, M. (1998): Subduction controls on the compositions of lavas from the Ecuadorian Andes. *Earth Planet. Sci. Letters*, **154**, 153-166.

Barragàn, R. & Baby, P. (2004): Evoluciòn magmàtica actual de la zona subandina. *In*: "La Cuenca Oriente: Geologìa y Petròleo", P. Baby, M. Rivadeneira & R. Barragàn, eds. Petroecuador, Quito, 295 p.

Bourdon, E., Eissen, J.P., Gutscher, M.A., Monzier, M., Samaniego, P., Robin, C., Bollinger, C., Cotten, J. (2002): Slab melting and slab melt metasomatism in the Northern Andean Volcanic Zone: adakites and high-Mg andesites from Pichincha volcano (Ecuador). *Bull. Soc. Geol. France*, **173**, 195-206.

Bourdon, E., Eissen, J.P., Gutscher, M.A., Monzier, M., Hall, M.L., Cotten, J. (2003): Magmatic response to early aseismic ridge subduction: the Ecuadorian margin case (South America). *Earth Planet. Sci. Letters*, **205**, 123-138.

Bryant, J.A., Yogodzinski, G.M., Hall, M.L., Lewicky, J.L., Bailey, D.G. (2006): Geochemical constraints on the origin of volcanic rocks from the Andean Northern Volcanic Zone, Ecuador. *J. Petrol.*, **47**, 1147-1175.

Colony, R.J. & Sinclair, J.H. (1928): The lavas of the Sumaco, eastern Ecuador. *Am. J. Sci.*, **216**, 299-312.

Garrison, J.M. & Davidson, J.P. (2003): Dubious case for slab melting in the Northern volcanic zone of the Andes. *Geology*, **31**, 565-568.

Gutscher, M.A., Malavieille, J., Lallemand, S., Collot, J.Y. (1999): Tectonic segmentation of the North Andean margin: impact of the Carnegie Ridge collision. *Earth Planet. Sci. Letters*, **168**, 255-270.

Hichey, R., Frey, F., Gerlach, D., Lopez-Escobar, L. (1986): Multiple source for basaltic arc rocks from the southern volcanic zone of Andes (34°-41°S): Trace element and isotopic evidence for contribution from subducted oceanic crust, mantle and continental crust. *J. Geophys. Res.*, **91**, 5963-5983.

Hall, M.L. (1977): El volcanismo en el Ecuador. PhD Thesis, Biblioteca Ecuador Instituto Panamericano Geografia y Historia), 120 p.

Hall, M., Ramon, P., Mothes, P., Le Pennec, J.L., Garcia, A., Samaniego, P., Yepes, H. (2004): Volcanic eruptions with little warning: the case of Volcan Reventador's Surprise November 3, 2002, Eruption, Ecuador. *Rev. Geol. Chile*, **31**, 349-358.

Hantke, G. & Parodi, I.A. (1966): Catalogue of the active volcanoes of the world including Solfatara Fields; part XIX, Colombia, Ecuador and Perù. *Geol. Soc. Am. Pub.*, 1-48.

Irvine, T.N. & Baragar, W.R.A. (1971): A guide to the chemical classification of the common volcanic rocks. *Canad. J. Earth Sci.*, **8**, 523-548.

Monzier, M., Robin, C., Hall, M.L., Cotten, J., Mothes, P., Eissen, J.P., Samaniego, P. (1997): Les adakites d'Equateur: modèle préliminaire. *Compt. Rend. Acad. Sci.*, IIa, **324**, 545-552.

Pedersen, R.B. & Furnes, H. (2001): Nd- and Pb-isotopic variation through the upper oceanic crust in DSDP/ODP Hole 504B, Costa Rica Rift. *Earth Planet. Sci. Letters*, **189**, 221-235.

Plank, T. & Langmuir, C.H. (1998): The chemical composition of subducting sediment and its consequences for the crust and mantle. *Chem. Geol.*, **145**, 325-394.

Ridolfi, F., Puerini, M., Renzulli, A., Menna, M., Toulkeridis, T. (2008): The magmatic feeding system of El Reventador volcano (Sub-Andean zone, Ecuador) constrained by texture, mineralogy and thermobarometry of the 2002 erupted products. *J. Volcanol. Geotherm. Res.*, **176**, 94-106.

Sajona, F.G., Maury, R.C., Bellon, H., Cotten, J., Defant, M.J. (1996): High field strength element enrichment of Pliocene-Pleistocene island arc basalts, Zamboanga Peninsula, Western Mindanao (Philippines). *J. Petrol.*, **37**, 693-726.

Tatsumi, Y. & Eggins, S. (1995): Subduction zone magmatism. Blackwell, Oxford, 211 p.

GEOCHEMICAL AND ISOTOPIC COMPOSITION OF NATURAL WATERS IN THE CENTRAL MAIN ETHIOPAN RIFT: EMPHASIS ON THE STUDY OF THE SOURCE AND GENESIS OF FLUORIDE

TEWODROS RANGO GODEBO
Dipartimento di Scienze della Terra, Università di Ferrara, Via Saragat 1, 44100 Ferrara

GENERAL INTRODUCTION

In the Main Ethiopian rift (MER) system, groundwater resources from wells and springs as well as from rivers are a very important supply of drinking water for millions of people living in the area. The MER is characterized by semi-arid to arid climate conditions where water scarcity is often associated with water quality problems (Fig. 1).

The natural waters of this region are characterized by geochemical anomalies of high fluoride concentration (Kilham & Hecky, 1973; Gizaw, 1996) often exceeding the 1.5 mg/l tolerance limit for drinking water (WHO, 2006). The local population is affected by diseases such as mottled teeth and skeletal fluorosis (Tekle-Haimanot *et al.*, 1987).

Many geochemical studies have addressed the fluoride problem in order to elucidate its origin (Gizaw, 1996; Yirgu *et al.*, 1999; Chernet *et al.*, 2001; Rango *et al.*, 2009) and to investigate the associated health problems (Tekle-Haimanot *et al.*, 1987; Kloos & Tekle-Haimanot, 1999). Although the health related impact of fluorine is well known, the hydrogeochemistry of fluorine, with respect to the controlling phases (minerals and/or amorphous), and the processes that induce its enrichment are not extensively studied in the Ethiopian rift system. Similarly, geochemical studies on trace elements are also not yet well investigated in the region.

Such kind of studies are extremely important especially in

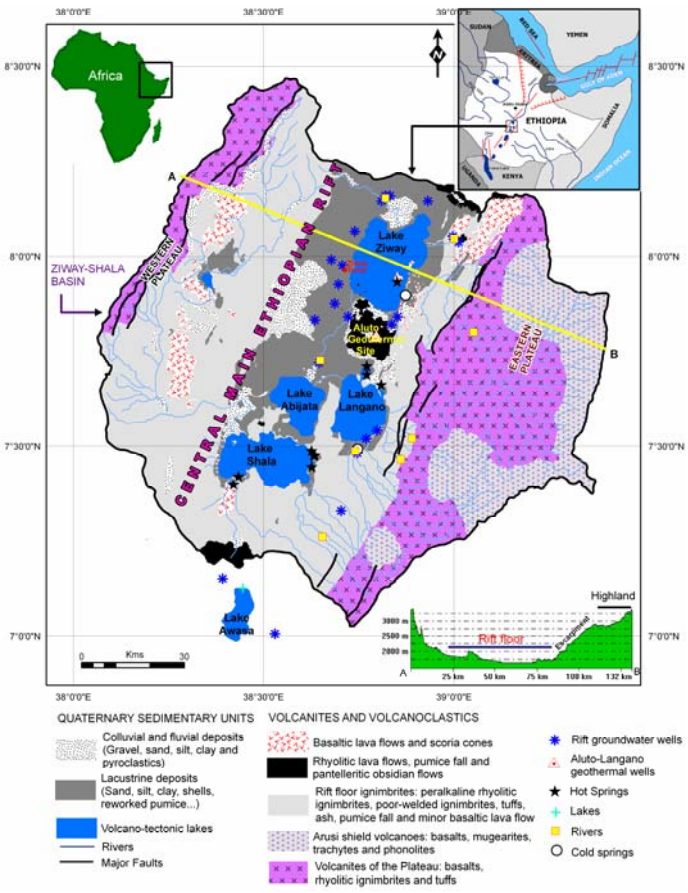

Fig. 1 - Simplified geologic map of Ziway-Shala lakes basin with water sampling points.

active volcanic areas which are characterized by extremely reactive lithotypes (that can release their chemical budget into the interacting water) and by persisting geothermal manifestations (possibly including juvenile fluids) that can pollute the shallow aquifers. This is the case of the Main Ethiopian rift (MER), where the presence of felsic-volcanic rocks (ashes, tuffs, rhyolitic ignimbrites) and their weathered and re-deposited fluvio-volcano lacustrine sediments, as well as the presence of active geothermal activities, could contribute to the existence of multiple geochemical anomalies with detrimental effects on human health.

This study mainly deals with the natural occurrence of these trace elements, particularly fluoride and arsenic. The other aspect addressed in this study is the isotopic composition of natural waters δD, $\delta^{18}O$ and strontium isotope ($^{87}Sr/^{86}Sr$) in order to understand surface water and groundwater circulation and their interactions, and water-rock interactions in the region.

Therefore, the objectives of this study can be summarized into three parts:

- To gain a better knowledge and understanding of fluoride problem with respect to its sources, genesis and distribution in order to support water quality management issues in the region;

- To perform a more general water quality assessment, and identifying other potentially toxic trace elements;

- To investigate the origin of waters, water/rock interactions and mixing processes in the basin using stable isotopes δD, $\delta^{18}O$ and radiogenic isotopes ($^{87}Sr/^{86}Sr$) in waters and lithotypes.

GEOCHEMISTRY OF ROCKS AND SEDIMENTS IN CENTRAL MAIN ETHIOPIAN RIFT

The results of bulk rock XRF analyses of the aquifer solid matrixes were reported in an alkali-silica classification diagram, indicating that the prevalent volcanic rocks are rhyolites, and that the fluvio-volcano lacustrine sediments simply represent the weathered - redeposited products of the above mentioned volcanic rocks. The petrographic investigation of representative thin sections shows that they are characterized by a few crystals of quartz, alkali-feldspar, orthopyroxene and amphibole within a prevalent glassy groundmass.

The microprobe analysis on ignimbrites revealed that the concentration of F is as high as 180 ppm in the glassy groundmass and up to 260 ppm in accessory phases such as alkali amphibole (riebeckite composition). Therefore, considering the modal proportions of the investigated rocks (hydrous mineral phases are extremely rare), we assume that most of the fluorine budget is concentrated in the glassy matrix.

Representative samples were subsequently selected for leaching experiments. In these experiments, powdered samples were mixed with distilled water having a *p*H of about 5.5, at a ratio of 1 to 5 (10 g / 50 ml; room temperature), and shaken for 12 months at a frequency of 100 rev/min. The test simulates the potential leachability of soluble components during water-rock/sediment interactions.

GEOCHEMISTRY OF MER WATERS

The major ions analyses of the different MER water types show extremely variable composition, ranging from low TDS (and *e.g.* low F^-) in rivers to very high TDS (and *e.g.* high F^-) in the rift groundwater wells, hot springs and lakes (sampling points on Fig. 1).

The average TDS values in the groundwater wells and hot springs (39-96°C) are 1050 and 3610 mg/l respectively. TDS is even more variable in lake waters, with values which vary from the fresh

water Ziway lake (379 mg/l), brackish water Langano lake (1377 mg/l) to the saline Shala, Abijata and Chitu lakes (11563, 52725 and 64267 mg/l respectively). *p*H ranges between 6.8-9.1 in groundwater wells, thermal springs and rivers whereas the lakes have pH range of 8.6-10, with the highest value recorded in the alkaline lake Chitu.

Hydrochemical facies of different water types, *i.e.* groundwater wells (in the rift and highlands), geothermal wells, hot springs, rivers and lakes were identified based on the Piper classification diagram. Groundwater from the highlands (Ayenew, 2005) typically show a $Ca^{2+}(Mg^{2+})$- HCO_3^- hydrochemical facies similar to that of rivers and cold springs where the sum of Ca^{2+} and Mg^{2+} exceeds Na^+ and K^+. On the contrary hot springs and most groundwater in the rift display a Na^+-HCO_3^- fingerprint, with Na^+ and HCO_3^- proportions constituting more than 80% of all the ionic species in the solution.

Fluoride concentration increases along the groundwater flow path displaying low values in Ca^{2+}-Mg^{2+}/HCO_3^- waters from the highlands and higher values in the Na^+-HCO_3^- waters from the rift. The average concentration of fluoride is 0.8 mg/l in rivers, 32 mg/l in thermal springs, 27 mg/l in deep (> 2 kms) geothermal wells, 6 mg/l in groundwater wells, and 121 mg/l in lakes. 38% of rivers, 87% of the groundwater wells and 100% of lakes, thermal and geothermal waters have fluoride value beyond 1.5 mg/l.

High F^- is associated with high *p*H, Na^+, and HCO_3^- values, whereas F^- is inversely related to Ca^{2+} and Mg^{2+} in the groundwater wells, hot springs and geothermal wells of the MER (Fig. 2). Accordingly, high fluoride concentration is found in leachates characterized by high *p*H, Na^+ and HCO_3^-.

Fluoride enrichment mechanism

Fluorine occurrence is associated with the presence of silicic rocks and their weathering products. The fluoride activity in the solution is controlled by the solubility product, $K_{fluorite}$ as expressed below:

$$CaF_2 = Ca^{2+} + 2\ F^-$$

$$K_{fluorite}: (Ca^{2+})\ (F^-)^2 = 10^{-10.57} \text{ at } 25ºC$$

This suggests that the fluoride concentration in natural waters is inversely related to Ca^{2+}. This permits free mobility of the fluoride ion into the solution at lower Ca^{2+} content. This effect (Ca^{2+} deficiency) is magnified in the rift (MER) where cation exchange took place within the sediments (fluvio-lacustrine, volcano-lacustrine) causing the removal of ions from the solution (mainly Ca^{2+}) by replacement with Na^+ ions from the clay exchange sites (Rango *et al.*, 2009).

$$Na^+\text{-clay} + (Ca^{2+} + Mg^{2+})\ \text{groundwater} = (Ca^{2+} + Mg^{2+})\ \text{clay} + (Na^+)\ \text{groundwater}$$

Such hydrogeochemical processes are responsible for the evolution of Ca^{2+}-Mg^{2+}/HCO_3^- to Na^+/HCO_3^- types of groundwater and thermal water with a parallel enrichment of fluoride.

In order to sort out other potentially hazardous geochemical anomalies, the measured concentrations of trace elements (and major ions) in MER natural waters were compared with existing drinking water standards recommended by the authorities (WHO 2006; EU directives, 1998; USEPA, 2003).

The result showed that major ions (F^-, Na^+, Cl^-, SO_4^{2-} and NO_3^-) and trace elements such as As, B, Mo, U, Fe, Al, and Mn often exceed the tolerance limit of drinking water fixed by the authorities.

Among trace elements, arsenic represents another geochemical anomaly that potentially induce serious health problem. The average concentration of arsenic is 0.9 µg/l in rivers, 39 µg/l in thermal springs, 236 µg/l in deep geothermal wells, 21.4 µg/l in groundwater wells and 77 µg/l in lakes, with maximum values of 3 µg/l, 156 µg/l, 278 µg/l, 157 µg/l and 405 µg/l respectively. It has to be noted that 35% of the MER groundwater wells (the main source of potable water) contain more than the safe limit 10 µg/l (WHO, 2006).

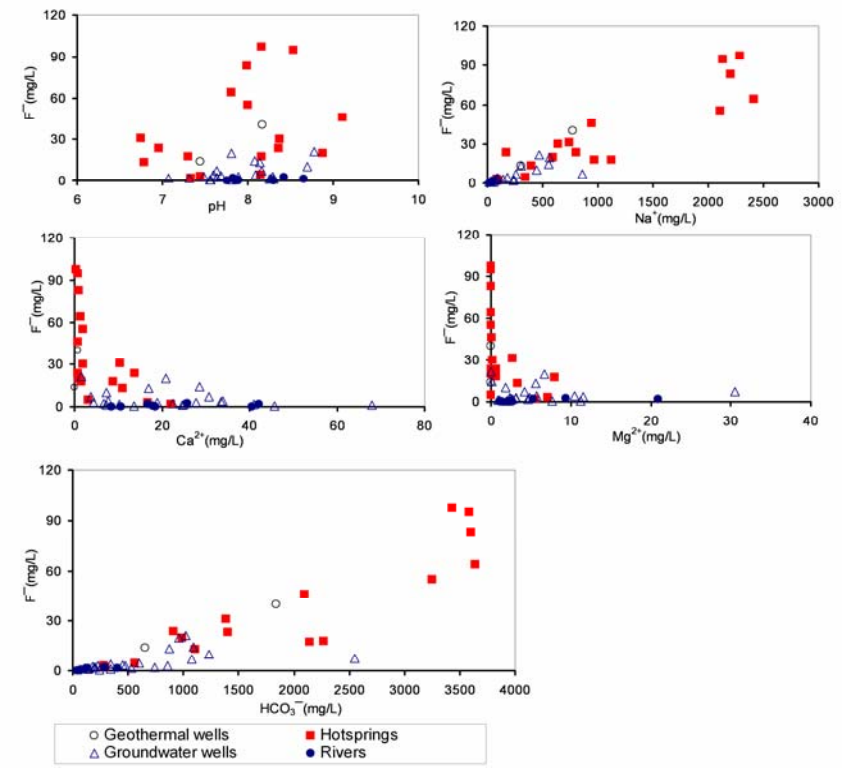

Fig. 2: Relationship between *p*H, F^-, Na^+, HCO_3^-, Ca^{2+} and Mg^{2+} in waters of the central MER.

F^- in MER groundwater wells positively correlated with Na^+ (R^2 = 0.7), HCO_3^- (R^2 = 0.5), TDS (R^2 = 0.64) and EC (R^2 = 0.73) and similarly arsenic shows a positive correlation with Na^+ (R^2 = 0.63), HCO_3^- (R^2 = 0.7), TDS (R^2 = 0.6) and EC (R^2 = 0.67). Arsenic also correlates with some trace elements such as Mo (R^2 = 0.79), V (R^2 = 0.68), and U (R^2 = 0.70), whereas no correlation with Fe and Mn were observed.

LEACHING EXPERIMENTS

The comparison with the tolerance limits indicated by international guidelines has been extended to the experimental leachates, showing that the concentration of elements potentially affecting human health such as F, As, Fe, Al, Mo, and U are often beyond the admissible limits. These comparisons simply define the higher relative vulnerability of natural waters to the above mentioned elements in the region.

For instance, fluoride concentrations exceeded the drinking water standard of 1.5 mg/l in 10 out of 11 leachates, arsenic concentrations exceeded the standard of 10 µg/l in 3 out of 11 leachates, iron concentrations exceeded the standard of 200 µg/l in 4 out of 11 leachates and aluminium concentrations exceeded the standard of 200 µg/l in 3 out of 11 leachates. It is also very interesting to note that leachates from sediments display higher concentration of toxic elements with respect to those obtained from volcanic rocks. This indicates that the sediments are the major reservoir and source of toxic elements. High arsenic and fluoride concentration is found in leachates characterized by high *p*H, Na^+, and HCO_3^-.

Column laboratory experiments were also employed to asses the leaching behavior of pyroclastic ash deposits so as to elucidate its source and simulate the water-rock interaction processes, and to quantify the distribution of F^- within different grain sizes. The pyroclastic ash was separated into coarse and fine fractions. Then, three columns were respectively filled with raw (unsieved), coarse and fine fraction and flushed with synthetic rain water in saturated conditions (Fig. 3).

Very fast F^- leaching was observed on the fine fraction column at the start of the experiment while in the other two columns F^- was slowly released; additionally, a strong accumulation of F^- was found in the fine fraction. The effect was more pronounced in the fine column due to the available effective adsorbing surface area in the fine grained fractions. Subsequent to elution experiments, the columns were characterized via moment analysis of tracer test. Finally, flow and transport modeling was employed to compute the amount of F^- adsorbed onto solid phase, comparing the calculated conservative transport of F^- and the observed concentrations. The results gained in this study confirm the sources of leachable F^-, is principally constituted by F^- adsorbed on to the silicate glass surfaces of pyroclastic particles.

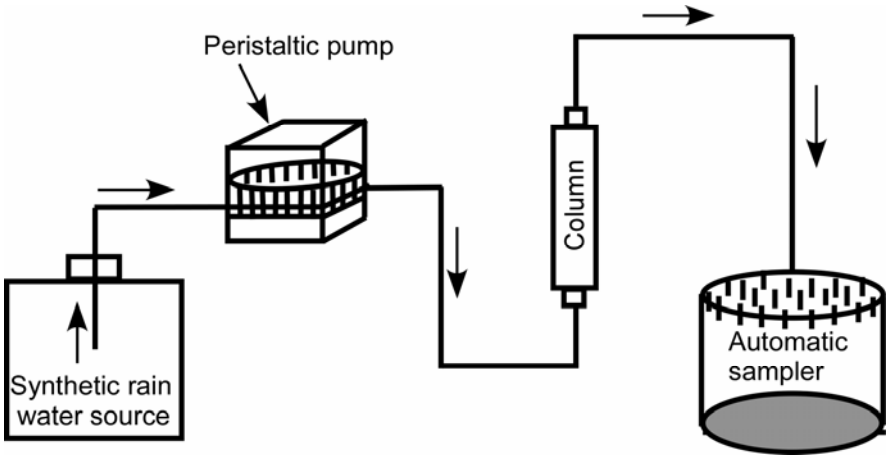

Fig. 3 - Schematic diagram of the column experimental set-up.

ISOTOPE GEOCHEMISTRY OF MER WATERS AND ROCKS

Defining the local meteoric water line (LMWL)

In the study area the local meteoric water line (LMWL; $\delta D = 7.02$, $\delta^{18}O + 9.1$) is defined based on the interpretation of isotopic data ($\delta^{18}O$, δD) of rain in the basin (at Asela, Ziway, Silte, Butagera, and Awasa towns) that were collected by (Chernet, 1998) in the period of June-August 1994 and 1995 with precipitation varying from 2.5 to 75 mm.

Samples from groundwater and geothermal wells, hot springs, lakes and rivers were analyzed for δD, $\delta^{18}O$, $^{87}Sr/^{86}Sr$ isotopes, and trace (Li, B, Sr, and Rb) elements in order to investigate groundwater and lake water interactions, water-rock interactions, and to evaluate groundwater flow path.

The principal groundwater recharge in the region, particularly east of Lake Ziway, are meteoric waters coming from highlands, mainly recharged by the NNE/SSW faults bounding the rift floor. Different ranges of isotopic values are recorded for different water types: hot springs $\delta^{18}O$ (-3.36–3.69)

and δD (-15.85–24.23), groundwater wells $\delta^{18}O$ (-3.99–5.14) and δD (-19.69–32.27) in contrast to the Lake $\delta^{18}O$ (3.98–7.92) and δD (26.19–45.71) (‰ V-SMOW). δD and $\delta^{18}O$ of the water types compared with LMWL and GMWL ($\delta^2H = 8\ \delta^{18}O + 10$).

Dissolved strontium isotopic ratios range from 0.7045 to 0.7076 in the hot springs, and the two deep geothermal wells situated along the fault at the up flow part of Aluto-Langano geothermal field, have 0.7043 and 0.7054 values, respectively. These ratios lie in the range of Sr isotopic signature of MER basalts and rhyolites, which showed overlapping signatures. The diversity in strontium isotopic ratios in waters is probably caused by complex mixings, interactions with multiple lithotypes, and different degree of water-rock/sediment interaction.

CONCLUSIONS AND RECOMMENDATIONS

The geochemical composition on natural waters of the central MER in Ziway-Shala basin has been investigated in order to understand the source, genesis and distribution of chemical elements with particular emphases to fluoride.

In this framework we performed an integrated study of both waters and coexisting representative solid aquifer matrixes, in order to unravel the water-rock/sediment interactions that ultimately lead to the peculiar geochemical features of the Ethiopian rift waters. Therefore, the hydrochemical investigation was coupled with the mineralogical/geochemical characterization of the lithologies outcropping in the area. Moreover, laboratory leaching tests (batch and column) were also carried out to evaluate the potential release of fluoride from the various rock/sediment types. These approaches serve to understand the lithologic sources and the enrichment mechanisms controlling the anomalous fluoride content in the water.

The geochemical anomalies in the studied natural waters are predominantly linked to the mode of emplacement of volcanism in the Ethiopian Rift system. The general hydrochemical evolution, in which $Ca^{2+}(Mg^{2+})$-HCO_3^- waters, typical of the highlands, are transformed along the flow path into alkaline *p*H and Na^+-HCO_3^- waters (typical of the rift area), is clearly related to water-rock/sediment interactions, is probably triggered/favoured by the high geothermal gradient and the high activity of CO_2 that characterize the rift valley. In these interactions, the matrixes are mainly rhyolites consisting of volcanic glass (usually more than 95% in proportion). This glassy material is extremely reactive, and its weathering products (*i.e.* the fluvio-volcano lacustrine sediments) can further concentrate geochemical elements. Therefore, the interaction of these "reworked" volcanic products with water and carbon dioxide (juvenile?) progressively lead to a "secondary" clay-bearing mineral assemblage that and under high *p*H conditions can release some chemical species (*e.g.*, F^-, As) into the interacting water.

A comparison of major and trace element concentrations of MER natural waters with standards set by three authorities (WHO, EU directives, USEPA), indicated significant quality problems (in all water groups at different percent proportions).

Together with the renowned F^- problem, the possible presence of geochemical anomalies in As, B, Mo, U, Al, Fe, and Mn have to be taken into consideration in water quality issues. Furthermore, future work has to be done to investigate their possible health impact on the population of MER and other sectors of the east African rift.

Column experiments were also conducted on volcanic ash (vitric ash) materials after separating into different grain size fractions (fine ash, coarse ash and raw ash) to characterize the behaviour of fluoride under flushing of synthetic rain water. The result showed that high concentrations of fluoride

were leached out particularly from the fine ash fraction which in turn suggests pyroclastic materials are the ultimate reservoir of fluoride.

Understanding the distribution and geochemistry of fluorine, arsenic and related elements along with their tolerance thresholds is essential in identifying high-risk areas and for the development of adequate remediation technologies, particularly where people live in scattered villages across the basin. However, considering that water treatments are expensive and barely efficient, we suggest avoiding (as far as possible) the drilling of new wells especially a) in those areas characterized by the presence of fluvio-lacustrine sediments b) close to the outpouring of hot springs. In any case activation of new wells should be preceded by chemical analysis including the above mentioned critical elements.

Moreover, we suggest starting to plan new strategies for water exploitation in the highlands (where elemental concentrations (such as F^- and As are typically low). This is mainly important for water supply of towns. These aqueduct infrastructures would imply an initial investment, but would be cost-effective in the long-term.

The stable $\delta^{18}O$, δD and radiogenic ($^{87}Sr/^{86}Sr$) isotopic composition indicate different ranges of stable isotopic values were recorded for different water groups. The Sr isotope signatures are typical of water that interacted with the main lithotypes covering the study area. Generally, the result shows that there exists a complex surface water and groundwater interactions that is reflected on a diversity of the stable and Sr isotopic signature in waters.

The general geochemical evolution of rift waters begins from eastern and western highlands following the regional groundwater flow direction; the pristine waters coming from the highlands should display isotopic compositions characterized by less radiogenic $^{87}Sr/^{86}Sr$ (and more depleted δD, $\delta^{18}O$). This isotopic signature subsequently evolves toward higher $^{87}Sr/^{86}Sr$ for an interaction with the more radiogenic rhyolites of the rift and their weathered and redeposited products.

The preliminary results of this study has showed that there is a need for future extended works on the geochemistry of solid samples (rocks, sediments and soils) as well as in waters. These studies should investigate a wide spectrum of chemical elements including all the components (trace/rare earth elements) that are potentially detrimental to human health and environment, in order to establish baseline geochemical atlases of the region.

Furthermore, from a water resource point of view, the following work must focus on a comprehensive study of various isotopes and geochemical data to constrain groundwater age dating, water-rock interaction and flow path and thus help to model and systematize the hydrologic cycles in the basin.

REFERENCES

Ayenew, T. (2005): Major ions composition of the groundwater and surface water systems and their geological and geochemical controls in the Ethiopian volcanic terrain. *Ethiopian J. Sci.*, **28**, 171-188.

Chernet, T. (1998): Etude des mécanismes de minéralisation en fluorure et éléments associés de la région des lacs du rift Ethiopien, Thèse Doctorat, Université d'Avignon, 210 p.

Chernet, T., Travi, Y., Valles, V. (2001): Mechanism of degradation of the quality of natural water in the lakes region of the Ethiopian rift valley. *Water Res.*, **35**, 2819-2832.

European Union (1998): Council Directive 98/83/EC of 3 November 1998 on the quality of water intended for human consumption. *Offic. J. Europ. Comm.*, L330/32-L330/54.

Gizaw, B. (1996): The origin of high bicarbonate and fluoride concentrations in waters of the Main Ethiopian Rift Valley, East African Rift System. *J. African Earth Sci.*, **22**, 391-402.

Kilham, P. & Hecky, R.E. (1973): Fluoride: geochemical and ecological significance in East African waters and sediments. *Limin. Oceanog.*, **18**, 932-945.

Kloos, H. & Tekle-Haimanot, R. (1999): Distribution of fluoride and fluorosis in Ethiopia and prospects for control. *Tropic. Medic. Intern. Health*, **4**, 355-364.

Rango, T., Bianchini, G., Beccaluva, L., Ayenew, T., Colombani, N. (2009): Hydrogeochemical study in the main Ethiopian rift: new insights to source and enrichment mechanism of fluoride. *Environ. Geol.*, **58**, 109-118.

Tekle-Haimanot, R,. Fekadu, A,. Bushra, B. (1987): Endemic fluorosis in the Ethiopian Rift Valley. *Trop. Geogr. Med.*, **39**, 209-217.

USEPA (2003): National primary drinking water regulations. EPA 816-F-03-016, United States Environmental Protection Agency.

WHO (2006): Guidelines for drinking-water quality. 1st Addendum to vol. 1. Recommendations, 3rd ed. Geneva, World Health Organisation, 595 p.

Yirgu, G., Ayalew, D., Peccerillo, M.R., Barberio, C., Donati, C., Donato, P. (1999): Fluorine and chlorine distribution in the volcanics rocks from the Gedemsa volcano, Ethiopian Rift Valley. *Acta Vulcanol.*, **11**, 169-176.

EVIDENCE OF ENRICHED MANTLE (EM-2) SOURCE CONTRIBUTION TO ETNEAN MAGMAS: A COMPREHENSIVE STUDY ON FLUID AND MELT INCLUSIONS OF 2001-2006 ERUPTIONS

ALBERTO ROSCIGLIONE
Dipartimento di Chimica e Fisica della Terra ad Applicazioni alle Georisorse ed ai Rischi Naturali,
Università di Palermo, Via Archirafi 36, 90123 Palermo

INTRODUCTION

Mt. Etna (Sicily, Italy) is one of the most active volcano in the world and the greatest one in Europe. Its activity probably started in the late-Pleistocene, ~ 0.5 Ma ago (Condomines *et al.*, 1982) and from then it was characterised by several changes in its eruptive style. Mt. Etna has the longest period of documented eruptions in the world and is noted for the wide variety of eruption styles.

Present-day Mt. Etna activity consists in summit and flank eruptions, prevailingly effusive accompanied by strombolian ejections of tephra (bombs and scoriaceous lapilli).

During the last ten years Mt. Etna activity has been characterised by frequent and sudden eruptions with many new and unusual geochemical and petrological features. In particular, the flank eruption of July-August 2001 and the dramatic flank eruption that lasted from October 2002 until late January 2003 are considered as two of the most unusual and complex eruptions recorded during the past 300 years.

These two eruptions had several similarities. Both were characterised by an extraordinary explosive activity and both affected two portions of the Etnean plumbing system. But the most striking feature of these two energetic eruptive events was the occurrence of textural and compositional differences in products contemporaneously erupted from distinct vents during a same eruption (Métrich *et al.*, 2004; Clocchiatti *et al.*, 2004; Spilliaert *et al.*, 2006; Corsaro *et al.*, 2007). In particular, lavas from the 2001 upper vents (≈ 2700 m; hereafter 2001 UV) and from the 2002-2003 northern fracture (hereafter 2002 N) are trachybasalts mineralogically similar to those that erupted in previous decades, while lavas from the 2001 lower vents (≈ 2100 and 2600 m; hereafter 2001 LV) and from the 2002-2003 southern fracture (thereafter 2002 S) are slightly more basic, primitive, and volatile-rich (Clocchiatti *et al.*, 2004; Corsaro *et al.*, 2007). After these two unusual events, at Mt. Etna occurred other two minor eruptions in 2004 and 2006.

Among the geochemical features that can be studied in the erupted products, fluid and melt inclusions hosted in olivine and clinopyroxene phenocrysts of the volcanic products (tephra and lavas) emitted during 2001-2006 eruptions, were selected for this study. It is well known in fact that melt and fluid inclusions could preserve more pristine characters of the related magmas providing useful constraints on the mantle source(s) and its evolution over space and time.

The aim of this study is to provide a contribution in acquiring further information on both the genesis and evolution of the recent erupted magmas, by better defining the characters of the magma source(s) and the dynamics of melts in the plumbing system. We are confident it will improve our knowledge on *how Mt. Etna works*, considering also the possible relations linking new data on the sampled volcanic rocks with those acquired during the geochemical monitoring. This work of thesis is basically divided into two main sections which regards respectively i) Fluid inclusions, and ii) Melt inclusions.

FLUID INCLUSIONS

In this section, are presented new data on noble gases obtained by *in-vacuo* crushing of olivines and pyroxenes extracted from the products erupted from Mt. Etna during 2001-2005.

Fluid inclusions are a common feature of minerals. During magma crystallization, when a crystal grows in the presence of a vapor phase, some of the gas may be trapped as imperfections in the growing crystal to form fluid inclusions (thereafter FIs). Their presence suggests oversaturation of magma with a fluid phase and partial degassing at the stage of host mineral crystallization. When properly interpreted, FIs provide information, which cannot be obtained otherwise: they are the only direct evidence for the role of the fluid during intratelluric processes.

Among the noble gases, the helium-isotope signature can be used to determine the source and processes ongoing during magma crystallization. In particular, during their growth within magma, olivines and pyroxenes trap FIs containing helium isotopes that are representative of the magmatic conditions, and can be investigated a long time after the eruption (Scarsi, 2000; Hilton *et al.*, 2002). The noble gases in FIs from etnean lavas have been investigated only by Marty *et al.* (1994) in selected historical lavas in order to constrain the origin and evolution of Mt. Etna magmatism.

In this work, He and Ar have been investigated in olivine and clinopyroxene FIs from lavas and pyroclastic deposits erupted at Mt. Etna during the 2001 (UV and LV), 2002-2003 (N and S), and 2004-2005 eruptions.

Analytical techniques

Rock samples were crushed to a grain size below 2 mm, taking into account that most of the minerals have a grain size below 1 mm. Then 0.5 mm crystals (olivine and clinopyroxene) were selected by hand under a binocular microscope. Separated minerals were ultrasonically cleaned in 5% HNO_3, and then in distilled water and high-purity acetone. During each analytical session, about 1 g of olivines or 2 g of pyroxenes were loaded in the crusher. Gases were extracted by *in-vacuo* crushing at about 200 bar pressure. Helium, neon, and argon were cleaned up in a stainless steel ultrahigh-vacuum line, by adsorbing reactive species in Zr-Al getter pumps, separating Ar from He and Ne by charcoal trap cooled at 77 K by liquid nitrogen. He and Ne were then adsorbed and concentrated in another charcoal trap (cryogenic pump), cooled down at 12 K by a cold-head. A temperature controller allowed to separate the two species by releasing He at 40 K and Ne at 85 K, that were then separately admitted in a split flight tube mass spectrometer (Helix SFT) for isotope analysis. Ar previously adsorbed was finally released from the charcoal by heating the trap at room temperature and then admitted in a multi-collector mass spectrometer (Argus). Analytical error in air standard He isotope analysis was generally below 1%, while in Ar analysis was generally below 0.1% (Nuccio *et al.*, 2008).

Results and discussion

The He and Ar abundances and relative isotope ratios are in agreement with the values reported by Marty *et al.* (1994) for olivine and pyroxene FIs from etnean historical lavas.

The measured helium isotope ratios (expressed as R/Ra, where R is $^3He/^4He$ of the sample and Ra is the same ratio in atmosphere) of olivine and pyroxene FIs vary widely, from 5.2 to 7.0 Ra, and $^{40}Ar/^{36}Ar$ ratios are between 300 and 310, which is near to the atmospheric value of 295.5.

By crushing co-genetic olivines and pyroxenes, they revealed that both helium abundance and $^3He/^4He$ ratio tends to be lower in pyroxenes (Fig. 1). This effect has been attributed to the closure temperature being lower for pyroxene than for olivines, that caused higher loss of magmatic volatiles and

fractionation in the formers, coupled to more evident effects of air contamination. Atmospheric contamination was also identified on the basis of argon isotopes, which were not used as a tracer of the magmatic source. We believe that the differences of air-corrected isotope ratios between olivines and pyroxenes mainly depend on the capability on the two minerals to provide a true barrier for He diffusion. Indeed, olivine has a crystal structure that reduce any secondary exchange, after crystallization, thus preserving the original magma signature (Craig & Lupton, 1976; Ozima & Podosek, 1983; Martelli *et al.*, 2004).

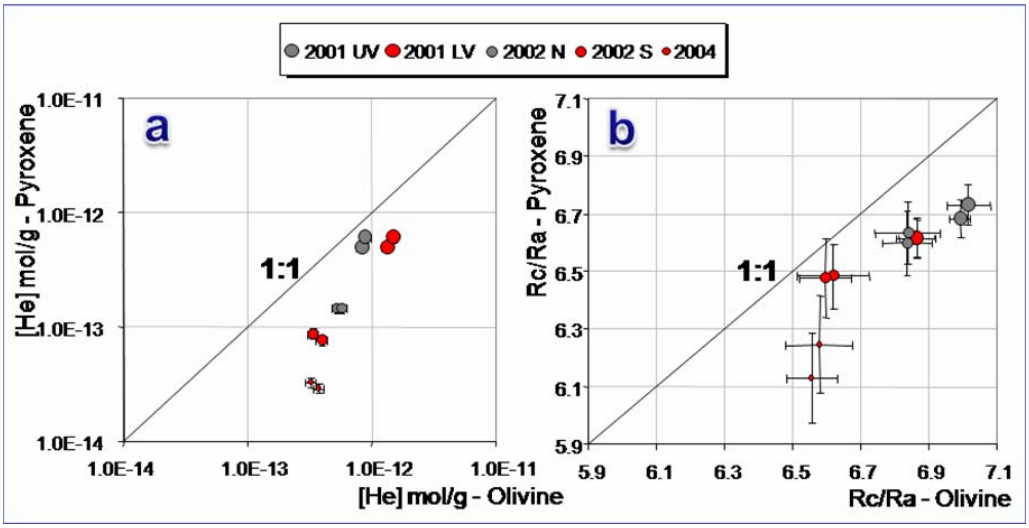

Fig. 1 - a) Comparison of He abundance between investigated olivines and pyroxenes. Grey and red colours indicate the two parental magma series. Circles progressively decrease in size from 2001 products to 2004-2005 products. Each point represents an individual mineral sample. b) $^{3}He/^{4}He$ ratios (expressed as Rc/Ra) of the investigated olivines and pyroxenes.

Another finding in our investigation was that the He and Ar contents as well as the helium isotope ratio generally decrease in both olivines and pyroxenes from the 2001 to the 2004-2005 products (Fig. 1 and Fig. 2). The decreasing trend of the helium isotope ratios from 2001 toward 2004-2005 lavas results in a difference of 0.5 Ra between 2001 UV and 2004-2005 olivines and up to 0.6 Ra in the cogenetic pyroxenes (Fig. 1). In accordance with the petrological evidence, we attributed the observed decreasing trend in He abundances to a progressive loss of volatiles due to magma degassing between the 2001 eruption and those of 2002-2003 and 2004-2005 and we suggest that this process could also induce a preferential ^{3}He loss in the residual magma. In agreement with the process described by Caracausi *et al.* (2003), the exsolving bubbles in etnean magmas could in fact grow far from equilibrium, and thus become kinetically enriched in ^{3}He. Accordingly, the progressive outgassing of ^{3}He-enriched bubbles can explain the decrease of the $^{3}He/^{4}He$ ratios measured in the FI of 2002-2003 and 2004-2005 phenocrysts with respect to the ones erupted in 2001.

The decrease in He-isotope ratios from 2001 to 2004-2005, recorded in olivine-hosted FI, was also found in the helium-isotope data obtained during the same period through the long-term monitoring of

volcanic gases at the surface (Rizzo *et al.*, 2006). To our knowledge, this is the first time that temporal trends from FIs and emitted gases have been compared. The results provide strong evidence of a direct link between gases discharged at the surface and the volatiles released from magma, and highlight the power of using Etnean peripheral gases as real-time indicators of magma dynamics at depth.

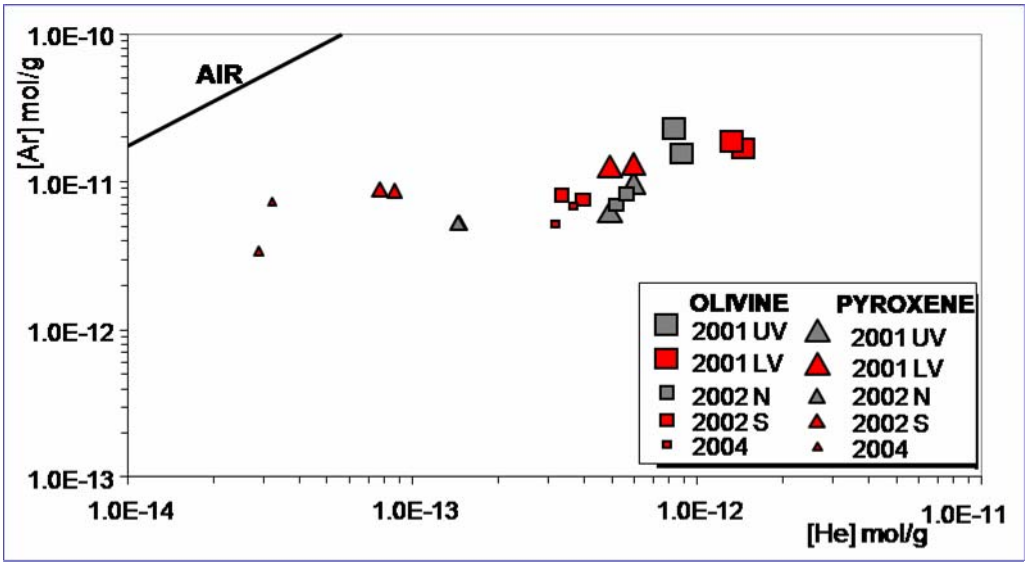

Fig. 2 - He *versus* Ar abundance in FIs of investigated olivines and pyroxenes. Squares and triangles have dimensions progressively smaller in size from 2001 products to 2004-2005 products. The line representing the He/Ar ratio in the atmosphere is also shown.

MELT INCLUSIONS

In this section were discussed data about the major, volatiles and trace elements compositions of olivine-hosted melt inclusions. Melt inclusions (thereafter MIs) trap small amounts of the unaltered and non-degassed silicate melt from which phenocrysts grow. Analyses of MIs can provide important geochemical information on the melt and help to better understand igneous petrogenesis. The use of MIs to study magmatic processes is based on the assumption that the inclusions represent the melt present at the time of trapping, and that nothing has been added to or lost from the inclusion since trapping (Bodnar & Student, 2006).

In this study, MIs occur as isolated inclusions or in assemblages defining crystal growth zones. Their size vary from < 10 μm to > 100 μm, however most inclusions are typically 5-50 μm. Typically, isolated inclusions are larger than those in well-defined crystal growth assemblages. MIs are composed of homogeneous glass with or without a small bubble, but without any trapped or daughter minerals and their shape is rounded to elongate. The MIs are assumed to be primary because they are trapped along crystal growth faces or between growth zones with no visible fractures.

Analytical techniques

Phenocrysts containing MIs were mounted in epoxy resin, and the MIs were brought closer to the surface of the crystal by continued grinding and polishing by hand on glass plates for better visual inspection. MIs located along fractures or near the edges of crystals were ignored as were those containing a shrinkage or vapor bubble.

The major and minor element compositions of exposed MI were determined using an Cameca SX-50 electron microprobe (EMPA) at CNR-IGG of Padova. Measured values were corrected for post-entrapment crystallization (PEC). The trace elements and H_2O analysis in the MIs were done with a Cameca IMS 4f ion microprobe (SIMS) installed at CNR-IGG of Pavia.

Results and discussions

One of the most important results of this study is a documentation of large chemical variability, among melt inclusions found in samples belonging to the different magmas, simultaneously emitted during 2001 and 2002-2003 eruptions, already recognised on the basis of petrographic investigations (Clocchiatti *et al.*, 2004). It is worth noticing that primitive melt inclusions within a single phenocryst or a single lava sample have relatively uniform major element compositions but their trace elements signature may be highly variable. On the basis of trace elements compositions, MIs can be clustered into two groups (Fig. 3) named “type 1” and “type 2”.

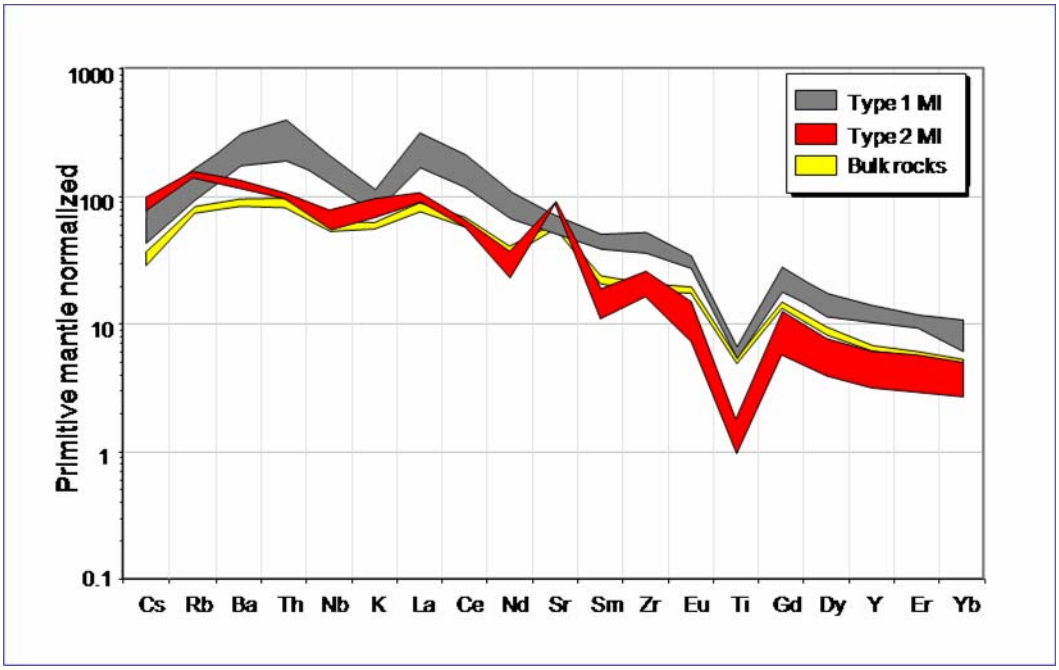

Fig. 3 - Trace element abundance normalised to the composition of the primitive mantle and plotted from left to right in order of increasing compatibility. Olivine-hosted MIs in etnean trachybasalts and alkali basalts belonging to the suites of different eruptions (2001, 2002 and 2006). Bulk rocks from Corsaro *et al.* (2007) were also plotted for comparison.

The different chemical composition of the two MI suites can be related to either source or en-route processes, such as fractional crystallisation or assimilation that modified the primitive melt chemistry. Simple arguments allow us to reject the latter possibility. Indeed, geochemical modelling shows that the two MI suites do not represent batches of the same parental magma that variously evolved by fractional crystallisation. On the other hand, the role of crust contamination cannot account for the different geochemical signatures of the two MI suites. Therefore, the different chemical composition of the two MI suites have been generated by either varying degrees of partial melting of the same mantle source or distinct magma sources. We first evaluate the former hypothesis and verified that the two recognised melts must derive from different mantle sources located at different mantle depths. The deeper source is probably asthenospheric and produces parental melts of type 1 MI; it has FOZO/C to HIMU isotopic signatures (Cadoux *et al.*, 2007) and is similar in composition to the mantle sectors that gave rise also to the older Hyblean lavas. The second source feeds parental melts of type 2 MIs and seems to be lithospheric and located at shallower depth relative to the source of type 1 MIs, possibly near the mantle-crust interface. With the aim of identifying the mantle sources involved in the melts production, ratios involving highly incompatible elements with nearly identical D (solid/melt) plotted against each other were used.

Because they remain uniform irrespective of their absolute concentrations and, therefore, do not vary with increasing concentrations in the magma during partial melting process, concentration ratios of these incompatible elements, namely Ce/Nb, K/La, Be/Nb, Rb/La and Ba/La primarily reflect those in present-day mantle magma sources (Hofmann *et al.*, 1986).

Schiano *et al.* (2001) used these ratios to postulate that the Etnean mantle source has changed from a HIMU-type to an arc-type, close in trace element composition to Vulcano primitive MIs**.** Instead, the trend defined by our samples falls far from the Vulcano Island subductive component and clearly point toward the EM-2 mantle source, namely a mantle source enriched by contribution of oceanic crust plus terrigenous sediments (Willbold & Stracke, 2006, and references therein).

The highest EM-2 contribution occurs in type 2 MIs erupted from 2001 LV and 2002 South fissures, which poured out products clearly different from any other one previously erupted from Mt. Etna. Rather than a general transition towards arc-type mantle sources beneath Mount Etna (Schiano *et al.*, 2001), we propose here that modern Etnean eruptions are supplied by magmas from two coexisting sources located at different depths within an Hyblean-like mantle. The contribution of magma with EM2-like signature seems to increase over time.

REFERENCES

Bodnar, R.J. & Student, J.J. (2006): Melt inclusions in plutonic rocks: Petrography and microthermometry. *In*: "Melt inclusions in plutonic rocks", J.D. Webster, ed. Mineral. Ass. Canada, Short Course, **36**, 1-26.

Cadoux, A., Blichert-Toft, J., Pinti, D.L., Albarede, F. (2007): A unique lower mantle source for Southern Italy volcanics. *Earth Planet. Sci. Letters*, **259**, 227-238.

Caracausi, A., Favara, R., Giammanco, S., Italiano, F., Paonita, A., Pecoraino, G., Rizzo, A., Nuccio, P.M. (2003): Mount Etna: Geochemical signals of magma ascent and unusually extensive plumbing system. *Geophys. Res. Lett.* **30**, doi:10.1029/2002GL015463.

Clocchiatti, R., Condomines, M., Guènot, N., Tanguy, J.C. (2004): Magma changes at Mount Etna: the 2001 and 2002-2003 eruptions. *Earth Planet. Sci. Letters*, **226**, 397-414.

Condomines, M., Tanguy, J.C., Kieffer, G., Allegre, C.J. (1982): Magmatic evolution of a volcano studied by ^{230}Th-^{238}U disequilibrium and trace elements systematics: the Etna case. *Geochim. Cosmochim. Acta*, **46**, 1397-1416.

Corsaro, R., Miraglia, L., Pompilio, M. (2007): Petrologic evidence of a complex plumbing system feeding the July-August 2001 eruption of Mt. Etna, Sicily, Italy. *Bull. Volcanol.*, **69**, 401-421.

Craig, H. & Lupton, J.E. (1976): Primordial neon, helium and hydrogen in oceanic basalts. *Earth Planet. Sci. Letters*, **31**, 369-385.

Hilton, D.R., Fischer, T.P., Marty, B. (2002): Noble gases in subduction zones and volatile recycling. MSA Special Volume: *Noble Gases Geochem. Cosmochem.*, **47**, 319-362.

Hofmann, A.W., Jochum, K.P., Seufert, M., White, W.M. (1986): Nb and Pb in oceanic basalts: new constraints on mantle evolution. *Earth Planet. Sci. Letters*, **79**, 33-45.

Martelli, M., Nuccio, P.M., Stuart, F.M., Burgess, R., Ellam, R.M., Italiano, F. (2004): Helium strontium isotope constraints on mantle evolution beneath the Roman Comagmatic Province, Italy. *Earth Planet. Sci. Letters*, **224**, 295-308.

Marty, B., Trull, T., Lussiez, P., Basile, I., Tanguy, J.C. (1994): He, Ar, O, Sr and Nd isotope constraints on the origin and evolution of Mount Etna magmatism. *Earth Planet. Sci. Letters*, **126**, 23-29.

Métrich, N., Allard, P., Spilliaert, N., Andronico, D, Burton, M. (2004): 2001 flank eruption of the alkali- and volatile-rich primitive basalt responsible for Mount Etna's evolution in the last three decades. *Earth Planet. Sci. Letters*, **228**, 1-17.

Nuccio, P.M., Paonita, A., Rizzo, A., Rosciglione, A. (2008): Elemental and isotope covariation of noble gases in mineral phases from Etnean volcanics erupted during 2001-2005, and genetic relation with peripheral gas discharges. *Earth Planet. Sci. Letters*, **272**, 683-690.

Ozima, M. & Podosek, F.A. (1983): Noble gas geochemistry. Cambridge University Press, Cambridge, 367 p.

Rizzo, A., Caracausi, A., Favara, R., Martelli, M., Paonita, A., Paternoster, M., Nuccio, P.M., Rosciglione, A. (2006): New insights into magma dynamics during last two eruptions of Mount Etna as inferred by geochemical monitoring from 2002 to 2005. *Geochem. Geophys. Geosyst.*, **7**, Q06008.

Scarsi, P. (2000): Fractional extraction of helium by cushing of olivine and clinopyroxene phenocrysts: effects on the $^{3}He/^{4}He$ measured ratio. *Geochim. Cosmochim. Acta*, **64**, 3751-3762.

Schiano, P., Clocchiatti, R., Ottolini, L., Busà, L. (2001): Transition of Mount Etna lavas from a mantle-plume to an island-arc magmatic source. *Nature*, **412**, 900-904.

Spilliaert, N., Allard, P., Mètrich, N., Sobolev, A.V. (2006): Melt inclusion record of the conditions of ascent, degassing, and extrusion of volatile-rich alkali basalt during the powerful 2002 flank eruption of Mount Etna (Italy). *J. Geophys. Res.*, **111**, B04203.

Willbold, M. & Stracke, A. (2006): Trace element composition of mantle end-members: Implications for recycling of oceanic and upper and lower continental crust. *Geochem. Geophys. Geosyst.*, **7**, Q04004.

RADON RELEASE: DETECTION PROBLEMS AND ASSESSMENT OF RISK FACTORS

MARTA ROSSETTI
Dipartimento di Scienze della Terra, Università di Ferrara, Via Saragat 1, 44100 Ferrara

The indoor radon exposition is internationally known as a health hazard. For this reason, many countries have introduced specific laws and regulations and radon-risk maps have been produced. In Italy the radon exposure legislation regards only workplaces (D. Lgs. n. 241/00, 2000) and only one National Survey in the 90's has been conducted by APAT, ISS and ARPA regional agencies (Bochicchio *et al.*, 2005). This survey assessed the exposure to indoor radon concentration in national dwellings on large scale. In absence of guidelines, only few Italian Regions have prepared a surveying protocol using independent standards in order to identify "radon prone areas", inducing bigger uncertainty on the definition of a national risk map. In the present work a standardized methodology for indoor radon measurements has been set up in collaboration with ENEA and U-Series Srl (Bologna), with attention to the development of a passive measurement technique (solid state nuclear track detectors). The developed technique has been validated through an interlaboratory comparison conducted by the German Federal Office for Radiation Protection (BfS).

An indoor radon monitoring survey has been conducted in all Italian Regions with the developed methodology and 5425 measurements have been elaborated, also to verify the relapse of seasonal fluctuations on radon concentrations. A new map of annual average radon concentration for each Italian Region has been produced and, as a consequence of our developed methodology (measurements only in underground rooms), indoor radon concentrations resulted generally higher than the concentrations obtained in the National Survey.

The project of a radon chamber for the evaluation of radon emanation from geomaterials has been followed and the chamber was built at U-Series Srl laboratory.

Data from a wide sampling (Lombardia, with the case studies of Milano Province and Milano city, Emilia Romagna, Toscana, Puglia) of radon indoor monitoring have been elaborated and georeferenced, using geo-statistical technique, to produce a map of annual average radon concentration. Appling the international approach (Dubois *et al.*, 2007; Zhu *et al.*, 2001) recently introduced, the maps have been integrated with geological knowledge of highest concentration macro-areas identified in order to better determine them. This study allowed to point out not negligible radon concentrations also in traditionally no-risk zone, for example the North plain zone of Milan Province and the city of Milan; so some hypothesis have been formulated to understand the geological origin of the radon source in these sites.

Indoor radon concentrations were measured hourly with a continuous radon monitor for two case studies; the analyzed data showed the influence of ventilation control on radon concentration variability.

The application of the developed methodology will be useful to give advices to fill legislation gaps or to draft urban development plans.

REFERENCES

Bochicchio, F., Campos Venuti, G., Piermattei, S., Nuccetelli, C., Risica, S., Tommasino, L., Torri, G., Magnoni, M., Agnesod, G., Sgorbati, G., Bonomi, M., Minach, L., Trotti, F., Malisan, M.R., Maggiolo, S., Gaidolfi, L.,

Giannardi, C., Rongoni, A., Lombardi, M., Cherubini, G., D'Ostilio, S., Cristofaro, C., Pugliese, M., Martucci, V., Crispino, A., Cuzzocrea, P., Sansone Santamaria, A., Cappai, M. (2005): Annual average and seasonal variations of residential radon concentration for all the Italian Regions. *Radiation Meas.*, **40**, 686-694.

D. Lgs. n. 241/00 (2000): Attuazione direttiva 96/29/EURATOM in materia di protezione contro i rischi derivanti dalle radiazioni ionizzanti. *Suppl. Ord. Gazz. Uff.*, **203**, 31-08-2000.

Dubois, G., Bossew, P., Friedmann, H. (2007): A geostatistical autopsy of the Austrian indoor radon survey (1992-2002). *Sci. Total Environ.*, **377**, 378-395.

Zhu, H.C., Charlet, J.M., Poffijn, A. (2001): Radon risk mapping in southern Belgium: an application of geostatistical and GIS techniques. *Sci. Total Environ.*, **272**, 203-210.

MINERALOGY OF EPICA - DOME C ICE CORE DUST

MARCO SALA
Dipartimento di Scienze della Terra "A. Desio", Università di Milano, Via Botticelli 23, 20133 Milano

ABSTRACT

Optimization of analytical procedures for mineralogical characterization of aeolian dust trapped in Antarctic ice has been developed in this work. The analytical protocol includes X-Ray Powder Diffraction (XRPD) and High Resolution-Transmission Electron Microscopy (HR-TEM) coupled to Energy Dispersive X-Ray Fluorescence (ED-XRF) techniques. This procedure has been applied on standard minerals and Antarctic ice samples, in order to combine powder and single crystal results of aeolian particles archived in the EPICA Dome C (EDC) ice core during the last two climatic cycles. Diffraction measurements were also done on samples from Potential dust Source Areas (PSAs) collected in southern South America (sSA), South Africa (Saf), Australia (Aus), New Zealand (NZ), and some Antarctic (Ant) non-glaciated areas. Differences between the climatic periods has been observed in term of mineral assemblages. The more concentrated glacial periods seem to confirm the southern South America origin, while the provenance of interglacial particles seem to be a mixing between southern South America and Australia. This work highlight the potentialities of the XRPD coupled with HR-TEM techniques to help in the interpretation of the dust transport and deposition from the PSA to the Antarctic continent, and the possibility to understand the role of the atmospheric dust on the history of the southern Hemisphere climate in the last 200 kyrs.

INTRODUCTION

Ice cores can be considered undisturbed archives of climatic information, if drilled in the internal part of Antarctic Plateau, in the centre of Topographic Dome, and can permit to recover climatic and environmental records at different timescales (Petit *et al.*, 1999; EPICA Community Members, 2004). The EPICA Dome C (EDC) ice core provide information about the last 800 kyrs. Aeolian mineral dust trapped in the EDC core providing information about environment and climate, atmospheric circulation and the hydrological cycle of the Southern Hemisphere during last nine glacial and interglacial climatic periods (Lambert *et al.*, 2008). In this respect we could observe a high dust concentration value followed by a rapid decrease in dust mass and flux occurring during all the glacial to interglacial climatic variations, respectively from ~ 800 to ~ 15 ppb on average and a ratio of 50 to 1 over the last climatic cycle (Lambert *et al.*, 2008). The very low concentration of dust during interglacials is an analytical challenge in understanding the mineralogical properties of particles trapped in the ice cores.

The insoluble material reaching the Antarctic ice sheet is composed by extremely small particles, which display a diameter (spherical equivalent) smaller than 5 μm, and the size distribution typically shows modal values of about 2 μm, which is a characteristic dimension for long range transport (Delmonte *et al.*, 2002; Lambert *et al.*, 2008).

The environmental and climatic factors producing the increase in dust concentration during glacial times are: (1) dryness of the source areas, (2) variations in the hydrological cycle, (3) changes in the atmospheric circulation, and finally (4) efficiency during dust deposition (Petit *et al.*, 1999; Lambert *et al.*, 2008).

Mineral particles that compose the dust fraction suspended in the high troposphere that reach the Antarctic ice sheet are quartz, feldspars, salts, volcanic materials and mainly clay minerals (Pye, 1987). Due to the morphology, size and weight, clay materials are the most diffuse aeolian particles all over the Earth (Tegen & Fung, 1994). Moreover, several studies using isotopic tracers indicate that the major source for dust is southern South America (SSA) during cold periods (Grousset *et al.*, 1992; Basile *et al.*, 1997; Delmonte *et al.*, 2004). Conversely, for the last interglacial several studies provide evidence of large differences, with the strong contribution of the East Australia deflation areas (Revel-Rolland *et al.*, 2006).

An important contribution in understanding the climatic variations occurred in the Southern Hemisphere is obtained by applying mineralogical study on EDC ice core microparticles. In this respect, mineralogical and crystal-chemical studies provide information about the weathering occurred within the most important Southern Hemisphere source areas. Moreover, diffraction patterns obtained on the more recent aeolian sediments allow comparing the *present day* with the past environmental conditions at the same source.

In this work, we focus on the set-up and on the inter-calibration of XRPD and TEM, whose results were extensively tested with the use of certified standard samples, and we present the first data obtained by coupling diffraction and electron microscope analyses on a few samples from the EPICA (*European Project for Ice Coring in Antarctica*) ice core drilled at Dome C. Also an XRPD investigation on a few fine selected sediments from possible source areas collected in the more active dust sources of the Southern Hemisphere (Delmonte *et al.*, 2004; Revel-Rolland *et al.*, 2006) provide additional information about the provenance of mineral dust trapped in the Antarctic ice.

MATERIAL AND METHODS

Samples preparation and ice core dust deposition is an analytical challenge due to the very low amount of mineral materials, which is generally around 10-100 ng of mineral particles per g of ice; the extremely low quantity of solid particles in the Antarctic ice cap makes sample preparation for the different analytical techniques very difficult and prone to external contamination.

The ice core samples analysed in this research were selected from the European Project for Ice Coring in Antarctica-Dome C ice core (EDC, 3320 m long, 75º06'S, 123º21'E, 3233 m a.s.l., mean accumulation rate: 2.7 cm w.e. yr^{-1}) (Fig. 1). Two ice pieces are representative of Holocene, three from MIS2, two from MIS3, three from MIS4, two from MIS5.5 and three from MIS6 climatic periods. The ice samples were decontaminated using a microtome swamp and melted in Teflon pot in a 1000 class clean room at environment temperature. Afterwards, an estimation of dust concentration and size distribution of ice dust were made by a particle counter at DISAT, University of Milano Bicocca. The same procedure were also done on PSAs and certified standard minerals in order to check the size of mineral materials.

XRPD analyses were applied on (1) certified standard minerals, (2) Antarctic dust, and (3) on the bulk and fine fraction (FF, $\varnothing < 5$ μm) of airborne PSA sediments. Moreover, a crystallo-chemical characterization on ice core dust were done using HR-TEM at the Earth Science Dept. - University of Milano.

The former group of samples allows evaluating the lowest amount of mineral dust detectable through XRPD, obtaining also some calibration lines for semi-quantitative mineral phase estimation (Dapiaggi *et al.*, 2007) and creating a crystallographic dataset by means of HR-TEM investigation. The second group of samples allows the mineralogical characterization of extremely small amounts of

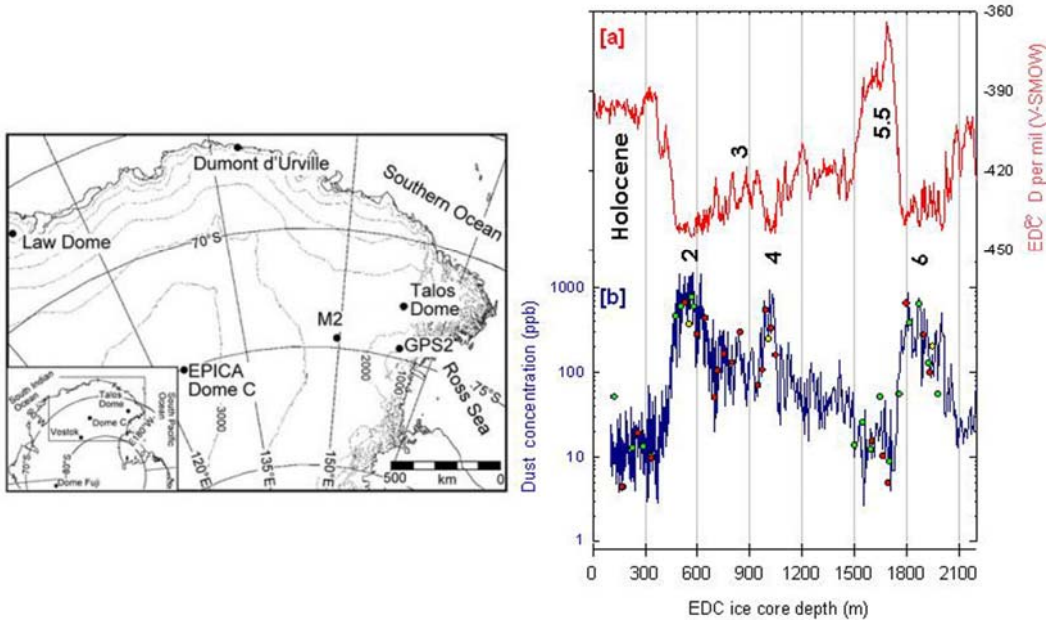

Fig. 1 - EDC drilling site and the EDC Deuterium (red) and dust (blue) record during the last 200 kyrs. Green dots show the I sampling, red dots the II and yellow dots the last (III) ice sampling.

Antarctic dust samples. The latter group of samples (11 Ant, 5 NZ, 18 SSA, 11 Saf and 22 Aus sediments) allows the identification of clay minerals in order to evaluate the provenance of the aeolian mineral dust trapped in the Antarctic ice (Sala, 2008).

All the diffraction patterns on standard minerals and ice samples were collected in a parallel beam geometry following the procedure described in Dapiaggi *et al.* (2007). Moreover, the PSA samples were analyzed working in Bragg-Brentano geometry both for bulk and fine selected fraction (Sala, 2008). Fine selected sediments were analyzed twice, comparing diffraction patterns of air-dried and ethylene glycol-solvated preparation. This analytical step allow to identify presence of expandable clay minerals in the samples.

The crystal-chemical investigation were performed as follows: single particles were looked for on the copper carbon grid, trying to avoid polycrystalline aggregates; then the crystal is tilted until the zone axis is found, and its diffraction pattern is collected. Moreover, by using the ED-XRF data it was also possible to evaluated the chemical composition of the crystal. The electron diffraction and imaging data collection were applied in the Eucentric position and focus the image (moving the sample along the *z*-axes).

RESULTS AND DISCUSSION

Here mineralogical assemblages and crystal-chemical characteristics of Antarctic ice dust were presented. A semi-quantitative estimation based on the calibration line obtained by analysing a few certified standard mineral was applied on the EDC ice core dust in the same way described in Dapiaggi *et*

al. (2007). Unfortunately, due to the very low and various quantity of mineral materials deposited on filter and to the high variability in the chemical composition of each mineral phases trapped in the ice, the quantification by the calibration line reconstruction is not available and representative for all the mineral dust materials archived in the Antarctic ice. For these reasons a semi quantitative estimation, based on the integrated peaks area calculation was applied on the EDC mineral particles. These method allow to evaluate a few mineral phase ratio as clay mineral *versus* quartz and feldspars.

The XRPD analyses on the aeolian particles trapped in the EDC core highlight that the mineralogical composition of Antarctic dust is very similar for all glacial climatic periods investigated. The diffraction pattern show presence of a few mineral phases archived in the ice (Fig. 2) as chlorite (Ch), kaolinite (K), mica (Mc), talc (T), amphibole (Am), quartz (Qz), K-feldspar (Kf) and plagioclase (Pl).

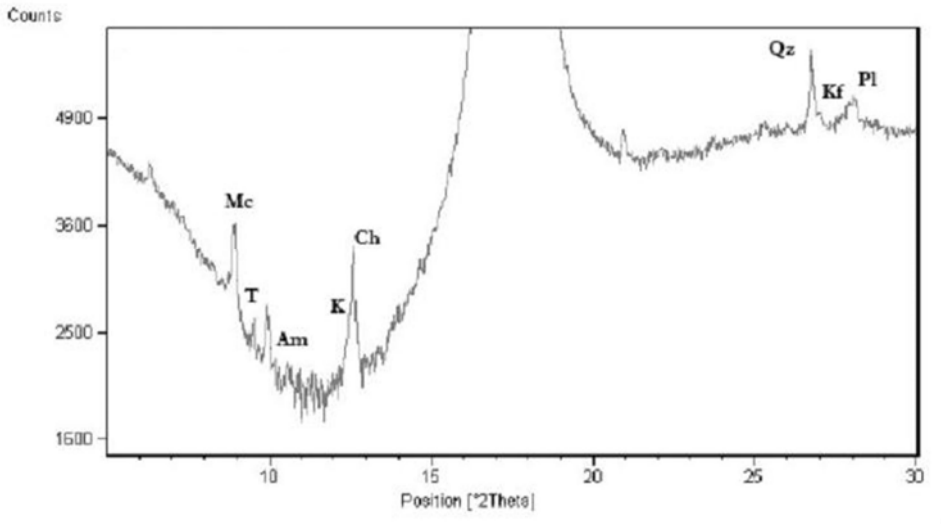

Mc:Qz	T:Qz	Am:Qz	K:Qz	Ch:Qz	Mc:F	T:F	Am:F	K:F	Ch:F	K:Ch	K:Mc	Ch:Mc
1:1.7	1:19	1:50	1:5	1:2	1:2	1:18	1:50	1:5	1:2	1:3	1:3	1:1

Fig. 2 - EDC-MIS2-I diffraction pattern and mineral phases ratio.

The low concentrated mineral dust filtered trough Nuclepore membrane make the diffraction peak identification for interglacial samples an analytical challenge; in this case only mica, talc and amphibole (Fig. 3) are detected against the background. The other mineral phases trapped are probably under the detection limit of 1 µg for each kind of materials. Due to the very low concentration of dust deposited on filter it's impossible to obtain the ratio between the mineral phases detected in the sample. The mineral ratios reported in Table 1 show the mean values of each clay material detected in the glacial ice against quartz and feldspar.

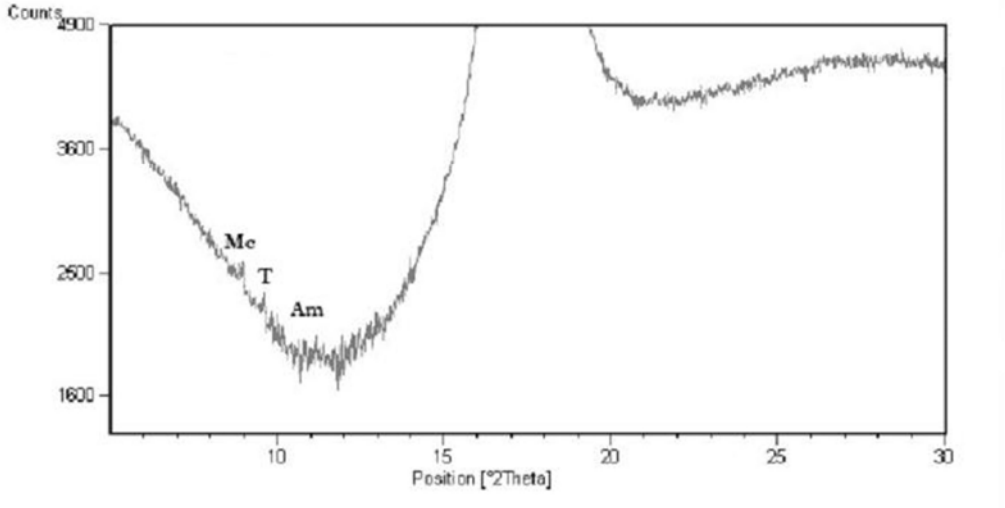

Fig. 3 - EDC-Holocene-I diffraction pattern.

The coupling with electron microscopy techniques on a shared quota of the same ice sample provide supplementary information about the structure of each mineral particle and also confirm the mineralogical results described above for the bulk fraction during Glacial periods (Table 2). Moreover, only single crystal HR-TEM analyses coupled to ED-XRF investigation allowing the mineralogical characterization of Interglacial Antarctic ice core dust are also presented in Table 2.

The most important characteristics observed during Glacial periods are summarized as follow:

- chlorite, mica, illite-smectite, quartz and feldspars are the most abundant mineral phases trapped in the ice samples. Mica and illite-smectite are detected in a very high concentration in all the climatic stages. In all the samples many polycrystalline illite-smectite, probably an interstratified layer, were observed using electron diffraction;

- only one particle of kaolinite was detected both in MIS2 and MIS4 climatic stage, to low for any statistical analyses, but significant in term of source characterization;

- comparing the XRPD and the HR-TEM abundances of calcite is clearly visible a large discrepancies both for MIS2 and MIS6 climatic periods;

- talc, pyrophyllite and titanium oxide are observed in a very low quantity, while for the iron oxide we have more or less the same percentage with the exception of MIS4 that show a little increase.

Table 1 - Mean mineral phases ratio of EDC ice core dust archived during Glacial periods obtained from XRPD investigation.

	MIS2	MIS3	MIS4	MIS6
Mc:Qz	1:1.3	2:1	1:1.1	1:1.2
T:Qz	1:11	1:1	1:20	1:12
Am:Qz	1:27	0	1:4	1:19
K:Qz	1:5.3	0	1:2.6	1:10
Ch:Qz	1:1.8	1:1.5	1:1.8	1:1.7
Ca:Qz	1:8.7	0	0	1:2
Mc:F	1:1.2	2.5:1	1:1.4	1:1.1
T:F	1:10	1.3:1	1:13	1:14
Am:F	1:25	0	1:2.8	1:23
K:F	1:5	0	1:1.7	1:12
Ch:F	1:1.6	1:1.3	1:1.3	1:2.1
Ca:F	1:8	0	0	1:2.4
K:Ch	1:3	0	1:1.4	1:6
K:Mc	1:4	0	1:2.7	1:11
Ch:Mc	1:1.3	1:3	1:2	1:2

Table 2 - Mineral phases detected during Glacial and Interglacial periods coupling HR-TEM and ED-XRF investigation. Numbers and percentage are referred to the number of particles analysed.

Mineral	Glacial				Interglacial	
	MIS2	MIS3	MIS4	MIS6	Holocene	MIS5.5
chlorite	8 (10.5%)	7 (26.9%)	7 (18%)	4 (9.1%)	3 (5.6%)	13 (19.1%)
kaolinite	1 (1.3%)	0	1 (2.6%)	0	4 (7.6%)	2 (3.1%)
quartz	10 (13.2%)	1 (3.8%)	6 (15.4%)	5 (11.4%)	5 (9.4%)	5 (7.3%)
feldpsar	7 (9.2%)	1 (3.8%)	0	3 (6.8%)	4 (7.6%)	6 (8.8%)
illite-smectite	23 (30.3%)	7 (26.9%)	12 (30.8%)	19 (43.2%)	7 (13.2%)	14 (20.5%)
mica	15 (19.7%)	8 (30.8%)	5 (12.8%)	6 (13.7%)	21 (39.7%)	18 (26.5%)
talc	1 (1.3%)	0	1 (2.6%)	0	2 (3.7%)	0
calcite	6 (7.9%)	0	0	0	4 (7.6%)	4 (5.8%)
pyrophyllite	1 (1.3%)	0	1 (2.6%)	3 (6.8%)	0	0
titanium oxide	0	0	1 (2.6%)	1 (2.2%)	0	2 (3.1%)
iron oxide	4 (5.3%)	2 (7.8%)	5 (12.6%)	3 (6.8%)	3 (5.6%)	4 (5.8%)
TOTAL dust	76	26	39	44	53	68

In opposition to the mineral assemblages observed mainly during the Last Glacial time (MIS2) and also along the other three Glacial periods (MIS3, MIS4 and MIS6) we could observe a considerable increase in kaolinite and a decrease in illite-smectite and chlorite during Holocene. Also quartz and feldspars percentage decrease from MIS2 to the Holocene. The concentration of iron oxide is like the same of Glacials as well as talc and calcite. Contrarily to the ice core dust identification discussed for the Holocene ice samples, during MIS5.5 are visible some differences. In this respect we could observe an increase in chlorite and illite-smectite, while mica was detected in low concentration than during Holocene; quartz and feldspars did not show strong variation. Iron oxide and calcite do not vary, while kaolinite is very scarce and an increase in titanium oxide is appreciable.

Comparing the EDC ice core dust with the mineral assemblages observed in the Southern Hemisphere (Table 3) continental land some clear differences are appreciable:

- sSA sediments show an high concentration of smectite, feldspars, quartz, illite and chlorite; moreover a considerable concentration of kaolinite and amphibole is detected but not in all the samples analysed;

- SAf sediments highlight a very high concentration of kaolinite besides quartz and illite. Kaolinite should be considered as tracer SAf sediments;

- Aus sediments show a dominant concentration of kaolinite. As in the case of SAf and sSA sediments, quartz and illite are detected in high concentration and represents the mean mineral composition of Aus samples;

- NZ sediments show a common mineral assemblages formed by chlorite, illite and quartz;

- Ant sediments display the most variable mineralogical composition of the Southern Hemisphere; high concentrations of quartz and illite have been observed as in the case of all the other continents and a relevant abundances of smectite, talc, pyrophyllite, amphibole, chlorite and feldspars.

Mineralogical characterization of aeolian mineral dust trapped in the EDC ice core coupling powder and single crystal investigation confirms and improve the results obtained by Gaudichet *et al.* (1992) on the old Dome C and Vostok ice core using electron microscopy. The XRD and HR-TEM results revealed that the mineral assemblages of dust reaching the inland East Antarctica during Glacial periods is composed mainly by chlorite, mica, illite-smectite, quartz and feldspar, while during the Interglacials we could observe a decrease in illite-smectite and chlorite, an increase in mica and the detection of a considerable concentration of kaolinite.

The comparison of the EDC ice core dust with the aeolian sediments collected in the Southern Hemisphere continental lands suggests that sSA is the most probable dust source area during Glacial periods, while the mineralogical evidence observed for the Interglacial ice core dust highlights a mixed provenance from sSA and Aus during warm periods.

Table 3 - Mean mineral phases ratio obtained from XRPD analyses of southern South America (sSA), southern South Africa (SAf), Australia (Aus), New Zealand (NZ) and Antarctic (Ant) sediments.

	SSA	SSAf	AUS	NZ	ANT
Sm:Qz	1.7:1	1:1.4	1:1	1:5	1:1.8
I:Qz	4.3:1	3:1	3:1	3:1	3.7:1
T:Qz	1:61	1:23	1:92	0	1:13
Py:Qz	0	1:68	0	0	1:5.5
Am:Qz	1:13	0	0	1:10	1:17
K:Qz	1:3.2	1.7:1	6.4:1	0	1:20
Ch:Qz	1:1.5	1:2	0	1.5:1	1:3.5
Sm:F	4:1	47.5:1	17.2:1	2.7:1	1.8:1
I:F	10:1	207.1:1	47:1	40.2:1	12:1
T:F	1:26	3:1	1:6	1:9	1:4
Py:F	0	1:1	0	0	1:1.3
Am:F	1:5	0	0	1.3:1	1:5.5
K:F	1:1.3	119:1	99:1	0	1:8
Ch:F	1.4:1	35:1	0	19.4:1	1:1.3
K:I	1:14	1:2	2.1:1	0	1:90
Ch:I	1:7.3	1:6	0	1:2	1:14
Sm:I	1:2.3	1:4.2	1:3	1:15	1:6
K:Ch	1:1.9	3.2:1	0	0	1:6.5

Moreover, this mineralogical observation are also confirmed by a few complementary information concerning the atmospheric circulation models and the system of air trajectories (Mahowald *et al.*, 1999) over the Antarctica, the material supplies in the source areas and many other studies applied on Antarctic ice core dust (Delmonte *et al.*, 2004, 2007; Revel-Rolland *et al.*, 2006; Basile *et al.*, 1997; Grousset *et al.*, 1992; Gaudichet *et al.*, 1992).

CONCLUSION

The analytical protocol developed in this work provides an improved way to evaluate the mineralogical phase composition of dust trapped in the Antarctic ice cores. The very sensitive X'Celerator detector mounted on the X-Ray diffractometer allows to investigate a very tiny quantity of material, down to 1 µg for each mineral species deposited on the polycarbonate substrate.

The mineralogical and crystal-chemical composition of dust trapped in the EDC ice core highlight a dominant provenance from sSA during Glacial time and a mixing of Aus and sSA mineral particles

during warm Interglacial periods. This results were also confirmed by atmospheric circulation model (Mahowald *et al.*, 1999), isotopic signature of dust particles (Delmonte *et al.*, 2004; Revel-Rolland, 2006) and some other complementary information strictly related to the environmental and climatic condition of the Potential dust Source Areas during the last 200 kyrs as described in Delmonte *et al.* (2004).

The coupling of XRPD and HR-TEM allows to understand the role of the atmospheric dust from the southern Hemisphere continents during the last two climatic cycles, and provides new dataset of boundaries conditions for the general models used for the hydrological cycle and the Circum Antarctic atmospheric circulation studies.

REFERENCES

Basile, I., Grousset, F.E., Revel, M., Petit, J.R., Biscaye, P.E., Barkov, N.I. (1997): Patagonian origin of glacial dust deposited in East Antarctica (Vostok and Dome C) during glacial stages 2, 4 and 6. *Earth Planet. Sci. Letters*, **146**, 573-589.

Dapiaggi, M., Sala, M., Artioli, G., Fransen, M.J. (2007): Evaluation of the phase detection limit on filter-deposited dust particles from Antarctic ice cores. *Kristallogr. Suppl.*, **26**, 73-78.

Delmonte, B., Petit, J.R., Maggi, V. (2002): Glacial to Holocene implications of the new 27000-year dust record from the EPICA Dome C (East Antarctica) ice core. *Clim. Dyn.*, **18**, 647-660.

Delmonte, B., Basile-Doelsch, I., Petit, J.R., Maggi, V., Revel-Rolland, M., Michard, A., Jagoutz, E., Grousset, F. (2004): Comparing the Epica and Vostok dust records during the last 220,000 years: stratigraphical correlation and provenance in glacial periods. *Earth Sci. Rev.*, **66**, 63-87.

Delmonte, B., Petit, J.R., Basile-Doelsch, I., Jagoutz, E., Maggi, V. (2007): Late Quaternary Interglacials in East Antarctica from ice core dust records. *In*: "The climate of past interglacials", F. Sirocko, T. Litt & M. Claussen, eds. Elsevier, Amsterdam, 53-73.

EPICA Community Members (2004): Eight glacial cycles from an Antarctic ice core. *Nature*, **429**, 623-628.

Gaudichet, A., De Angelis, M., Joussaume, S., Petit, J.R., Korotkevitch, Y.S., Petrov, V.N. (1992): Comments on the origin of dust in East Antarctica for present and ice age conditions. *Atmos. Chem.*, **14**, 129-142.

Grousset, F.E., Biscaye, P.E., Revel, M., Petit, J.R., Pye, K., Jossaume, S., Jouzel, J. (1992): Antarctic (Dome C) ice-core dust a 18 k.y. B.P.: isotopic constraints and origins. *Earth Planet. Sci. Letters*, **111**, 175-182.

Lambert, F., Delmonte, B., Petit, J.R., Bigler, M., Kaufmann, P.R., Hutterli, M.A., Stocker, T.F., Ruth, U., Steffensen, J.P., Maggi, V. (2008): Dust-climate couplings over the past 800,000 years from the EPICA Dome C ice core. *Nature*, **452**, 616-619.

Mahowald, N., Kohfeld, K., Hansson, M., Balkanski, Y., Harrison, S.P., Prentice, I.C., Schulz, M., Rodhe, H. (1999): Dust sources and deposition during the Last Glacial Maximum and current climate: a comparison of model results with paleodata from ice cores and marine sediments. *J. Geophys. Res.*, **104**, 15895-15916.

Petit, J.R., Jouzel, J., Raynaud, D., Barkov, N.I., Barnola, J.M., Basile, I., Bender, M., Chappellaz, J., Davis, M., Delaygue, G., Delmotte, M., Kotlyakov, V.M., Legrand, M., Lipenkov, V.Y., Lorius, C., Pépin, L., Ritz, C., Saltzman, E., Stievenard, M. (1999): Climate and atmospheric history of the past 420,000 years from the Vostok ice core, Antarctica. *Nature*, **399**, 429-436.

Pye, K. (1987): Aeolian dust and dust deposits. Academic Press, San Diego, 265 p.

Revel-Rolland, M., De Deckker, P., Delmonte, B., Hesse, P.P., Magee, J.W., Basile-Doelsch, I., Grousset, F., Bosch, D. (2006): Eastern Australia: A possible source of dust in East Antarctica interglacial ice. *Earth Planet. Sci. Letters*, **249**, 1-13.

Sala, M. (2008): Mineralogy of Antarctic ice dust and Potential dust Source Areas in the Southern Hemisphere. PhD Thesis, Università di Milano.

Tegen, I. & Fung, I. (1994): Modeling of mineral dust in the atmosphere: sources, transport, and optical thickness. *J. Geophys. Res.*, **99**, 22897-22914.

MODELLING OF WATER-ROCK INTERACTIONS IN CARBONATE AQUIFERS: INSIGHTS FROM A CASE STUDY IN THE MADONIE AREA (SICILY)

ELISA TAMBURO
Dipartimento di Chimica e Fisica della Terra ed Applicazioni alle Georisorse e ai Rischi Naturali,
Università di Palermo, Via Archirafi 36, 90123 Palermo

Weathering reactions between natural waters and the minerals that constitute the soils and underlying rocks are the major geologic control on natural water chemistry. The chemical action of water, oxygen, carbon dioxide and other components cause the chemical dissolution of primary minerals and the release of dissolved constituents to natural waters. As a result of these processes, the chemical features of groundwaters are strictly dependent on the characteristics of the host rocks.

This research attempts at a comprehensive and systematic characterization of water-rock interaction processes taking place in the aquifers of the Madonie area.

The Madonie is one of the main massifs in Sicily and is located in the centre of the Mediterranean region. The study area is characterized by several distinct kinds of landscape, resulting from heterogeneous outcropping lithologies as well as from the tectonic and modelling action of morphodynamic factors.

The hydrogeology of the Madonie area is characterized by the presence of both of carbonate rocks, generally acting as aquifers and clayey Flysch deposits.

The characteristics of outcropping rocks, the density of fractures and other structural features, the morphogeological setting, and the presence of karst processes, all contribute to the complex hydrogeological setting of the Madonie area.

Carbonate outcrops are of particular hydrogeologic interest because they represent the highly productive reservoirs.

Previous geochemical researches in the Madonie area focused on the isotopic composition of springs and rains (*e.g.*, Mangano *et al.*, 1970; Hauser *et al.*, 1980; Favara *et al.*, 1984). More recently, the first hydrogeochemical results on the chemistry of major elements dissolved in groundwaters were presented by Cusimano *et al.* (1992). These Authors suggested that the Madonie springs can be clustered into four homogeneous groups: springs with Ca/Mg > 1, typical of calcite-dominated hydrostructures of the Panormide Unit; springs with Ca/Mg < 1, characteristic of dolomite hydrostructures of the Panormide Unit; springs with low salinity, typical of Flysch aquifers; and springs with high salinity, related to seawater ingression.

The gap of data on the abundance and distribution of major, minor and trace elements in the area is the first reason for this work. Here, we report data collected from 241 different sites, including springs and wells, during an extensive hydrogeochemical survey. Analytical data are used to produce geochemical maps, and to draw geochemical considerations on compositional diversity in the Madonie area.

Water-rock interaction is the principal processes controlling the cycling of chemical elements in the Madonie groundwaters. In fact, the wide compositional range of groundwaters mostly reflects variable extents of weathering of carbonate rocks (see below). Limestones represent the main sedimentary rocks cropping out in the study area, and they are also highly productive reservoirs. As such, the mineralogical

and chemical characterization of the Madonie limestones is an indispensable step for understanding the chemical evolution of local groundwaters.

Previous studies on the petrography and geochemistry of outcropping rocks in the study area have been limited in number; therefore, a sampling survey of the main rocks in the area, and their geochemical characterization (through optical microscopy, SEM-EDS observations, XRF whole rock analyses and LA-ICP-MS determinations on selected minerals) have been required to fulfil the objectives of this work. In fact, major, minor and trace elements data described below have been used as input parameters in the reaction path simulations that are to define the solid reactant.

In this work, we have also collected 21 rock samples from different lithologies cropping out in this study area, with a special focus on limestones, which represent the prevalent sedimentary formations and are also highly productive reservoirs. The mineralogical and chemical characterization of the Madonie limestones is an indispensable step for an understanding of the chemical evolution of local groundwaters.

Microscopic characterization reveals that carbonate clasts are generally rounded to sub-angular or have irregular shapes. In general, the Madonie carbonate rocks are characterized by different fossil associations.

Selected samples were subsequently studied by scanning electron microscopy (SEM) to ascertain mineral textures, textural relationships, and element distributions in mineral phases. EDS has been used for quantitative mineral chemistry. SEM images allowed to characterise the textural features of the carbonates, and confirmed the results of optical observations, in that clasts essentially consist of carbonate minerals with variable proportions of secondary minerals. In thin and polished sections of carbonate rocks, apatite grains with size ranging from some microns to 100 microns are relatively common. Cryptocrystalline apatite crystals are associated with accessory amounts of pyrrhotite, quartz and Fe-oxides.

Petrographic and geochemical analyses have also been carried out in dolostone showing the typical feature of euhedral crystals.

Geochemical characteristics of the Madonie sediments have been first evaluated through detailed investigation by X-Ray Fluorescence (XRF). Whole rock chemistry of limestones shows significant variability in the amounts of SiO_2 (0.284-5.413 wt.%), Al_2O_3 (0.1-2.6 wt.%), P_2O_5 (0.008-1.01 wt.%), MgO (1.1-31.4 wt.%), MnO (0.05-0.96 wt.%) and CaO (21.0-54.4 wt.%).

Earth alkalis (Mg and Ca) are manifestly the two major components of the studied rocks. The variable MgO and CaO concentrations reflect variable proportions of calcite and dolomite in the rocks. Variations in Fe_2O_3 content are likely due to variable amounts of pyrite and Fe-oxides in the samples, and subordinately to presence of a siderite and ankerite component in carbonate minerals.

Scanning electron microscopy reveals a notable compositional homogeneity in the selected samples, highlighting the need of spot analyses to complement whole-rock determinations. High-resolution electronic images, obtained by SEM-EDS, were then used to select adequate areas where to perform Laser Ablation-Inductively Coupled Plasma-Mass Spectrometry (LA-ICP-MS).

The present study has proposed the first detailed geochemical mapping of the distribution of major, minor and trace elements in the Madonie area. Geochemical data acquired in this work allow understanding the processes controlling the abundance and mobility of metals in this groundwater system.

The wide compositional range of groundwaters circulating in the Madonie area is initially investigated by the study of major element abundance.

An initial assessment of the chemical composition of groundwaters of the Madonie area is obtained from the Langelier Ludwig (L-L) diagram of Fig. 1.

Waters samples have been differentiated in six families, according to their composition. Groundwaters circulating in carbonate aquifers have a typical bicarbonate alkaline-earth composition.

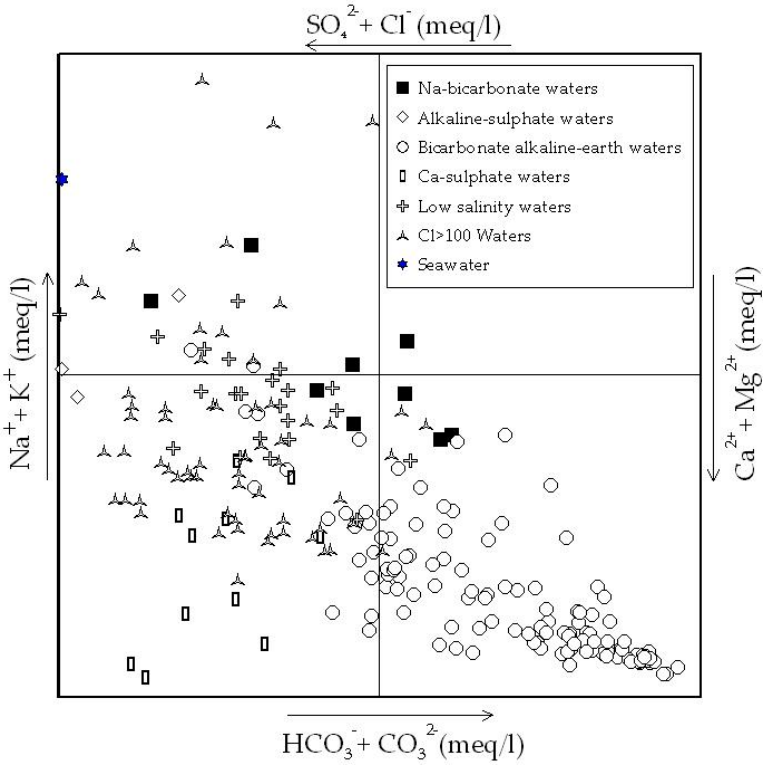

Fig. 1 - Square diagram of Langelier-Ludwig.

These samples have been collected in areas where the carbonate rocks of the Imerese and Panormide Formations crop out. A few waters, coming from the Flysch Numidico Units, also cluster in the bicarbonate alkaline-earth group. A common feature of these sediments is the presence of clays interposed between the quartz-arenaceous levels. The apparent incongruity between water composition and lithology can be explained either by the presence of carbonates in form of calc-arenaceous levels, calcirudites and silty breccias Mesozoic, called Wildflysch (Ogniben, 1963), or by dissolution of limestone cement in quartz-arenaceous sediments.

Some samples of this group show a trend towards the point representative of seawater point, suggesting a some extent, mixing with seawater. These samples have been collected near the seacoast.

The Na-bicarbonate waters are depleted in calcium and magnesium, and enriched in sodium and potassium, compared to the bicarbonate alkaline-earth waters described above. The enrichment in sodium and potassium displayed by these waters is likely the result of ionic exchange processes. These processes are very common in the water circulation in the phreatic aquifers (Stumm & Morgan, 1996), where clayey sediments remove calcium and magnesium and release sodium and potassium. A small group of samples are characterized by high sulphate contents and prevalence of Ca among the cations; in fact, these Ca-sulphate waters stretch toward the bottom-left corner of Fig. 1, their chemical characteristics likely reflecting leaching of the Messinian evaporites.

The group of low salinity waters is characterized by conductivities between 44 µS/cm and 564 µS/cm, and by an average *p*H of 6.6. These samples have measured bicarbonate concentrations of 0.1-76.3 mg/l, and are mostly distributed in Fig. 1 in the compositional domain of chloride-sulphate waters. Their low conductivity can be explained by minor water-rock interaction because of very short residence time in the aquifer system. As such, low-salinity waters can be interpreted as shallow infiltrated rain waters weakly modified by water-rock interactions. The remaining groundwaters display a fair compositional trend toward seawater composition. These samples (hereafter referred as Cl > 100 waters) are characterized by chloride contents higher than 100 mg/l, and are likely produced through mixing with seawater. This is also consistent with their coastal location.

The chemical characteristics of Madonie groundwaters typically evolve under oxidizing redox conditions (range from 200 to 500 mV), consistent with the superficial groundwater system; in contrast reducing redox conditions are less frequent and often found for natural waters with significant residence times in aquifers. The water samples have conductivity between 31.7 µS/cm and 8220 µS/cm; their total dissolved solids (TDS) content is higher near the coast area, where contribution from saline components (seawater) becomes important.

The good correlation between sodium and chloride of Fig. 2 and the high contents of these dissolved constituents are an indications of significant seawater contribution in several samples. The same diagram also indicates that groundwaters consistently plot along a mixing line between low salinity (meteoric) waters and seawater, suggesting the presence of a marine component in virtually all the waters of the study area. It is likely of atmospheric derivation at the low Na, Cl contents, whereas it is ascribable to seawater ingression at the high Na, Cl concentrations.

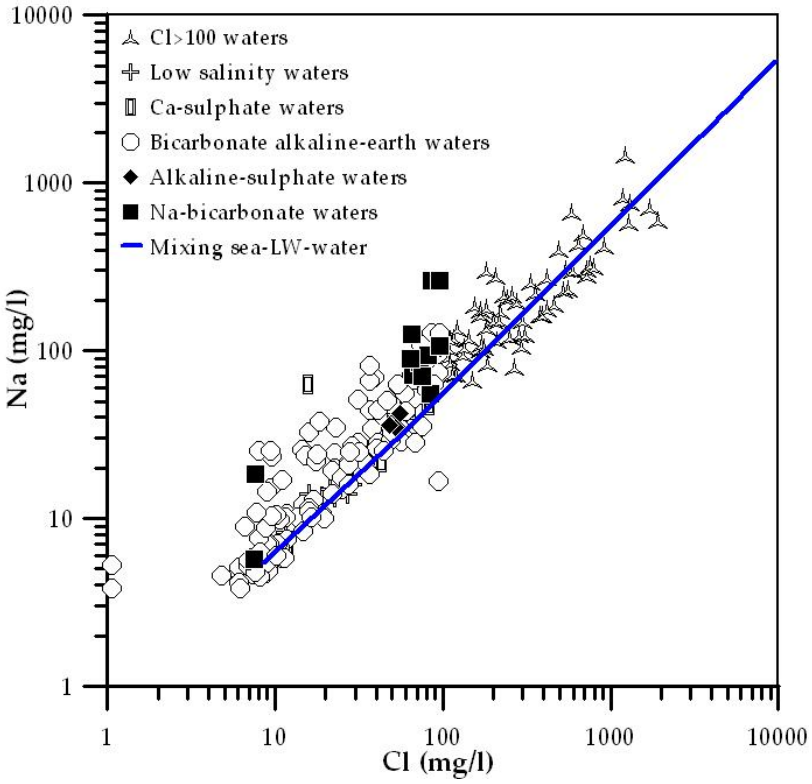

Fig. 2 - Na-Cl scatter diagram. The figure demonstrates that the groundwaters of the "Cl > 100 group" are contaminated by seawater.

In fact, groundwaters collected in coastal area display a fair compositional trend toward seawater composition. The significance of seawater ingression is also consistent with the Na and B distribution maps; the amount of both elements increasing from inner sites toward the coast.

The wide compositional range of groundwaters circulating in the Madonie area is also related to lithological feature of host rocks, and particularly to variable extents of water-rock interaction. Calcium and bicarbonate excess concentrations in groundwaters suggest the occurrence of other process as in addition to seawater mixing, namely water-rock interaction in carbonate aquifers.

Simple thermodynamic considerations suggest that congruent carbonate dissolution takes place in the investigated area. Relationships between carbonate and groundwaters are illustrated in the HCO_3/*p*H plot of Fig. 3 which shows the evolution trend of groundwaters from under-saturated waters to saturated and slightly oversaturated conditions.

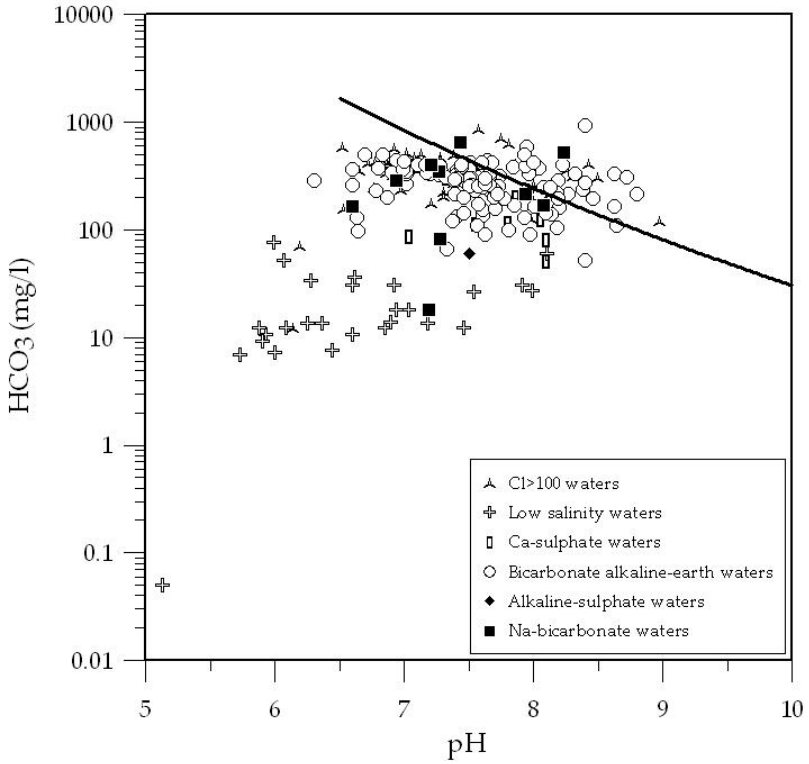

Fig. 3 - HCO_3-*p*H scatter diagram with the theoretical equilibrium curve for calcite. The figure suggests that the inverse relationship between *p*H and HCO_3 contents for most groundwaters from the study area is related to attainment of saturation with calcite (and dolomite).

Ca and HCO_3 concentrations (≈ 500 mg/l) are higher in the northern sector than in the southern one; this allows hypothesizing that the weathering process is more important in the northern area. High values of PCO_2 associated to the lower *p*H values confirm the presence of aggressive water with respect to carbonates.

The contribution of solutes from the weathering process is confirmed by the good correlation between Ca and Mg (Fig. 4), suggestive of a common origin for the two elements. The Mg/Ca ratio of groundwaters falls within the range of Mg/Ca ratios of the two main carbonate lithologies in the area, namely the limestones of the Imerese Unit (black line), and the dolostones of the Quacella Formation (grey line), respectively. This shows that leaching of carbonate rocks is the main source of calcium and magnesium in the groundwaters samples.

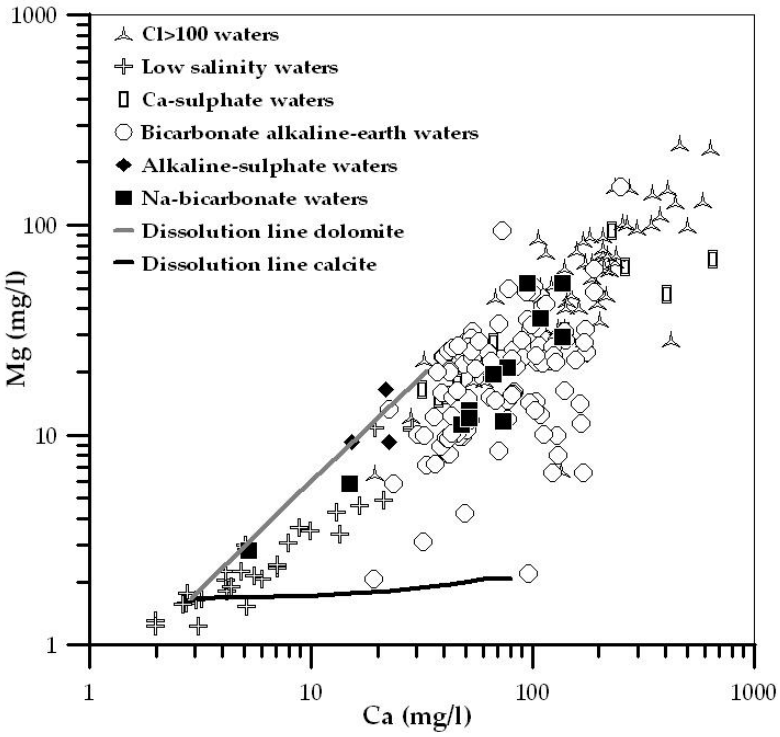

Fig. 4 - Diagram of Mg^{+2} *vs.* Ca^{+2}. Dissolution lines were computed at the average temperature (14.6°C) by reaction path modelling, carried out by mean of the EQ3/6 software package, version 7.2b (Wolery & Daveler, 1992).

Also we report a study of trace metals in Madonie groundwater. Minor elements (Fe, Sr and Mn) display a concentration range from 0.1 μg/l up to 10 mg/l, whilst trace elements (Ag, Pb, Sb and Cd) are comprised between 0.01 and 0.1 μg/l, and ultra-trace elements from 0.01 up to 1 μg/l.

The abundance and distribution of minor and trace elements in the Madonie aquifers reflects the variable extent of water-rock interaction, and eventually the presence of additional sources of chemical elements (*i.e.*, anthropogenic pollution).

Correlation diagram of median concentration of metals in groundwaters (Cg, in μg/l) *vs.* average content in carbonates from the Madonie area (Cr, in mg/kg) suggests that carbonate leaching is a controlling factor on groundwater chemistry. This is confirmed by a fair correlation between Ca and Sr and U. However, metal partitioning between aqueous solution and rock-forming minerals also depends on their geochemical behavior. Al, Fe, Mn and Cr are typically depleted in groundwaters, compared to more mobile elements (*e.g.* alkalis), supporting their affinity for the solid phase during water-rock interaction.

The geochemical mobility of chemical elements during the water-rock interaction is related to their speciation, namely the partitioning of an element among its different chemical species. Speciation computation and mineral-solution equilibria are important to understand the processes controlling the abundance and mobility of major and trace elements in the groundwater system. Speciation calculations indicate control of environmental parameters (mostly the *p*H and redox potential) on trace element mobility in waters. Most water types are typical of oxidant redox conditions (range from 200 to 500 mV), consistent with the superficial groundwater, favouring low aqueous mobility of Fe and Mn; while reducing redox conditions are less frequent, and often found for natural waters with significant residence times in aquifers.

The chemical fractionation of elements during the water-rock interaction processes is closely related to the relative tendencies of primary minerals to dissolve and of secondary minerals to form. The

primary minerals release their own chemical constituents, whereas the secondary minerals behave as a possible sink for the elements. This process was quantitatively evaluated in this work by use of reaction path modelling, carried out by EQ3/6 code adopting the Double Solid Reactant Method (DSRM) (suggestion of Accornero and Marini (2007)). Theoretical simulations were performed in time mode, using as solid reactant either a carbonate solid solution (representative of Mg-calcites of the Imerese units) or a dolomite, each one with its associated special reactant (dissolving at the same rate, as required by the DSRM). Based on these input parameters (also including a guess of the composition of the original solution at in open-system conditions at f_{CO2} ranging from $10^{-1.5}$ to 10^{-3}), a sequence of model solution were calculated upon increasing extents of reaction (*e.g.*, on increasing values of the overall reaction progress ξ); which were then compared with observed composition of natural waters, highlighting a general agreement.

Fig. 5 shows the cumulative moles of reactant minerals that are dissolved during the model runs, plotted against corresponding *p*H's of the model solutions. The diagram highlights that, as the model reaction progresses (the overall progress variable increases from bottom to top in the diagram), the reactant minerals are increasingly dissolved, and the *p*H increases from acidic conditions at the onset of the reaction, to basic conditions at the end of the simulation. The diagram also shows that, independently on the composition of the reactant (Mg-calcites or dolomite), and at all f_{CO2} investigated, the *p*H does not vary significantly in the first part of the simulations, whereas it shows a remarkable shift towards basic conditions in the second part of the runs, when important amounts of the solid reactants are dissolved.

Upon advancement of the irreversible model reaction path, a set of secondary minerals sequentially attains saturation with the model solution, and these "stable" minerals are allowed to precipitate and act as sinks of selected chemicals from the model solution. The sequence of "model" secondary minerals that are formed is similar in all model runs, albeit the actual amount (cumulative moles) of any given mineral formed changes with composition of the reactant and f_{CO2}. Taking the runs

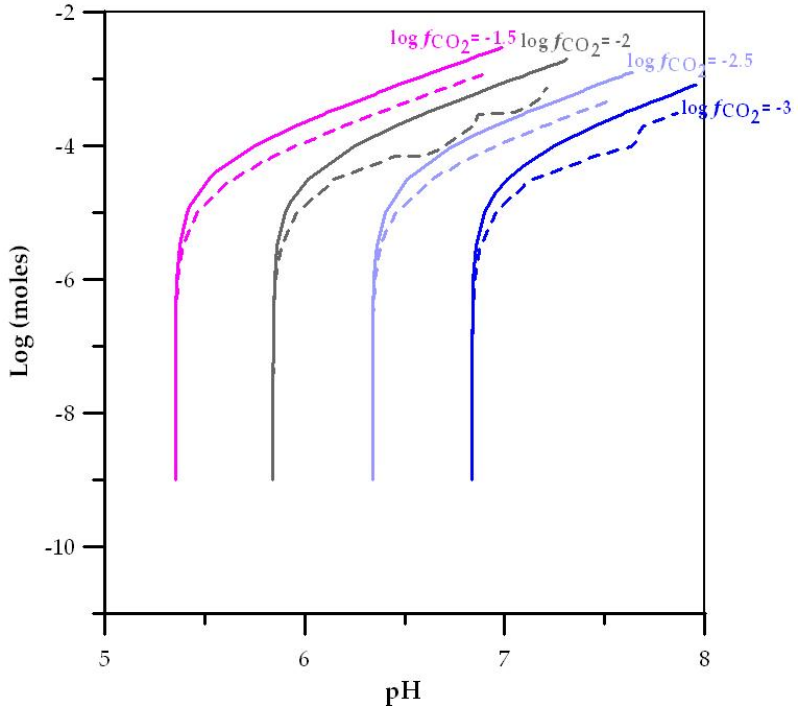

Fig. 5 - Cumulative moles of primary solid phases destroyed through weathering of Mg-calcites (solid lines) and dolomite (dashed lines) at 14.6°C and CO_2 fugacity of 10^{-3}, $10^{-2.5}$, 10^{-2} and $10^{-1.5}$ bar.

calculated at $f_{CO2} = 10^{-2}$ bar as reference (Fig. 6), the run calculated with the Mg-calcites as the reactant (solid lines) indicates that kaolinite and ferrihydrite are the first-formed and most abundant secondary minerals along the reaction path; implying that these minerals act as principal sinks for the elements Si, Al (kaolinite), Fe, Mn, Cr, Zn, Co, Cu, and Ni (ferrihydrite).

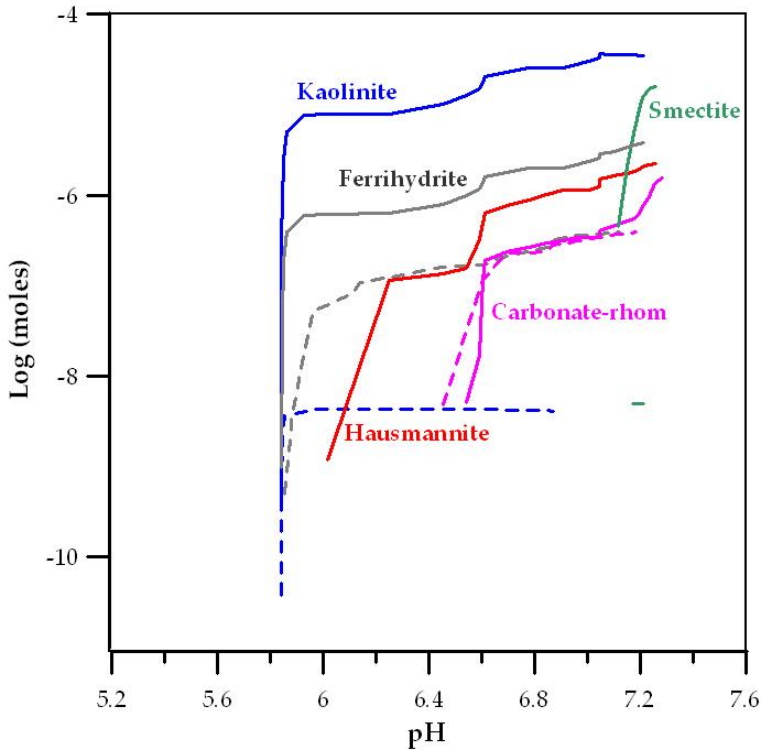

Fig. 6 - Cumulative moles of secondary minerals solid phases precipitated through weathering of Mg-calcites at 14.6°C and CO_2 fugacity of 10^{-2} bar.

Upon increasing extent of reaction, as the *p*H becomes more basic, the minerals hausmannite, the ortho-rombic carbonate solid solution, and smectite, also become progressively stable. It is noteworthy that the sequence of secondary minerals formed in the reaction path modelling is consistent with the set of minerals that have shown to attain saturation in natural samples.

In a second set of simulations, also carried out using the DRSM, the presence of fluoro-apatite and pyrite in the mineral assemblage of the leached carbonate rock was also taken into account, revealing that these accessory minerals provide a negligible contribution to the mineralisation of natural waters.

The measurements and simulations presented here represent a step forward in the interpretation of water-rock interaction processes in the carbonate environment, and should contribute to stimulate farther studies in this relevant field of geochemistry.

REFERENCES

Accornero, M. & Marini, L. (2008): The Double Solid Reactant Method for modeling the release of trace elements from dissolving solid phases: I. Outline and limitations. *Environ. Geol.*, **55**, 1627-1635.

Cusimano, G., Favara, R., Francofonte, S., Madonia, P., Valenza, M. (1992): Lineamenti idrogeologici ed idrogeochimici del gruppo montuoso carbonatico delle Madonie (Sicilia). Proceeding of workshop on "Alpin Caves and Alpine Karst System and their Environmental Context", Asiago, Giugno 1992, 189-192.

Favara, R., Dongarrà, G., Hauser, S., Longinelli, A. (1984): Studio geochimico isotopico di una serie di sorgenti nell'area di Scillato (PA). *Rend. Soc. It. Mineral. Petrol.*, **39**, 421-427.

Hauser, S., Dongarrà, G., Favara, R., Longinelli, A. (1980): Composizione isotopica delle piogge in Sicilia. Riferimenti di base per studi idrogeologici e relazione con altre aree mediterranee. *Rend. Soc. It. Mineral. Petrol.*, **36**, 671-680.

Mangano, F., Marcè, A., Meybeck, M., Olive, P., Pratelli, W. (1970): Idrologia isotopica: metodologia e prime applicazioni alle sorgenti Fiume e Bella (Madonie orientali). Convegno Internazionale sulle acque sotterranee, Palermo, 6-8 dicembre 1970, 609-616.

Ogniben, L. (1963): Le formazioni tipo Wildflysch delle Madonie. Società Cooperativa Tipografica, Padova, 56 p.

Stumm, W. & Morgan, J.J. (1996): Aquatic chemistry: chemical equilibria and rates in natural waters. Wiley, New York, 1022 p.

Wolery, T.J. & Daveler, S.A. (1992): EQ3/6, a software package for geochemical modelling of aqueous systems. Lawrence Livermore National Laboratory, UCRL-MA-110772PT I-IV.

DEVELOPMENT OF METHODOLOGIES FOR THE STUDY OF RADON RISK AREAS

MATTIA TARONI
Dipartimento di Scienze della Terra, Università di Ferrara, Via Saragat 1, 44100 Ferrara

The PhD's thesis has designed a methodology for the study of radon risk areas; radon gas (^{222}Rn) is the only gaseous element of the ^{238}U natural decay series.

This radioactive gas is present everywhere at different concentrations in terms of geological characteristics of the study area. So close a correlation between geomorphologic characteristics, structural subsoil characteristics and specific situations of the investigated area allow the identification of areas with different radon potential risk.

The methodology developed is the result of a synergy of several areas of research and study: nuclear physics, study and interpretation of the ^{222}Rn detection systems and their application to *in situ* measures (liquid scintillation method for the determination of Radon in groundwater and measures with semiconductor chambers to measure the Radon in subsoil air).

The methodology so developed is based on the development of:

1. Demarcation of investigated area.

2. Geological general study: collection and study of geological maps, geomorphological, hydrogeological and tectonic.

3. Geological detail study (where possible): collection and study of information about specific characteristics of the area of study, as different lithologic areas in contact, the subsoil and basement structure, presence of ascending geothermal, vulnerable character of the soil, phenomena of dissolution of basement rock, such as karst, etc.

4. Geological conclusions: identification of the Radon potential risk. The potential risk is a direct function of the presence of structural conditions that allow the formation, the emanation and diffusion of Radon towards the soil surface. A key role are the subsoil structure more or less altered, permeability, presence of hydrologic structure, lithologic genesis and development environment of geological formations, if with low energy lead to the formation of intercalation of biological origin, and so rich in elements such as the uranium, again the presence of abnormal situations which may alter the natural, anthropic interventions for example.

5. *In situ* measures distribution based on the potential risk (in the subsoil air and any points of groundwater), the most dense distribution where the hazard is higher, and outcrops lithologic sampling.

6. Processing and interpretation of results through Box-Plot of the Radon measures in the underground and creation of thematic maps.

The test areas identified are: the Trieste's Area and the Lecce's Area.

These zones are particularly significant because the results can be compared with each other and also with those of existing maps of concentration, produced in Italy in 1999 and 2002, obtained by other methods that are not based on geological studies, but on a distribution to regular mesh of indoor measures.

The methodology thus developed can then identify the likely source of high concentrations of radon gas and may allow the formulation of remedial measures to solve the problem both in terms of efficiency and optimization of available economic resources.

The study of general and detailed geology of the two areas has identified a Radon risk potential about Trieste is in line with that of papers produced in Italy in 1999 and 2002 and about Lecce, however, differs: from low to high.

In both test site that makes the high potential risk are:

- Areas of contact between lithologic at different degrees of porosity and permeability;
- High permeability for fracting, cracking and karst;
- Bituminous and argillaceous intercalations in lithologic, a sign that the environment formation was the anoxic type, therefore the immobilization of uranium ions.

Using Box-Plot (Fig. 1 and Fig. 2), allowed to provide an initial interpretation of the results about measurements of radon in the subsoil air comparing the lithological formations in the same test area identifying alleged anomalies that may be brought in preparation of the final data in natural or anthropic situations.

The processing of point data like continuous data, digital processing, has made it possible to generate thematic maps of the Radon concentration in subsoil (Fig. 3 and Fig. 4).

The Trieste's area, in line with previous papers generated at the national level, presents higher average values with a distribution to spot leopard; the largest concentration area is the central part, limestone bioclasts, which are deposits of opened platform with bituminous intercalations and a degree of karstification which has a rang from middle to higher, and high permeability for cracking and karstification.

The Lecce's area gave a final result that differs from that obtained from the national survey of 1999, in particular, as shown by the Fig. 2 and Fig. 4, the area is characterized by Hot-spot of Radon concentrations, have been recorded point with over 60.000 Bq/m^3; the direct study of area,

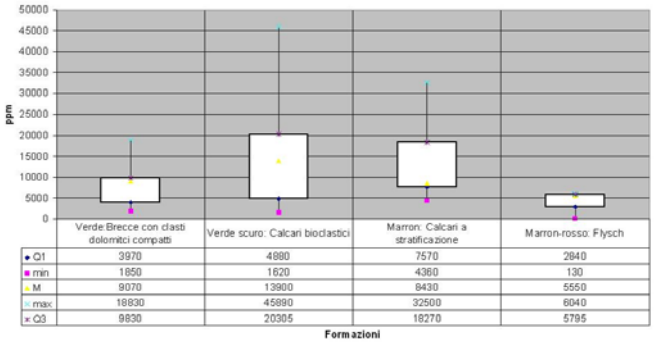

Fig. 1 – Box Plot Trieste Area

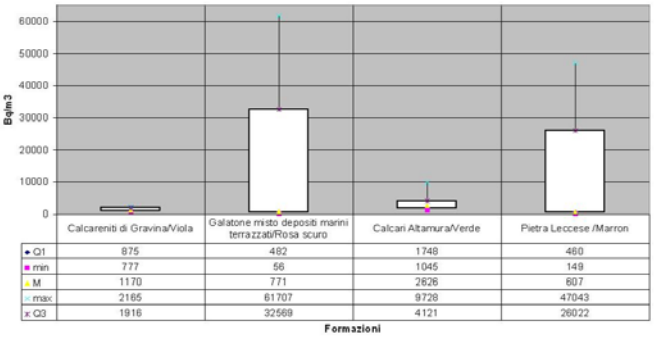

Fig. 2 – Box Plot Lecce Area

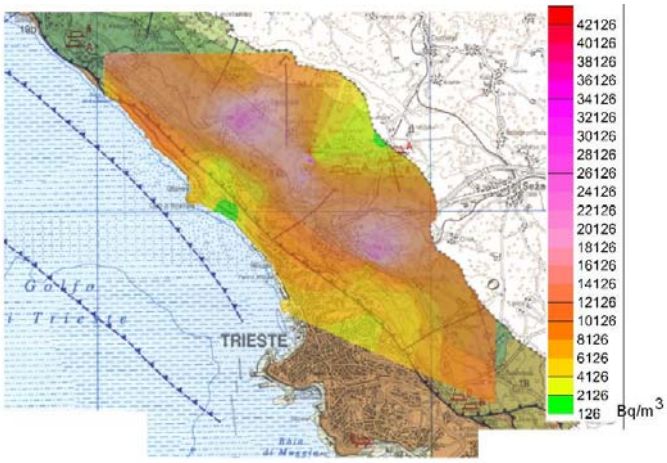

Fig. 3 – Radon Map Trieste Area

together with general and detailed geologic information and with gas measures in the underground, enabled to identify points of measurement like measures such "distorted"; these are all located in areas close to man, whose common feature is to have penetrated the layer of soil and bedrock to resolve the area and to construct buildings with higher volume.

Fig. 5 and Fig. 6 show the elaboration of Radon concentration maps in the air of subsoil, respectively of the measures called "Not disturbed" and measures called "disturbed"; it was noted that the absence of the latter allows to identify an area characterized by radon values are not too high and by small changes in concentrations between different lithological species.

Among the measures affected the higher were obtained in geological formation with greater permeability and fracturing and in contact areas between the different lithologic areas.

The complete study of a building, Radon indoor measures coupled with measures of Radon in the subsoil, with the characteristics listed above and positioned to straddle two different lithologic areas finally allowed to identify a situation of real danger to the residents' building concerned (Fig. 7 and Fig. 8).

The abnormal situation generated by a distracted human intervention, has encouraged a formation and release of radon gas in high quantities.

In conclusion, this methodology allows analysis of the area investigated able to plan the distribution of measures in the subsoil and more importantly allows you to interpret the results obtained by identifying the factors, both natural and anthropogenic, that can characterize and generate abnormal situations.

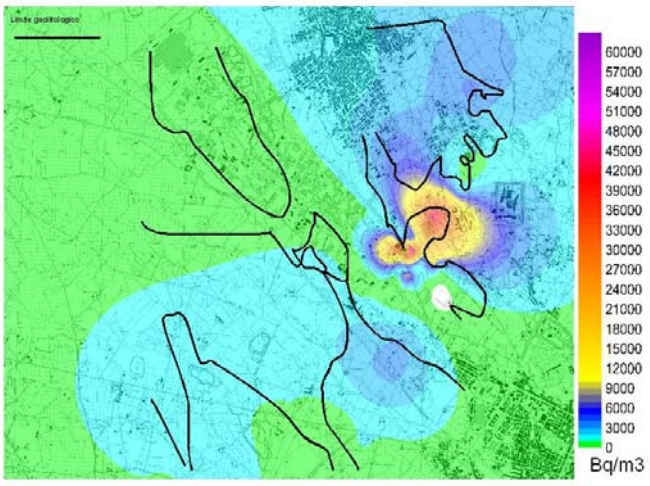

Fig. 4 – Radon Map Lecce Area

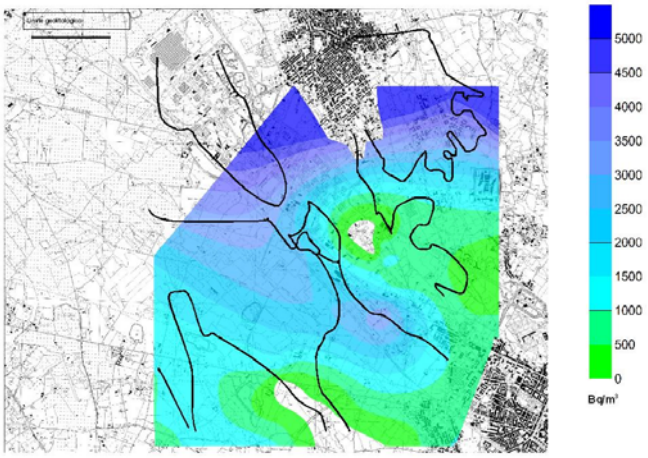

Fig. 5 – Measures "Not disturbed"

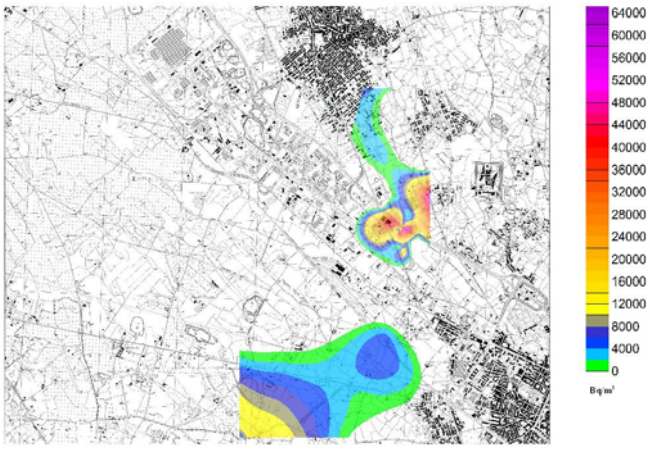

Fig. 6 – Measures "Disturbed"

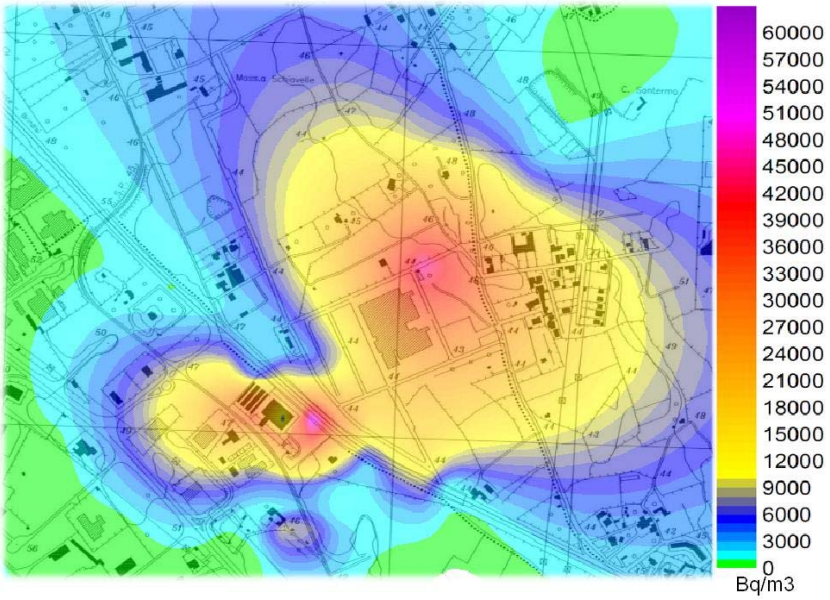

Fig. 7 – Anthropic Area

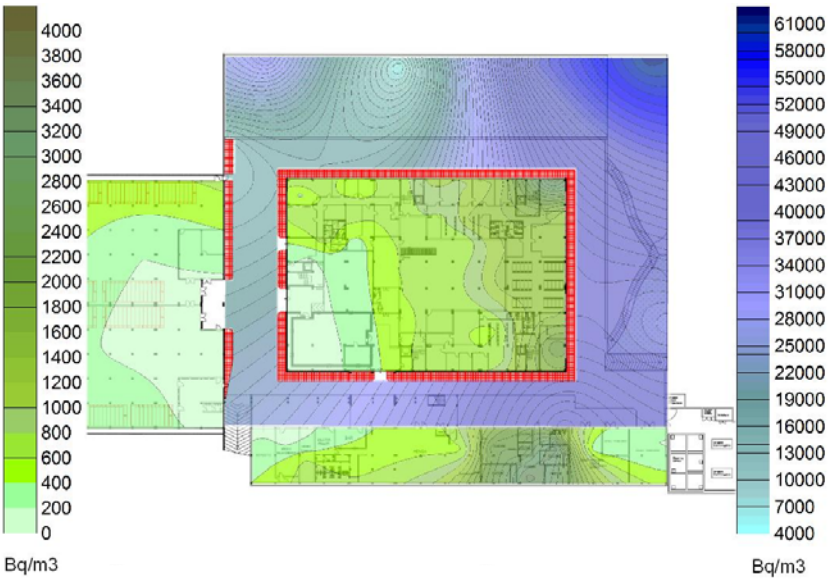

Fig. 8 – Measure indoor and outdoor Anthropic Area

This methodology also identified the structure of the subsoil, the presence of faults, the primary and secondary porosity, like the phenomenon able to adjust the lift of Radon gas, creating situations of strong accumulation and fast rising in areas where this problem seemed not present.

PETROCHEMICAL AND PETROPHYSICAL CHARACTERISATION OF CONSTRUCTION AND DEMOLITION INERT MATERIALS FOR THE PREPARATION OF CERAMIC MIXES AND CONCRETE

ALICE TOFFANO
Dipartimento di Scienze della Terra, Università di Ferrara, Via Saragat 1, 44100 Ferrara

INTRODUCTION

Building activity is currently demanding noticeable amounts of natural inert materials, such as gravel and sand, usually provided by natural sediments. The extraction of sediments can modify river-profiles and their equilibrium as well as quarrying activities could induce environmental problems.

The use of recycled aggregates is promoted by the EU which has provided guidelines for common strategies for a correct re-use of construction and demolition (C&D as proposed by Poon *et al.*, 2001) (DG ENV E. 3, 2000). As for the Italian situation, currently the legislation (D.L. 152/06, 2006) is encouraging the re-use of C&D inert materials but the re-utilisation of these materials is hampered by the scarcity of suitable plants for processing, as a result this resource is used as a lower quality materials for low grade application (*i.e.* road sub-base). In this study, different grain-size fractions, obtained by a grain-size sorting, from a C&D processing plant in Rovigo (NE Italy), were compared with other data (Bianchini *et al.*, 2005) and investigated through chemical and physical analyses (according to UNI EN 206-1, 2001). The results indicate that, through an opportune crushing and sorting operation for C&D material, it is possible to obtain grain-size fractions with roughly homogenous chemical and mineralogical composition on each fraction. The homogeneity of the materials can be considerably improved if a careful differentiation takes place during the initial stages of C&D production (Poon, 1997; Poon *et al.*, 2001).

DISCUSSION

Fine recycled fractions were used in high grade application as starting materials for ceramic mixes prepared and tested in collaboration with CNR-IRTEC Faenza laboratories. Preliminary results, in fact had shown that there is a real possibility to use this materials for preparing suitable ceramic mixing.

Fine recycled fractions (TA1d e TA2d sands) were used for preparing 6 different mixes (two recycled sands plus two different kind of clay) compared with 3 mixes prepared using natural sand (Colombara) plus the same clays. Clays used (Sila, Mosso, Giomo) were selected on geographical basis, quarried not far from the Fenza Daniela plant (Table 1).

Were produced:

- 3 standard mixes (Colombara plus Sila, Mosso, Giomo respectively)
- 3 mixes (TA1 plus Sila, Mosso, Giomo respectively)
- 3 mixes (TA2 plus Sila, Mosso, Giomo respectively)

All the materials used were characterized in the CNR-IRTEC of Faenza laboratories and then were also characterized all the mixes produced.

Table 1 - Ceramic mixes prepared and tested in collaboration with CNR-IRTEC Faenza laboratories.

S0		STA1		STA2	
Sila clay	85%	Sila clay	85%	Sila clay	85%
Colombara	15%	TA1d	15%	TA2d	15%
M0		MTA1		MTA2	
Mosso clay	85%	Mosso clay	85%	Mosso clay	85%
Colombara	15%	TA1d	15%	TA2d	15%
G0		GTA1		GTA2	
Giomo clay	85%	Giomo clay	85%	Giomo clay	85%
Colombara	15%	TA1d	15%	TA2d	15%

The results have shown that using the recycled sands, produced for these experimental study, it is possible to prepare ceramics mixes for bricks with the very similar characteristic when compared with mixes produced with natural materials (Marsigli & Dondi, 1997; Dondi *et al.*, 1998a, 1998b, 1998c).

Recycled sand and a medium grade fraction (0-30 mm) were used for preparation of concrete mixes in collaboration with CTG-Italcementi Group laboratories. More in detail were investigated some fractions usually produced in the plant:

- recycled sand (TA1)
- recycled fraction 0-30 mm (TA2).

Chemical-mineralogical and physical analysis have shown that the material is roughly homogenous. The homogeneity of the materials can be considerably improved if a careful differentiation takes place during the initial stages of C&D production (Poon, 1997; Poon *et al.*, 2001). This aspect is relevant for the use of this materials in the preparation of concrete mixes. Several concrete mixes were prepared using different percentage of recycled aggregate and tested. The data obtained have shown, accordingly with Limbachiya *et al.* (2006) that the introduction of 30% of inert recycled coarse fraction, substituting the natural coarse aggregate, does not affect the concrete.

REFERENCES

Bianchini, G., Marrocchino, E., Vaccaro, C. (2005): Recycling of construction and demolition waste materials: a chemical-mineralogical appraisal. *Waste Manag.*, **25**, 149-159.

D.L. 152/06 (2006): Decreto Legislativo 152/06: Norme in materia ambientale, parte IV.

DG ENV E. 3 (2000): European Commission, Directorate - General Environment. Management of construction and demolition waste. Working document No. 1, 1-26.

Limbachiya, M.C., Marrocchino, E., Koulouris, A. (2006): Chemical-mineralogical characterisation of coarse recycled concrete aggregate. *Waste Manag.*, **27**, 201-208.

Dondi, M., Marsigli, M., Venturi, I. (1998a): Comportamento in cottura delle argille italiane per laterizi. *Ind. Laterizi*, **54**, 382-394.

Dondi, M., Marsigli, M., Venturi, I. (1998b): Sensibilità all'essiccamento e caratteristiche porosimetriche delle italiane per laterizi. *Ceramurgia*, **28**, 1-8.

Dondi, M., Marsigli, M., Venturi, I. (1998c): Technological requirements of raw materials for heavy clay products (1998c) Proc. 2nd Mediterranean Clay Meeting, Aveiro, 204-207.

Marsigli, M. & Dondi, M. (1997): Plasticità delle argille italiane per laterizi e previsione del loro comportamento in foggiatura. *Ind. Laterizi*, **46**, 214-222.

Poon, C.S. (1997): Management and recycling of demolition waste in Hong Kong. *Waste Manag. Res.*, **15**, 561-572.
Poon, C.S., Yu, A.T.W., Ng, L.H. (2001): On-site sorting of construction and demolition waste in Hong Kong. *Resources Conserv. Recycling*, **32**, 157-172.
UNI-EN 206-1 (2001): Calcestruzzo-parte 1: specificazione, prestazione, puroduzione e conformità.